KAUNAS UNIVERSITY OF TECHNOLOGY

IEVA PETRIKYTĖ-VALIONIENĖ

SYNTHESIS AND PROPERTIES OF EFFECTIVE HOLE TRANSPORTING MATERIALS WITH π-CONJUGATION EXTENDED *via* PHENYLETHENYL MOIETIES

Doctoral dissertation
Physical Sciences, Chemistry (03P)

2018, Kaunas

This doctoral dissertation was prepared at Kaunas University of Technology, Faculty of Chemical Technology, Department of Organic Chemistry during the period of 2013–2017. The studies were supported by Research Council of Lithuania and Scientific Exchange Programme SCIEX-NMS^{ch}.

Scientific Supervisor:

Prof. Dr. Vytautas Getautis (Kaunas University of Technology, Physical Sciences, Chemistry, 03P).

Scientific Advisor:

Dr. Marytė Daškevičienė (Kaunas University of Technology, Physical Sciences, Chemistry, 03P).

Doctoral dissertation has been published in:
http://ktu.edu

Editor:

Tony Bexon (Publishing Office “Technologija”)

ISBN/ISMN 978-609-02-1523-4

The bibliographic information about the publication is available in the National Bibliographic Data Bank (NBDB) of the Martynas Mažvydas National Library of Lithuania.

KAUNO TECHNOLOGIJOS UNIVERSITETAS

IEVA PETRIKYTĖ-VALIONIENĖ

EFEKTYVIŲ SKYLES TRANSPORTUOJANČIŲ MEDŽIAGŲ SU FENILETENILGRUPĖMIS PRAPLĖSTA KONJUGUOTA π-ELEKTRONŲ SISTEMA SINTEZĖ IR SAVYBIŲ TYRIMAS

Daktaro disertacija
Fiziniai mokslai, Chemija (03P)

2018, Kaunas

Disertacija rengta 2013-2017 metais Kauno technologijos universiteto Cheminės technologijos fakultete Organinės chemijos katedroje. Mokslinius tyrimus rėmė Lietuvos mokslo taryba ir Šveicarijos stipendijų fondas (SCIEX-NMS^{ch}).

Mokslinis vadovas:

Prof. dr. Vytautas GETAUTIS (Kauno technologijos universitetas, Fiziniai mokslai, Chemija (03P).

Mokslinis konsultantas:

Dr. Marytė DAŠKEVIČIENĖ (Kauno technologijos universitetas, Fiziniai mokslai, Chemija (03P)).

Interneto svetainės, kurioje skelbiama disertacija, adresas:
http://ktu.edu

Redagavo:

Tony Bexon (leidykla “Technologija”)

ISBN/ISMN 978-609-02-1523-4

Leidinio bibliografinė informacija pateikiama Lietuvos nacionalinės Martyno Mažvydo bibliotekos Nacionalinės bibliografijos duomenų banke (NBDB).

CONTENTS

LIST OF ABBREVIATIONS AND PHYSICAL UNITS

Bn-Cbz	*N*-benzylcarbazole;
*t*BP	4-*tert*-butylpyridine;
Cbz	9*H*-carbazole;
^{13}C NMR	carbon nuclear magnetic resonance;
CGL	charge generation layer;
CoTFSI	tris(2-(1*H*-pyrazol-1-yl)-4-*tert*-butylpyridine)-cobalt(III) tris(bis(trifluoromethylsulfonyl)imide);
CSA	(±)-camphor-10-sulfonic acid;
CTL	charge transporting layer;
CV	cyclic voltammetry;
DMF	dimethyl formamide;
DMSO	dimethyl sulfoxide;
DSC	differential scanning calorimetry;
E_g^{opt}	optical band gap;
E_{ox}	ground-state oxidation potential;
FDT	fluorine-dithiophene;
FET	field effect transistor;
FF	fill factor;
FTO	fluorine doped tin oxide;
^{1}H NMR	proton nuclear magnetic resonance;
HOMO	highest occupied molecular orbital;
HTM	hole-transporting materials;
ICZ	indolo[3,2-*b*]carbazole;
I_p	ionization potential;
J_{sc}	current density;
J_V	current density-voltage;
LiTFSI	bis(trifluoromethylsulfonyl)imide lithium salt;
PCE	power conversion efficiency;
PC-*Z*	bisphenol-*Z* polycarbonate;
PESA	photoelectron spectroscopy in air;
PhOLED	phosphorescent organic light-emitting devices;
PSC	perovskite solar cell;
PTAA	poly-[bis(4-phenyl)(2,4,6-trimethylphenyl)amine];
$MAPbI_3$	methylammonium lead iodide;
MHz	megahertz;
MPPT	maximum power point tracking;
NBS	*N*-bromosucciniminde;
OLED	organic light-emitting diode;
PS	polystyrene;
spiro-OMeTAD	2,2′,7,7′tetrakis(*N*,*N*-di-*p*-methoxyphenylamine)-9-9′-spirobifluorene;
T_{dest}	5% mass loss temperature;
T_g	glass transition temperature;

T_m	melting point;
TAT	triazatruxene;
TBABr	tetra-*n*-butylammonium bromide;
THF	tetrahydrofuran;
TGA	thermogravimetric analysis;
TMS	tetramethylsilane
TPA	triphenylamine;
TPD	*N*,*N*′-bis(3-methylphenyl)-*N*,*N*′-diphenylbenzidine;
U_R/U_0	relative residual potential;
UV/VIS	ultraviolet/visible;
V_{oc}	open-circuit voltage;
Φ_F	fluorescence quantum yield;
XTOF	xerographic time of flight technique;
α	Poole–Frenkel parameter;
λ	wavelength;
μ	charge carrier mobility;
μ_0	zero field charge carrier mobility.

1. INTRODUCTION

Organic molecules with a π-conjugated system have attracted growing interest over recent years, owing to their applications in a wide range of electronic and optoelectronic devices [1,2]. Such materials can be used for various applications, such as electrophotography, organic light emitting diodes (OLED), photovoltaic cells, field-effect transistors, and other semiconductor devices [3,4]. Electronic and optoelectronic devices using organic materials as active elements involve a charge transport as an essential operation process and hence, require charge-transporting materials. Therefore, the development of high-performance charge-transporting materials is a key issue for the fabrication of high-performance devices. Realization of the organic electronics potential for simple processing requires the ability to create form devices by solution deposition methods, preferably using simple, inexpensive and easily purified materials.

Organic charge transport materials used in optoelectronic devices can be divided into polymers, molecularly doped polymers and molecular glasses. Molecularly doped polymers represent small electroactive molecules doped into a polymer matrix. Molecular glasses are low-molecular-weight amorphous materials that form stable amorphous glasses having glass transition temperatures above room temperature. All these classes have their own advantages and drawbacks. Polymers and molecularly doped polymers usually possess good film forming properties and mechanical resistance of their films is superior to that of amorphous films of molecular glasses. However, the main drawback encountered so far with polymers in optoelectronic devices has been their operation stability, which is largely connected with their chemical purity. Indeed, polymerization products are usually polluted by impurities, such as catalyst residues that cannot be separated by distillation or sublimation. Therefore, the impurity trap charge carriers lead to a decrease in the devices' efficiency and shortening of its lifetime. Another problem, which arises with the preparation of the thin films, is poor solubility of many polymeric materials in common organic solvents. On the other hand, thorough purification of molecular glasses, which can be performed by such methods as sublimation, crystallization, chromatography, *etc*., is a serious advantage over polymeric materials.

In recent years, several families of hole transporting materials have been increasingly studied [5,6]. Numerous investigations are being carried out aimed at enhancement of hole drift mobility; however, until now only a few concrete recommendations have been made with regard to the molecular structure modification. Although, it is evident that the alternating double bonds present in both small molecules and polymers gives rise to their interesting electronic properties [7]. There are many possibilities for the enhancement of its π-conjugated systems of organic molecules into dimers, trimers or oligomers utilizing Suzuki or Yamamoto cross-coupling, Wittig or Knoevenagel condensation, or Heck reaction; also by adding diarylamino (usually applying Buchwald-Hartwig reaction) or hydrazone fragments. Similar compounds, bearing phenylethenyl or diphenylethenyl fragments, have been reported in the literature [8,9]. However, they are obtained using either a multistep synthesis procedure, involving the McMurry cross-coupling

reaction, or by palladium-catalyzed cross-coupling, facilitated by a tailor-made ligand or employing quite high loading of the catalyst.

For the synthesis of effective hole transporting materials with π-conjugation extended *via* phenylethenyl moieties, this study has employed a different approach. The method utilizes commercially available and relatively inexpensive precursors and catalyst, with the reaction not oxygen sensitive, therefore the final product could be obtained in one step.

The main aims of this work is the synthesis and characterization of effective hole transporting materials with π-conjugation extended *via* phenylethenyl moieties for semiconductive devices.

The tasks proposed for the achievement of the above stated aims are as follows:

1. Synthesis and investigation of effective hole transporting carbazole-based small molecules with π-conjugation extended *via* phenylethenyl moieties.
2. Synthesis and investigation of effective hole transporting triphenylamine-based small molecules with π-conjugation extended *via* phenylethenyl moieties.
3. Synthesis and investigation of effective hole transporting triphenylamine-based polymers with π-conjugation extended *via* phenylethenyl moieties.

Scientific novelty: A series of novel carbazole based derivatives possessing diarylethenyl fragments have been synthesized and investigated. This is the first report dealing with the interaction of diphenylacetaldehyde and its dimethoxy analogous with *C*-unsubstituted carbazole derivatives. The neat films of these carbazole-based derivatives wet-casted in ambient conditions exhibited high drift mobilities in strong electric fields ($>10^{-3}$ $cm^2 V^{-1} s^{-1}$ at 3.6×10^5 V cm^{-1}). Commercially available and the relative cheapness of the starting materials, simple synthetic method, number of sites available for easy functionalization and covalent linking to other molecules, good charge drift mobility, solubility in common organic solvents and glass-forming properties make these compounds attractive for optoelectronic applications, and also as promising building blocks for the construction of more complex low-molecular-weight or polymeric materials.

A rapid and efficient synthesis of novel indolocarbazole-based two-dimensional hole transporting materials (HTMs), comprising electron-rich methoxy substituents in phenylethenyl-engineered side arms was demonstrated. The HTMs were obtained in three scalable synthetic steps, offering potentially much lower production costs in comparison with the most widely used *spiro*-OMeTAD. Remarkable power conversion efficiency (PCE) of 15.24% was achieved using 3,8,13–tris[2,2-bis(4-methoxyphenyl)ethenyl]-5,10,15-triethyl-10,15-dihydro-5*H*-indole-[3,2-*a*:3′,2′-*c*]carbazole as a hole transporting material and compositive perovskite as absorber, which is on par with that of *spiro*-OMeTAD (17.03%).

A simple one step synthesis method to obtain solution processable star-shaped charge transporting materials with a triphenylamine core and a varying number of

different phenylethenyl sidearms from commercially available and relatively inexpensive starting materials was proposed. Substitutions in the phenylethenyl fragment could noticeably influence HTMs glass transition temperatures and the tendency to crystallize. By structurally modifying the sidearms, one can also significantly influence the size of the π-conjugated system, energy levels, and the way molecules pack in the solid state. Optical measurements revealed that increasing the number of the side arms effectively suppressed intramolecular motions of the TPA core in the solution, whereas in the solid state it facilitated an exciton migration *via* the dense sidearm network formed. In turn, this dense network enables charges to move more rapidly through the HTM layer, resulting in very good charge drift mobilities of up to 0.017 $cm^2 V^{-1} s^{-1}$ in strong electric fields.

New polymeric triarylamine derivatives with methyl phenylethenyl and diphenylethenyl functional groups were synthesized and used as HTMs for the perovskite solar cells (PSC) construction. These materials work without any additives, which the study showed to be particularly detrimental for PSC stability. Polymer containing poly[bis(4-phenyl)(3,5-dimethylphenyl)amine] main chain with methyl phenylethenyl fragments attached to it, demonstrates a PCE of 12.3% without any additives, which is better than the usually used poly-[bis(4-phenyl)(2,4,6-trimethylphenyl)amine]. Furthermore, research showed stable PSCs with **38** under full sun illumination for around 40 h, and under elevated temperature (85 °C) in the dark for more than 140 h. These results indicate that this polymer is a very attractive HTM for highly stable PSCs. More generally, this finding is very promising towards the prospect of commercializing PSCs, because with the astonishing rise in efficiency, the next big step is to demonstrate the stability of the PSCs under industrially compatible stress tests.

The main statements of the doctoral dissertation are:

1. The newly synthesized organic solution processability, film-forming carbazole based derivatives possessing diarylethenyl fragments are applicable as semiconducting materials in optoelectronic devices, particularly in the perovskite solar cells.
2. By a simple one step synthesis method, obtainable star-shaped charge transporting materials with a triphenylamine core and a varying number of different phenylethenyl side arms are solution processable semiconducting materials with extremely high hole mobilities.
3. New polymers, containing poly[bis(4-phenyl)(3,5-dimethylphenyl)amine] main chain with phenylethenyl fragments attached to it, exhibiting high thermal stability and high charge mobility, are applicable as hole transporting materials for highly stable perovskite solar cells.

2. LITERATURE REVIEW

2.1 Conjugated organic systems

Conjugated organic materials, and mainly aromatic compounds, are widely used in numerous fields in todays science and technologies, *e.g.* as semiconductors in organic light-emitting diodes (OLEDs), organic photovoltaics (OPVs), organic field transistors (OFETs). Additionally, conjugated organic materials are the key materials in functional fluorescent dyes, pharmaceuticals and agrochemicals [10-12]. Conjugated organic molecules with their extended π-electrons systems, due to better optical properties and conductivity, allows the organic optoelectronics as a fact. There are several different methods known for the enlargement of conjugation in organic molecules. Widely used metal-catalysed Buchwald-Hartwig [13, 14], Ullman [15], Suzuki-Miyaura [16, 17] reactions are well known as a tool for π-extention *via* sidearms. Due to these reactions, a wide spectrum of organic materials have been created in the last few centuries. In the case of non-metal catalysed reactions, synthesis of hydrazones plays a significant role [18].

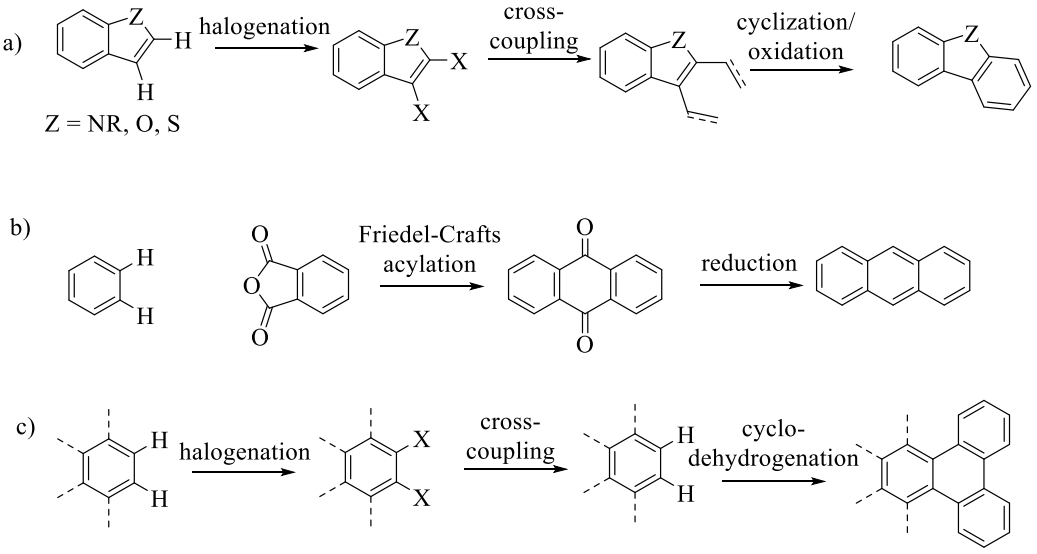

Scheme 2.1. Multistep synthesis of fused compounds; a) halogenation/cross-coupling/cyclization/oxidation based synthesis of heterocycles, b) Friedel-Crafts acylation/reduction based synthesis of acenes, c) cyclohydrogenation based synthesis of PAHs, nanographenes and GNRs

The classical methods for synthesis of fused aromatic compounds are based on the multistep π-extension reactions of small arenes [19-51]. Scheme 2.1. demonstrates three examples of step-wise synthesis of fused organic molecules. First representative shows the synthetic sequence of three rings-bearing heterocyclic compounds, such as carbazoles and benzothiophenes, including halogenation of smaller heterocycle (indole or benzothiophene), cross-coupling of halogenated intermediate and cyclization/oxidation procedure. The next illustration demonstrates Friedel-Crafts acylation with the following reduction, when benzene reacts with

phtalic anhydride and yields antracene. Polycyclic aromatic hydrocarbons, nanographenes, graphene nanoribbons could be synthesized *via* cyclodehydrogenation of polyarylated compounds.

In the cases of the above mentioned examples, complicated pathways with purification of intermediate are the limiting factors for good yields and overall synthetic efficiency. However, Itami and co-workers defined a single-step annulative π-extension reaction of a template arene (APEX) as a perfect method to construct one or more new fused aromatic rings [52]. Scheme 2.2. demonstrates the principled idea of APEX reactions, when the starting material is a non-functionalized aromatic template.

Scheme 2.2. The idea of annulative π-extention reaction of non-functionalized aromatic templates

The main advantages of this method are the passing of prefunctionalization, such as metalation or halogenation, which leads to a faster synthesis and great potential of formed structures in one step reactions. This review is focused on the APEX reactions of π-extended fused heterocycles, including classical and recent examples.

2.2 Annulative π-extension (APEX)

Annulative π-extension is a great synthetical tool in both hydrocarbons and heterocyclic materials. Depending on the two rings connection type, polycyclic aromatic hydrocarbons (PAHs) contain three different edge structures: bay regions (concave armchair edges), *K*-regions (convex armchair edge) and *L*-regions (zigzag edge) [53]. As a consequence of regioselective APEX reactions, synthesis of structurally well-defined aromatic compounds, *e.g.*, π-extended PAHs, nanographenes, GNRs, it is possible in a programmable fashion.

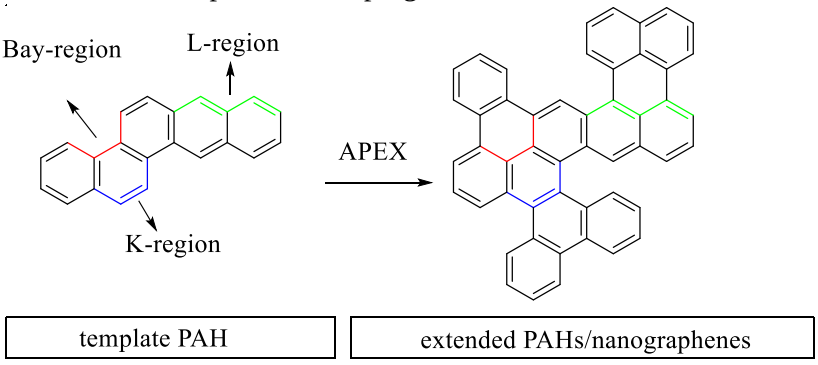

Scheme 2.3. Regioselective annulative π-extension reactions of smaller arenes for synthesis of PAHs, nanographenes, and GNRs. Bay region=concave armchair edge, *K*-region= convex armchair edge, *L*-region=zigzag edge

Nevertheless, as this work is based on nitrogen bearing hole transporting materials, full attention is orientated on the synthesis of fused heterocycles. To elaborate, three main methodologies are most popular in this case: 1) transition metal catalysed *C-H* functionalization, 2) nucleophilic addition and 3) [4+2] cycloaddition. Fused aromatic compounds show better physical and biological properties *versus* small aromatic compounds; as a consequence of their extended π-conjugation, narrow HOMO-LUMO gaps, longer-wavelength (both absorption and emission), lower oxidation and/or reduction potentials, strong π-π interactions, and higher mechanical strengths. Multistep π-extension reactions of small molecules such as indoles, pyrroles or benzene is the classic methods for π-extended fused heterocyclical compounds.

Aromatic hydrocarbons are key fragments in both life and material science [54-61]. More than two fused rings bearing molecules, such in the cases of anthracene, phenanthrene, pyrene and perylene show perfect π-conjugation, which plays a significant role in narrow HOMO–LUMO gaps, long-wavelength absorptions and emissions, lower oxidation and/or reduction potentials, strong π-π interactions, and high mechanical strengths.

Nowadays, organic synthesis is unthinkable without the attendance of fused heterocyclic molecules. The greatest part of heterocyclic compounds contains nitrogen, sulfur or oxygen in the fused piece of a molecule. A large amount of main cyclic molecules, such as carbazole, or thiophene could be found in natural sources of organic materials –fossils, like oil or coal, but in the case of requirements for smart materials, functionalization and optimization of small skeletons using different substituents and/or their positions is necessary. The before mentioned advantages of fused heterocycles dictate a tendency to synthesize molecules with extended π-electron system. The starting materials for this target are the simple one or two rings bearing heterocycles and different additives, for example, unsaturated aliphatic compounds. The three main courses- transition metal catalysed *C-H* functionalization, nucleophilic addition and [4+2] cycloaddition are reviewed below.

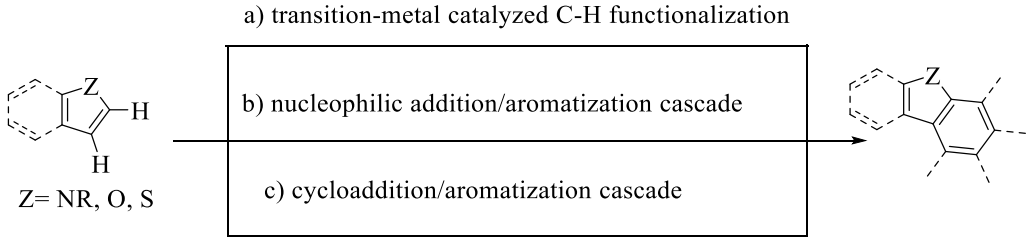

Scheme 2.4. Three main APEX methods for unfuncionalized heteroarenes

2.2.1. Transition-metal-catalyzed *C-H* functionalization

Activation of aromatic *C-H* bonds by a transition metal catalyst has received significant attention in the synthetic chemistry community. The main metals for catalyst function are from the platinum group – platinum, palladium, rhodium, rhutenium, and other noble elements like gold and silver. The leading catalysts are salts, for example, chlorides, or complexes of noble metals. The catalysts containing

the organic parts (mainly acetates of precious metals) are found as perfect for synthesis of fused heterocycles.

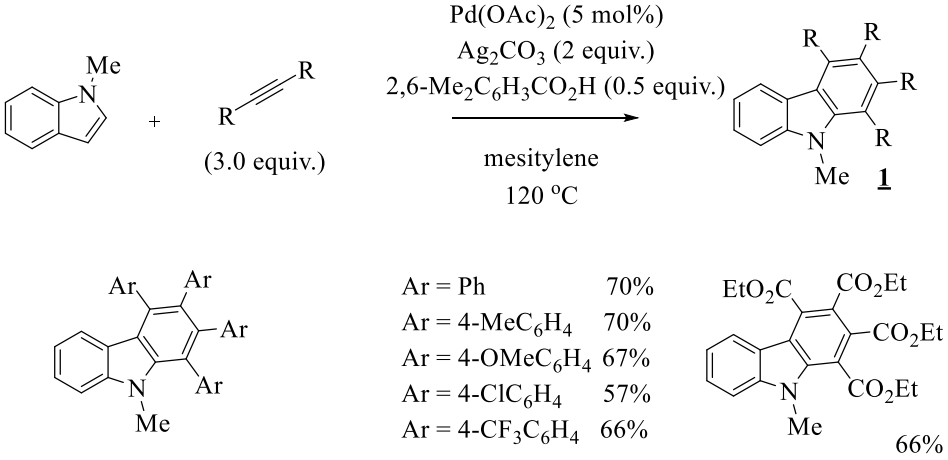

Scheme 2.5. Pd-catalyzed indole-to carbazole reaction with alkynes

In recent years, rapid and site selective extension of π-electron systems by *C–H* activation has emerged as an ideal methodology for preparing organic materials with extended π-systems. *C-H* functionalization powered by catalysis of transition metals is one of the widely used methods to create new organic materials. The fused heteroaromatic systems are also synthesizing using this technology. An important step was made by Miura, Sotah *et al.* in 2009 by the indole to carbazole report [62]. In this example, *N*-methylindole reacted with aromatic alkynes and yielded tetrasubstituted carbazoles. This reaction was catalysed by palladium acetate, assisted by 2 equivalents of silver carbonate and 0.5 equivalents of 2,6-dimethylbenzoic acid. Yields of this reaction are good and depending on the substituent in the aromatic ring are variable between 57 and 70%. The highest efficiency of reaction was reached with phenyl and (*p*-methyl)phenyl substituents, when more complex substituents reduce yields of the final three fused rings possessing compound.

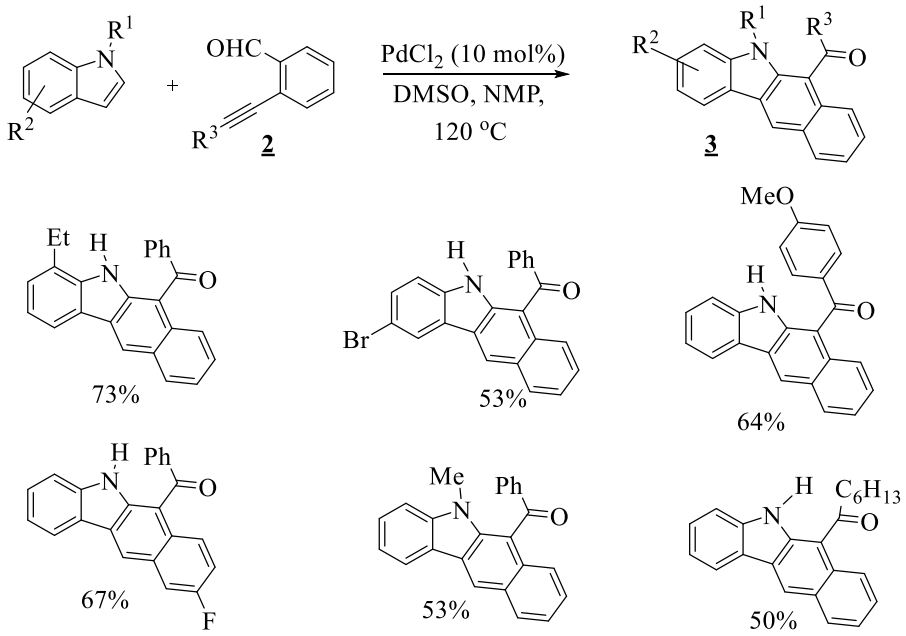

Scheme 2.6. Pd-catalyzed naphth-annulative reaction of indoles with alkynylbenzaldehydes (NMP-*N*-methylpyrrolidone)

The same authors described this reaction as initiated by direct palladation at 3rd C of indole. Palladium chloride was chosen as the catalyst. After two alkynes come into the indolyl-palladium complex and then cyclopalladation situated at the 2nd C of indole provide a seven members palladacycle. The last step is the reductive elimination of palladium with the release of the substituted carbazole. The same reaction conditions yielded a variety of diaryacetylenes and acetylene carboxylates [63].

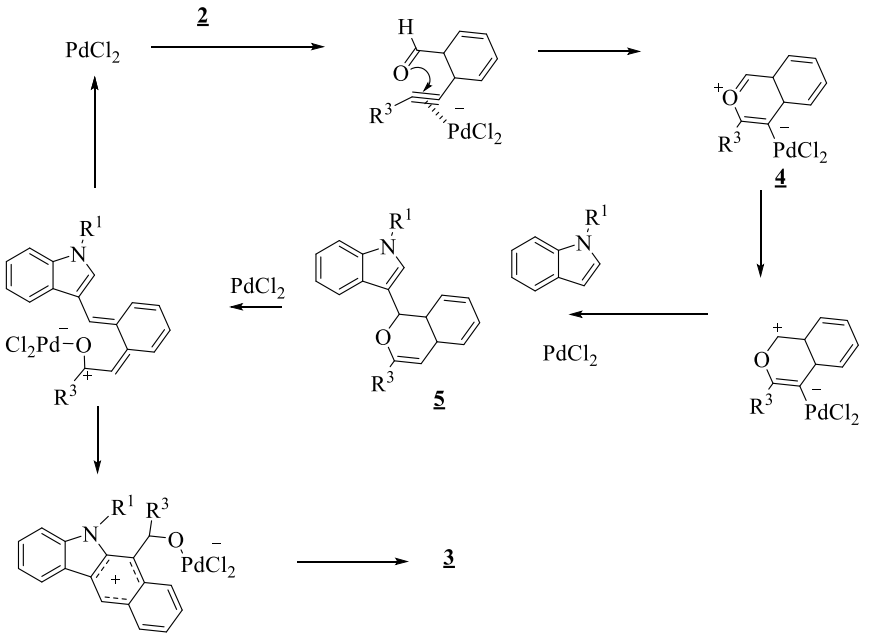

Scheme 2.7. Mechanism of Pd-catalyzed naphth-annulative reaction of indoles with alkynylbenzaldehydes

The selective synthesis of 1,2,3,4-tetrasubstituted carbazoles can be performed effectively through the palladium-catalyzed oxidative coupling reactions of *N*-substituted indoles or their carboxylic acid derivatives with alkynes. Unsymmetrically octasubstituted carbazoles can also be obtained by the stepwise couplings of 1-methylpyrrole-2-carboxylic acid with two different alkynes. In addition, the present coupling procedure is applicable to the synthesis of other various heteroarenes possessing di-, tri-, and tetracyclic cores. Some of the products exhibit intense fluorescence in the solid state. The related strategy was used by Li and co-workers with another precious metal – rhodium(III)- catalysis for the pyridine to chinoline synthesis. The use of pyridine derivatives as a substrate was found as an efficient and straightforvard strategy in the case of Rh(III)-catalyzed *C-H* functionalization. The rhodium complexs salt $[Cp^*RhCl_2]_2$ and stoichiometric amounts of $Cu(OAc)_2$ catalyzed the direct benzoquinolines transformation from isonicotinamides, when two equivalents of alkyne are used to extend π-conjugation and the amide group is used as a directing group [64].

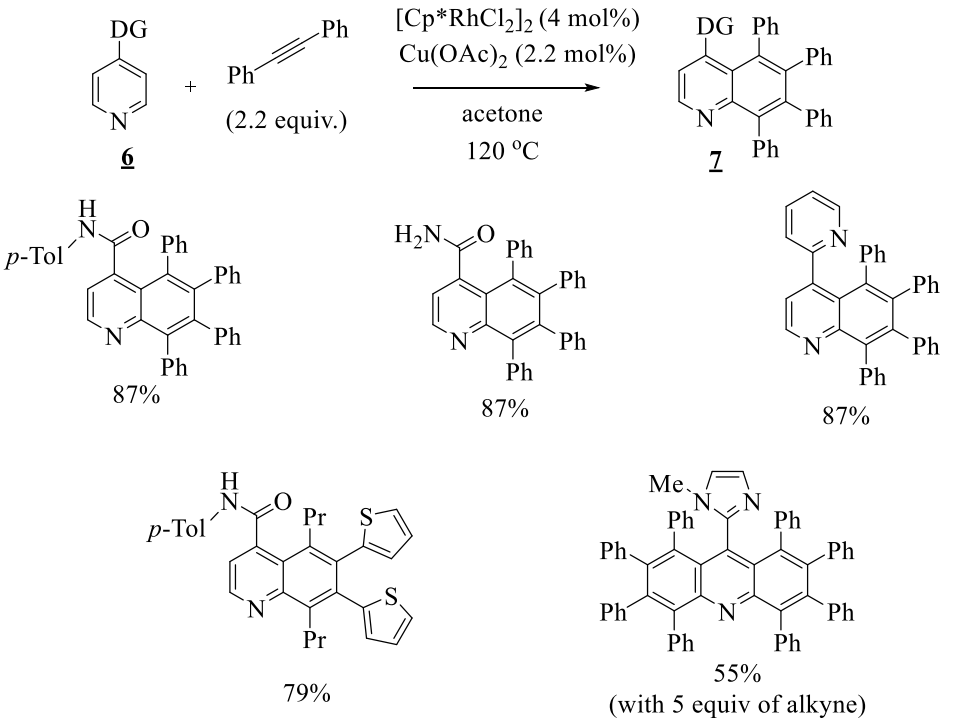

Scheme 2.8. Rh-catalyzed pyridine to quinolone reaction assisted by the directing group (DG)

In addition, double APEX reaction on the starting pyridine is possible and the synthesis of acridine derivatives was mentioned in Li paper as well.

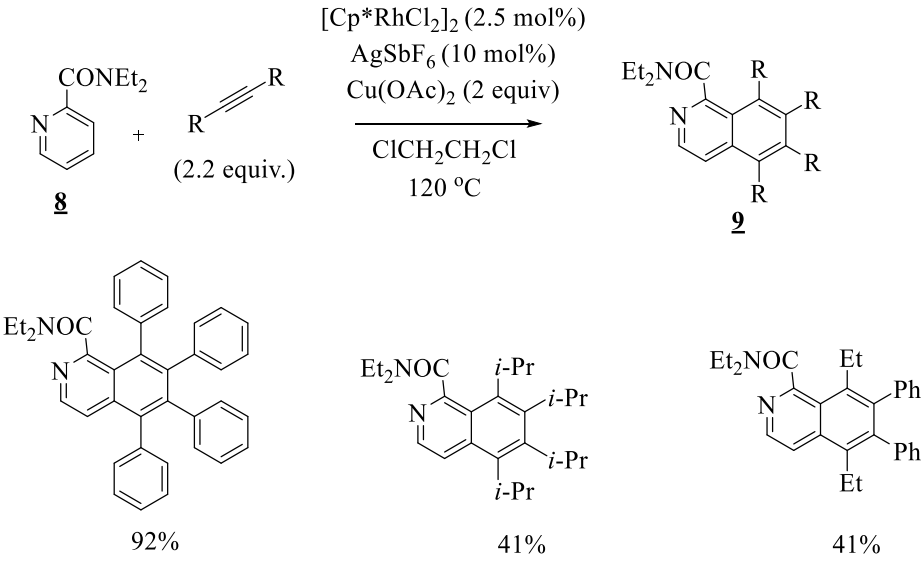

Scheme 2.9. Rh-catalyzed pyridine to isoquinolone reaction assisted by the amido group

Synthesis of isoquinolines from picolineamide catalyzed by $[RhCp^*Cl_2]_2$ and $AgSbF_6$ was reported relatetively in the previous mentioned research [65]. Interestingly, an excellent yield was obtained in the case of tetraphenylsubstituted compound.

Selective synthesis of quinolines has been achieved *via* oxidative annulation of functionalized pyridines with two alkyne molecules under Rh(III)-catalyzed cascade *C–H* activation of pyridines using $Cu(OAc)_2$ as an oxidant. The selectivity of this reaction is oxidant-dependent, particularly on the anion of the oxidant. An efficient synthesis of isoquinolines *via* Rh(III)-catalyzed oxidative annulation of picolinamides with alkynes using $Cu(OAc)_2$ as an oxidant has been developed. The scope of the reaction was studied with a selection of various picolinamides and alkynes, and the desired isoquinolines were obtained in good to excellent yields.

Ohno, Fujii, and coworkers tried cationic gold catalyst to formal [4+2] cycloaddition of 1,3-butadiynes to pyrroles and indoles [66]. Pyrrole-to-indole and indole-to carbazole APEX reactions were made through the formation of enyne intermediates. Indole synthesis by a gold(I)-catalyzed intermolecular formal [4+2] reaction between 1,3-diynes and pyrroles has been developed. This reaction involves the hydroarylation of 1,3-diynes with pyrroles followed by an intramolecular hydroarylation to give the 4,7-disubstituted indoles. This reaction can also be applied to the synthesis of carbazoles when indoles are used as the nucleophiles instead of pyrroles. Depending on site substituents, yields vary between 35 and 90%.

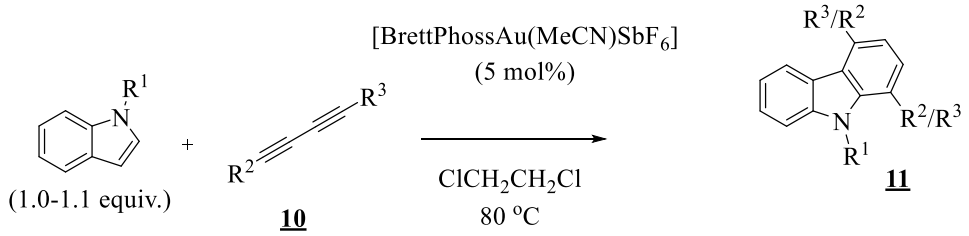

R_1=H, R_2=Ph, R_3=H 50%
R_1=Me, R_2=Ph, R_3=H 57%
R_1=Me, R_2=Ph, R_3=OMe 70%
R_1=Me, R_2=Ph, R_3=CO_2Me 45%
R_1=Bn, R_2=Ph, R_3=H 78%

Scheme 2.10. Gold-catalyzed APEX reaction of indoles with 1,3-butadiynes

As triple bond bearing alkines, double-bonded alkenes with electron-withdrawing groups are good *π*-extending reagents for APEX reactions. Electron-deficient alkenes, such as methyl vinyl ketone or methyl acrylate in the presence of the trimetallic Pd-Cu-Ag system, formed carbazoles from indoles [67].

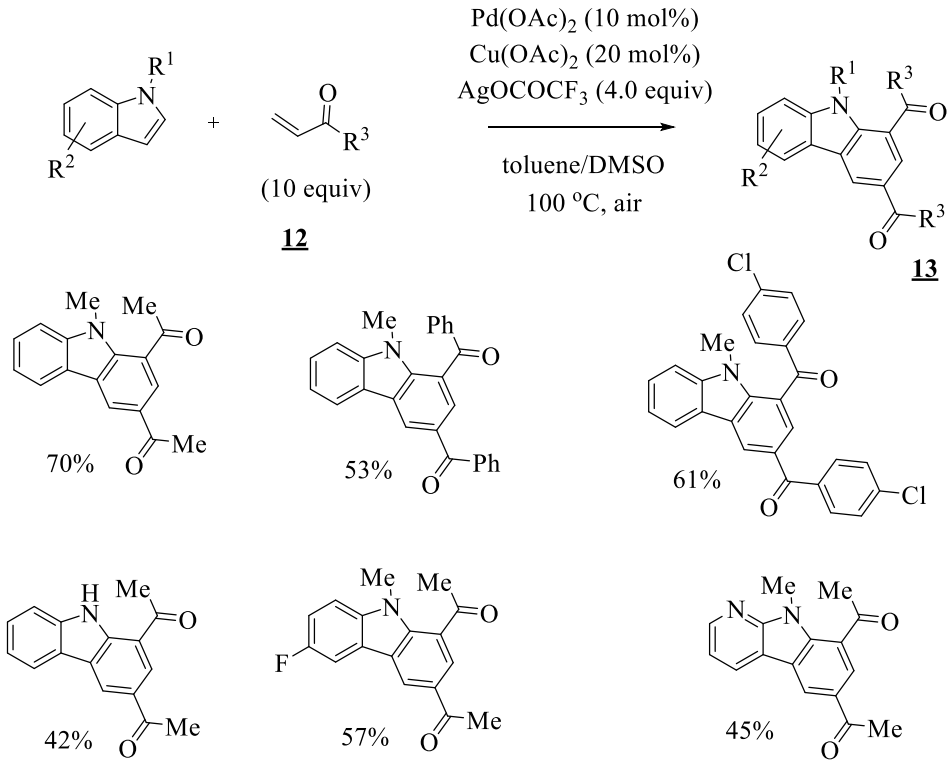

Scheme 2.11. Triple metallic catalyzed one step indole-to-carbazole reaction with electron deficient groups

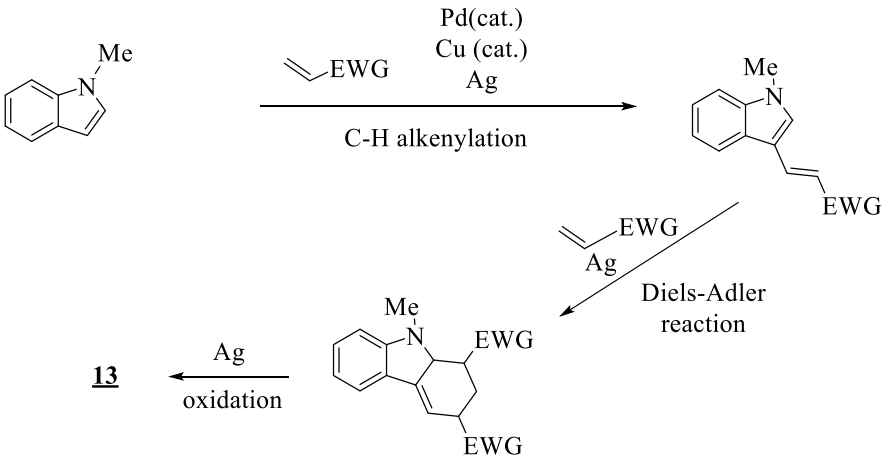

Scheme 2.12. The mechanism of one step indole-to-carbazole reaction with electron deficient groups promoted by Pd-Cu-Ag catalytic system (EWG – electron-withdrawing group)

Most probably, this reaction starts with tandem *C3*-selective *C-H* alkenylation of indole, catalyzed by palladium and copper and proceeds through regioselective

Diels-Alders reaction and aromatization. Unfortunately, polymerization of vinyl compounds plays a significant role in the yield of the desired product, so 10 equivalents of starting π-conjugation extending compound are necessary for good yields of 1,3-diarolylcarbazoles. To summarize, it was developed a Pd–Cu–Ag trimetallic system that can convert indoles to carbazoles using electron-deficient alkenes as two-carbon units. Investigation of the reaction mechanism revealed that this one-shot indole-to-carbazole π-extension is likely to proceed through the sequence of Pd/Cu-catalyzed indole *C–H* alkenylation, Ag-promoted Diels–Alder reaction and dehydrogenative aromatization. The successful one-pot synthesis of a five-rings-membered granulatimide derivative, an interesting example of Chk1 kinase inhibitors, highlights the potential of the present reaction for further development and applications.

One more example of direct synthesis of differentially substituted carbazoles from the *NH*-group possessing indoles is regioselective triple successive oxidative Heck (Fujiwara-Moritani) reaction. Verma *et al*. demonstrated that both electron-deficient and electron-rich alkenes could be used successively and form products with two different nature substituents.

The Yu group worked by the same strategy with metallic catalyst, and developed that a 3-chloropropiophenone could form both – carbazoles in the presence of indole, and enones. APEX reactions are suitable for synthesis of mixed aroyl-substituted carbazoles [68].

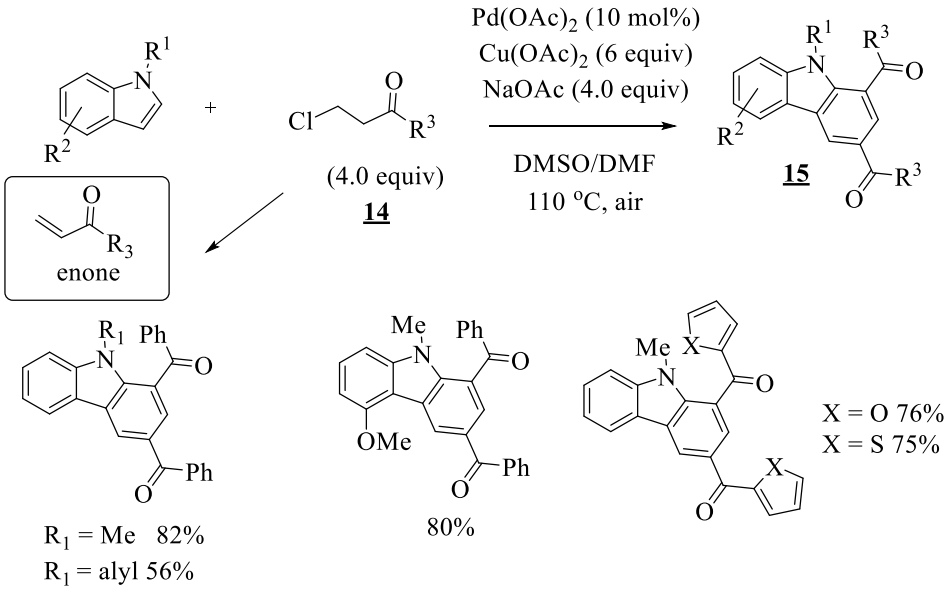

Scheme 2.13. Indole to carbazole reaction from 3-chloropropiophenones, catalyzed by Pd- and Cu

Construction of the benzene ring in carbazoles was efficiently realized through a domino dehydrochlorination/alkenylation/cycloaddition–oxidation sequence by

means of palladium(II)-catalyzed, copper(II)-mediated reactions of *N*-protected 2,3-unsubstituted indoles with 3-chloropropiophenones in the presence of a base. 3-Alkenylated indole was confirmed to be formed as the reaction intermediate, which then underwent Diels–Alder cycloaddition to the initially *in situ* generated enone from a 3-chloropropiophenones substrate, and the subsequent dehydrogenative aromatization yielded the carbazole product. The strategy to employ *in situ* generated enones as the reactive species avoided the use of a large excess of labile substrates and lessened the side reactions. For example, Verma *et al*. used Pd/Cu bimetallic catalysis for indole-to-carbazole reaction involving acrylic esters.

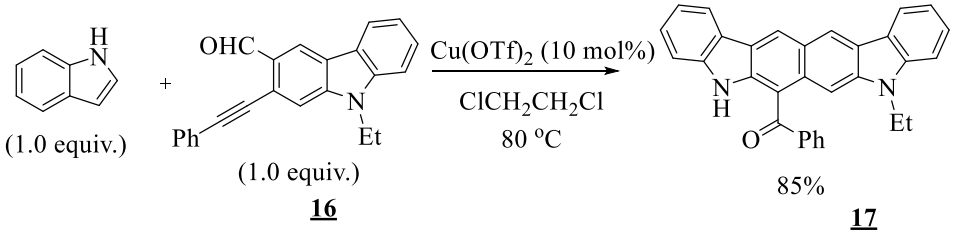

Scheme 2.14. Cu-catalyzed naphtha-annulative APEX reaction of indole with alkynylformylcarbazole

A novel Pd (II)-catalyzed approach for the direct synthesis of differentially substituted carbazoles from free (*NH*) indoles *via* regioselective triple successive oxidative Heck (Fujiwara–Moritani reaction) has been achieved [69]. It is demonstrated that both electron-deficient and electron-rich alkenes could be used successively for the incorporation of two different functional groups into the product. The proposed pathway was well supported by isolating the first and second successive oxidative Heck intermediates as well as by trapping with styrene-d3.

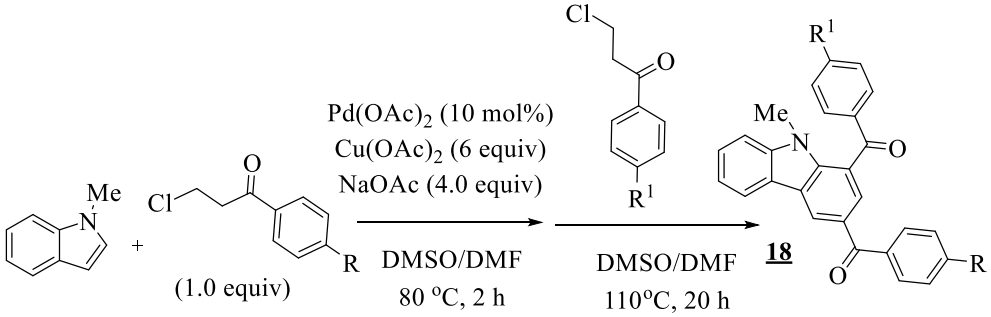

R = H; R_1 = Me 63%
R = H; R_1 = Cl 59%
R = OMe; R_1 = H 62%
R = OMe; R_1 = Me 55%

Scheme 2.15. Indole to carbazole reaction from 3-chloropropiophenones, catalyzed by Pd- and Cu

After the research of Laha and Dayal, it could be mentioned that the Pd/Ag catalyst system is selective and provides exclusively 2,3-disubstituted carbazoles.

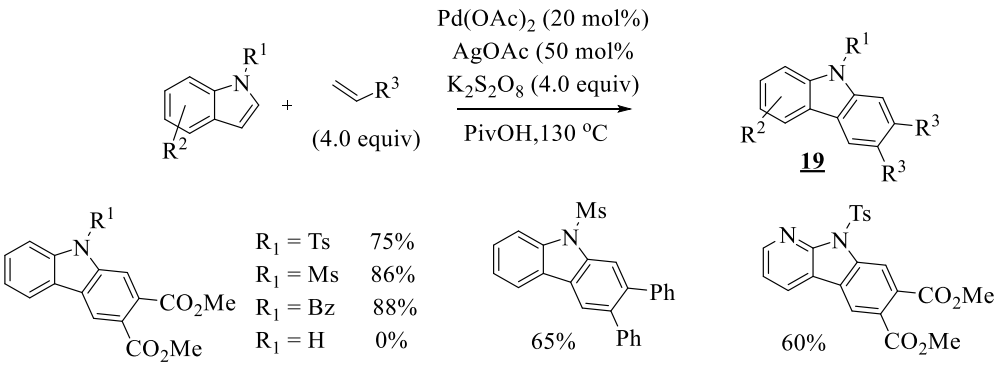

Scheme 2.16. Palladium and silver catalyzed indole to carbazole reaction with double bonded derivatives to obtain 2,3-disubstituted carbazoles (Bz-benzoyl, Piv –pivalic acid)

Most probably, the first step in the reaction is alkenylation of double bond at the 3rd and 2nd C of indoles. After this, follows the electrocyclization and oxidation. It was observed that electron withdrawing groups, such as tosyl, mesyl and benzoyl on the *N*-position in indole, give a positive effect in this reaction. A direct one-pot approach to the synthesis of carbazoles (mono-, di-, and trisubstituted) and *α*-carbolines from readily available indoles or 7-azaindoles and alkenes was described. Based on mechanistic studies, the tandem reaction follows the sequence: palladium-catalyzed regioselective *C-3* alkenylation/palladium-catalyzed *C-2* alkenylation/thermal electrocyclization. It is important to note that this reaction works in the case of *N*-substituted compound, but indole with free *NH* group does not form carbazole in this condition.

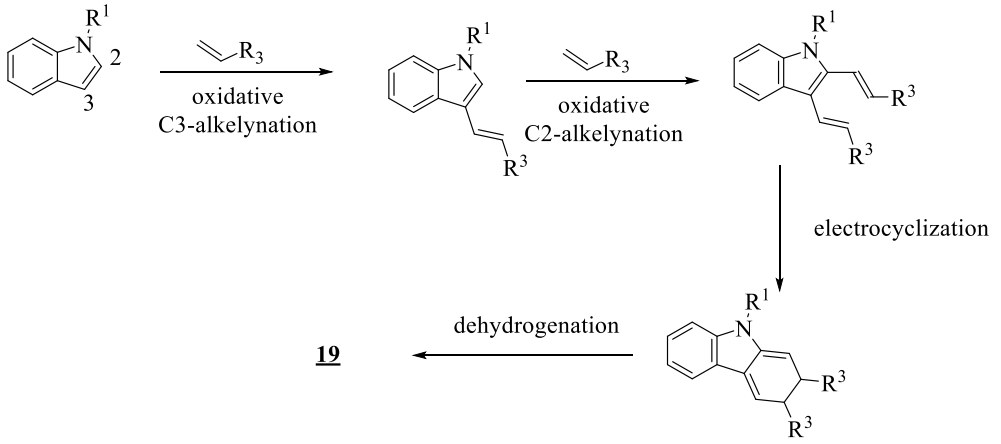

Scheme 2.17. Mechanism of palladium and silver catalyzed indole to carbazole reaction with double bonded derivatives to obtain 2,3-disubstituted carbazoles (Bz-benzoyl, Piv –pivalic acid)

The second ring forming pyrrole-to-indole reaction can be catalyzed by another platoid - ruthenium - catalyst and trifluoracetic acid. First of all, *Z*-enyne, which is a sterically less-hindered intermediate, is formed from pyrolle and

propargyl alcohol. The Ru-bounded derivative is in equilibrium with π-complex and alkenylidene, so cyclization can occur from intermediate. The next step is the 1,5-shift and reductive elimination from the ruthenium complex, which then forms the desired indole with traces of regioisomer. Several ruthenium-catalyzed atom-economic transformations of propargyl alcohols with pyrroles or indoles leading to alkylated, propargylated, or annulated heteroaromatics are reported. The mechanistically distinct reactions are catalyzed by a single ruthenium(0) complex containing a redox-coupled dienone ligand. The mode of activation regarding the propargyl alcohols determines the reaction pathway and depends on the alcohols' substitution pattern. Secondary substrates form alkenyl complexes by a 1,2-hydrogen shift, whereas the transformation of tertiary substrates involves allenylidene intermediates. 1-Vinyl propargyl alcohols are converted by a cascade allylation/cyclization sequence. The environmentally benign processes are of broad scope and allow the selective synthesis of highly functionalized pyrroles and indoles generating water as the only waste product [70].

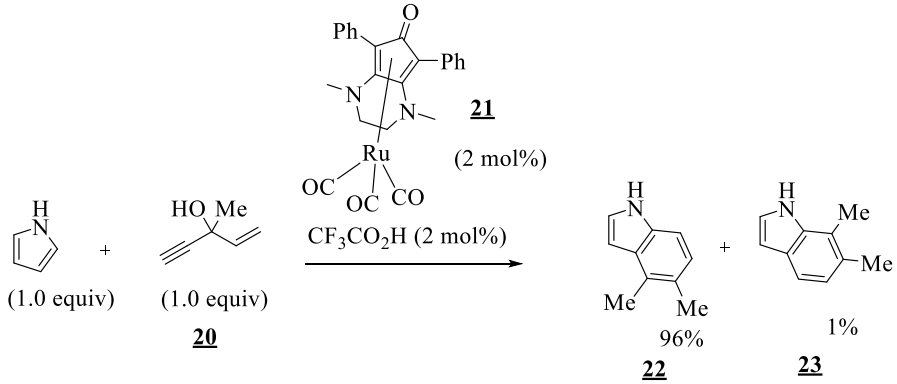

Scheme 2.18. Ruthenium-catalyzed pyrrole to indole reaction with 1-vinyl-propargyl alcohol

The proved catalyst for synthesis of 4-substituted carbazoles from indoles is $Rh_2(OAc)_4$. This type of reaction starts with *C3*-C-H insertion of indole into rhodium carbenoid, followed by protodemetalation, as well as an electrophilic cyclization and aromatization catalyzed by 1,1′-binaphtyl-2,2′-phosphoric acid to give ester substituted carbazoles. Regioselectivity of pyrroles-to-indoles and indoles-to-carbazoles reactions can be rationalized by the higher nucleophilic nature in *C2* pyrolle and *C3* indole position. Disclosed herein is the design of an unprecedented electrophilic rhodium enalcarbenoid, which results from rhodium(II)-catalyzed decomposition of a new class of enaldiazo compounds. The synthetic utility of these enalcarbenoids has been successfully demonstrated in the first transition-metal-catalyzed [4+2] benzannulation of pyrroles, thus leading to substituted indoles. The new benzannulation has been applied to the efficient synthesis of the natural product leiocarpone, as well as a potential adipocyte fatty-acid binding protein inhibitor [71].

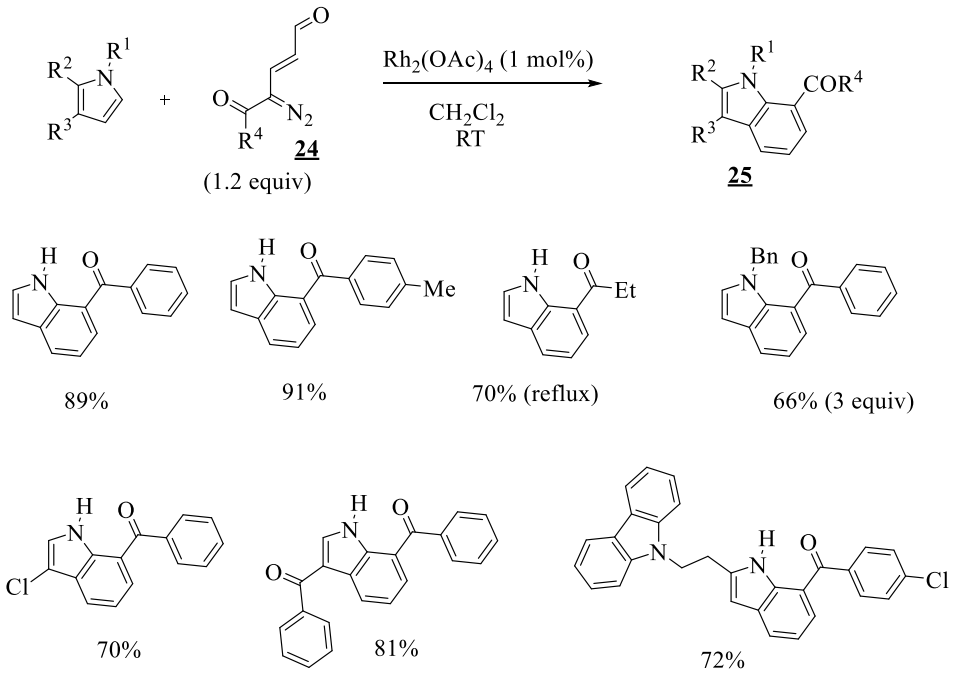

Scheme 2.19. Rhodium catalyzed pyrrole to indole reaction with *α*-diazocarbonyl compounds

Cationic rhodium catalyst and diphenyl phosphoric acid were catalyst in the *N*-pirimidyl substituted indoles reaction to carbazoles. In similar reactions, done by the Katukojvala group as well, only 2-acylcarbazoles were obtained [72]. It is possible that coordination of a pyrimidyl directing group to rhodium(I) complex activate *C-H* bond at the 2nd position of indole selectively. The next Rh-carbene formation, migratory insertion, protodemetallation and the final cyclization is mentioned as the most probable reaction way to obtain 2-acylcarbazoles with good yields. Discovery of this methodology assisted molecular biologists to synthesize the analogues of a *hepatitis C* virus replication inhibitor and a secreted phospholipase inhibitor [73].

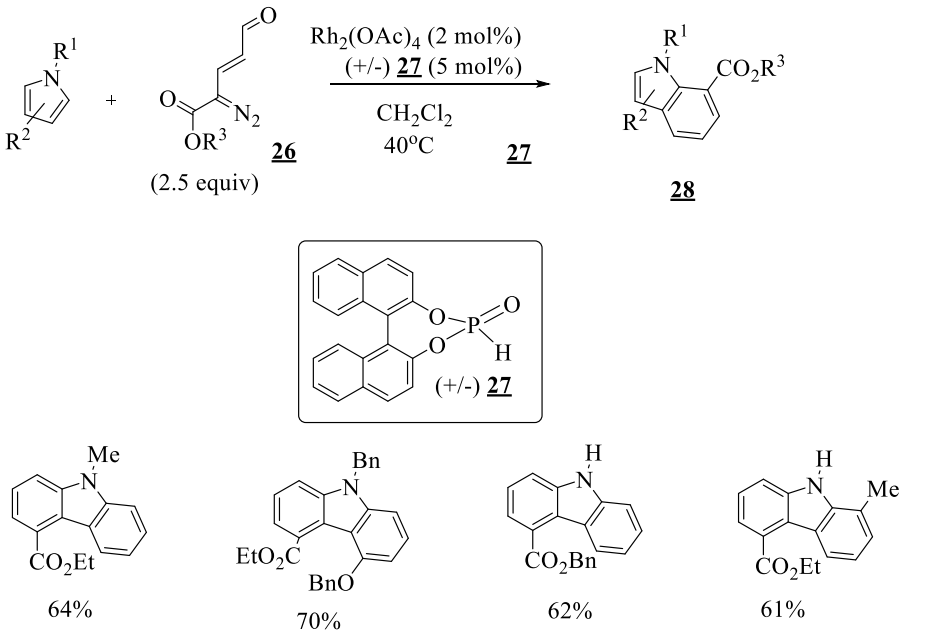

Scheme 2.20. Rhodium catalyzed indole to carbazole reaction with *α*-diazoester

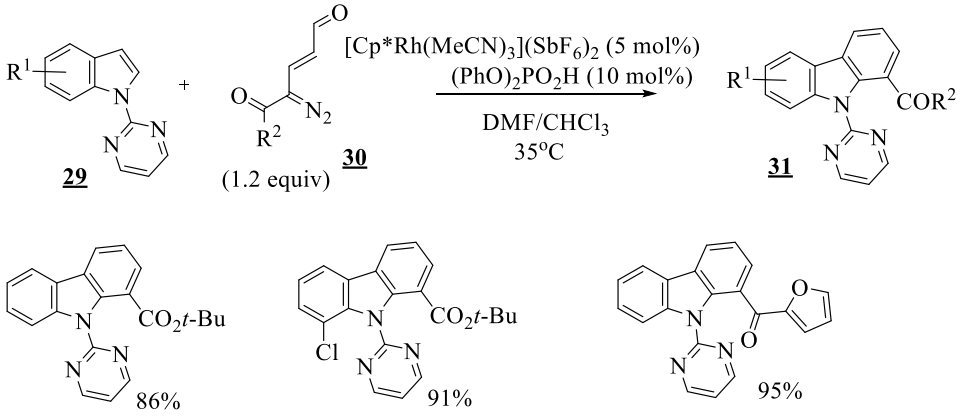

Scheme 2.21. Rhodium/diphenyl phosphoric acid catalyzed indole to carbazole reaction with *α*-diazoester

Nowadays, photoredox reactions with visible light are very popular because of the substrate activation in mild conditions. One of the APEX with 420 nm LED radiation examples is reported by Paria and Reiser. Iridium complex catalyzed pyrolle and furan reaction with *α*-bromochalcone or *α*-bromocinnamate. New fused heteroarenes formed by excited Ir^{3+}*(III)-catalyzed generation of vinyl radical, which cyclizes to carbocation and then dehydrogenation. Vinyl radicals were generated from *α*-bromochalcones or *α*-bromocinnamate ethyl ester under visible light photoredox catalyzed conditions *via* an oxidative quenching cycle of the iridium complex $[Ir\{dF(CF_3)ppy\}_2(dtbbpy)]PF_6$ and subjected to cascade

cyclizations with heteroarenes entailing two consecutive *C-C* bond formations and three *C-H* activations. The process is amenable to furans, benzofurans, pyrroles, and indoles, giving rise to a broad variety of novel polycyclic frameworks in high yields under mild and environmentally benign reaction conditions [74].

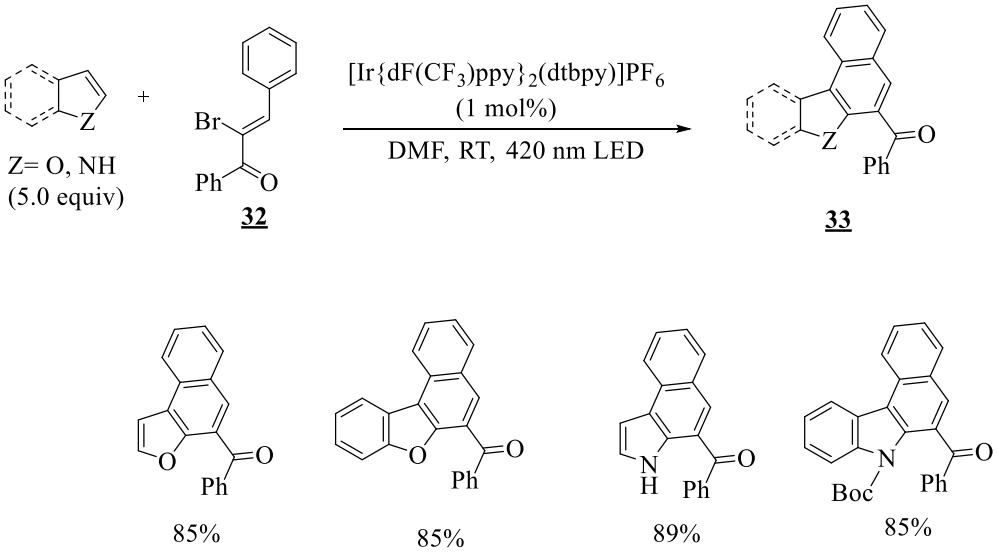

Scheme 2.22. Furan, benzofuran, pyrrole and *N*-Boc-indole reaction with α-bromochalcone

The employment of diaryliodonium salts as π-extending agents in the APEX reaction with *N*-substituted and unsubstituted indoles yielded corresponding dibenzocarbazoles in a one step reaction [75]. This double *C-H* arylation is catalyzed by palladium acetate. Most probably, the pathway of this reaction proceeds through a) electrophilic palladation to form intermediate, b) formation of palladium(IV) derivative by oxidative addition of diarylindonium salt to palladium, and c) reductive elimination and intramolecular *C-H* arylation.

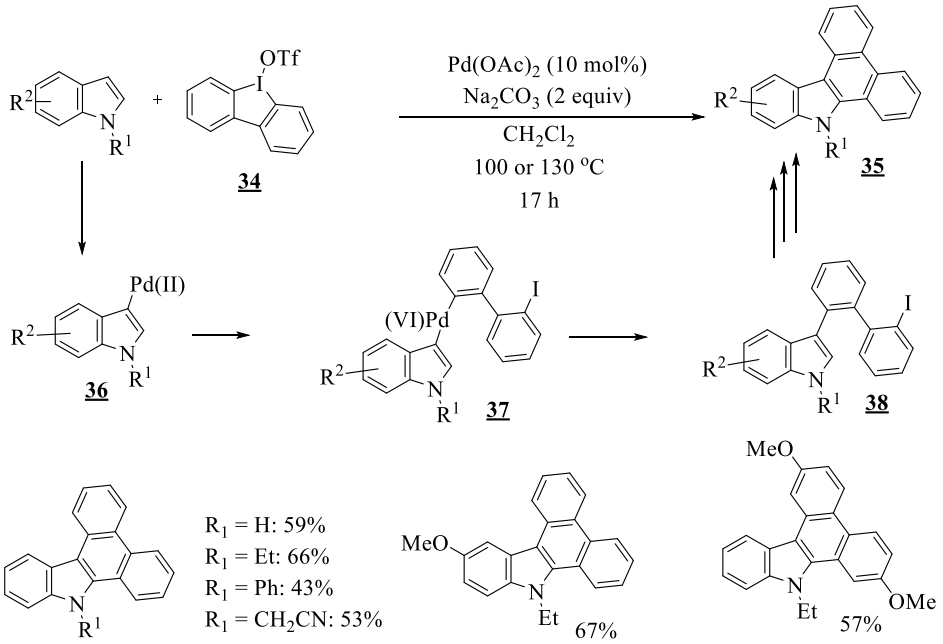

Scheme 2.23. Palladium-catalyzed indole-to-carbazole reaction through diaryliodonium salts

Palladium(II)-catalyzed dual *C–H* functionalization of indoles with cyclic diaryliodoniums was successfully achieved, providing a concise method to synthesize dibenzocarbazoles [76]. In a single operation, two *C–C* bonds and one ring were formed. The reaction was ligand free and tolerated air and moisture conditions. Close to this method, Itami, Ito *et al*, have reported synthesis of various heteroarenes, basically thiophenes, proceeded by a palladium catalyzed APEX reaction.

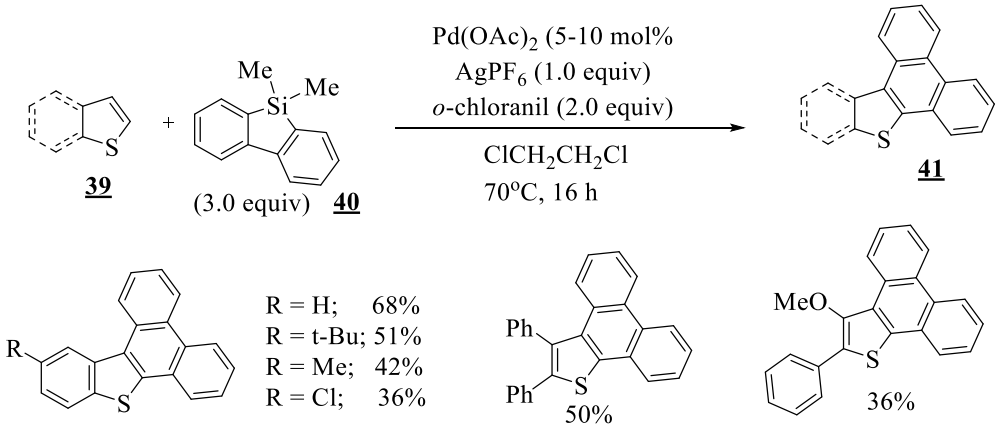

Scheme 2.24. Palladium/silver catalyzed reaction of tiophenes, *N*-tosylindole, and benzofuran with dibenzosilole

In this case, dibenzosilole derivative played the role of the π-extending fragment in the palladium/*o*-chloranil catalytic system. Following this method, a series of fused π-extended thiophenes in moderated yields were synthesized. The mentioned conditions are acceptable to the *N*-tosylindole and benzofuran reaction with dibenzogermole as an alternative agent to improve conjugation and yield dibenzocarbazole, and benzonaphthofuran, respectively.

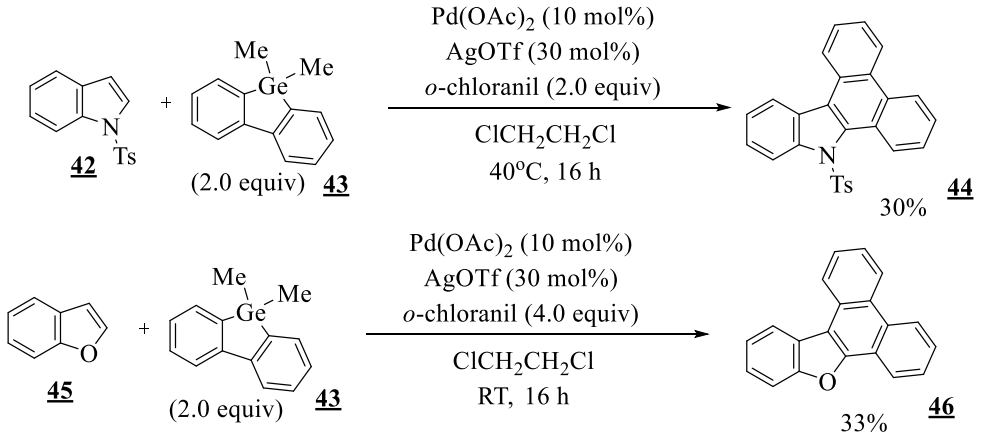

Scheme 2.25. Palladium/silver catalyzed reaction of tiophenes, *N*-tosylindole, and benzofuran with dibenzogermole

Palladium(II)-catalyzed dual *C–H* functionalization of indoles with cyclic diaryliodoniums was successfully achieved, providing a concise method to synthesize dibenzocarbazoles. In a single operation, two *C–C* bonds and one ring were formed. The reaction was ligand free and tolerated air and moisture conditions [77].

2.2.2. Nucleofilic addition and aromatization cascade

Another type of nucleophilic addition – benzannulation - was first reported in 1954 by Dann *et al* [78]. This nucleophilic addition reaction of heteroarenes with carbonyl compounds was found by the synthesis of pharmaceutical 1,3,4,7-tetramethylbenzo[*c*]thiophene from 2,5-hexanedione and 2,5-dimethylthiophene. In the case of aqueous hydrofluoric acid catalysis, dehydrative aromatization follows electrophilic addition in *C3*- and *C4*- positions of thiophene.

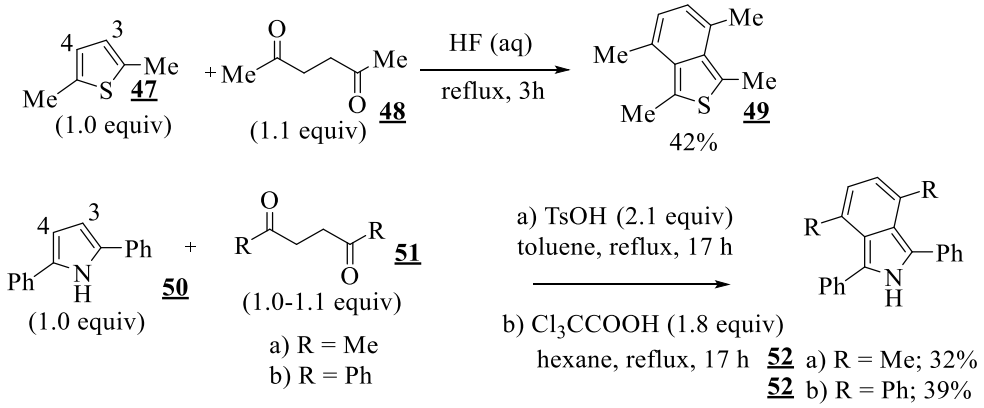

Scheme 2.26. Nucleophilic-addition reactions of 2,5-disubstituted thiophene and pyrrole under acidic conditions

In the next decade, Fletcher reported on 4,7-dimethyl-1,3-diphenylisoindole and 1,3,4,7-tetraphenylisoindole transformation from 2,5-diphenylpyrrole through the use of 2,5-hexanedione and 1,4-diphenyl-1,4-butanedione in an acidic environment (in the presence of toluenesulfonic acid (TsOH) or trichloroacetic acid) [79]. Depending on the substituents in the starting π-extending dione, reaction yields reach 32% (R=methyl) and 39% (R=phenyl).

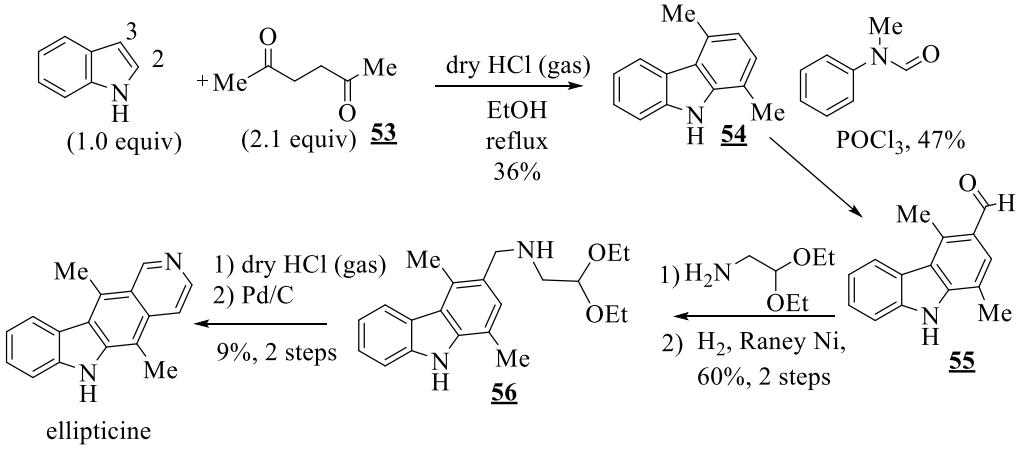

Scheme 2.27. Ellipticine synthesis from indole following APEX reaction

Dry hydrogen chloride was used as the catalyst in the nucleophilic addition of 2,5-hexanedione to the indole to provide 1,4-dimethylcarbazole in a 36% yield. Corresponding carbazole allowed the synthesis of the naturally occurring element in *Aspidosperma subincanum* plants in creating alkaloid ellipticine [80]. The low yield and undesirable conditions, as the gas state HCl, inspired Torok and co-workers to try montmorillonite *K*-10 as a strong acid catalyst during solvent-free microwave irradiation of pyrroles and indoles with 2,5-hexanedione [81].

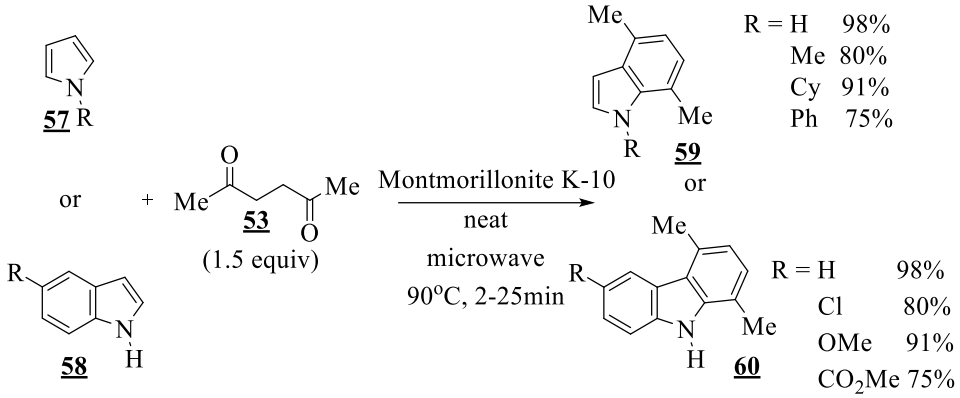

Scheme 2.28. Microwave-initiated pyrroles and indoles reaction with 2,5-hexadione

This improvement of reaction allowed a one step synthesis of different 4,7-dimethylindoles and 1,4-dimethylcarbazoles in good-to-excellent yields (75-98%). The same conditions were tried with indole and 2,5-hexanediol instead of diketone. Unfortunately, this reaction required a longer time (0.5h-1h) and a higher temperature (160°C) but gained lower yields [82].

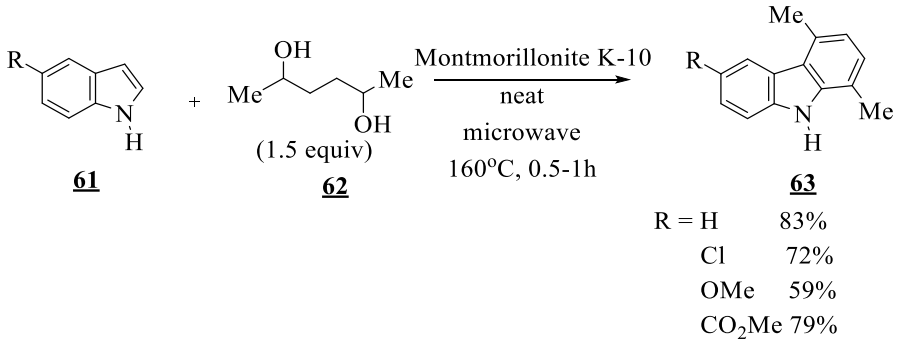

Scheme 2.29. Microwave-initiated indoles reaction with 2,5-hexadione using montmorillonite as catalyst

Both the cycloalkylation of amines and annelation of pyrroles and indoles have been completed within minutes, with practically 100 % selectivity. Most probably, the mechanism of this reaction could be explained by the acid promoted electrophilic substitution of the indole with diol and aerobic oxidation forming unsaturated ring.

APEX reactions of indoles in the presence of TfOH may yield carbazoles with free *NH* groups. For example, the indole reaction with *γ*-carbonyl *tert*-butylperoxide provide 1,2-disubstituted carbazoles with active *NH* group. The synthetic utility of this method is demonstrated by concise and selective total syntheses of naturally occurring carbazole alkaloids, olivacine, and asteropusazole *A*. In the case of *N*-methyl substituted starting indole, regioisomer was observed [83].

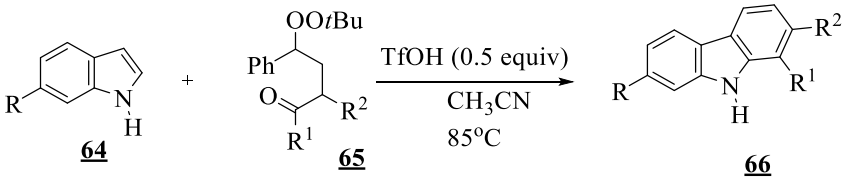

R= H, R_1=Me, R_2=CO_2Et 51%
R= Br, R_1=(3,4-dimethoxy)Ph, R_2=CO_2Me 66%

Scheme 2.30. Triflic acid-promoted *NH*-free indole-to-carbazole APEX reaction. Products are the preursosrs of olivacine and asteropusazole A

Tetrahydropyridine-based compounds have been developed as the *π*-extending reagents. For example, in the presence of acetic acid, *NH*-free indole was used in an APEX reaction and 2-(2-aminoethyl)indoles were observed [84].

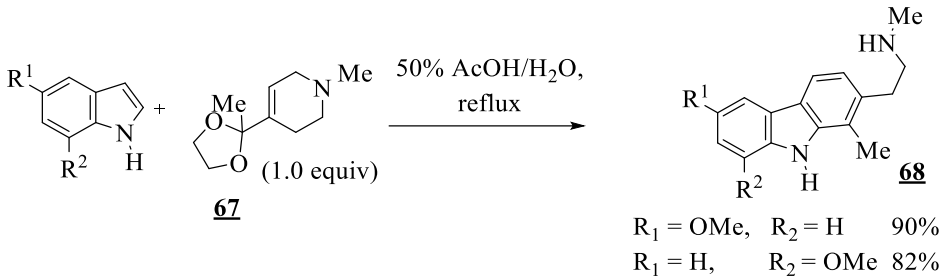

Scheme 2.31. Acetic acid promoted indoles reaction with tetrahydropyridine

To extend the π-electron system with more than one benzene ring, the Brønsted acid catalyzed naphthoannulations of indoles were tested with *ortho*-[α-(hydroxy)benzyl]benzaldehyde acetals [85]. In addition, heteroatoms bearing conjugated rings, as benzothiophene was added to the starting indole. Suarez *et al.* suggested APEX reactions proceeds through a sequence of Friedel–Crafts reactions and aromatization. Highly selective migration processes are key steps in the overall cascade sequence that involves the one-pot formation of two new bonds and a cycle in a regioselective fashion.

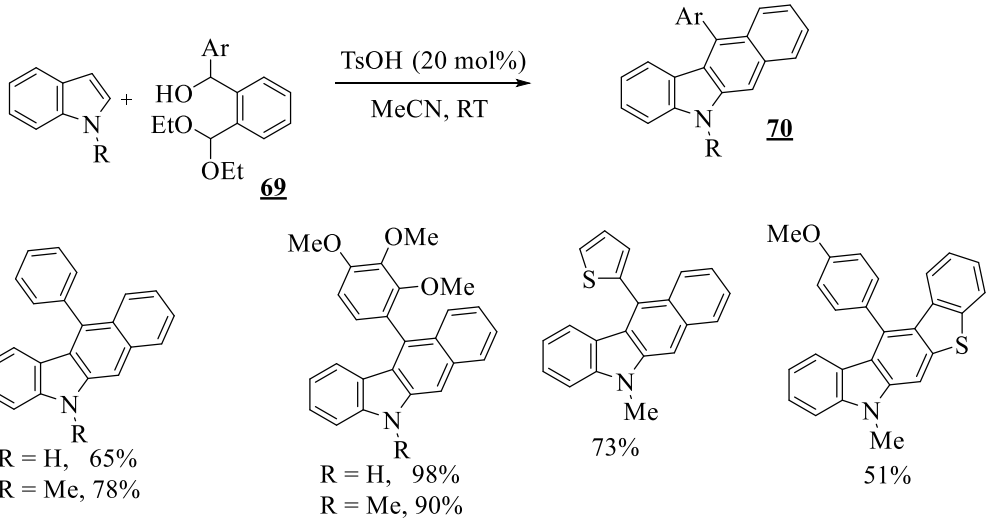

Scheme 2.32. Brønsted acid catalyzed benzo- and naphtilannulation reactions of indoles with aromatic acetals

Indolo[3,2-*b*]carbazole was obtained in a one-pot synthesis using indole and isobutylaldehyde APEX reaction under reflux in a sulphuric acid/methanol solution [86]. Most notably, 5,11-dihydroindolo[3,2-*b*]carbazole-6,12-dicarbaldehyde has been synthesized, whereby a previously assigned structure has been confirmed. This compound is an extremely efficient ligand for the TCDD (Ah) receptor.

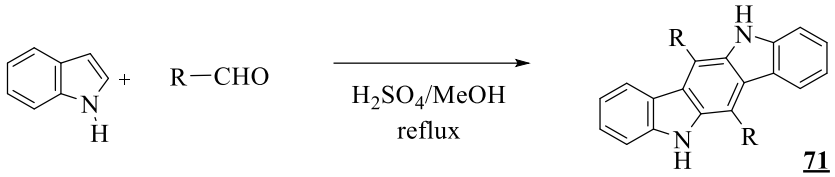

R = Ph 37%
R = *i*-Pr 80%
R = *n*-Bu 72%

Scheme 2.33. Synthesis of indolo[3,2-b]carbazoles from indole and aldehydes

To archieve compound with additional electron-donating (4-diphenylamino)phenyl rings, Jiang and co-workers used the same reaction conditions. Two triphenylamine-substituted indolo[3,2-*b*]carbazole compounds, 2,8-bis(4-diphenylaminophenyl)-5,11-di-*n*-octylindolo[3,2-*b*]carbazole and 6,12-bis(4-diphenylaminophenyl)-5,11-di-*n*-octylindolo[3,2-*b*]carbazole, have been designed and synthesized as hole transporting materials. The theoretical and experimental studies show that the difference of the substituted positions has great effects on the optical and electrochemical properties. Hole drift mobility results indicate that indolo[3,2-*b*]carbazole compound with 6,12-disubstituted by triphenylamine possess a better hole transporting performance than the 2,8-disubstituted one [87].

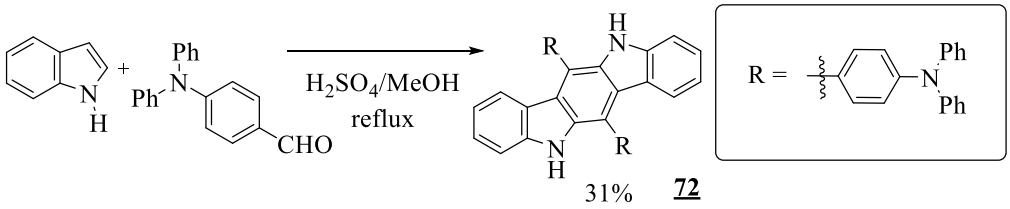

Scheme 2.34. Synthesis of indolo[3,2-*b*]carbazoles from indole and aromatic aldehyde

As described above, indolo[3,2-*b*]carbazole, its regioisomer indolo[2,3-*b*]carbazole can be obtained *via* APEX reactions from indole and relevant aldehydes, depending on the preferred product [88]. Novel annulated pyrido[2,3-*d*]pyrimidines were synthesized stereoselectively by intramolecular hetero Diels–Alder reactions involving 1-oxa-1,3-butadienes. Instead of strong acidic conditions in previous cases, Bhuyan and co-workers reached yields of up to 85% by iodine catalysis in acetonitrile.

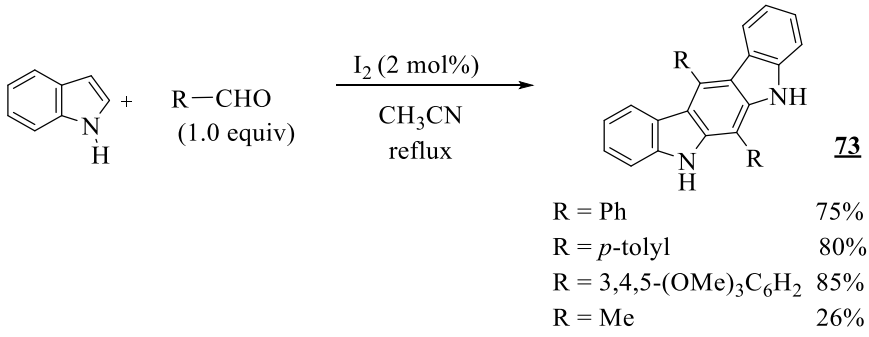

Scheme 2.35. Synthesis of indolo[2,3-*b*]carbazoles from indole and aldehydes using molecular iodine

The synthesis may be explained by the Friedel-Crafts reaction process between the aldehyde and *C*-3 positions of two indoles with following dehydration, second step of reaction is Friedel/Crafts reaction with one more dehydration, catalyzed by molecular iodine yielding dehydroindolo[2,3-*b*] carbazole. The final product indolo[2,3-*b*]carbazole is received after aromatization. This reaction, which can also be investigated for the synthesis of many other heterocyclic compounds of biological importance, is a valuable addition to the chemistry of uracils.

Other isomers of indolo [3,2-*a*]carbazole, as homodimeric 7-phenylindolo[3,2-*a*]carbazole, were synthesized by the Cachet group using six steps of a one-pot reaction from indole and *β*-nitrostyrenes, in the presence of $SnCl_2 \cdot 2H_2O$ [89].

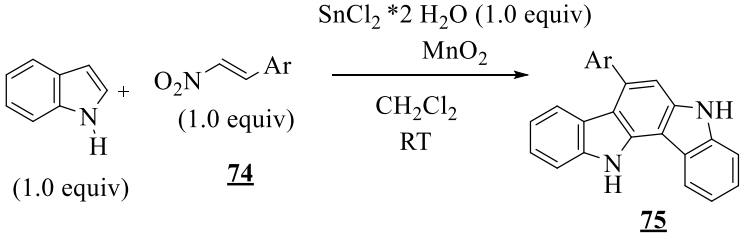

Scheme 2.36. Synthesis of 7-arylindolo[3,2-*b*]carbazoles by tin and manganese catalysis

In this case, the first step of reaction is dimerization of the indole in to the indole dimer under very mild conditions, followed by the Michael addition, where it is transformed to alkenyl indole, and after his the heterogenous oxidation tranfers to the 6*π*-electron system. The electrocyclic closure though denitration and aromatization of previously mentioned molecule proceeds to give the indolo[3,2-*a*]carbazole. An unprecedented mechanism involving sequential indole dimerization, regioselective nucleophilic conjugate addition of the resulting 2,3′-biindole to *β*-nitrostyrene and formal intramolecular [4 +2]-cycloaddition was proposed.

Mohanakrishnan and co-workers paid a lot of attention to domino APEX reactions with diacetoxyacetal-functionalized indolylmethyl bromide using Lewis acids, for example, $ZnBr_2$ [90, 91]. This three-steps one-pot transformation proceeds by sequential Lewis acid catalysed Friedel–Crafts alkylation, electrocyclization and aromatization reactions. The strategy is highly efficient for the assembly of complex

aryl/heteroaryl-fused carbazoles. APEX process yielded indole, thiophene and furan derivatives with π-extended heteroarenes in high yields. A $ZnBr_2$ mediated arylation of aryl/heteroaryl methyl bromides with arenes at 80 °C led to the formation of arylated products, which underwent subsequent 1,5-sigmatropic rearrangement followed by electrocyclization and aromatization with loss of a diethylmalonate unit to afford the corresponding annulated products.

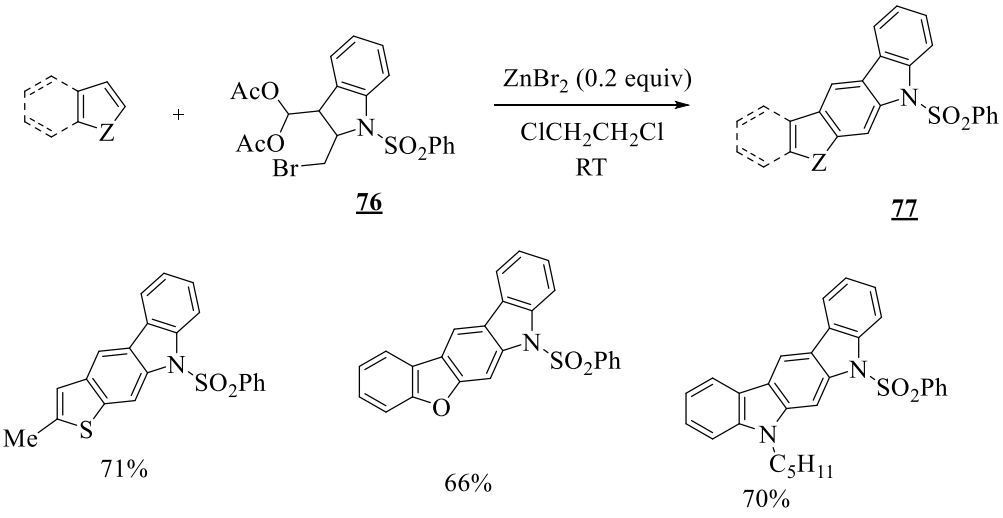

Scheme 2.37. Zinc(II) catalyzed APEX reaction of heteroarenes with π-extending agent

The next step of the Mohanakrishnan group was the synthesis of naphtha-annulation products from phtalaldehyde-derived tetraacetate catalyzed by $BF_3 \cdot Et_2O$ [92]. The reaction of the tetraacetates with arenes and heteroarenes leads to the formation of 1,1-bis-arylated diacetates upon elimination, followed by electrocyclohetero-arylated intermediate may lead to the formation of bis-arylated 1,1-diacetates, which on cyclization is followed by aromatization furnish annulated heterocycles.

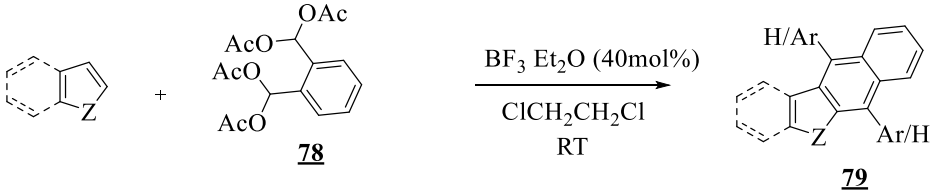

Scheme 2.38. Naphtannulative APEX reaction of heteroarenes and tetraacetoxyxylene

Fused aromatic rings with different heteroatom were synthesized by benzaannulative reactions from electron-rich heteroarenes. For example, 2,5-dimethyltetrahydrofuran was tested as the π-extending agent in reaction with *S*, *Se*, and *O* heteroatoms bearing heterocycles [93]. These one-pot reactions were catalyzed by TfOH or $ZnBr_2$ and similar conditions were used for benzene-to-antracene reactions from 1,2-dimethoxybenzene. A facile preparation of benz-

annulated heterocycles were achieved at RT involving a Lewis acid/Brønsted acid mediated annulation of heterocycles using 2,5-dimethoxytetrahydrofuran as a four-carbon synthon. The benz-/naphth-annulation was found to be successful with electron-rich arenes as well.

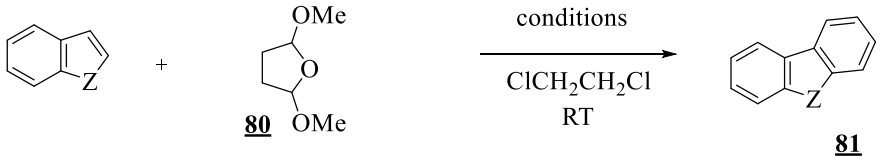

80 **81**

	Condition a	Condition b	Condition c
Z= S	88%	87%	-
Z= Se	83%	81%	-
Z= O	81%	35%	76%

Condition a: 2,5-dimethxytetrahydofuran (2.0 equiv) and ZnBr2 (1.0 equiv)
Condition b: 2,5-dimethxytetrahydofuran (2.2 equiv) and TfOH (1.0 equiv)
Condition c: 2,5-dimethxytetrahydofuran (4.4 equiv) and TfOH (2.0 equiv)

Scheme 2.39. Benzannulative APEX reaction of benzoheteroles and dimethoxyfuran

2.2.3. [4+2] cycloaddition and aromatization cascades

The [4+2] cycloaddition is a widely used method for obtaining six-membered aromatic compounds. 4,5-dicyanopyridazine as the electron-deficient diene was tested in the Diels-Alder reaction with both indole and *N*-substituted pyrrole, and 2,3-dicyanocarbazole and 5,6-dicyano-*N*-methylindole were obtained with outgoing H_2 and N_2 gas. These simple examples demonstrates that cycloaddition is a good method of obtaining indoles from pyrroles and carbazoles from indoles without metal-bearing catalysis [94].

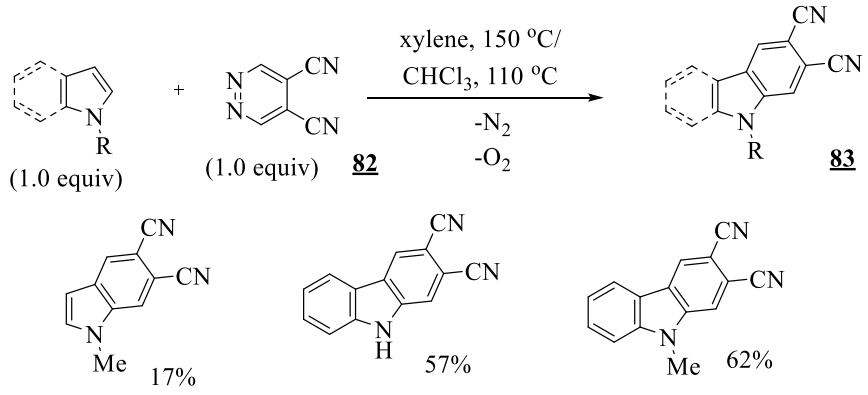

82 **83**

Scheme 2.40. Inverse-electron-demand Diels-Alder cycloaddition of pyrrole and indoles with dicyanopyrridazine

In 1987, Prota and colleagues reported the APEX reaction by a cascade of Michael addition and [4+2] cycloaddition [95]. By acetic acid catalysed reaction, seven fused rings bearing compound was obtained from 5,6-dihydro-*N*-methylindole and 1,4-naphtochinone. The Menéndez group tested a similar reaction with 2,5,8-

quinolinetriones in an ethanol/HCl solution and heptacyclic reaction products arising from a cascade of two regioselective Michael addition–Diels–Alder cycloaddition steps were obtained [96-97]. In another approach to polyheterocyclic quinone systems, double Diels–Alder reactions between indolylquinolinetriones and 2,5- or 2,6-dihalogenated benzoquinones provided a regioisomeric 11-cycle products in good yields.

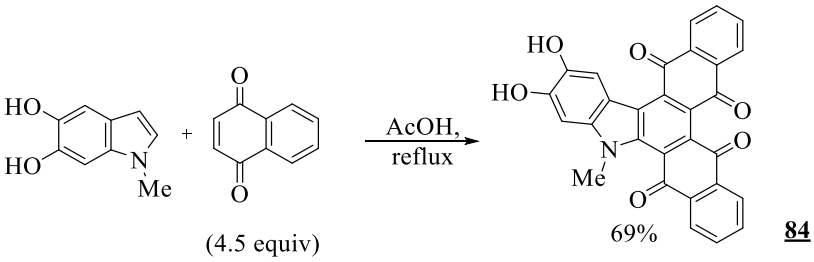

Scheme 2.41. Naphtoquinone cycloaddition to indole by Michael addition procedure

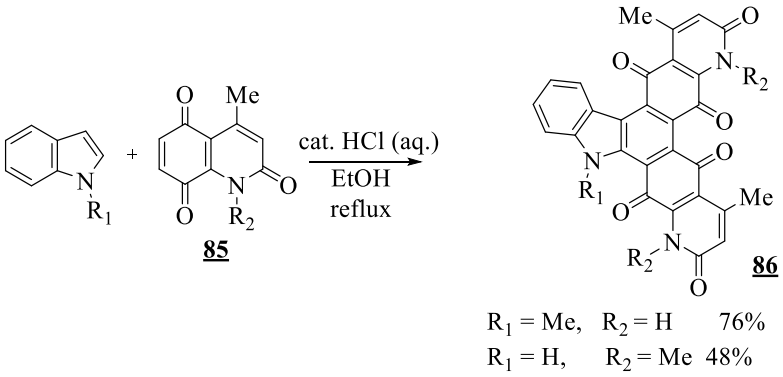

Scheme 2.42. 2,5,8-quinolinetrione cycloaddition to indole by Michael addition procedure

Copper(II) triflate catalyzed heteroannulation has been employed for the construction of 5*H*-benzo[*b*]-, carbazolo[2,3-*b*] and indolo[2,3:*b*]carbazole derivatives [98].

2.3. Conclusions

As the new technologies requires effective organic materials, the research on π-conjugation extending is still on going. The main annulative π-extension methods enable rapid access to fused arenes and heteroarenes, otherwise synthesized by classical multistep operations. This synthetical method has great potential in nanocarbon science. In addition, this method is very useful in synthesis of fused heterocycles. Three representative APEX reactions of unfunctionalized heteroarenes were reviewed, such as a) transition metal-catalyzed *C-H* functionalization, b) nucleophilic addition and aromatization cascades, and c) [4+2] cycloaddition and aromatization cascades. The simple five-membered heterocycles, such as pyrrole, thiophene, furan, were found to be perfect templates that leads to the generation of

higher molecular weight heterocycles, for example, carbazole, dibenzothiophene, dibenzofuran.

Transition-metal-catalyzed *C-H* functionalization in heteroarenes is very important in todays synthesis, because it enables a number of one step reactions instead of different long multistep synthesis with lower yields. The series of precious metals, such as copper, palladium, rhodium, gold, ruthenium and iridium are effective in catalysis for various π-extending reagents, for example alkene, alkyne or diazo compounds.

The acidic environment in nucleofilic addition and aromatization cascade type reactions assists in the creation of the full spectrum of fused heterocycled molecules. In the case of the reviewed literature, different conditions were used, such as microwave reactor, dry hydrochloride gas, varied temperatures. The quality of this method is selectivity and it benefits in pharmaceutical chemistry, where synthesis of compounds found in nature plays an important role. A volume of carbazoles or indolocarbazoles with specific relevant elements of substituents addition were found after this method in one-pot reactions.

Due to the high nucleophilicity of heteroarenes, a variety of electrophilic π-extending reagents, such as aldehydes, acetals, and alkyl bromides, react with them easily in the presence of Brønsted or Lewis basis. The main advantage of the [4+2] cycloaddition is simplicity of reaction. The minimum of reagents and waste makes this method promising for experiments in both a laboratory and at an industrial scale.

After the short view to these methods, it is clear, that single step synthesis is user-friendly and very attractive for both the economical and time aspects. Of course, the research for new synthetical routes of π-extending groups bearing compounds is still not finished, because of the lack in both the catalysts and the π-extending groups variety. Additionally, these reactions are tested mostly with just pyrroles and indoles. The development of a new one step synthesis method to extend the conjugated systems of different arenes and heteroarenes may provide rapid reactions yielding π-extended molecules with the desired substitution.

3. RESULTS AND DISCUCCIONS

3.1. Carbazole-based hole transporting materials with π-conjugation extended *via* phenylethenyl moieties

Intensive development in the field of various electronic and optoelectronic devices requires efficient materials suitable for such applications. Organic materials in this area are advantageous and receive attention because they allow the construction of flexible, thin-film capable, large-area, light weight and potentially low cost devices. Among such organic materials, carbazole-based derivatives are attractive and widely used for optoelectronic and electronic applications because of their facile chemical functionalization, high thermal stability, film-forming ability and electron-donating properties enabling hole transporting mobility [99]. Compounds possessing carbazole moieties are important hole transporting materials (HTM) in various types of organic solar cells [100]. Wu *et al*. [101] reported on the

perovskite solar cell (PSC) with HTM based on carbazole, with power conversion efficiency (PCE) exceeding 12 %. Recently, a new HTM (*V886*) was reported, based on methoxydiphenylamine-substituted carbazole. The perovskite device with *V886* shows a maximum PCE of 16.9% under AM1.5G illumination, whereas PCE values exceeding 14% are routinely observed [102]. The simple two-step synthesis made this HTM very appealing for the commercial prospects of PSCs. Carbazole-based derivatives, such as 2,7-carbazole, indolo[3,2-*b*]carbazole containing donors coupled with various acceptors, namely, benzothiadiazole, thiazolothiazole, diketopyrrolopyrrole, quinoxaline and fullerene, show interesting properties in the bulk heterojunction organic or dye-sensitized solar cells, and also in PSC devices [100, 103]. Carbazole-based donor-acceptor polymers, exhibiting excellent thermal and air stability have also been successfully applied in photovoltaic devices [104]. Such materials possessing bipolar charge-transport properties are currently of great interest, due to the demonstrated enhanced stability and performance [105, 106]. Besides, the use of such materials would allow the construction of efficient single-layer OLEDs that are attractive to industrial applications because of the simpler manufacturing and lower production costs [107, 108].

Materials with pendant carbazole moieties are also promising candidates as hosts in blue, green or red phosphorescent organic light-emitting devices (PhOLEDs), due to their triplet energies, suitable HOMO levels, and outstanding hole-transporting properties [109-111]. Carbazole-based materials that could be used as emitting layers in non-doped blue OLEDs have also been reported [112-115]. As 3,6-position and *N* atom can be easily functionalized or covalently linked to other molecules, carbazole offers wide possibilities for tuning the properties (such as charge carrier mobility, ionization potential, film-forming, glass transition temperature *etc*.) of the synthesized derivatives. There are many possibilities for the enhancement of its π-conjugated systems by 2,7- or 3,6- linking of carbazole molecules into dimers, trimers or oligomers [116, 117] utilizing Suzuki or Yamamoto cross-coupling, Wittig or Knoevenagel condensation, or Heck reaction; also by adding diarylamino [10, 118, 119] (usually applying Buchwald-Hartwig reaction) or hydrazone [120-122] fragments. The synthesis of the latter compounds generally includes the steps of Vilsmeier reaction and then interaction of the obtained formyl derivatives with various hydrazines.

3.1.1. Monomeric carbazole-based hole transporting materials with π conjugation extended *via* 3 and 6 positions

Bubniene and coworkers have reported on the synthesis, thermal, optical, electrochemical, and photophysical properties of β,β-disubstituted 1,3-divinyl carbazole derivatives that were obtained by condensation of 2-hydroxycarbazole and diphenylacetaldehyde [123]. However, the change of the synthesis sequence (*i.e.*, substitution at the hydroxyl and *NH* groups, followed by the condensation reaction) resulted in the corresponding 3,6-divinylcarbazoles. Commercial availability and relative cheapness of the starting materials, simple synthetic method, number of sites available for easy functionalization and covalent linking to other molecules, glass-forming properties, good charge drift mobility, and solubility in common organic

solvents makes these precursors attractive building blocks for the construction of more complex materials for optoelectronic applications [124, 125].These findings and the potential of such carbazole-based compounds encourage their further synthesis and investigation. This part of the doctoral thesis describes the synthesis and properties of a novel series of carbazole derivatives with extended conjugation bearing different peripheral diarylethenyl moieties, *i.e*. diphenylethenyl and bis(4-methoxyphenyl)ethenyl fragments. This is the first report dealing with the interaction of diphenylacetaldehyde and its dimethoxy analogue with *C*-unsubstituted carbazole derivatives.

3.1.1.1. Synthesis of novel carbazole derivatives

The reported compounds were obtained by the condensation of *N*-substituted carbazoles with relevant acetaldehyde in toluene (Dean–Stark trap was used to remove water generated in the course of the reaction according to the procedure described in [126]). The reaction mixture was heated at reflux in the presence of (±)-camphor-10-sulfonic acid (CSA) (Scheme 3.1.) for 1.5-17 h to afford the target compound series **1-6a** and **1-3,7b** in 25-72% yields. It was observed that the presence of *p*-methoxy groups in phenyl fragments of the aldehyde resulted in longer reaction times and lower yields of the target products **1-3b** and **7b**. The synthesized compounds are soluble in common organic solvents, such as toluene, chloroform, tetrahydrofuran or 1,4-dioxane, which makes them suitable for solution processing.

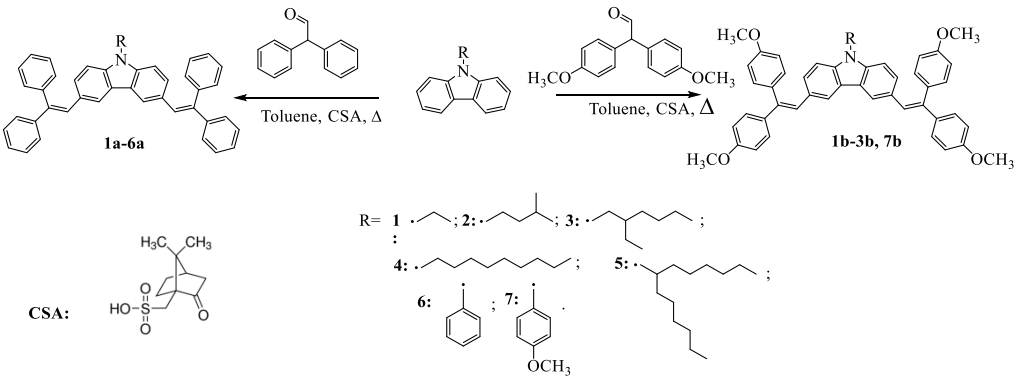

Scheme 3.1. Synthesis of novel compounds bearing diphenylethenyl fragments

The structure of novel compounds was confirmed by the data of ^{1}H and ^{13}C NMR spectra, mass spectroscopy, and elemental analysis.

The formation of 3,6-disubstituted compounds could be explained by the reaction mechanism presented in Scheme 3.2.

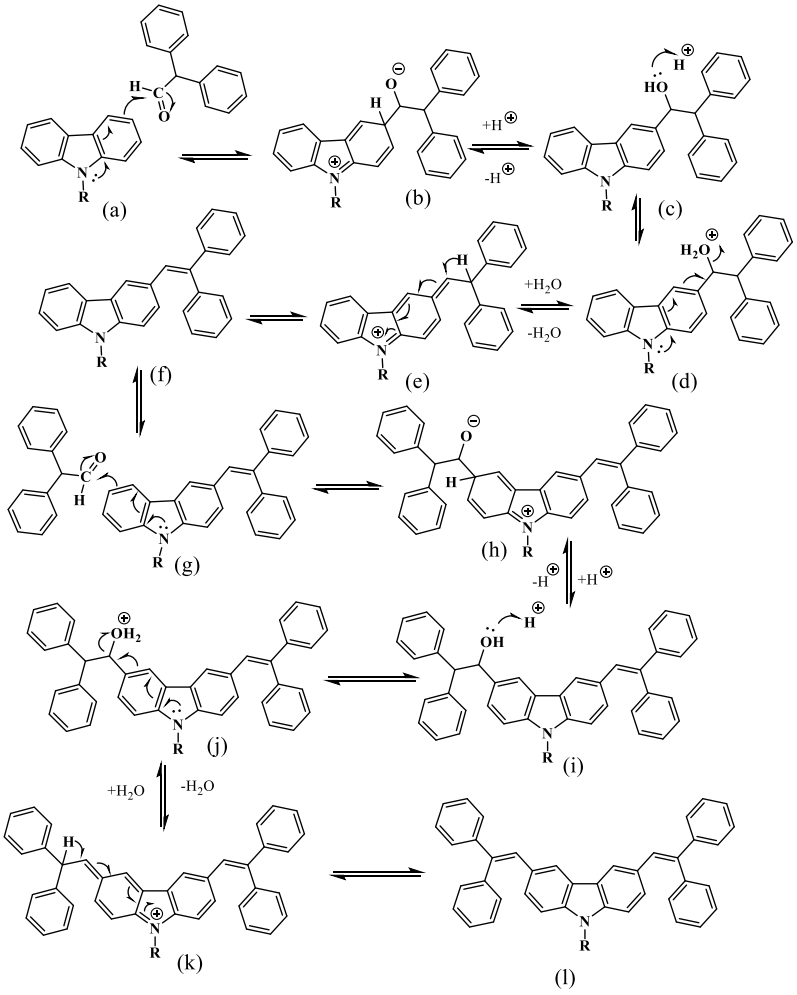

Scheme 3.2. Suggested reaction mechanism of *N*-substituted carbazole condensation with diphenylacetaldehyde

Most probably, delocalization of the electron pair pushes electrons from the nitrogen atom into the carbazole ring and the heterocycle becomes electron-rich at *3*- and *6*-positions, thus these positions are more susceptible to the electrophilic attack. During the electrophilic substitution, a σ bond is formed between diphenylacetaldehyde and 9-substituted carbazole (a), the carbonyl π bond becomes polarized forming an oxyanion and an iminium cation (b) is created. This is followed by a loss of a proton at 3-position of the carbazole ring, and acceptance of the proton by the former oxyanion to form the hydroxyl group (c). Protonation of the hydroxyl group (d) and subsequent loss of water by elimination (e) followed by the loss of a proton leads to the formation of the mono substituted compound (f). Reaction to the 6-position proceeds by the same route yielding the final product (l).

3.1.1.2. Thermal properties

Successful application of hole transporting materials in devices requires formation of homogeneous and thermal resistant layers. Knowledge about material crystallinity and glass-transition temperature is important, therefore thermal measurements were performed for the estimation of possible application of the synthesized carbazoles in charge transporting layers. Thermal characteristics of the reported compounds were investigated by differential scanning calorimetry (DSC).

Table 3.1. Thermal properties of 3,6-diphenylethenyl *N*-substituted carbazoles

Compound	**1a**	**1b**	**2a**	**2b**	**3a**	**3b**	**4a**	**5a**	**6a**	**7b**
T_g (°C)	74	94	50	72	38	56	41	43	99	82
T_m (°C)	176;184	-	-	-	-	-	100	60	205	-

Results, presented in Table 1, confirmed the glassy state of compound **1a** at 74°C. In the thermogram of the first heating, crystalline form and polymorphism are observed (*i.e.* compound melts at 176 °C and 184°C).

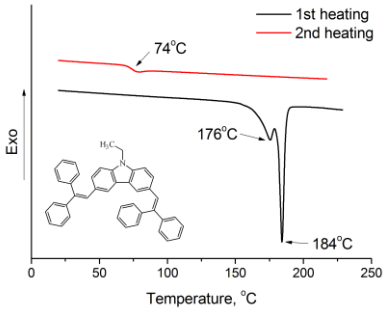

Figure 3. 1. Thermograms of compound **1a**

The extension of the aliphatic chain reduced both the glass transition temperature (T_g) and the tendency to crystallize, and only the glass transition was registered for compounds **2a** and **3a** (Figure 2a and 3a).

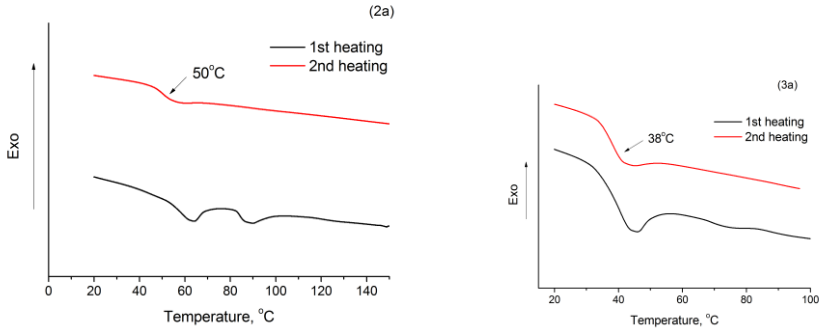

Figure 3.2. Thermograms of compounds **2a** and **3a.**

However, the further enlargement of alkyl fragment resulted in both glass transition and melting observed for derivatives **4a** and **5a** possessing nonyl and tridecan-7-yl groups, respectively (Table 1).

In spite of similar T_g values of **4a** and **5a**, melting points of these compounds differ by 40°C (100 °C and 60°C, respectively). Melting peak of compound **4a** bearing the *n*-nonyl chain was more intensive compared to that of branched derivative **5a**. This demonstrates that the branched chain reduces both the value of melting point and the possibility to crystallize, as only a small part of material **5a** melted at 60 °C.

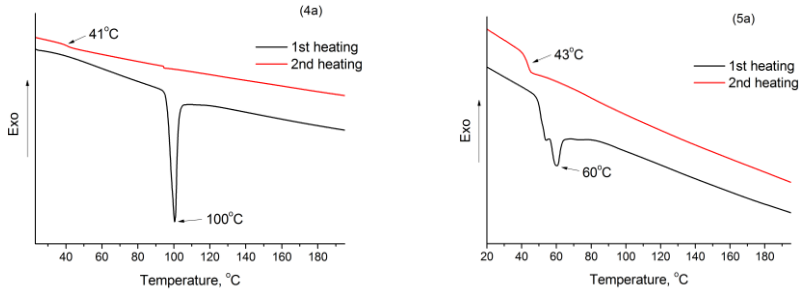

Figure 3.3. DSC thermograms of compounds **4a** and **5a**.

Introduction of methoxy groups in phenylethenyl fragments resulted in 18–24 °C higher T_g. *p*-Methoxy substituents also ensured a stable amorphous state of compound **1b**.

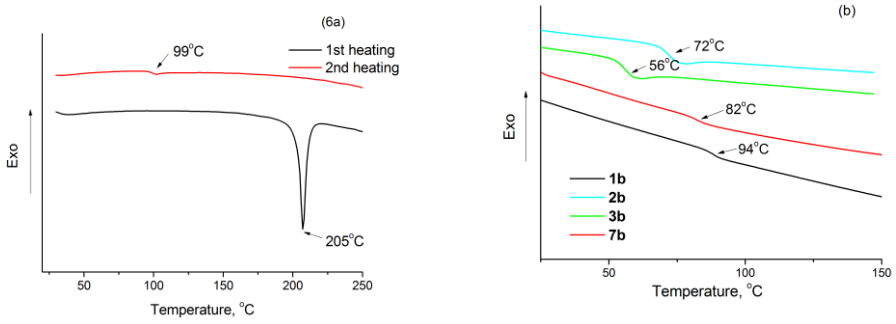

Figure 3.4. Second heating thermograms of compounds **1b-3b, 7b, 6a**.

N-Phenylsubstituent caused higher T_g (99 °C) and increased the tendency to crystalize as compound **6a** melted at 205 °C.

Replacement of *N*-alkyl substituent with phenyl fragment also caused higher T_g (99 °C) and increased the tendency to crystalize, as the compound **6a** melted at 205 °C (Figure 4). Introduction of methoxy groups in all of the benzene rings (**7b**) resulted in lower T_g and the stable amorphous state of this compound (Figure 4).

3.1.1.3. Optical properties

Influence of different *N*-substituents and peripheral *p*-methoxy groups on the optical properties of carbazole compounds was elucidated in different environments, *i.e.* low molar concentration tetrahydrofuran (THF) and toluene solutions, low concentration polystyrene films, and neat films. The absorption spectra of the dilute solutions of the studied compounds are presented in Figure 6a and 6b, whereas the main optical parameters are listed in Table 2. The spectrum of 9-nonylcarbazole (**4**) was added for a comparison.

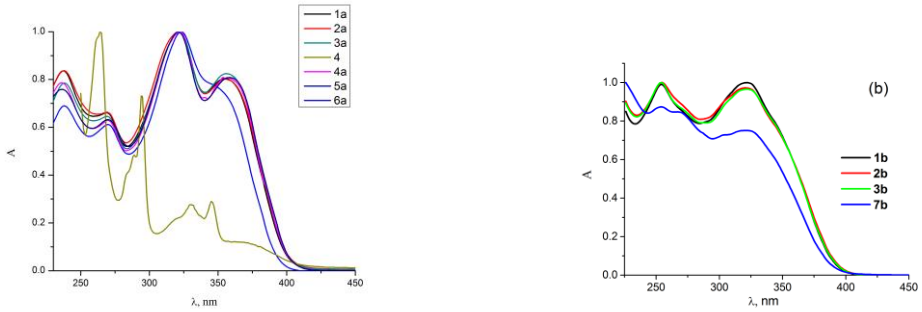

Figure 3.5. Light absorption spectra of 9-nonylcarbazole and 3,6-diphenylethenylsubstituted carbazoles **1a-6a**, **1b-3b**, **7b**

The absorption spectra of 3,6-diphenyl substituted compounds **1-6a** are batochromically and hyperchromically shifted with respect to the spectrum of 3,6-unsubstituted compound **4**. All the compounds with diphenylethenyl groups **1-6a** (as well as derivatives with bis(4-methoxyphenylethenyl groups **1-3**,**7b**) exhibit a similar absorption spectra with maxima peaking at about 235 nm, 270 nm, 322 nm, and 355 nm and corresponding to π-π* optical transitions. Such a great similarity of the spectra indicates that *N*-substituents (mostly alkyls) have negligible impact on the molecule's conjugation length. Even in the case of phenyl or *p*-methoxy phenyl substituents (compounds **6a** and **7b**, respectively) the spectral differences are minor due to the steric hindrance-induced severe twisting of the substituents, which strongly reduces π-conjugation.

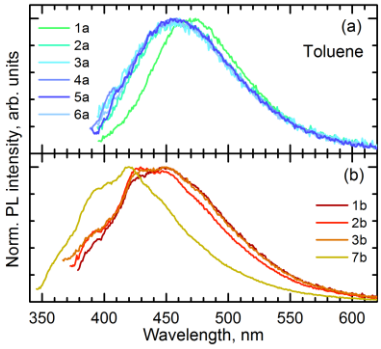

Figure 3.6. Fluorescence spectra of carbazole derivatives **1-6a** (**a**) and **1-3, 7b** (**b**) in 10^{-5} M toluene solutions

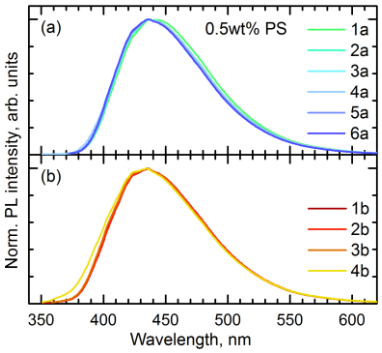

Figure 3.7. Fluorescence spectra of carbazole derivatives **1-6a** (**a**) and **1-3**, **7b** (**b**), dispersed in PS matrix at the 0.5 wt% concentration

Similarly to *N*-substituents, peripheral *p*-methoxy groups have a minor impact on the conjugation of carbazole derivatives, although a slight lowering in absorption intensity of the lowest transitions is observed (Figure 7b). Due to the effect of *p*-methoxy groups on vibrational modes by hampering intramolecular vibrations, intensity redistribution among the vibrational modes diminishes the lowest vibrational peak at 355 nm in the absorption spectra of series **b** compounds as compared to that of series **a** (Figure 7b).

Figure 6 shows the fluorescence spectra of dilute toluene solutions of the series **a** and **b** carbazole compounds. As expected, the series **a** compounds expressed a similar fluorescence spectra in the blue spectral range (peaking at ~457 nm) indicating a negligible role of different *N*-substituents in the emission (Figure 7a). Fluorescence spectra of the series **b** compounds are slightly blueshifted as compared to those of series **a,** due to the polarity changes induced by the presence of peripheral *p*-methoxy groups (Figure 7b). The strongest blueshift of ~30 nm was observed for the compound **7b,** possessing additional *p*-methoxy phenyl group at the *N*-position of the carbazole.

Fluorescence quantum yields (Φ_F) of both series of carbazole derivatives in toluene solutions were estimated to be very low and ranged from 0.1 % to 0.4 %. Such low Φ_F is obviously caused by labile diphenylethenyl substituents, which are known to facilitate intramolecular torsional motions promoting nonradiative deactivation of the excited state [127].

To suppress efficient excited state relaxation *via* intramolecular torsional motions, the investigated compounds were incorporated into a rigid polystyrene (PS) matrix at low concentration (0.5 wt%). The fluorescence spectra of the compounds dispersed in PS films exhibited blue shift ~20 nm (with the maximum at 436 nm) as compared to those in solutions, likely due to the different polarity of the surroundings (Figure 7, Table 2). As expected, the rigid polymer environment strongly suppressed molecular torsions resulting in more than one order of magnitude higher Φ_F in respect to that in solution (Table 2). Φ_F values for the series **a** compounds were found to be in the range of 16 - 22%, whereas for the series **b** compounds containing peripheral *p*-methoxy moieties it ranged from 25 % to 28 % (Table 2).

Table 3.2. Optical properties of monomeric carbazole derivatives

Compound	Absorption	Fluorescence						
	Abs_{max} [a] (nm)	Toluene solution		0.5wt% PS film		Neat film		
		Fl_{max} [b] (nm)	Φ_F (%)	Fl_{max} [b] (nm)	Φ_F (%)	Abs_{max} (nm)	Fl_{max} [b] (nm)	Φ_F (%)
1a	237 269 322 355	471	0.3	437	16	323 361	474	2
1b	254 322	447	0.4	435	26	318	468	5
2a	238 269 322 356	458	0.4	437	16	325 360	470	1
2b	254 321	429 447	0.3	436	28	319	468	3
3a	238 269 323 355	457	0.1	436	17	324 360	470	2
3b	254 322	430 449	0.1	435	25	322	464	7
4a	236 270 322 354	458	0.1	436	22	323 362	463	3
5a	236 270 321 358	458	0.1	436	22	323 361	465	3
6a	238 270 323 350	456	0.1	436	18	236	469	2
7b	254 267 322	420	0.4	435	28	301 314 327	473	1

[a] Measured in 10^{-4} M THF solution. [b] Measured in 10^{-4} M THF solution. Measurements made in Organic optoelectronic research group (leader prof. habil. dr. S. Juršėnas) at the Faculty of Physics of Vilnius University

3.1.1.4. Electrochemical and photoelectrical properties

To reveal the energetic conditions for energy and electron transfer in dilute solutions, the E_{HOMO} and E_{LUMO} values were also estimated from cyclic voltammetry (CV) measurements (Table 3). These values do not represent any absolute solid-state or gas-phase ionization potentials, but can be used to compare different compounds

relative to one another. The cyclic voltammograms of the synthesized compounds in dichloromethane show reversible oxidation and reduction couples (Figure 9).

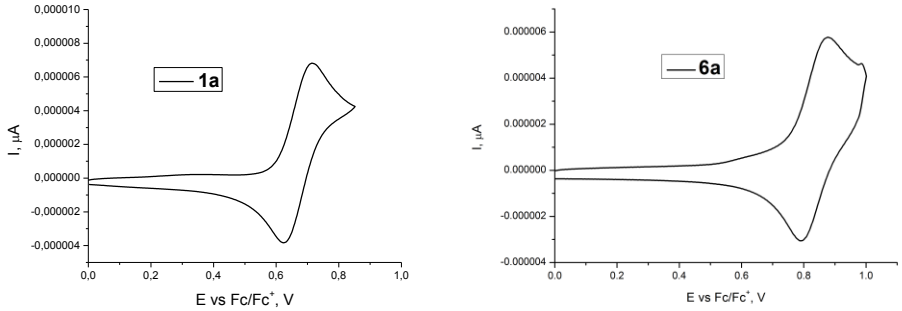

Figure 3.8. Cyclic voltammograms of compounds **1a** and **6a**.

The length of *N*-alkyl substituent did not have a significant influence on energy levels in compounds **1-5a**, though replacement of *N*-alkyl chain with *N*-phenyl fragment resulted in the increase of E_{HOMO} value by ca. 0.10-0.17 V for compound **6a** compared to alkyl analogues. The introduction of methoxy groups in **1-3b** decreased E_{HOMO} by 0.07-0.09 V in comparison to derivatives **1-3a** without methoxy substituents. It was also observed that the additional methoxy fragment in compound **7b** promoted the decrease of E_{HOMO} value by 0.15 V compared to **6a**.

However, solid state ionization potential (I_p) of HTM is an important characteristic when considering the application of such a compound in optoelectronic devices. The ionization potentials of synthesized compounds were measured by the photoelectron spectroscopy in air (*PESA*) method (Figure 10a and 10b) and the results are presented in Table 3. The I_p values of all investigated compounds were quite similar and varied from 5.39 to 5.62 eV.

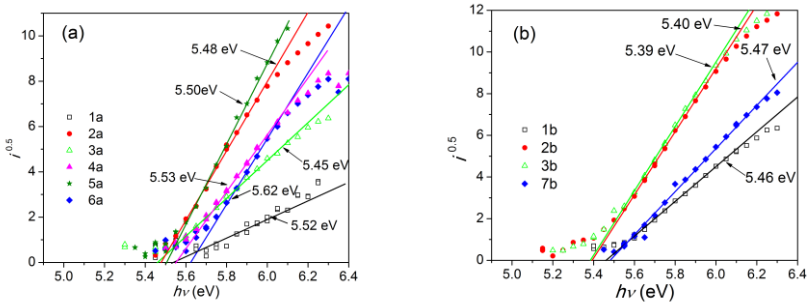

Figure 3.9. I_p of compounds **1-6a** (**a**) and **1-3,7b** (**b**) Measurements were done at the Faculty of Physics, Vilnius University by habil. dr. V. Gaidelis and dr. E. Kamarauskas

Compound **6a** possessing *N*-phenyl fragment demonstrated the highest I_p, showing that *N*-alkyl substituents influenced the decrease of ionization potential. The I_p values of derivatives **1-3b** with bis(4-methoxyphenyl)ethenyl moieties (Figure 10b) were ca. 0.07 eV lower compared to their analogues **1-3a** without

methoxy groups. The introduction of additional *p*-methoxy group in the *N*-benzene ring as well as the replacement of diphenylethenyl fragments with bis(4-methoxyphenyl)ethenyl moieties resulted in a decrease of I_p by 0.15 eV in compound **7b** (5.47 eV) in comparison to 5.62 eV determined for compound **6a**.

To evaluate the charge transport properties of synthesized materials, the hole drift mobility of new carbazole derivatives was measured by the xerographic time of flight (XTOF) technique from the films of neat samples (Figure **8a** and **8b**). The values of the parameters defining charge mobility (zero field mobility μ_0, Poole–Frenkel parameter α and the mobility (μ) at 6.4×10^5 V cm^{-1} electric field strength) are given in Table **3**.

Table 3.3. E_{HOMO}, E_{LUMO}, I_p, band gap energies, and hole mobility data for **a** and **b** compounds[a].

Compound	E_g^{opt} [b] (eV)	E_{HOMO} (V vs Fc+/Fc)	E_{LUMO} [c] (V vs Fc+/Fc)	I_p [d] (eV)	d (μm)	μ_0 [e] ($cm^2V^{-1}s^{-1}$)	μ [f] ($cm^2V^{-1}s^{-1}$)	α ($cm^{1/2}V^{-1/2}$)
1a	3.09	0.39	–2.70	5.52	4.0	2.1×10^{-5}	7.7×10^{-4}	0.0045
2a	3.10	0.37	–2.73	5.48	2.2	1.5×10^{-4}	2.0×10^{-3}	0.0032
3a	3.08	0.38	–2.70	5.45	12.0	6.3×10^{-5}	3.3×10^{-3}	0.0049
4a	3.02	0.32	–2.70	5.53	3.2	8.0×10^{-5}	2.0×10^{-3}	0.004
5a	3.00	0.34	–2.66	5.50	5.3	1.6×10^{-4}	3.6×10^{-3}	0.0039
6a	3.15	0.49	–2.66	5.62	1.5	–	1.4×10^{-3}[g]	–
1b	3.18	0.30	–2.88	5.46	2.0	6.1×10^{-6}	3.3×10^{-4}	0.0050
2b	3.16	0.30	–2.86	5.40	3.0	1.7×10^{-6}	2.1×10^{-4}	0.0060
3b	3.17	0.31	–2.86	5.39	1.5	8.6×10^{-6}	4.1×10^{-4}	0.0048
7b	3.20	0.34	–2.86	5.47	1.1	1.3×10^{-8}	2.7×10^{-6}	0.0067

[a] The CV measurements were carried out at a glassy carbon electrode in dichloromethane solutions containing 0.1 M tetrabutylammonium hexafluorophosphate as electrolyte and $Ag/AgNO_3$ as the reference electrode. Each measurement was calibrated with ferrocene (Fc). Potentials measured vs Fc+/Fc. [b] The optical band gaps E_g^{opt} estimated from the edges of electronic absorption spectra. [c] $E_{LUMO} = E_{HOMO} - E_g^{opt}$. [d] Ionization potential was measured by the photoemission in air method from films. [e] Mobility value at zero field strength. [f] Mobility value at 6.4×10^5 V cm^{-1} field strength. [g] The material was not sufficiently soluble; mobility was measured from vacuum deposited layers using TOF technique; mobility value at 3.6×10^5 V cm^{-1} field strength

The results of hole drift mobility of *N*-alkylated carbazole derivatives have revealed that the introduction of methoxy groups has a negative influence on

mobility values that are much lower at strong electric fields compared to those of the respective compounds without methoxy groups (Table 3). The decrease of μ value in methoxy-substituted carbazole derivatives (series **b** compounds) confirms the reduced intermolecular couping, which is in good agreement with enhanced Φ_F in the neat films of these compounds.

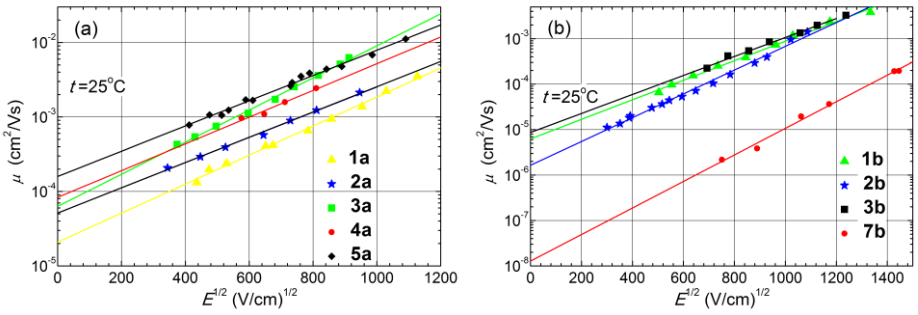

Figure 3.10. Hole drift mobilities of compounds **1**-**5a** (**a**) and **1**-**3,7b** (**b**). Measurements were done at the Department of Solid State Electronics, Vilnius University by dr.V. Jankauskas

Evaluation of the influence of the *N*-aliphatic substituent length (compounds **1**-**5a**) has allowed to state that the extension of the aliphatic chain results in a positive effect on hole drift mobility. Figure 11a illustrates this observation: mobility varies from 3.0×10^{-4} cm^2/V·s in **1a** with ethyl fragment to 3.6×10^{-3} in compound **5a** possessing the branched group. *N*-Phenyl substituted derivative **6a** also demonstrated good charge transport properties, *i.e*. the value of hole drift mobility approached 1.4×10^{-3} cm^2/V·s. However, the introduction of *p*-methoxy group into *N*-substituent had a negative influence on both the compound's film-forming and charge transport properties, resulting in the significant decrease of hole mobility in compound **7b** (2.7×10^{-6} cm^2/V·s at strong electric fields) (Figure 11b). It is possible that the inhomogeneity of the layer significantly affected the results of the mobility measurements.

Summarizing, it can be noted that longer aliphatic chains in *N*-alkylated carbazole derivatives enhance hole drift mobility, likely caused *via* the improved molecular ordering. Replacement of alkyl groups with phenyl fragment (compound **6a**) did not have much influence and the value of mobility was similar to those of alkylated derivatives, while additional *p*-methoxy moiety in the corresponding benzene ring resulted in a significant drop of the mobility. It should be mentioned that ethylhexyl and tridecan-7-yl fragments had a particularly good effect on charge transport of the respective compounds (**3a**, **3b** and **5a**). The reason for this could be that branched chains allow proper arrangement and good packing density of the molecules, thus resulting in a better quality of the prepared layers.

Series of novel carbazole based derivatives bearing diarylethenyl fragments have been synthesized and investigated. Diphenylethenyl-substituted carbazole compounds were found to be poor emitters, both in dilute solutions (Φ_F <0.4%) and

neat films (Φ_F <7%). Low Φ_F in solution was caused by labile diphenylethenyl moieties facilitating intramolecular torsions and torsion-induced nonradiative deactivation. This finding was confirmed by incorporating the compounds in a rigid polymer matrix, which resulted in suppressed torsional motions and enhancement of Φ_F over one order of magnitude. Notably, the neat films of carbazole derivatives wet-casted in ambient conditions exhibited high drift mobilities ($>10^{-3}$ $cm^2 V^{-1} s^{-1}$) at strong electric fields (3.6×10^5 V cm^{-1}). The mobility enhancement was achieved for the compounds containing longer aliphatic *N*-substituents, likely due to improved molecular ordering. The attachment of peripheral *p*-methoxy groups was found to diminish carrier drift mobility, due to reduced intermolecular coupling. Commercial availability and relative cheapness of the starting materials, simple synthetic method, number of sites available for facile functionalization and covalent linking to other molecules, good charge drift mobility, solubility in common organic solvents, and glass-forming properties make these compounds attractive for optoelectronic applications and also promising building blocks for the construction of more complex low-molecular-weight or polymeric materials.

3.1.2. Monomeric carbazole-based hole transporting materials with π-conjugation extended *via* 3,6 and 9 positions

Carbazole-based derivatives are attractive and widely used for optoelectronic and electronic applications because of their facile chemical functionalization. In the previous chapter, the synthesis and properties of carbazole-based HTMs with extended conjugation via 3 and 6 positions were reported. All these HTMs have different alkyl or phenyl substituents at 9 positions. Even in the case of phenyl or *p*-methoxy phenyl substituents differences in the conjugated π electron system are minor, due to the steric hindrance. Since π electrons are very important for the charge transporting process, the additional conjugation extension via 9 positions should improve the charge mobility of carbazole-based photoconductors. The idea behind this work described in the next chapter was to increase the π conjugation of the carbazole-based HTMs *via 3, 6* and *9* positions.

3.1.2.1. Synthesis of 3-, 6-, and 9-substituted carbazoles

In the previous part of this work, the novel synthetic methodology for the synthesis of the 3,6-bifunctional carbazole-based HTMs from 9-substituted carbazoles was successively realized through the reaction with diphenylacetaldehyde or bis(4-methoxyphenyl)aldehyde in the presence of (±)-camphor-10-sulfonic acid as a catalyst. In addition, it is known that under the same conditions the *NH* group in carbazole reacts with the mentioned aldehydes; providing the corresponding [128] enamines. Accordingly, these procedures were applied for the synthesis of the target 3,6,9-diphenylethenyl substituted carbazoles starting from 9*H*-carbazole (Scheme 3.3.). Unfortunately, the attempts to obtain 3,6,9-trifunctional carbazole-based compound 3,6,9-tris(2,2-diphenylvinyl)-*9H*-carbazole (**10a**) in a moderate yield failed. The target product could not be isolated because of the numerous by-products. Most probably, the enamine was formed at the first stage in this case and the electron density at 3 and 6 positions was reduced. Efforts to develop an

alternative synthesis for the target product **10a** were made. Thus, the synthesis of **10a** was easily performed by a four-step procedure from *9H*-carbazole (**Cbz**). The reaction between **Cbz** and benzyl bromide in the presence of KOH was carried out in order to obtain derivative **Bn-Cbz** with the protected *NH* group. In the next step, **Bn-Cbz** was treated with diphenylacetaldehyde to obtain 9-benzyl-3,6-bis(2,2-diphenylvinyl)-*9H*-carbazole (**8a**), which was transformed to the deprotected 3,6-disubstituted carbazole-based precursor **9a**. Finally, 3,6,9-trifunctional product **10a** was prepared by the reaction of diphenylacetaldehyde in the presence of a catalyst CSA. Based on the developed method, the analogues bearing methoxy and methyl groups, 3,6,9-tris(2,2-bis(4-methoxyphenyl)vinyl)-*9H*-carbazole (**10b**) and 3,6,9-tris(2,2-di-*p*-tolylvinyl)-*9H*-carbazole (**10c**), were synthesized.

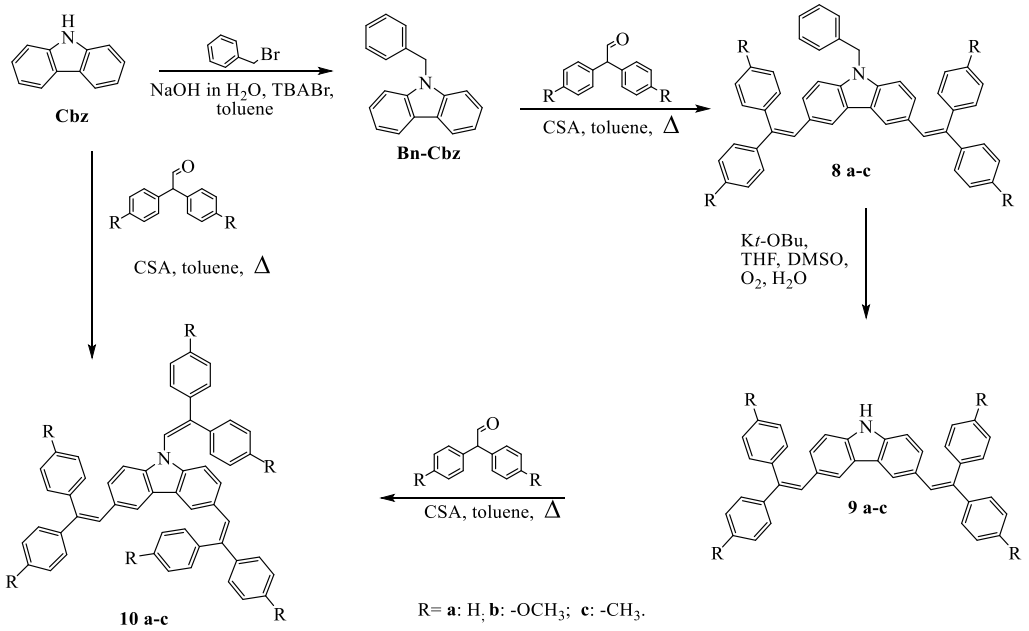

Scheme 3.3. Synthesis of 3,6,9-diphenylethenyl substituted carbazoles **10a-c**

3.1.2.2. Thermal and optical properties

It is noteworthy to mention, that the addition of substituents in diphenylethenyl groups slightly decreases thermal stability. The results of thermogravimetric analysis (TGA) are shown in Figure 12. All the enamine group containing carbazolyl compounds are stable above 380°C (**10a** T_{dest} = 404°C, **10b** T_{dest} = 396°C, **10c** T_{dest} = 380°C).

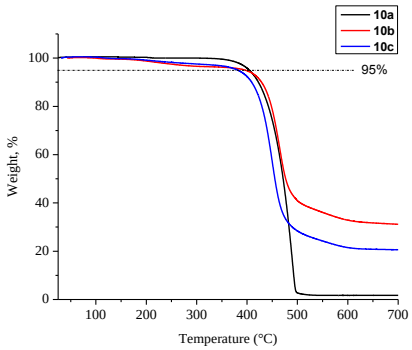

Figure 3.11. Thermogravimetrical analysis curves of **10a-c**

The morphological stability of synthesized HTMs was investigated by DSC under a nitrogen atmosphere. At the first heating, *p*-phenyl unsubstituted compound **10a** demonstrated melting at 215 °C and in the curves of cooling and during the second heating; no peaks due to crystallization and melting were observed. Just the glass transition temperature at 112 °C was registered during the second heating.

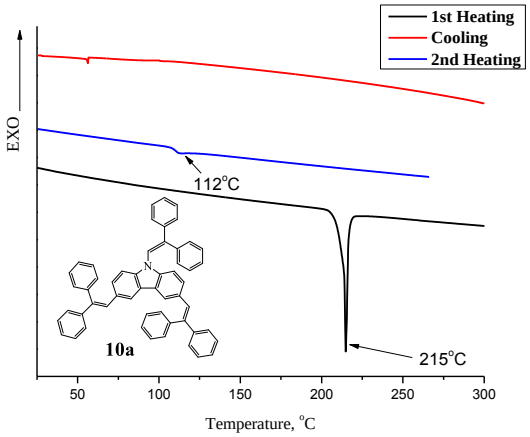

Figure 3.12. DSC analysis curves of the compound **10a** (heating rate 10 °C/min)

Methoxy and methyl substituents in HTMs **10b** and **10c** increase molecular weight of the investigated molecules and also decrease their packing density, therefore the melting point was not observed in thermograms of these carbazolyl compounds. Figure 13 presents DSC second heating curves of molecular glasses **10b** and **10c** with glass transition at 111 °C and 110 °C, respectively.

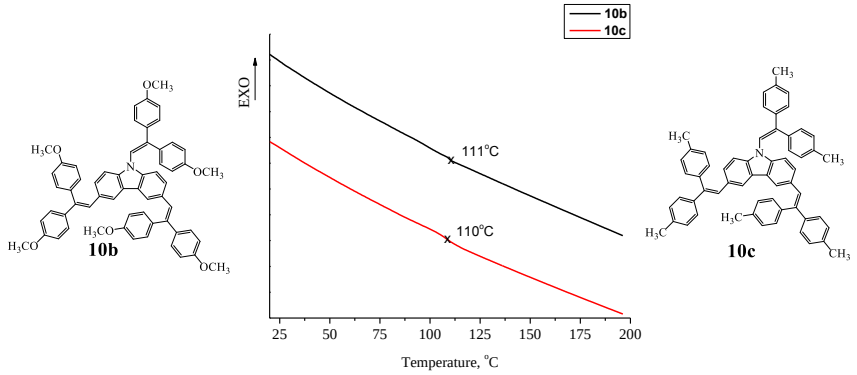

Figure 3.13. DSC second heating curves of the molecular glasses **10b** and **10c** (heating rate 10°C/min)

The optical properties of synthesized compounds **10a-c** were analyzed by UV-VIS spectroscopy from dilute THF solutions withthe spectra presented in Figure 15. The absorption spectra of *N* and *C* unsubstituted carbazole is given for comparison. The addition of three substituents increases significantly the intensity and expands the absorption region comparing with the starting carbazole. All the investigated compounds **10a-c** exhibited a broad absorption in the region up to 400 nm. UV spectrum of compound **10a** is very similar to that of methyl groups-containing molecule **10c,** in both intensity and absorption region (λ_{max} =357 nm). In the case of compound **10b**, peripheral *p*-methoxy groups have a minor impact on the conjugation of carbazolyl derivative, although a slight lowering in absorption intensity of the lowest transitions is observed (Figure 21). Additionally, 10 nm blueshift of bordering peak is observed (**10a**, **10c** λ_{max} =357, **10b** λ_{max} =347 nm).

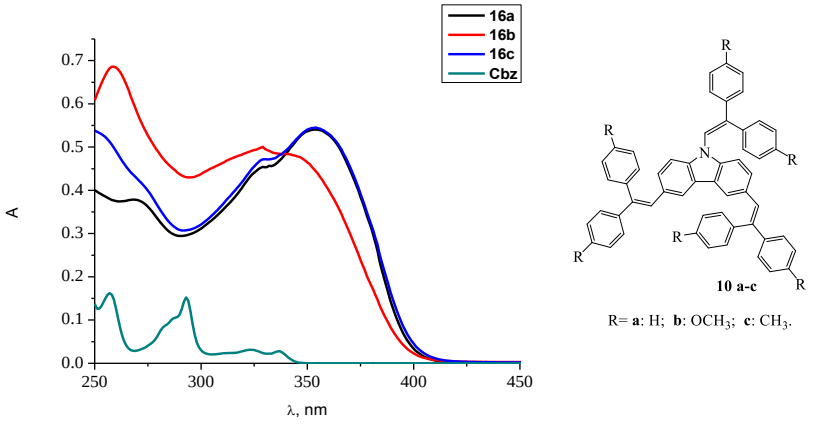

Figure 3.14. UV-VIS absorption spectra of compounds **10a-c** and carbazole in diluted 10-4 mol/l THF solutions

3.1.2.3. Ionization potentials and carrier mobility properties

Summarized values of ionization potential and carrier mobility properties are provided in Table 4. Ionization potentials of trisubstituted carbazoles **10a-c** are in the range of 5.24 eV (**10b**) to 5.38 eV (**10c**). Compound **10a**, without substituents in phenyl rings, has suitable ionization potential and shows a particularly high carrier mobility value at $6.4 \cdot 10^5$ V/cm field reaching $9 \cdot 10^{-3}$ cm^2/Vs (Figure 15). This result is one of the highest known for the carbazole-based hole transporting materials. Methoxy substituents influenced both ionization potential and hole drift mobility, but the positive effect was obtained just in the I_p case. This parameter decreased by 0.06 eV.

Table 3.4. Ionization potentials and hole drift mobility properties of **10a-c**. Measurements were done at the Department of Solid State Electronics, Vilnius University by dr.E.Kamarauskas and dr.V. Jankauskas

Compound	I_p, eV	d, μm	μ_0, cm^2/Vs	$\mu(6.4 \cdot 10^5$ V/cm), cm^2/Vs	α, $(cm/V)^{1/2}$
10a	5.31	4.8	$2.5 \cdot 10^{-3}$	$9 \cdot 10^{-3}$	0.0016
10a+PC-*Z* (1:1)		4.7	$4 \cdot 10^{-5}$	$1.5 \cdot 10^{-4}$	0.0017
10b	5.24*	3.5	$1 \cdot 10^{-7}$	$5 \cdot 10^{-5**}$	0.006
10b+PC-*Z* (1:1)		4.5	$7 \cdot 10^{-9}$	$2.7 \cdot 10^{-6*}$	0.0059
10c	5.38				

*Fixed by PESA method.**Fixed at $1 \cdot 10^6$ V/cm.

Carbazole **10b** bearing methoxy groups demonstrated quite low μ_0 and μ, additionally, the hole drift mobility depends on the electric field strength, which is an adverse property. On the other hand, methyl substituents had a negative influence on the ionization potential (**10c**: 5.38 eV), therefore further research on this compound was discontinued.

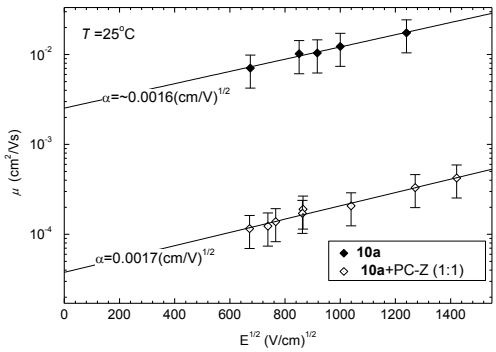

Figure 3.15. Hole drift mobility values of neat **10a** film and **10a**+PC-*Z* (1:1). Measurements were done at the Department of Solid State Electronics, Vilnius University by dr.V. Jankauskas

3.1.3. Twin type 3,6-diphenylethenyl substituted *N*-alkyl carbazoles

In the previous chapter, monomeric carbazolyl compounds with extended π electron system, which are low-molar-mass glasses and exhibit high hole drift mobility, were described. However, some of them (**1**,**4-6a**) can exist both in crystalline and amorphous states, which limit their use in photoelectronic devices. To prevent this problem, compounds that do not readily crystallize are required. According to Wirth postulates [129], there are several ways to achieve the desired results. The amorphous materials should contain non-planar chemical structures, which can prevent easy packing of molecules and hence hinder crystallization. Increasing the number of conformers and incorporation of bulky substituents in the molecule also improves the formation of the amorphous state. Glass transition temperature can be increased by increasing molecular size, incorporation of bulky substituents in the molecule, and enhancing molecular interaction, which can hinder molecular motions. In addition, aliphatic groups and linkages increase the inclination to form glasses, and also reduce the undesired brittleness of an organic glass. Therefore, in this chapter the efforts to synthesize the molecular glasses that exist only in an amorphous state will be presented. Furthermore, thermal, optical properties, and investigation of photoconductive properties will be discussed.

3.1.3.1. Synthesis of 3,6-diphenylethenylsubstituted twin type *N*-alkyl carbazoles

The synthesis route to the twin type 3,6-diphenylethenyl substituted carbazoles is shown in Scheme 3.4. First of all, carbazole twins **11-13** were synthesized from carbazole and different length dibromoalkanes using tetra-*n*-butylammonium bromide (TBABr) as a catalyst. Then these twin type carbazoles possessing four active groups (3, 3′, 6, 6′) reacted with diphenylacetaldehyde or 2,2-bis(4-methoxyphenyl)acetaldehyde under the same conditions as the synthesis of compounds **1-3 a**,**b** described in the previous chapter. Unfortunately, the yields of target products **14-16a**,**b** were low, even if the reaction conditions (molar ratio, temperature, and solvent) were systematically varied. It was noticed that at a higher reaction temperature and in an acidic environment, double bonds in the diphenylacetaldehydes underwent polymerisation. Consequently, in order to obtain the target compound 1,3-bis(3,6-bis(2,2-diphenylvinyl)-9*H*-carbazol-9-yl)propane (**14a)** an alternative synthesis method to the twin molecule was developed. It proved to be successful when carbazole **Bn-Cbz** containing the protected *NH* group was treated with diphenylacetaldehyde to obtain 9-benzyl-3,6-bis(2,2-diphenylvinyl)-9*H*-carbazole (**8a**), which in turn was transformed to the unprotected 3,6-disubstituted carbazole derivative **9a**. Finally, the target product **14a** was prepared by the reaction of 1,3-dibromopropane with two equivalents of **9a** in the presence of KOH and interphase catalyst TBABr. The last method holds greater promise, since the overall yield (62%) is higher compared with the yield (17%) in the first method. Based on the developed method, interaction of the intermediate **9a** with 1,6-dibromohexane and 1,9-dibromononane provided corresponding twin type carbazole derivatives 1,6-

bis(3,6-bis(2,2-diphenylvinyl)-9*H*-carbazol-9-yl)hexane (**15a**) and 1,9-bis(3,6-bis(2,2-diphenylvinyl)-9*H*-carbazol-9-yl)nonane (**16a**).

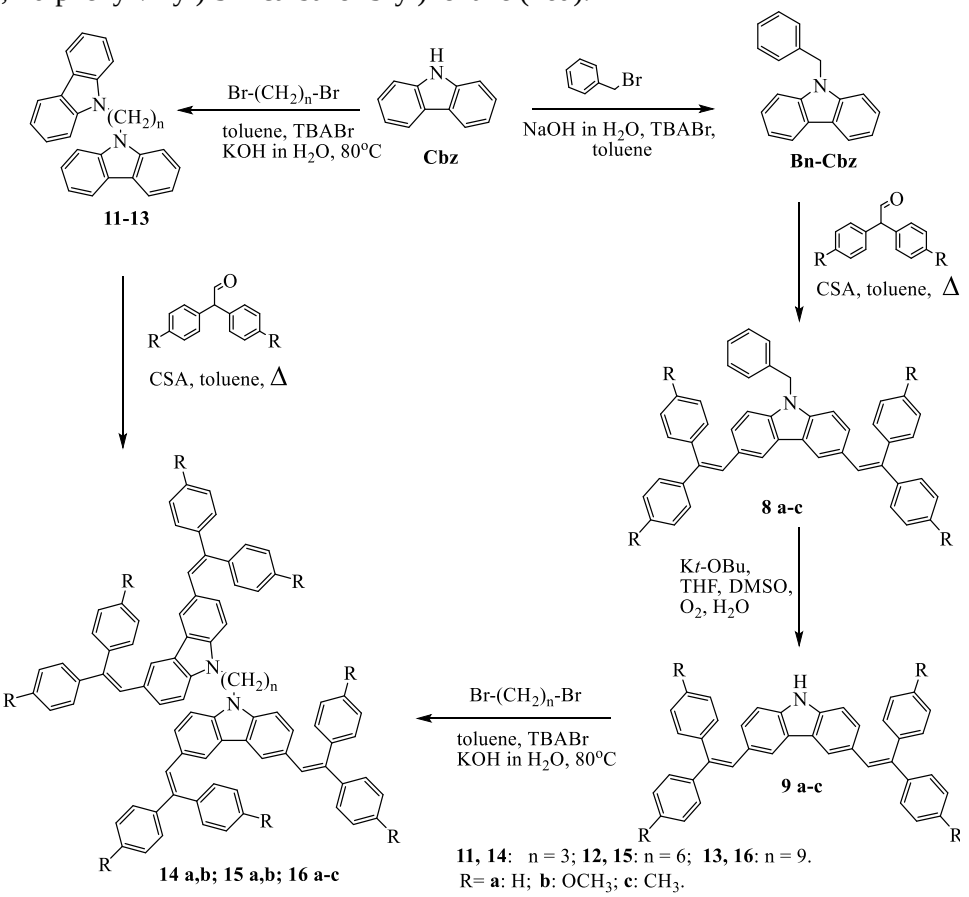

Scheme 3.4. Synthesis of twin type 3,6-substutituted carbazoles **14a**,**b**; **15a**,**b**; **16a-c**

Moreover, the analogues possessing methoxy and methyl groups were prepared in reasonable yields as follows: 1,3-bis(3,6-bis(2,2-bis(4-methoxyphenyl)vinyl)-9*H*-carbazol-9-yl)propane (**14b**) – 69%, 1,6-bis(3,6-bis(2,2-bis(4-methoxyphenyl)vinyl)-9*H*-carbazol-9-yl)hexane (**15b**) – 67%, 1,9-bis(3,6-bis(2,2-bis(4-methoxyphenyl)vinyl)-9*H*-carbazol-9-yl)nonane (**16b**) – 63%, and 1,9-bis(3,6-bis(2,2-di-p-tolylvinyl)-9*H*-carbazol-9-yl)nonane – 70% (**16c**).

The structure of novel compounds was confirmed by the ^{1}H and ^{13}C NMR spectra.

Characteristic peaks of aromatic protons of the novel synthesized twin type carbazole derivatives are found in the 7.55-6.75 region of the ^{1}H NMR spectra. Figure **16** demonstrates the fragment of ^{1}H NMR spectrum of compound **14a**. The singlet at 7.50 ppm (4-H) has been assigned to 4- and 5- protons of carbazoles, while the singlet attributable to the CH=C is located at 7.11 ppm (4H). Two pairs of

protons 2-H, 7-H and 1-H, 8-H of carbazole core gave two doublets at 7.00 and 6.83 ppm, respectively. Other aromatic protons in the phenyl rings resonated in the region of 7.40-7.20 ppm.

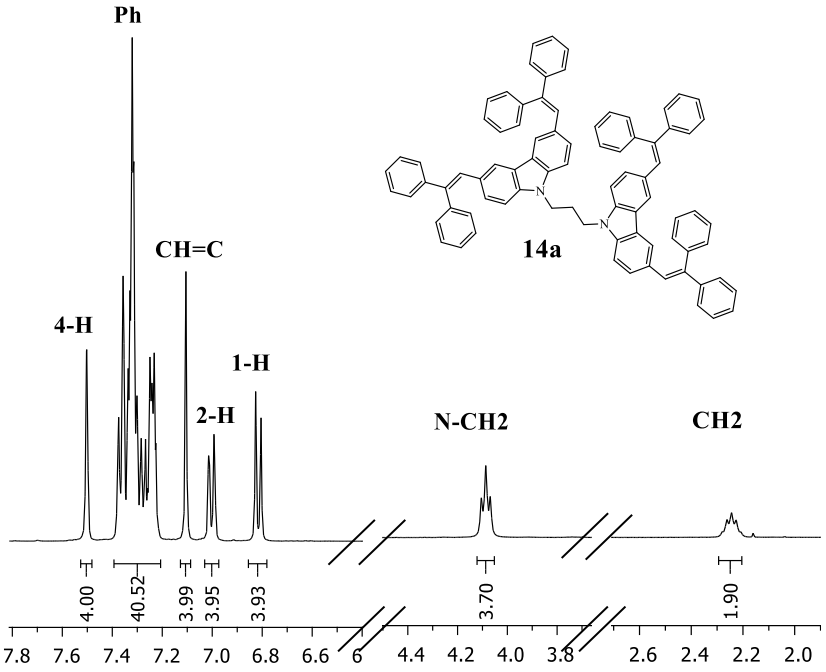

Figure 3.16. ^{1}H NMR spectrum of **14a** (400 MHz, $CDCl_3$)

3.1.3.2. Thermal properties

The thermal stability of compounds **16a-c** were analyzed using the TGA method with the recorded 5% mass loss to examine the influence of methoxy and methyl groups in the peripheral phenyl rings on the thermal stability. The unsubstituted compound **16a** was the most thermally stable with 5% mass loss at 440°C (Figure 17). Methyl groups reduced stability insignificantly (**16c**: 433 °C), and attachment of methoxy groups gave a noticeable decrease to 403°C in the case of compound **16b**. In conclusion, the synthesized twin type carbazole compounds exhibit high thermal stability up to ~ 400 ºC.

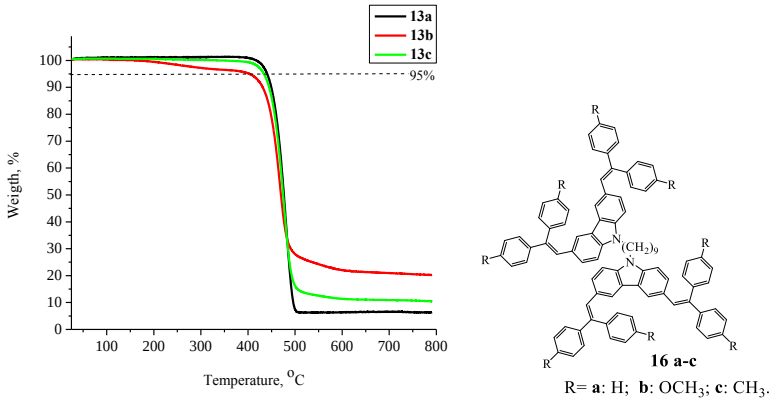

Figure 3.17. TGA curves of twin type 3,6-substutituted carbazoles **16-16c**

The glass-forming capability of the investigated twin type molecules was determined by DSC analysis. The detailed data is presented in Table 5. All the synthesized compounds described in this chapter showed glass transition with T_g ranging from 107-128 °C. These investigations revealed that all investigated compounds, except twin molecule **15a**, were found only in the amorphous phase in the experiments. For example, glass transition occurred at 126 ºC for **14a**, but no melting was observed (Figure 20). This means that the original state of the sample was amorphous. This is a common feature for **14b**, **15b**, and **16a-c**. Compound **15a** underwent not only glass transition but also melting. However, no crystallization exotherm and melting endotherm were observed in the second heating scan. The DSC thermograms of compound **15a** are shown in Figure 18. The material remained in the glassy state after melting and subsequent cooling. Interestingly, this substance was identified as polymorphic based on its first thermogram, with melting peaks - at 197 °C and 208 °C.

Table 3.5. Results of DSC analysis of twin type carbazoles **14a-b**, **15a-b**, **16a-c**.

Compound	**Glass transition T_g, °C**	**Melting point T_m, °C**
14a	126	-
14b	128*	-
15a	116	173, 197, 208
15b	122*	-
16a	107	-
16b	111	-
16c	118	-

*fixed at the 3rd heating (rate 20°/min.).

The comparison of the DSC analysis results for **14-16a** and **14-16b** has revealed a significant role of the aliphatic linking fragment of the conductive chromophores. In the case of **16a** and **16b**, the glass transition points are lower than

those of **14a**,**b**, **15a**,**b,** due to more flexible alkyl units in the linking fragment. The structure of the charge transporting chromophores also affects the glass transition points of the presented HTMs. The introduction of methoxy or methyl group into the peripheral phenyls (**14a** *vs* **14b**, **15a** *vs* **15b**, **16a** *vs* **16b**, **16a** *vs* **16c**) increases the glass transition temperature. However, this influence is much weaker in the case of the twin molecules **14** bearing propyl central unit.

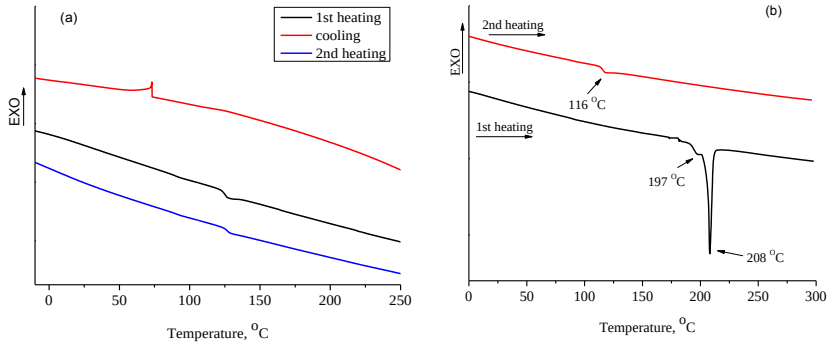

Figure 3.18. (**a**) DSC thermograms of carbazole-containing twin type compound **14a**.(**b**) Thermograms of polymorphic compound **15a** (heating rate 10 °C/min, N_2 atmosphere)

3.1.3.3. Optical properties

Since π-electrons are very important for the charge transporting process in the HTM structures, the absorption spectra of dilute THF solutions of the target carbazole-containing twin type molecules and their 3,6-substituted precursor **9a** were recorded and are shown in Figure 18. The comparison of UV spectra of compounds **14-16a**,**b** has revealed that the length of the alkyl chain does not play a significant role on $\pi \rightarrow \pi^*$ transitions in both diphenylethenyl and bis(4-methoxyphenyl)ethenyl substituted samples, thus indicating that there is no interaction between the photoconductive moieties at the ground state. Additionally, the $\pi \rightarrow \pi^*$ absorption bands are more intensive (hyperchromic shift) in comparison with the ones for precursor **9a**, indicating the increased number of chromophores.

In addition, the patterns of UV/VIS curves are very similar to the ones of the monomeric carbazoles discussed in chapter **3.1.1.3**: compounds with diphenylethenyl substituents **14a-16a** display the same absorption bands at 270, 322, and 355 nm with insignificant deviation. There is not much difference in the $\pi \rightarrow \pi^*$ absorption bands between the UV/VIS spectra of compounds **16a** and **16b**. The addition of methoxy groups reduces absorption negligibly at 270 and 355 nm (**14b-16b**), while the peripheral *p*-methoxy groups have a minor impact on the conjugation of carbazole derivatives, although a slight lowering in absorption intensity of the lowest transitions are observed. The influence of methyl groups is low (**16c** *vs* **16a**).

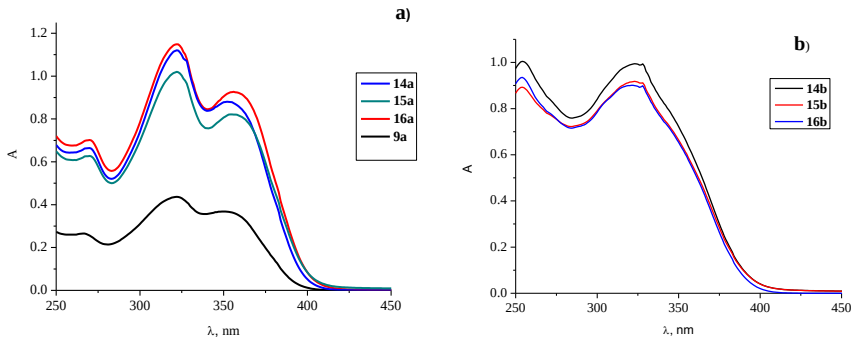

Figure 3.19. UV/VIS spectra of dilute THF solutions (10^{-4}M) of twin molecules a) **14a-16a** and their precursor **9a**; b) **14b-16b**

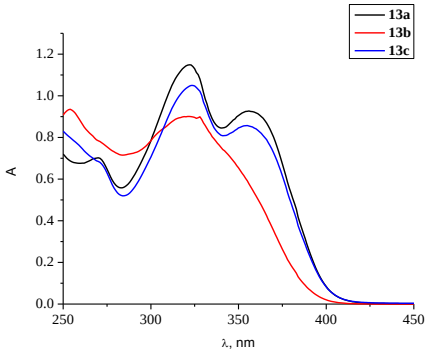

Figure 3.20. UV/VIS spectra of dilute THF solutions (10^{-4} M) of twin type carbazoles **16a-c**

3.1.3.4. Ionization potentials and hole transporting properties

Ionization potential measurements of this series were made at Vilnius University by dr. E. Kamarauskas. The values of ionization potentials are in the 5.44-5.71 eV range, and, unfortunately, this result does not correspond to the requirements for hole transporting compounds in organic perovskite solar cells. From the substituents aspect, additional methoxy and methyl groups have a positive effect. In addition, this effect depends on the length of the connecting aliphatic chain. In the case of the shortest one – propyl- chain containing pair **14a** (without substituents) and **14b** (with $–OCH_3$ groups), four additional methoxy groups lower ionization potential by 0.28 eV (**14a**: 5.74eV *vs* **14b**: 5.46 eV).

Table 3.6. Ionization potentials of twin type carbazoles **14-16 a-c.** Measurements were made at Vilnius University by dr. E.Kamarauskas.

Compound	**14a**	**14b**	**15a**	**15b**	**16a**	**16b**	**16c**
I_p, **eV**	5.74	5.46	5.64	5.44	5.71	5.54	5.56

In the example of compounds **15a** and **15b** with six CH_2 groups between two carbazolyl fragments, the role of this effect is less significant, where the difference is 0.20 eV (**15a**: 5.64eV *vs* **15b**: 5.44 eV). Ionization potentials of compound **16a** with unsusbstituted phenyl rings and the longest nonyl chain is 5.71 eV, which is higher by just 0.17 eV *versus* compound **16b** with methoxy groups (5.54 eV). Methyl groups behave similarly to methoxy ones and ionization potentials of **16c** (-CH_3) and **16b** (-OCH_3) are almost the same (**16b**: 5.54eV *vs* **16c**: 5.56 eV).

As the ionization potentials are too high for applications in perovskite solar cells, the measurements of hole transporting properties are not significant any more. The measurements by xerographic time of flight method were carried out only for the pair of **16a** and **16b** to identify the carriers transporting properties of these series. The compounds were tested in layers of neat material and in mixtures in PC-*Z* (weight ratio 1:1). In the case of twin-type carbazoles, the values of *XTOF* measurements are higher than those of single carbazoles (chapter 3.1.1.4) and, despite undesirable ionization potential, the results of the pure material layers in the $6.4 \cdot 10^5$ V/cm energy field are in the range of $3 \cdot 10^{-3}$ (**16a**) to $1.7 \cdot 10^{-4}$ cm^2/Vs (**16b**).

Table 3.7. Hole drift mobility values of **16a** and **16b**. Measured at Vilnius University by dr. V.Jankauskas.

Compound	*d*, μm	μ_0, cm^2/Vs	$\mu(6.4 \cdot 10^5$ V/cm), cm^2/Vs	α, $(cm/V)^{1/2}$
16a	7.5	$9 \cdot 10^{-5}$	$3 \cdot 10^{-3}$	0.0044
16a+PC-Z (1:1)	5	$2.3 \cdot 10^{-6}$	$4.6 \cdot 10^{-5}$	0.0038
16b+PC-Z (1:1)	2.8	$2.3 \cdot 10^{-7}$	$1.6 \cdot 10^{-5}$	0.0053

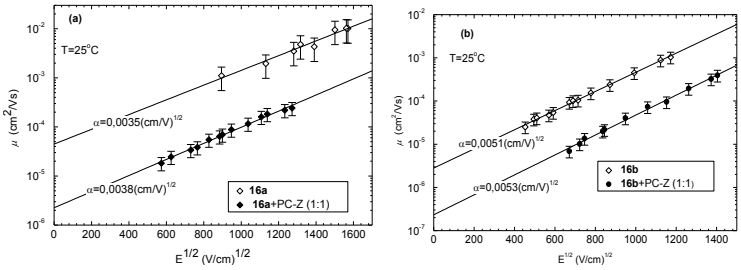

Figure 3.21. Hole drift mobility of **16a** (a) and **16b** (b), measured in neat films and in PC-*Z* (1:1). Measurements were done at the Department of Solid State Electronics, Vilnius University by dr.V. Jankauskas

Lower results of methoxy substituted twin type carbazole **16b** *versus* unsubstituted **16a** were expected, as the same tendency was observed in the case of single type carbazoles. Generally, in the case of a mixture with PC-*Z*, carrier drift mobility values are noticeably lower, but at this time are still quite high and reach from $4.6 \cdot 10^{-5}$ (**16a**) to $1.6 \cdot 10^{-5}$ cm^2/Vs (**16b**).

In summary, twin-type carbazoles with phenylethenyl groups were synthesized in two different ways, and, despite an additional synthesis step, the method with precursor was identified as more suitable. Due to the high molecular mass and flexible double bonds in the phenylethenyl groups, these compounds are molecular glasses with glass transition temperatures in the range of 107 to 128 °C, although only in one thermogram of material **15a** melting points were demonstrated. As expected, the different length of alkyl chain does not influence UV/Vis absorption and the twin type molecules with the same 3, 6 substituents in carbazole fragments (**14-16a** and **14-16b**, respectively) have the same λ_{max} in dilute THF solutions. Even though hole drift mobility of neat film (**16a)** approached $3 \cdot 10^{-3}$ cm^2/Vs at $6.4 \cdot 10^5$ V/cm field, ionization potential values of these phenylethenyl substituted twin type carbazoles are not suitable for applications in perovskite solar cells.

3.1.4. Siamese-twin type indolocarbazole-based hole transporting materials with extended π conjugation

The promising candidates for HTMs are indolocarbazole derivatives, particularly, indolo[3,2-*b*]carbazoles (ICZ) and triazatruxenes (TAT), which have been known as HTMs for the active layer of various optoelectronic devices. The core of these Siamese twin type molecules structured from two and three indole units condensed via benzene ring can be considered as a two-dimensional π-system, which provides a large aromatic surface overlapping with each other for efficient intermolecular charge transport. Hu *et al*. reported ICZ naphthyl derivative, which shows an unusual atropisomerism and excellent hole transporting properties in organic light-emitting diodes [130]. In 2004, the first organic field effect transistor (FET) using ICZ derivative as an active layer was successfully fabricated [131]. *N*,*N*-Disubstituted indolo[3,2-*b*]carbazoles and polymeric analogues have also been reported as new HTMs for fabrication of organic FETs [130-134]. Previous studies have shown that 5,11-bis(4-octylphenyl)indolo[3,2-*b*]carbazole provides a self-organized layered structure upon vacuum deposition and, thus, high FET mobility can be achieved [135]. Furthermore, due to sufficient charge mobilities and suitable ionization potentials the ICZ-based derivatives can be applied in the organic photoreceptors [136]. TAT-based HTMs were earlier used both in organic [137, 138] and hybrid perovskite solar cells (PSC) [139, 140]. Remarkable power conversion efficiency of 17.7% was achieved using TAT derivatives with extended π-conjugate system *via* Suzuki and Buchwald coupling reactions [140]. However, these HTMs require inert reaction conditions, boronic precursors or transition metal catalysts; making large scale production more costly.

In previous chapters, a simple one-step synthesis providing charge transporting materials with a varied number of different phenylethenyl side arms, which extend the π conjugate system of molecule significantly, was reported. Such molecularly engineered carbazole-based HTMs demonstrate comparatively high hole drift mobility (up to 0.017 $cm^2\ V^{-1}\ s^{-1}$). Therefore, new Siamese twin type HTMs, obtained by adopting a facile synthetic strategy, for efficient PSCs, were synthesized.

3.1.4.1. Synthesis of indolocarbazole-based hole transporting materials

Two novel indolocarbazole derivatives **19** (Scheme 3.5.) and **22** (Scheme 3.6.) were synthesized from inexpensive precursor materials and characterized to reveal their electrochemical and optoelectronic properties.

The general synthesis procedure for the preparation of 2,8-bis-[2,2-bis(4-methoxyphenyl)ethenyl]-5,11-diethyl-5,11-dihydroindolo[3,2-*b*]carbazole (**19**) and 3,8,13–tris[2,2-bis(4-methoxyphenyl)ethenyl]-5,10,15-triethyl-10,15-dihydro-5*H*-indo-lo-[3,2-*a*:3`,2`-c]carbazole (**22**) is shown in Schemes 3.5. and 3.6., respectively. Indolocarbazole (ICZ) core **17** was prepared by intermolecular condensation of commercially available 3,3′-bisindolylmethane *via* a one-step procedure [141]. The obtained planar ICZ core was then attached *via* ethyl chains to obtain an alkylated precursor **18**, which in condensation with 2,2-bis(4-methoxyphenyl)acetaldehyde in the presence of (+/-)-camphor-10-sulfonic acid provided the final **19** containing phenylethenyl-engineered side arms. The presence of methoxy groups permits tuning of the HOMO level in order to adapt the molecule's donor nature. Furthermore, the methoxy groups have been described in literature as effective anchors for the interface between perovskite and HTM [142].

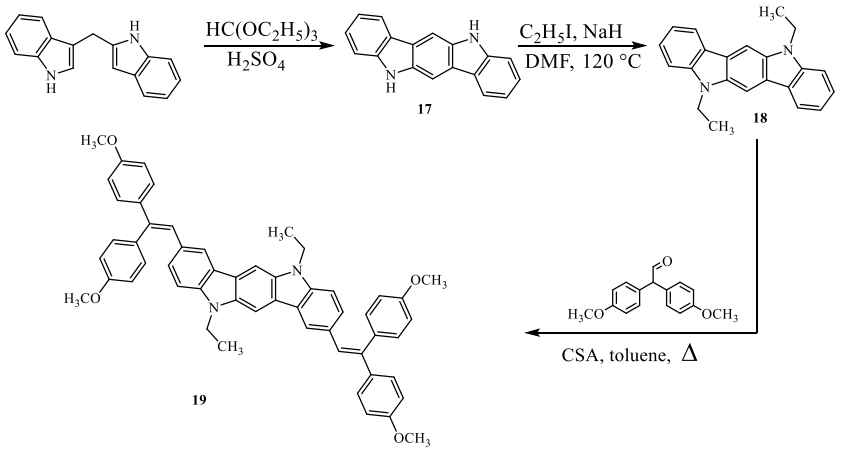

Scheme 3.5. Synthesis of 2,8-bis-[2,2-bis(4-methoxyphenyl)ethenyl]-5,11-diethyl-5,11-dihidroindolo[3,2-*b*]carbazole (**19**)

Compound **22** containing the triazatruxene core with phenylethenyl-engineered side arms was prepared in the analogous procedures from triazatruxene **20**, which was synthesized from commercially available 2-indolinone *via* a one-step reaction [143] (Scheme 3.6.). The structures of the synthesized compounds were verified by the data from $^{1}H/^{13}C$ NMR spectroscopy, mass spectrometry, and elemental analysis.

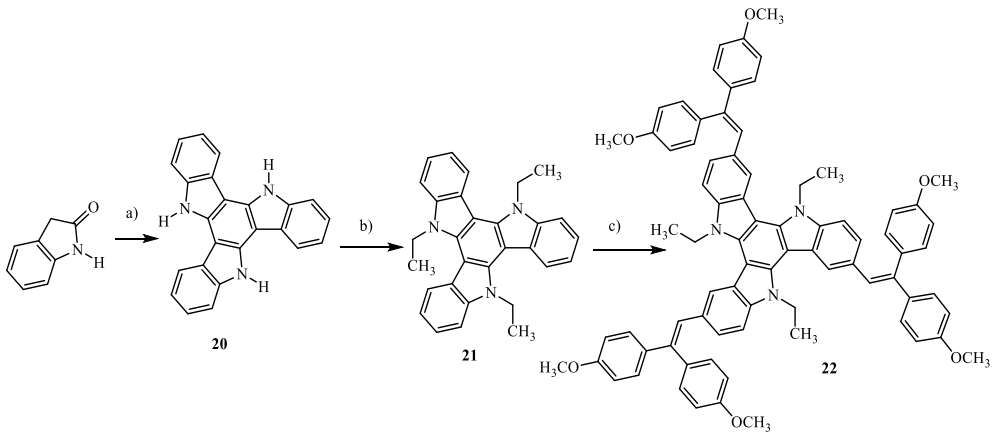

Scheme 3.6. Synthesis of 3,8,13–tris[2,2-bis(4-methoxyphenyl)ethenyl]-5,10,15-triethyl-10,15-dihydro-5*H*-indo-lo-[3,2-*a*:3`,2`-*c*]carbazole (22). (a) $POCl_3$, 100°C, (b) C_2H_5I, NaH, in DMF, 120°C; (c) 2,2-bis(4-methoxyphenyl)acetaldehyde, CSA, at reflux in toluene

Unfortunately, the yield of trisubstituted triazatruxene **22** was low (35%) as in the cases of monomeric carbazoles with three substituents at *3*, *6*, and *9* positions or direct substitution in four positions in the twin type carbazoles. These examples demonstrate, that condensation of the carbazolyl core with diphenylacetaldehydes in the presence of (+/-)-camphor-10-sulfonic acid is successful and efficient only in the case of substitution at two positions. A larger number of substituents requires a longer reaction time, in addition, the acidic environment and high reaction temperature play a significant role in the formation of side products and significantly reduce the yield of promising holes transporting materials with an extended π-electron system. An alternative synthesis route of HTM **22** was tried (Scheme 3.7.) as the results of PCE (Chapter 3.1.4.4.) are very promising.

Isatin was alkylated with iodoethane in the presence of NaH in DMF and the subsequent reaction with hydrazine-hydrate in H_2O provided *N*-ethyl-2-oxo-indole (**23**). Bromine was introduced into 4 position *via* halogenization with a slight excess of *N*-bromosuccinimide (NBS) in acetonitrile; starting the reaction at -5 °C and finishing it at room temperature after 2h. An alkylated triazatruxene core **25** was obtained *via* condensation in phosphorus oxychloride at 100 °C in 8 h in quite low yield, as well as *N*-unsubstituted analogue **20**. The diphenylethyl borolane **26** was obtained from 4-bromoanisole and vinylboronate pinacol ester in toluene at 80 °C in the presence of $Pd[P(t\text{-}Bu)_3]_2$/*i*-Pr_2NH. The Suzuki coupling reaction [144, 145] of 3,8,13-tribromo-5,10,15-triethyl-10,15-dihydro-5*H*-diindolo[3,2-*a*:3′,2′-*c*]carbazole with 2-(2,2-bis(4-methoxyphenyl)ethenyl)-4,4,5,5-tetramethyl- 1,3,2-dioxaborolane (Scheme 3.7.) yielded HTM **22** at 50% yield. The analytical and spectroscopic data of HTMs are consistent with the expected structures.

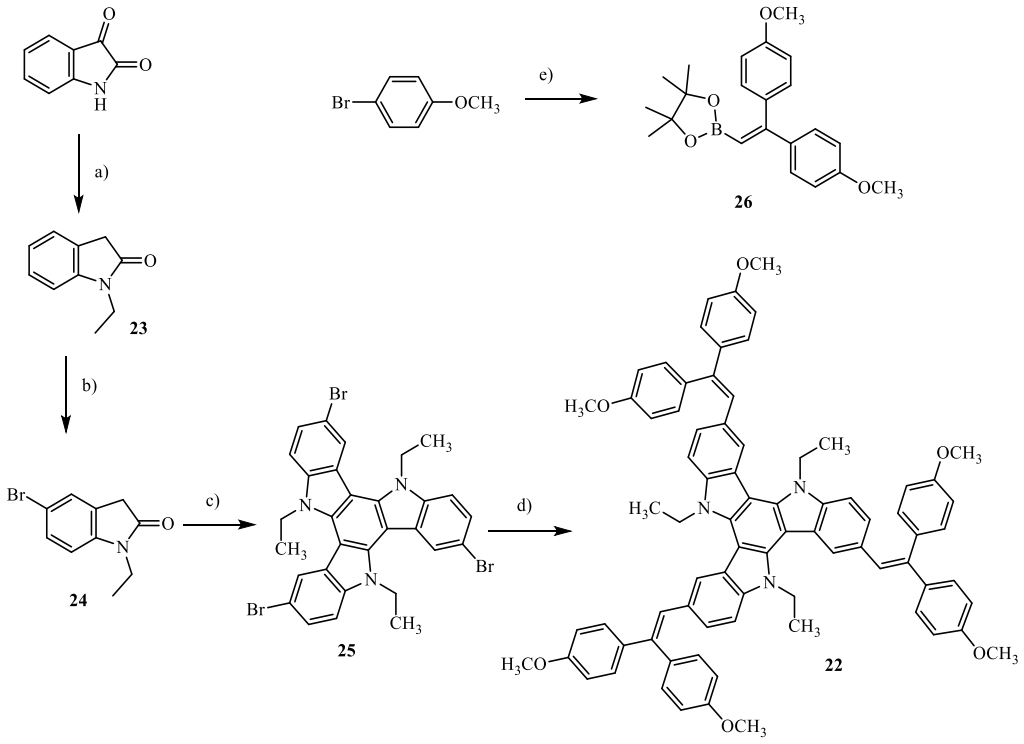

Scheme 3.7. Alternative synthesis route towards 3,8,13–tris[2,2-bis(4-methoxyphenyl)ethenyl]-5,10,15-triethyl-10,15-dihydro-5H-indo-lo-[3,2-a:3`,2`-c]carbazole (22) (a) *I*: C_2H_5I, NaH, in DMF, *II*: $NH_2NH_2 \cdot H_2O$; (b) NBS, acetonitrile, -5°C→rt; (c) $POCl_3$, 100°C, (d) 26 (2-(2,2-bis(4-methoxyphenyl)ethenyl)-4,4,5,5-tetramethyl- 1,3,2-dioxaborolane), $Pd(PPh_3)_4$, K_2CO_3, THF, H_2O, 80°C, 5h; (e) vinylboronate pinacol ester, $Pd[P(t\text{-}Bu)_3]_2/i\text{-}Pr_2NH$, toluene, 80°C, 24h

3.1.4.2. Thermal and optical properties

The thermal properties were studied by thermogravimetric analysis and differential scanning calorimetry. Compounds **19** and **22** are stable up to 414 °C (Figure 23a) and 427 °C (Figure 22a), respectively, which confirms their good thermal stability and states practical utilization. DSC scans demonstrate that TAT core-based HTM **22** is fully amorphous and only shows a glass transition temperature at 138 °C (Figure 21b, Table 4). T_g of **22** is higher than that of the best performance, showing 2,2′,7,7′-tetrakis(*N*,*N*-di-*p*-methoxyphenylamine)-9-9′-spirobifluorene (*spiro*-OMeTAD) (126 °C); indicating a more stable amorphous state and reduced tendency to crystallize, which is beneficial for the overall device stability [146].

Table 3.8. Thermal and optical properties of **19**, **22**, and spiro-OMeTAD.

Compound	T_m (°C)	T_g [a] (°C)	T_{dec} (°C)	Abs_{max} [b] (nm)	ε (M^{-1} cm^{-1})
19	284, 299	-	414	356	4.6×10^5
22	–	138	427	321, 351	7.6×10^4, 7.3×10^4
Spiro-OMeTAD	245	126	449	387	6.9×10^4

[a]Determined by DSC: scan rate, 10 K min^{-1}; N_2 atmosphere; second run. [b]Measured in 10^{-4} M THF solution

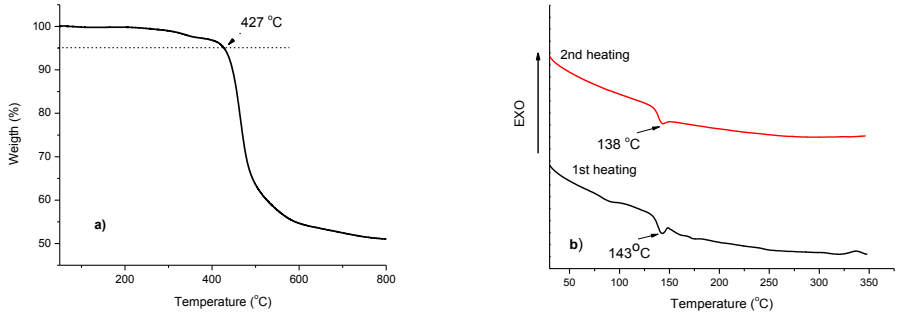

Figure 3.22. (**a**) Thermogravimetric heating curve; (**b**) differential scanning calorimetry first and second curves of **22**

On the contrary, the endothermic melting peaks have been observed in both the first and second heatings of DSC scans for **19** with ICZ core. Interestingly, the DSC curve for **19** at the first heating reveals a number of polymorphous changes before melting at 299 °C (Figure 22b).

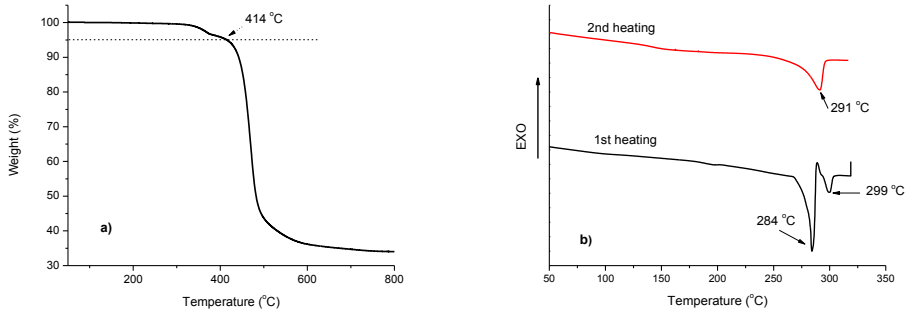

Figure 3.23. Thermogravimetric heating curve (**a**), the first and second heating differential scanning calorimetry curves (**b**) of **19** (heating rate 10 °K min^{-1})

The UV-VIS absorption bands of the ICZ core-based **19** and TAT core-based **22**, measured in THF, are shown in Figure 23. The spectra of the parent compounds **18** and **21** are given for comparison reasons. Indeed, the spectrum of alkylated ICZ

core **18** consists of weak band in the long wavelength region due to *n*-π* transition followed by a broad and intense band in the UV region due to π-π* transitions.

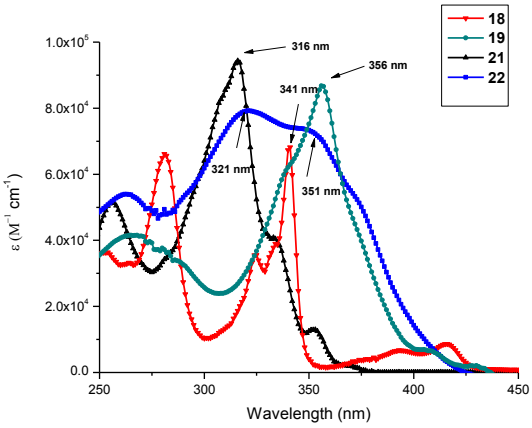

Figure 3.24. Absorption spectra of 10^{-4} M THF solutions of the compounds **19** and **22**. The absorption spectra of the intermediates **18** and **21** are shown for comparison

These results are typical of planar conjugated systems, which is obviously the case for these bridged indolocarbazole derivatives [147]. The π-π* absorption bands for **19** are bathochromically shifted with respect to the reference **18** by 15 nm, indicating an increase in the size of the π-conjugated system due to the ICZ core engineered by phenylethenyl side arms. Obviously, this is more expressed in the case of compound **22**: the π-π* absorption band is bathochromically shifted by 35 nm.

3.1.4.3. Ionization potential measurements

When considering the use of an organic material for hole transporting applications, it is important to have an understanding of its solid state ionization energies. This understanding can help in identifying a suitable partner for organic transport and inorganic electrode materials. The ionization potential was measured by the *PESA* method (Figure 25) and results are presented in Table 5; the measurement error is evaluated as 0.03 eV. ICZ and TAT core-based HTMs have similar I*p* values, 5.28 eV and 5.34 eV, respectively. The energy offset of the E_{HOMO} (ca. –5.30 eV) relative to that of the $MAPbI_3$ (–5.40 eV) present enough driving force for the charge injection process [148].

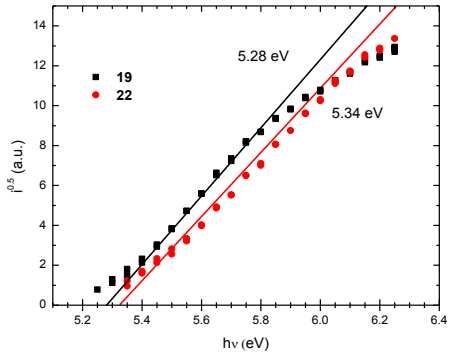

Figure 3.25. Photoemission in air spectra of **19** and **22**. Measurements were done at the Department of Solid State Electronics, Vilnius University by dr. V.Gaidelis and dr.V. Jankauskas

The ground-state oxidation (E_{ox}) potentials of the indolocarbazole-based **19** and **22** were measured by employing the cyclic voltammetry (CV) technique (Table 8). These values do not represent any absolute solid-state or gas-phase ionization energies, but can be used to compare different compounds relative to one another. The cyclic voltammograms of both synthesized HTMs show quasi-reversible oxidation signals (Figure 25) and differences in the CV results are quite small. The E_{HOMO} energy levels determined in CV experiments are in agreement with the PESA measurement results.

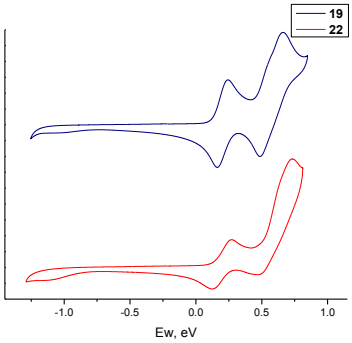

Figure 3.26. Oxidation waves of **19** and **22** (scan rate = 50 mV·s^{-1}) in argon-purged dichloromethane solution

Table 3.9. Electrochemical properties of **19** and **22**

Compound	I_p [a] (eV)	E_{pc}^{ox} vs Fc (V)	E_{pa}^{ox} vs Fc (V)	$E_{1/2}$ vs Fc [b] (V)
19	5.28	0.27	0.19	0.23
22	5.34	0.40	0.25	0.33

[a]Ionization potential was measured by the photoemission in air method from films. [b]$E_{1/2}$= (E_{pa}+E_{pc})/2; E_{pa} and E_{pc} are peak anodic and peak cathodic potentials, respectively

3.1.4.4. Fabrication and characterization of perovskite solar cells and hole drift mobility properties

New indolocarbazole-based semiconductors **19** and **22** were tested as HTMs in PSCs (where the perovskite precursor contained a cation and anion mixture) using a device stack of fluorine doped tin oxide (FTO)/compact TiO_2/ mesoporous TiO_2/perovskite/HTM/ Au. In Figure 27, current density-voltage (*JV*) characteristics are shown. Maximum power conversion efficiency of 15.24% under AM 1.5 G illumination was recorded in the perovskite device containing the TAT core-based **22** as hole transporting material. The measured fill factor was 0.70, the current density (J_{sc}) was 20.53 mA cm^{-2}, and the open-circuit voltage (V_{oc}) was 1042 mV (Figure 25).

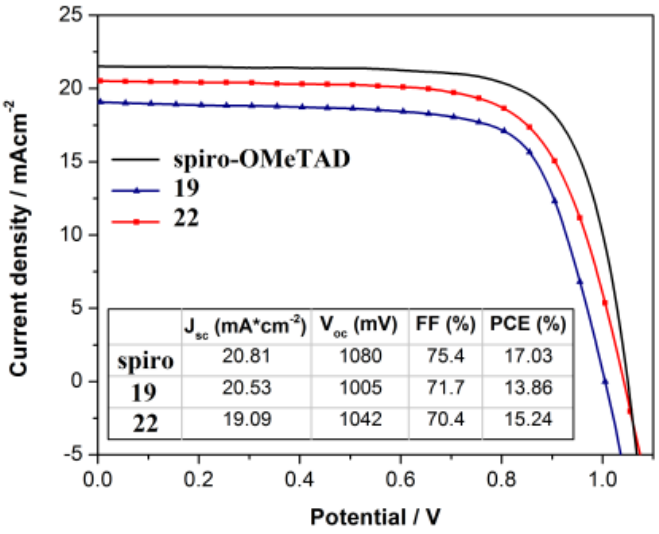

	J_{sc} (mA*cm^{-2})	V_{oc} (mV)	FF (%)	PCE (%)
spiro	20.81	1080	75.4	17.03
19	20.53	1005	71.7	13.86
22	19.09	1042	70.4	15.24

Figure 3.27. Best performing current density-voltage characteristics of **19**, **22** and spiro-OMeTAD as HTM. The voltage scan rate was 10 $mVs^{-1}$and no device preconditioning, such as light soaking or forward voltage bias applied for a long time, was applied before starting the measurement

Spiro-OMeTAD was used as a reference material and best device from the same batch of solar cells, prepared following the same device fabrication procedure, but using *spiro*-OMeTAD as the hole-extracting layer, displayed a PCE of 17.03%. PSCs are well known to exhibit hysteretic behavior, *i.e*. a discrepancy between the forward and backward scan, which can result in largely distorted performance parameters [149, 150]. For example, seemingly high PCEs can be achieved upon a fast scanning of the device from open-circuit to short-circuit conditions (reverse scan), but these values drop significantly at slower scan rates. Therefore, all *JV* measurements were taken at a slow scan rate of 10 mV s^{-1}, resembling quasi steady-

state conditions as suggested independently by Unger *et al.* and Kamat and co-workers [150, 151].

Time-of-flight measurements were used to characterize charge transporting properties of the synthesized HTMs. The obtained layers of neat compound **22** appeared to be uniform and transparent, while those of compound **19** became opaque rapidly after the deposition. Therefore, a uniform layer of **19** was obtained by casting the solution of its mixture with bisphenol-*Z* polycarbonate (PC-*Z*) in a weight ratio of 1:1. The corresponding layers of *spiro*-OMeTAD were also prepared in order to compare the charge-transporting ability of new HTMs. Examples of mobility field dependencies are given in Figure. 27. In all cases, mobility μ may be well approximated by the formula:

$$\mu = \mu_0 \exp(\alpha\sqrt{E})$$

here μ_0 is the zero field mobility, α is Pool-Frenkel parameter and E is electric field strength.

Table 3.10. Electrochemical characteristics, I_p and hole mobility for **19**, **22**, and *spiro*-OMeTAD in composition with PC-*Z* in weight ratio 1:1.

HTM	E_{ox} [a] (V vs Fc)	μ_0 [b] ($cm^2 V^{-1} s^{-1}$)	μ [c] ($cm^2 V^{-1} s^{-1}$)	α ($cm^{1/2} V^{-1/2}$)
19	0.23	1.8×10^{-7}	3.0×10^{-6}	0.0028
22	0.32	3.0×10^{-7}	2.2×10^{-5}	0.0043
Spiro-OMeTAD	-0.01	3.0×10^{-6}	6.7×10^{-5}	0.0032

[a]CV measurements were carried out at a glassy carbon electrode in dichloromethane solutions containing 0.1 M tetrabutylammonium hexafluorophosphate as electrolyte and Pt wire as the reference electrode. Each measurement was calibrated with ferrocene (Fc). [b]Mobility value at zero field strength. [c]Mobility value at 6.4×10^5 V cm^{-1} field strength. Hole drift mobility measurements were done at the Department of Solid State Electronics, Vilnius University by dr. V.Gaidelis and dr.V. Jankauskas

Such mobility dependence is explained by terms of the Borsenberger and Weiss [152], and Borsenberger [153] *et al.* disorder formalism. The mobility defining parameters μ_0 and α values, as well as the mobility value at the 6.4×10^5 Vcm^{-1} field, are given in Table 10.

As seen from the results presented, the hole drift mobility values in amorphous film of composition **22** with PC-*Z* are higher than the ones for **19** and at the strong electric field are similar to the ones of *spiro*-OMeTAD measured under the same conditions. Nevertheless, the difference is only up to one order of magnitude at weak electric field. These results are fully in agreement with the obtained parameters of the constructed PSC in this work.

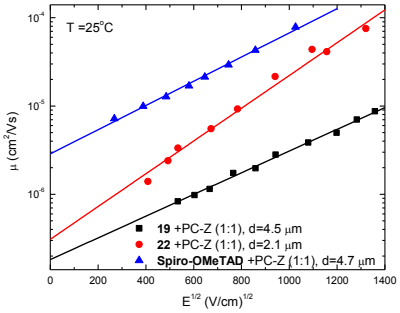

Figure 3.28. The dependence of hole drift mobility on the applied electric field in the amorphous layers of compounds **19**, **22**, and spiro-OMeTAD in composition with PC-*Z*, 1:1

In conclusion, a rapid and efficient synthesis of novel indolocarbazole-based two-dimensional HTMs comprising of electron-rich methoxy substituents in phenylethenyl-engineered side arms has been demonstrated. HTMs were obtained in three scalable synthetic steps, potentially offering much lower production costs in comparison with the most widely used *spiro*-OMeTAD. Remarkable power conversion efficiency of 15.24% was achieved using **22** as the hole transporting material and composite perovskite as absorber, which is on par with that of *spiro*-OMeTAD (17.03%). Triazatruxene core-based **22** is an especially promising candidate, because it can be handled in air, requires no high temperature annealing steps, can be solution deposited, possesses comparatively high mobility, and could be synthesized without using expensive catalysts.

3.2. Triphenylamine-based holes transporting materials with π-conjugation extended *via* phenylethenyl moieties

Another large group of charge-transporting materials are nitrogen-bearing triarylamines. These compounds class have long been known as hole transporting materials for the active layer of photocopiers, OLEDs, and organic solar cells. Typically they show very good solubility in common organic solvents, stability towards air and humidity [154-156], and adequately high charge-carrier mobilities (0.01 $cm^2\ V^{-1}\ s^{-1}$ in vapor deposited [157], and spin coated [158] films). That said, however, it is important to emphasize that mobility results in the spin coated films were obtained using conjugated polymers of triphenylamine (TPA). Currently, solution processed low molecular weight triarylamine derivatives demonstrate significantly lower results ($10^{-4}\ cm^2\ V^{-1}\ s^{-1}$) [159]. Therefore, development of simple, inexpensive, easily purified, very well soluble triarylamine based low molecular weight compounds with optimal electronic properties remains an attractive and important goal.

3.2.1. Monomeric diphenylethenyl substituted triphenylamines

In this chapter, star-shaped charge transporting materials with a triphenylamine core and a varying number of diphenylethenyl sidearms are being

discussed. These hole transporting organic semiconductors are obtained in a one step synthesis procedure, can be solution processed, handled in air, require no high temperature annealing steps, and possess comparatively high charge drift mobility (up to 0.017 $cm^2 V^{-1} s^{-1}$).

3.2.1.1. Synthesis of diphenylethenyl substituted triphenylamines

Similar compounds, bearing phenylethenyl or diphenylethenyl fragments, have been reported in the literature. However, they were obtained using either a multistep synthesis procedure, involving McMurry cross-coupling reaction [8], or by palladium-catalyzed cross-coupling, facilitated by tailor-made ligand [9] or employing quite high loading of the expensive catalyst. For the synthesis of the herein reported compounds, different approaches have been employed.

As the carbazole condensation with diphenylacetaldehyde was productive, the same synthesis pathway was tested for triphenylamine. Due to the active *p*-positions in phenyl rings of triphenylamine, the reported method utilizes commercially available and relatively inexpensive precursors and catalyst, the reaction is not oxygen sensitive and the final product could be obtained in one step. Chapter 2. described problems with reaction yields and complicated purification of the final product in the case of one step condensation in more then two positions of carbazole, experiments of reactions with triphenylamine core bearing materials were started by condensation in a single position. To avoid the multisubstitution possibility, diphenylacetaldehyde was condensated with 4,4′-dimethyltriphenylamine (**27**), synthesized *via* Buchwald-Hartwig reaction from aniline and 4-bromotoluene. 4-(2,2-diphenylvinyl)-*N*,*N*-di-*p*-tolylaniline (**27a**) was obtained in presence of the CSA catalyst in the reaction mixture. To estimate the influence of substituents in phenylethenyl fragments, reactions with bis(4-methoxyphenyl) and bis(4-methylphenyl)acetaldehhydes were tested and two novel triphenylamines **27b** and **27c** were obtained. To identify the role of the phenyl rings for properties of the molecule, (*E*)-4-methyl-*N*-(4-(2-phenylprop-1-en-1-yl)phenyl)-*N*-(*p*-tolyl)aniline (**27d**) was designed and yielded in the case of 4-(2,2-diphenylvinyl)-*N*,*N*-di-*p*-tolylaniline condensation with 2-phenylpropionaldehyde. Scheme 3.8. demonstrates synthesis of single phenylethenyl and phenylpropenyl branch bearing triphenylamines **27a-d**.

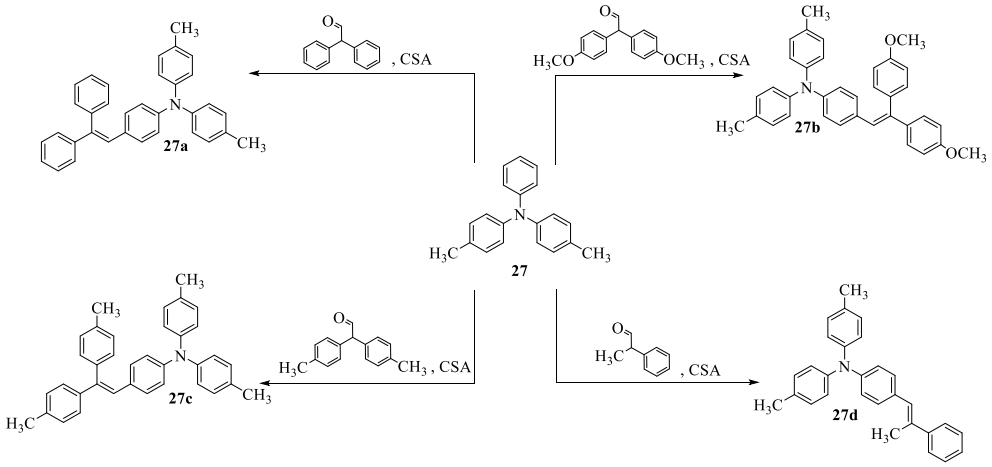

Scheme 3.8. Synthesis of *N*,*N*-di-*p*-tolylaniline core bearing HTMs **27a-d**

Figure 29 demonstrates the ^{1}H NMR spectrum fragments of compound **27c**. The aromatic part of this spectrum is interesting because of the overlapping signal at 6.84 ppm. This is the typical place of C<u>H</u>=C proton as a singlet signal should be found, but in this case signals of phenyl rings protons are in the same place as dublet. Three singlets at 2.28, 2.33 and 2.36 ppm belong to four CH_3 groups. This example suggests that CH_3 groups in peripherial bis(4-methylphenyl) fragment or central 4-methylphenyl rings are not magnetic equivalent. To clearly indentify this, the NMR spectrum of analogue **27b** with methoxygroups was analysed. As was expected, three singlets were obtained at 3.81 ppm (3 protons), 3.79 ppm (3 protons) and 2.28 ppm (6 protons), which proves that the substituents in the peripherial diphenylethenyl rings are not magnetic equivalent with each other.

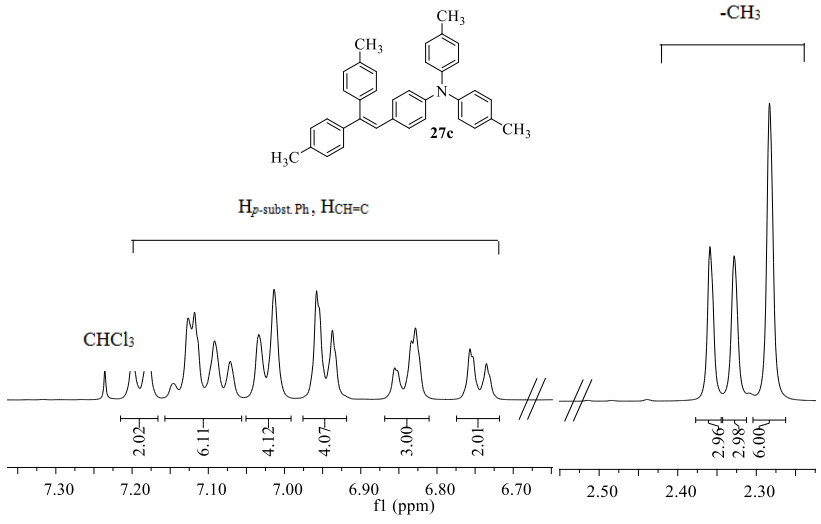

Figure 3.29. Fragment of ^{1}H NMR spectrum of of **27c** (400 MHz, $CDCl_3$)

To prove this reaction process in the case of triphenylamine disubstitution, aldehyde condensation with *para*-methyl monosubstituted triphenylamine **28** was tested. Due to the similarity of 4-methyl triphenylamine chemical reactivity to those of *N*-substituted carbazole, it was expected to obtain a product substituted in both free *para*-positions. As a result of successful condensation, reactions lasted from 3 to 7 hours for the new central triphenylamine core containing compounds **28a-d** with two diphenyl-, bis(4-methoxy)phenyl-, bis(4-methylphenyl)etenyl, and 2-phenylpropenyl sidearms were obtained.

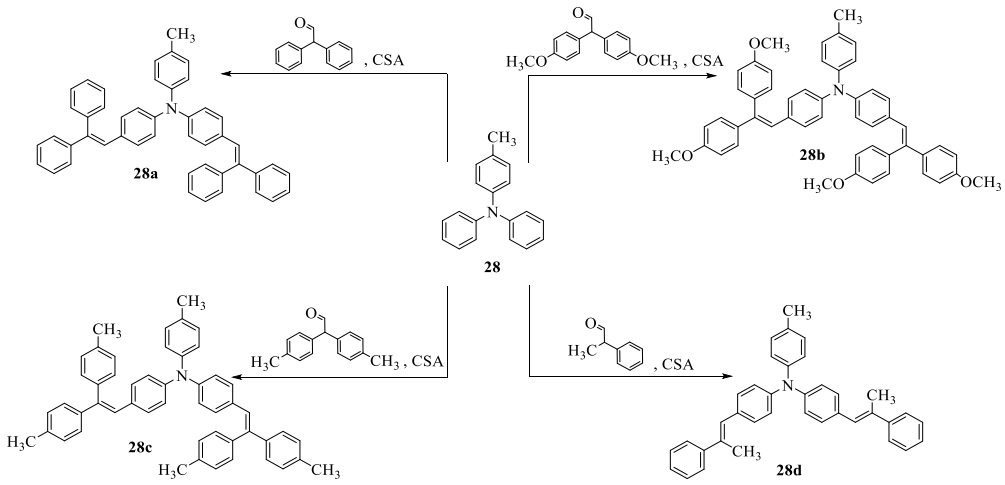

Scheme 3.9. Synthesis of two phenylethenyl substituents bearing HTMs **28a-d**

Accomplished experiments demonstrated that, different from carbazoles, the problem of multisubstitution is not actual in the triphenylamines case. Triphenylamine condensation with an excess of diphenylacetaldehyde, bis(4-methoxyphenyl)aldehyde, bis(4-methylphenyl)aldehyde or 2-phenylpropionaldehyde formed four new tri-*p*-substituted compounds **29a-d** in good yields and the quantity of undesirable polymeric derivatives was insignificant. Scheme 3.10. illustrates CSA catalyzed reactions between triphenylamine and four different aldehydes yielded new triphenylamines with phenylethenyl side arms in three *para*-positions.

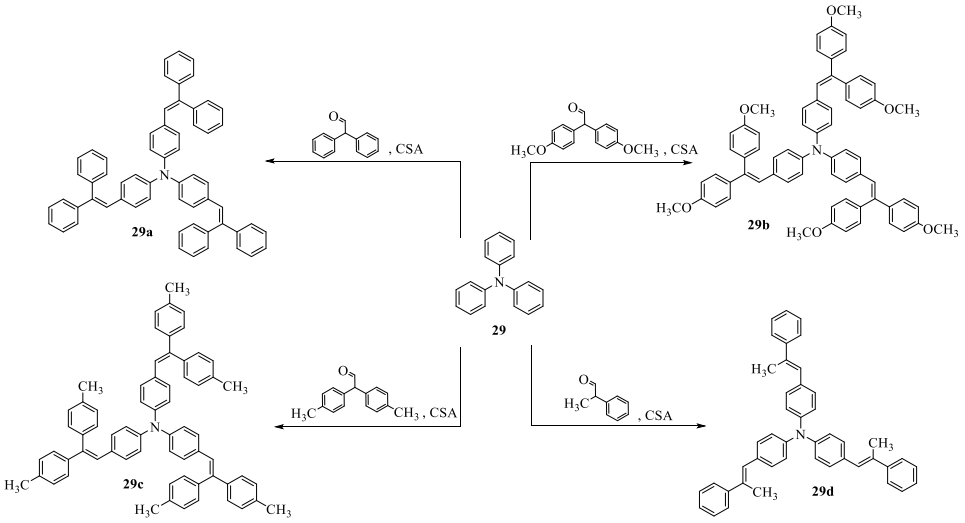

Scheme 3.10. Synthesis of TPA bearing HTMs **29a-d**.

Although compound **29a** has already been reported in the literature [160-162], it was included in this dissertation as a reference material and a demonstration of the method's scope and potential.

3.2.1.2. Thermal properties

Isolated derivatives **27-29 a-d** are soluble in common organic solvents such as THF, toluene and chloroform. Their thermal properties were determined by differential scanning calorimetry (DSC) (Figure 30, Table 7). The DSC measurements indicate that additional bulky phenylethenyl fragments increases the glass transition temperature (T_g) in all investigated compounds. Addition of the methoxy groups has a very noticeable effect on thermal characteristics of **29b**, increasing its melting point by 36 °C (*versus* **29a**) and allowing it to form stable molecular glass.

In the case of smaller molecule **27b,** methoxy groups also introduce more structural disorder compared with **27a** without methoxy groups, making it fully amorphous. Interestingly however, the glass transition (T_g) temperatures of **28a** and **28b** remain almost unchanged. Substitution of a single phenyl ring with methyl group lowers T_g close to (**27d**) or even below (**28d**) room temperature. Due to their very low T_g **27d** and **28d** could be applied as plasticizers or as HTM in applications where good pore filling is needed, for example; solid-state dye-sensitized solar cells [163-165].

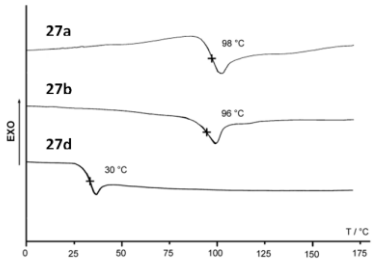

Figure 3.30. DSC second heating curves for the TPA derivatives **27a,b,d**

Monosubstituted TPA derivatives **27a-d** behave similarly as HTM with two or three side-arms. Diphenylethenyl substituted compound **27a** is fully crystalline and does not form a stable amorphous state. Introduction of the methoxy and methyl groups into **27b** and **27c** allows it to exist in both crystalline and amorphous state, while exchange of one phenyl ring with methyl group in **27d** yields a fully amorphous material.

Table 3.11. Thermal characteristics of the synthesized derivatives

Compound	**27a**	**28a**	**29a**	**27b**	**28b**	**29b**	**27c**	**28c**	**29c**	**27d**	**28d**	**29d**
T_g [a] (°C)	-	73	98	48	77	96	54	89	104	1	1	30
T_m [b] (°C)	136	-	201	172	-	-	134, 163	-	-	-	-	-

[a] Determined by DSC: scan rate, 10 K/min; N_2 atmosphere; second run. [b] Melting point was only detected during the first heating; the compound vitrified on cooling to room temperature with 10 K/min

Stability of compounds **27-29c** with bis(4-methylphenyl)ethenyl groups were tested by the TGA method. These three triphenylamine are thermally stable and stability increases together with the molecular weight and reaches up to 400°C in the case of three sidearms (Figure 31).

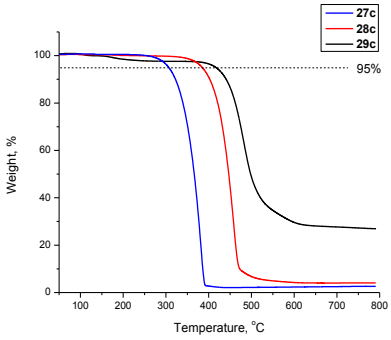

Figure 3.31. TGA curves of bis(4-methylphenyl)ethenyl substituents bearing triphenylamines **27-29c**

3.2.1.3. Optical properties

The absorption bands of the compounds **27-29 a-d** measured in 10^{-4} M tetrahydrofuran solution are shown in Figure 32 and summarized in Table 10.

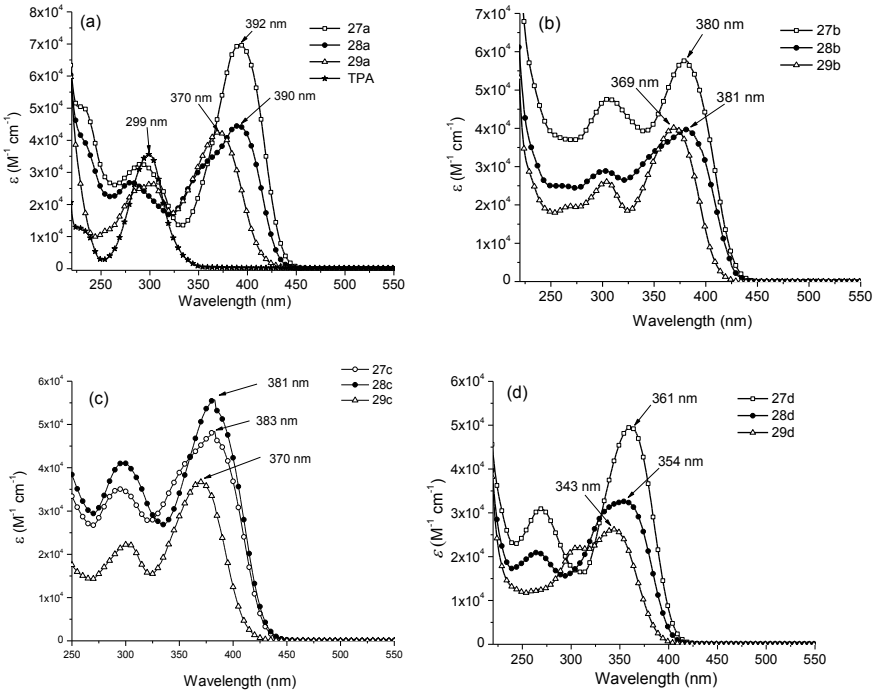

Figure 3.32. Absorption spectra of 10^{-4} M THF solutions of the TPA derivatives **27-29a** (**a**), **27-29b** (**b**), **27-29c** (**c**), and **27-29d** (**d**)

The bathochromic shift of the absorption of **27a** and **28a** compared to that of TPA is attributed to the extension of the core π-conjugated system by one and two diphenylethenyl units respectively (Figure 32a). The maximum of the absorption spectra of **27a** is shifted by about 71 nm with respect to the TPA and is located at 370 nm. In line with expectations, the absorption of **28a** is shifted even more bathochromically by about 91 nm compared with TPA. Additionally, diphenylethenyl fragment in **29a** has a very limited effect on the overall π-conjugated system of the molecule, the bathochromic shift going from di- to tri-substituted TPA derivative is very small (≈2 nm). However, absorption intensity increases quite noticeably. This indicates that the transition is accompanied by a larger change in the electronic charge distribution upon excitation. Addition of the methoxy groups in **27**,**28b** (Figure 32b) yields an overall smaller π-conjugated system (hypsochromic shift of ≈10 nm), compared with **27**,**28a**, indicating that **27**,**28b** adopt less planar configuration. As expected, the substitution of the aromatic phenyl ring with the methyl group in **27**–**29d** (Figure 32c) affects the overall π-conjugated system quite noticeably, compared with **27**–**29a** a hypsochromic shift of

≈30 nm is observed. However, TPA derivatives **27**,**28d** are slightly less bulky than their analogues **27,28a** or **27,28b**; therefore, it is easier for molecules to adopt a more planar conformation. Addition of the third sidearm in **29a** and **29b** had almost no effect on the position of the $\pi \rightarrow \pi^*$ transition band, in the case of **29d** however, the bathochromic shift is more noticeable (≈7 nm).

Table 3.12. Optical characteristics of the TPA derivatives measured in 10^{-4} M THF solutions

Compound	**27a**	**28a**	**29a**	**27b**	**28b**	**29b**	**27c**	**28c**	**29c**	**27d**	**28d**	**29d**
Abs_{max} (nm)	392	390	370	380	381	369	381	383	370	361	354	343
ε (M^{-1} cm^{-1}), $\times 10^{-4}$	6.9	4.4	4.2	5.7	3.9	4.0	5.4	4.2	3.7	4.9	3.2	2.6

3.2.1.4. Charge transport properties

Charge transport properties of the synthesized TPA derivatives **27-29 a-d** were studied by the xerographic time-of-flight (XTOF) technique [80-82] (Figure 36). The values of charge mobility defining parameters: zero field mobility (μ_0), Poole–Frenkel parameter (α), and the mobility at the electric field of 6.4×10^5 V cm^{-1} for the compounds **27-29 a-d** are given in Table 13. To elucidate the energetic conditions for energy and electron transfer in dilute solutions, the E_{HOMO} values were also determined using CV (Table 13).

Table 3.13. E_{HOMO}, I_p, band gap energies, and hole mobility data for **27-29 a-d**[a]

Compound	E_{HOMO}[c] **(eV)**	I_p **(eV)**	[e] d **(μm)**	μ_0[f] **($cm^2 V^{-1} s^{-1}$)**	μ[g] **($cm^2 V^{-1} s^{-1}$)**	α **($cm^{1/2} V^{-1/2}$)**
27a	–5.09	5.41	6.3	3×10^{-3}	0.017	0.0022
28a	–5.09	5.35	2.9	2×10^{-3}	0.014	0.0025
29a	–5.11	5.43	4.9	5.6×10^{-4}	4.3×10^{-4}	0.0045
27b	–5.03	5.27	3.4	5.6×10^{-6}	3.9×10^{-4}	0.0053
28b	–5.01	5.23	4.8	2.2×10^{-5}	6×10^{-4}	0.0041
29b	–5.02	5.35	2.3	3×10^{-5}	1.1×10^{-3}	0.0045
27c	-4.98					
28c	-4.99	5.41	5.0	1.5×10^{-4}	2.7×10^{-3}	0.0036
29c	-4.95	5.32	5.1	4.3×10^{-4}	3.7×10^{-3}	0.0027
27d	–5.10	5.45	6	1.5×10^{-3}	0.013	0.0027
28d	–5.10	5.47	6.4	1.4×10^{-3}	0.012	0.0027
29d	–5.11	5.45	6.3	1.1×10^{-3}	0.014	0.0032

These values do not represent any absolute solid-state or gas-phase ionization potentials, but can be used to compare different compounds relative to one another. The cyclic voltammograms of the synthesized compounds in dichloromethane show one quasi-reversible oxidation couples and no reduction waves.

These results are quite similar to those demonstrated by mono-substituted TPA **27a**, only a very slight increase in E_{HOMO} is observed. Very similar E_{HOMO} values are also determined for **27**–**29d**. Methoxy groups in **27**–**29b** succeed in increasing E_{HOMO} by ~0.1 eV, compared with **27**–**29a**. However, as with all other examples, there is almost no difference between E_{HOMO} levels in mono-, di-, and tri-substituted TPA derivatives.

When considering the use of an organic material for optoelectronic applications it is important to have an understanding of its solid state ionization potentials (I_p). This understanding can help in identifying suitable partner organic transport materials and inorganic electrode materials. The ionization potential was measured by the electron photoemission in air method (Figure 33) and the results are presented in Table 13, the measurement error is evaluated as 0.03 eV [166-168].

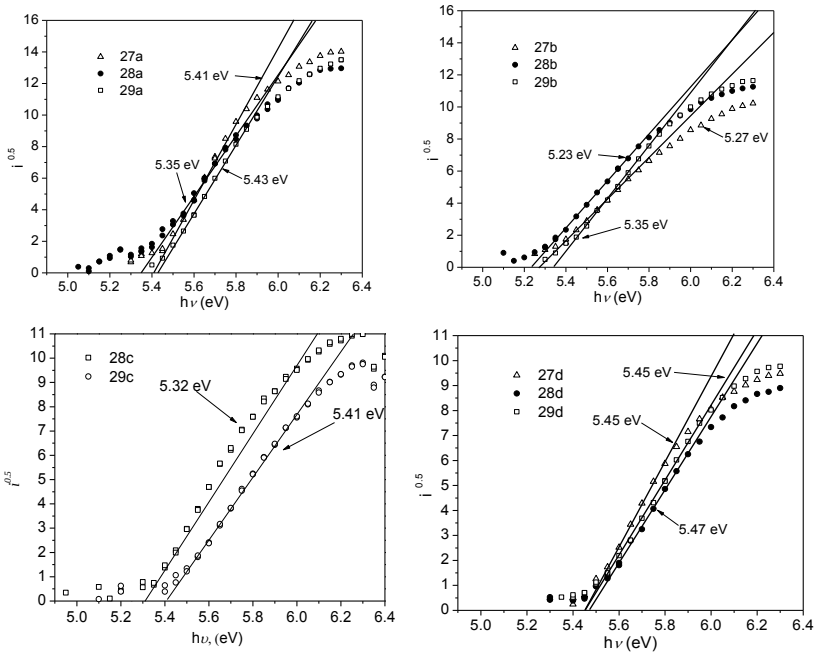

Figure 3.33. Photoemission in air spectra of **27-29 a-d**. Ionization potential measurements were made at Vilnius University, Department of Solid-state Electronics by dr. E. Kamarauskas

Usually the photoemission experiments are carried out in a vacuum and a high vacuum is one of the main requirements for these measurements. If the vacuum is not high enough, the sample surface oxidation and gas adsorption influence the measurement results. In this case, however, the organic materials investigated are stable enough to oxygen and the measurements may be carried out in the air. The measured I_p values are about 0.3 eV higher as compared with the E_{HOMO} levels found

in the CV experiments. The difference may result from different measurement techniques and conditions (solution in CV and solid film in the photoemission method). **27**–**29d** demonstrate the highest I_p values of all four groups investigated. Interestingly, **27**–**29a** have similar E_{HOMO} levels in solution, however, their ionization potentials are slightly lower. Most likely this is caused by differences in the way these molecules pack in the solid state. Presence of methoxy groups in **27**–**29b** lowers the I_p by ~0.1 eV, compared with **27**–**29a**.

3.2.1.5. Organic photoreceptor device fabrication and parameters

Triphenylamine core bearing *N*,*N*′-bis(3-methylphenyl)-*N*,*N*′-diphenylbenzidine (TPD) is one of the most used compounds in the fabrication of organic photoreceptors. Synthesized series of hole transporting materials is structurally similar to the mentioned commercially available TDP. Therefore compounds **29a**, **b**, **d** with three sidearms were in the construction of the organic photoreceptor devices (Figure 34). The device consisted of conducting Al layer, 0.5 μm thick charge generation layer (CGL) composed of a 2:1 mass proportion of titanyl phthalocyanine and polyvinyl butyral BX-1, and the charge transporting layer (CTL) consisting of a 1:1 mass proportion mixtures of the triphenylamine based transporting material and polycarbonate *Z*-200 (PC-*Z*).

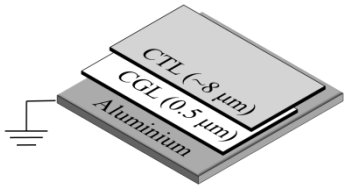

Figure 3.34. Structure of the organic photoreceptor device. Photoreceptor was made at Vilnius University Department of Solid-state Electronics by habil. dr. V.Gaidelis

Characteristics of the constructed devices bearing the investigated materials **29a**, **b**, **d** were compared with a well-known and efficient HTM *N*,*N*′-bis(3-methylphenyl)-*N*,*N*′-diphenylbenzidine (TPD) (Table 12). Photosensitivity (*S*) of the synthesized TPA derivatives with phenylethenyl sidearms is very similar or better than that of TPD. Relative residual potential (U_R/ U_0) is lowest for **29a**, while the device with **29b** demonstrates similar results as the one with TPD. In the case of **29d**, despite higher mobility compared with **29b**, the remaining residual potential is larger, most likely this could be attributed to a higher rate of trap formation. Figure 34 shows the spectral distribution of photosensitivity of organic photoreceptor with **29b** and TPD. Both compositions exhibit good xerographic photosensitivity across most of the visible light region of the spectrum, albeit somewhat better results are observed for **29b**.

Table 3.14. Characteristics of the organic photoreceptor devices bearing **29a**,**b**,**d**.

Compound	d [µm]	U_0 [V]	S [a] [m^2/J]	U_R [V]	U_R/U_0	$t_{1/2}$ [s]	μ_0 [b] [cm^2 V^{-} s^{-1}]	μ[c] [cm^2 V^{-1} s^{-1}]	α [$cm^{1/2}$ $V^{-1/2}$]
29a	7.2	–348	–478	–6.6	0.019	0.082	1.4×10^{-5}	7.5×10^{-4}	0.005
29b	9.9	–478	–396	–14.3	0.03	0.094	7.2×10^{-7}	1.8×10^{-4}	0.0069
29d	7.5	–495	–384	–30	0.061	0.104	3.1×10^{-5}	5.3×10^{-4}	0.0035
TPD	7.2	–461	–368	–13.2	0.029	0.102	4.6×10^{-6}	1.3×10^{-4}	0.0042

[a] λ= 780 nm. [b] Mobility value at zero field strength. [c] Mobility value at 6.4×10^5 V cm^{-1} field strength.

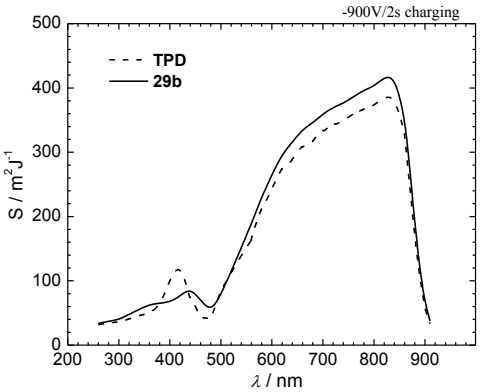

Figure 3.35. Electrophotographic spectral photosensitivity of **29b** and TPD. Measurements were made at Vilnius University Department of Solid-state Electronics by habil. dr. V. Gaidelis

Similar tendencies as with residual potential are observed when analysing the potential decay curves after illumination with 780 nm light pulse. The potential drops rapidly in the devices bearing hole transporting materials with diphenylethenyl and methoxy substituted sidearms **29a**,**b**, while **29d** performs slightly worse for the same reasons as explained above.

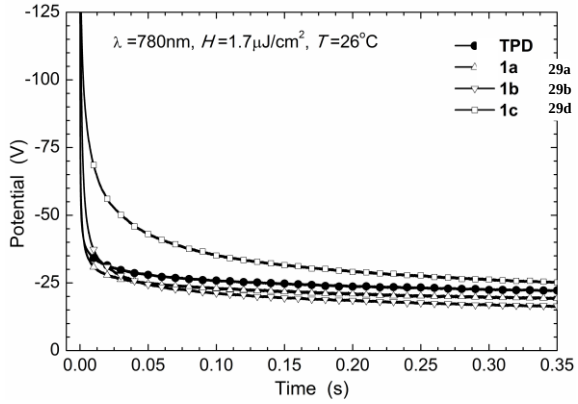

Figure 3.36. The potential decay curves of the photoreceptor devices with **29a**,**b**,**d** after illumination with 1 μs long xenon flash lamp with 780 nm filter pulse. The exposition *H* was 1.7 μJ/cm^2. Measurements were made at Vilnius University Department of Solid-state Electronics by habil. dr. V. Gaidelis

Despite the considerable reduction of the HTM concentration in the CTL layer, the hole mobility remains very good, in all cases it is better than the μ_h of the TPD under identical conditions (Figure 37). The best results (μ_h= 7.5 × 10^{-4} cm^2 V^{-1} s^{-1} at strong electric fields) are observed for the device with TPA derivative with diphenylethenyl sidearms **29a**.

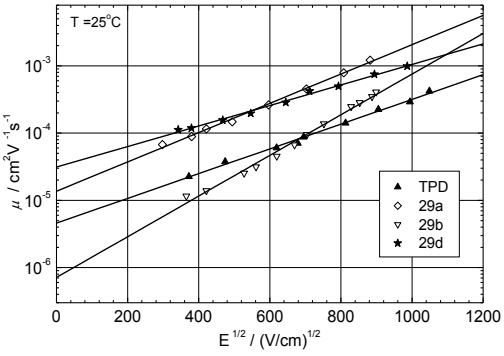

Figure 3.37. The mobility field dependencies of the electrophotographic samples. Measurements were made at Vilnius University Department of Solid-state Electronics by dr. V. Jankauskas

In conclusion, the study has demonstrated a simple one step synthesis method to obtain solution processable star-shaped charge transporting materials with a triphenylamine core and a varying number of different phenylethenyl sidearms from commercially available and relatively inexpensive starting materials. Substitutions in the phenylethenyl fragment could noticeably influence HTMs glass transition temperatures and the tendency to crystallize. By structurally modifying the sidearms can also significantly influence the size of the π-conjugated system, energy levels, and the way molecules pack in the solid state. Optical measurements revealed that

increasing the number of the side arms effectively suppressed intramolecular motions of the TPA core in solution, whereas in the solid state it facilitated exciton migration via the dense sidearm network formed. In turn, this dense network enables charges to move more rapidly through the HTM layer, resulting in very good charge drift mobilities of up to 0.017 $cm^2 V^{-1} s^{-1}$ at strong electric fields. The organic photoreceptor devices were constructed using HTMs **29a**,**b**,**d**. The test results demonstrate that these materials outperform a well-known hole transporting material TPD. Due to their low glass transition temperatures **29d** and **28d** could be used as HTMs in solid-state dye-sensitized solar cells, where good pore filling is needed. The investigated hole-transporting materials **29a** and **29d** are especially promising candidates for practical applications in solar cells, because they can be handled in air, require no high temperature annealing steps, can be solution deposited, possess comparatively high mobility, and could be synthesized in one step from commercially available and cheap triphenylamine.

3.2.2. Triphenylamine bearing polymers with phenylethenylside groups

In 2009, Kojima *et al*. demonstrated that methylammonium lead iodide ($MAPbI_3$) perovskite can work as a solar cell material with 3.8% power conversion efficiency [169] Since then, published values leapt to 21.1% [170] in only 5 years with an acurrently certified record PCE of 22.1%. Such values are already exceeding commercialized polycrystalline silicon solar cells and rapidly approach crystalline silicon solar cells with record efficiency around 25% [171]. Unfortunately, perovskite solar cells still have stability problems.

One promising avenue for stabilizing PSCs, is the appropriate choice of the hole transport material (*spiro*-OMeTAD), fluorine-dithiophene (FDT), or branched methoxydiphenylamine-substituted fluorene derivatives, employed as small-molecule HTMs in PSCs with efficiencies close to or exceeding 20% [172, 173]. However, *spiro*-OMeTAD, the most widely used small-molecule HTM, is problematic owing to chemical degradation by the Co III dopant, crystallization at temperatures as low as 60°C [60], or pinhole formation [174]. Recent studies showed that incorporating a Cr buffer layer between *spiro*-OMeTAD and the Au contact could partially remedy the sensitivity to heat, resulting in more thermally stable devices [175]. Additionally, because pristine *spiro*-OMeTAD has low conductivity, additives, such as bis(trifluoromethylsulfonyl)imide lithium salt (LiTFSI) and 4-*tert*-butylpyridine (tBP), are needed to enhance the conductivity of *spiro*-OMeTAD [176, 177].

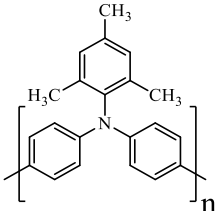

PTAA

Figure 3.38. Structure of PTAA

In addition to the classical *spiro*-OMeTAD and the recent reports of similar performances with other small molecules, polymer-based HTMs are being exploited in PSCs. For this, most of the classical polymers studied in OPVs were first employed to check their suitability in PSCs. Poly-[bis(4-phenyl)(2,4,6-trimethylphenyl)amine] (PTAA) (Figure 38) [178] was the first polymer to be tested in PSCs and holds the record for the highest PCE reported for any polymeric HTM [179]. In a seminal work in 2013, Seok *et al*. fabricated PSCs with PTAA as the HTM. Partially infiltrated PTAA forming a zig-zag like structure in the mesoscopic, PSCs gave a very competitive PCE of 12.0%. Therefore, although poly[bis(4-phenyl)(2,4,6-trimethylphenyl)amine] is a well-known polymeric HTM for PSCs, it also needs additives to obtain high PCE. However, the exact role of the additives and their interaction with the perovskite layer are not yet fully understood and, more importantly, the additives are suspected to directly degrade the perovskite during device operation [174, 180, 181]. Therefore, additive-free HTMs for PSCs are highly desired as they provide a more controlled system without interference from additives, and contribute towards developing long-term stable devices. Most reports on additive-free HTMs are on small-molecule HTMs with PCEs of up to 16% [182-187], while there are only a few reports of additive-free polymeric HTMs with PCEs exceeding 10% [188-190]. In addition, these reports did not focus on stability testing under working conditions, such as maximum power point tracking (MPPT), or under elevated temperature, which are the standard requirements for industrial solar cell certification [191]. From the technical point of view, the main advantage is that the film preparation from polymers is less complicated comparing with film preparation from low molar mass amorphous materials, because small molecules cannot frequently form stable neat films in devices. As a solution, compositions with polymers, as PC-*Z* are created. This causes better quality of films. On the other hand, hole drift mobility of small molecules measured in PC-*Z* as binding material matrix (1:1) are noticibly lower as they are of neat materials. An example of carbazole containing materials, discussed in chapter 3.1.2. shows hole drift mobility in polymerical solutions is by the ca. one order of magnitude lower than in neat films.

The solution processability, mechanical strength of the films, absence of crystallization, and suitable film thickness are the main issues, which make polymers very attractive for optoelectronic applications. Therefore, the principal idea for this part of the work was the design and synthesis of electroactive polymers, which are soluble in common organic solvents and could be used in devices without any additives and with high stability in the long term. As it has been demonstrated in the previous part of this work, addition of the phenylethenyl groups to the triphenylamine molecule provides charge-transporting materials with noticeably extended π-conjugated systems and comparatively high hole mobility values. A similar approach inspired the current investigation, where phenylethenyl groups were incorporated into the molecule with a poly(triarylamine) core to increase the size of the π-conjugated system with the aim to improve performance of the HTMs. Thus, new triarylamine-based polymeric HTMs that can function without additives in PSCs were synthesized. These devices are stable for extended periods under 1sun

illumination or elevated temperatures (85°C). Devices measured under elevated temperature showed remarkable thermal stability for 140 h. Four new hole-transporting polymeric triarylamine derivatives, **32a**, **32b**, **34a**, and **38a**, with methylphenylethenyl and diphenylethenyl functional groups were synthesized. These new materials have been inspired by the best performance shown by the molecules bearing PTAA motif.

3.2.2.1. Synthesis of polymeric triarylamine derivatives

The hole transporting polymer **32a**, containing 2-phenyl propenyl moieties, was synthesized according to Scheme 3.11. First of all, two *p*-positions of triphenylamine were brominated in the classical way with *N*-bromosuccinimide (NBS) in chloroform using a small excess of bromination agent. Dibrominated triphenylamine **30** was condensed with 2-phenylpropionaldehyde and yielded monomer **31**. The polymeric HTM **32a** was obtained from the corresponding monomer **31** through reductive Yamamoto homopolymerization in the presence of triphenylphosphine, Zn, 2,2′-bipyridine, and $NiCl_2$.

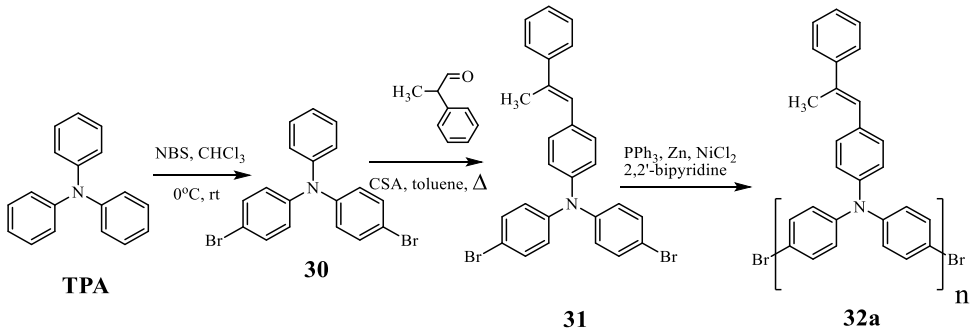

Scheme 3.11. Synhesis of monomer **31** and polymer **32a**

As the presence of halogen atoms can cause faster polymer decay and decrease the charge mobility as well, it is for this reason in the polymer **32a** the terminal bromine atoms were replaced with phenyl rings introducing chlorobenzene in the final phase of the polymerization reaction to give polymer **32b**. Based on the developed method, interaction of the intermediate **30** with diphenylacetaldehyde yielded polymer **34a** with diphenylethenyl sidearms and terminal phenyl rings. Detailed information on the average molecular weights of obtained polymers and their distribution detected by GPC are presented in Table 15.

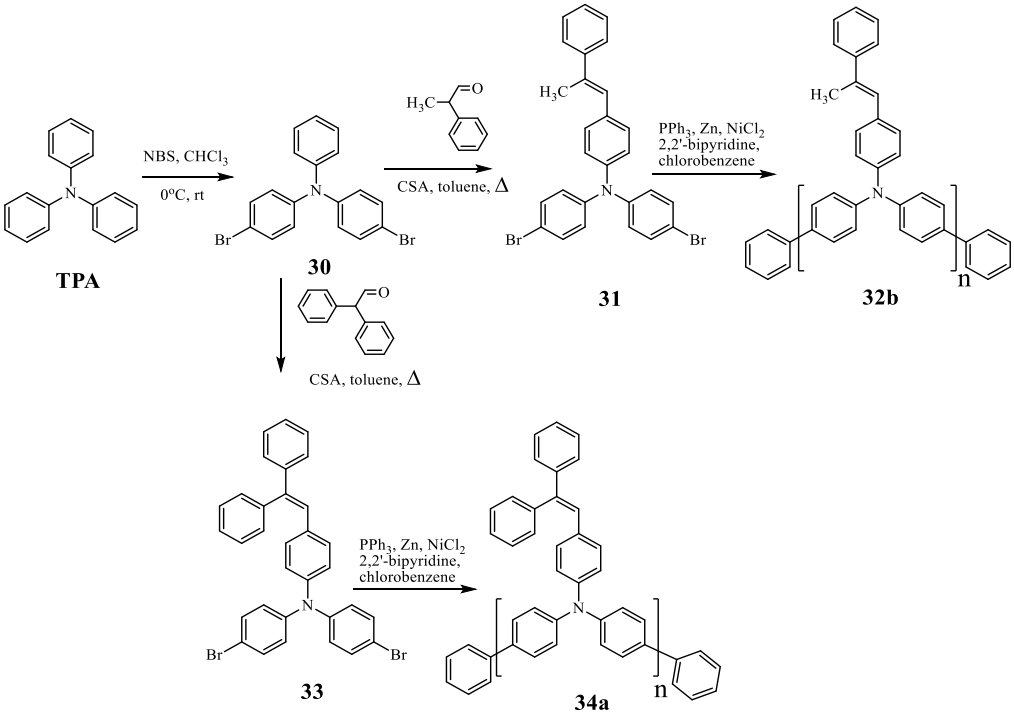

Scheme 3.12. Synthesis of monomers **31** and **32**, polymers **32b** and **34a**

The polymer **38a** with two additional methyl substituents in the side phenyl ring that does not belong to the main polymer chain was designed following the example of PTAA that showed good performance, only phenyl propenyl substituent was added in the *p*-position of the previously mentioned phenyl ring instead of the methyl group in PTAA. First of all, diphenylamine was brominated by NBS and 4,4′-dibromodiphenylamine **35** was obtained. This precursor reacted with 3,5-dimethyliodobenzene in the presence of copper (I) iodide and 1,10-phenanthroline to yield *N*,*N*-bis(4-bromophenyl)-3,5-dimethylaniline **36**. Phenyl propenyl group extending π-conjugation was added to the mentioned monomer *via* condensation with 2-phenylpropionaldehyde using Dean-Stark trap. Reductive Yamamoto homopolymerization of **37** was carried out under the same conditions as in the case of polymers **32a** and **34a**.

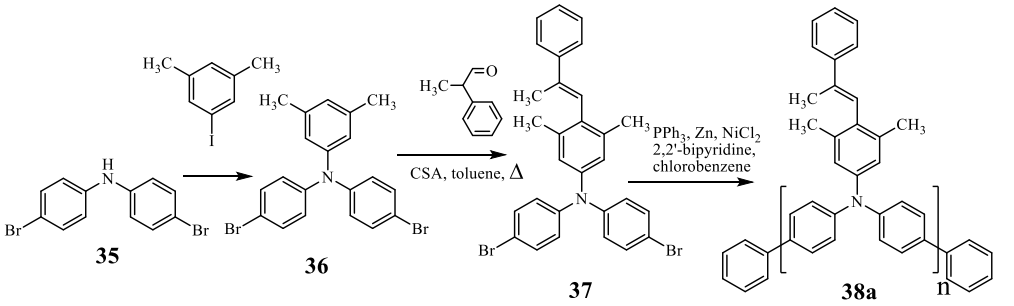

Scheme 3.13. Synthesis of PTAA-like polymer **38a**

Table 15. Characteristics of the polymers **32a**, **34a** and **38a**.

Polymer	M_n, kDa	M_w, kDa	M_w/M_n
32a	7.1	14.4	2.0
32b	6.4	12.4	1.9
34a	4.7	12.0	2.6
38a	7.5	12.5	1.7

[a]Molecular weights were measured using gel permeation chromatography (against polystyrene standards) in THF at the Department of Polymer Chemistry and Technology, Kaunas University of Technology, by prof. G.Buika.

The duration of polymerization reaction was the same for all the synthesized polymers to avoid time influence on molecular weights. The longest polymer chain and the highest average molecular weight were obtained in the case of the smallest monomer **31**. It could be explained by the less complex monomer structure **31**, containing no second phenyl ring in side chain as in **33**, or additional two methyl groups in central *N*-phenyl ring as they are in **37**. Analogously, the shortest chain and the lowest molecular weight were obtained from monomer **33** with the highest molecular weight.

As the main polymer chains for all the synthesized macromolecules were formed by multiple repetition of two *p*-nitrogen substituted phenyl rings, and the molecular weights of the synthesized polymers were higher *versus* commercially available PTAA, but similar with each other, the task of further investigation was to evaluate the influence of different substituents in the third phenyl ring, which does not react in polymerization reaction.

Preliminary measurements have demonstrated that **32b** has the highest ionization potential *Ip*=5.32 eV, which does not fit into the range of the recommended I_p values for HTMs in perovskite solar cells (5.0-5.30 eV). As a result, further investigations like optical, thermal measurements and device construction were made with three polymers having suitable ionization potentials (**32a**: 5.30 eV, **34a**: 5.25 eV, **38a**: 5.21 eV).

3.2.2.2. Optical and thermal properties

The absorption spectra of 10^{-4} M toluene solutions of the polymers **32**, **34**, **38a** are shown in Figure 39a. The redshifted absorption of **34a** indicates a slightly larger π-conjugated system, compared with the other two materials, mostly owing to an additional phenyl ring in the phenylethenyl fragment. Absorption peaks of the investigated polymers are located in the UV region and there is no significant absorption in the visible region. A noticeable hyperchromic effect of the absorption band of **32 - 34a**, compared with **38a**, indicates that the transition is accompanied by a larger change in the electronic charge distribution upon excitation. Interestingly, the absorption spectra of the thin films demonstrate an opposite trend in the position of the peaks (Figure 39b, Table 11), the lowest energy π–π* transitions are observed

for **38a**. Bulkier diphenylethenyl fragments in **34a** twist out of the plane in the solid state, where as smaller 2-phenylpropenyl moieties in **32a** and **38a** can arrange themselves more favourably. The studied polymeric HTMs demonstrate very little absorbance beyond the UV region in the solid state, indicating that this absorption property is advantageous for the construction of tandem solar cells bearing these HTMs. Furthermore, the investigated films were approximately 100 nm thick, whereas PSC devices were constructed using 20 nm-thick HTM films, diminishing the impact of the HTM absorbance in the NIR region even further.

Table 3.16. Optical and thermal characteristics of the polymers **32a**, **34a** and **38a**.

Polymer	λ_{abs} [a], nm	λ_{abs}^{film}, nm	T_g [b], °C	T_{dec} [c], °C
32a	375	373	217	439
34a	388	362	215	508
38a	371	383	129	459

[a]UV−Vis−NIR spectra measured in 10^{-4} M toluene solutions. [b]Determined by DSC: scan rate= 10 °Cmin^{-1}, N_2 atmosphere; second run. [c]Onset of decomposition determined by TGA: heating rate= 10 °Cmin^{-1}, N_2 atmosphere.

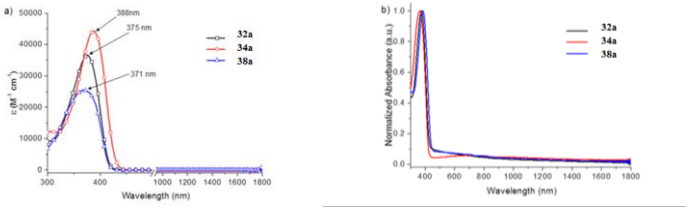

Figure 3.39. Absorption spectra of of the polymers **32**, **34** and **38** in 1×10^{-4} M toluene solutions (a) and thin films (b)

Thermogravimetric analysis (Figure 40a) measurements indicate that polymers **32a**, **34a**, and **38a** start to decompose at temperatures above 400 °C, which is well above operational conditions. A slight weight loss (~2%) at around 100– 200 °C is attributed to the evaporation of trace solvents that remained after purification of the material. Differential scanning calorimetry (DSC, Figure 40b) measurements show that the glass transition temperature (T_g) of **32** and **34a** are at 210°C, whereas the additional methyl groups in **38a** significantly influence the derivatives T_g, lowering it to 129 °C. However, it is still sufficiently above the required temperature of 85 °C for industrial requirements.

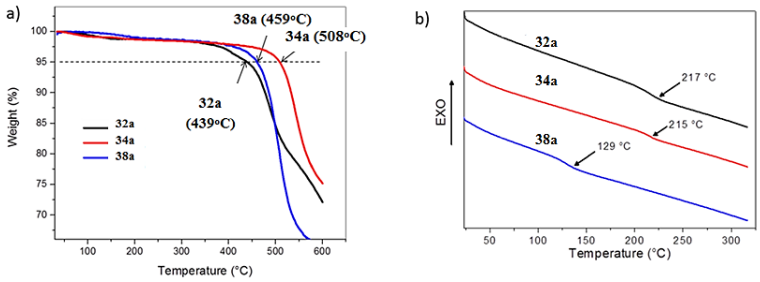

Figure 3.40. a) Thermogravimetric heating curves of **32a**, **34a** and **38a** (heating rate 10 °C min^{-1}) b) Differential scanning calorimetry second heating curves of **32a**, **34a** and **38a** (heating rate 10 °C min^{-1}). Measurements were made at Kaunas University of Technology, Department of Polymer Chemistry and Technology by dr.J.Simokaitienė

3.2.2.3. Ionization potential measurements and application in perovskite solar cell

The solid-state highest occupied molecular orbital (HOMO) levels obtained from the photoemission spectra in air are -5.30, -5.25, and -5.21 eV for **32a**, **34a**, and **38a**, respectively (Figure 41). These HOMO level values are slightly lower than those of *spiro*-OMeTAD (-5.00 eV) and PTAA (-5.16 eV) that are widely used for PSC applications [192-194].

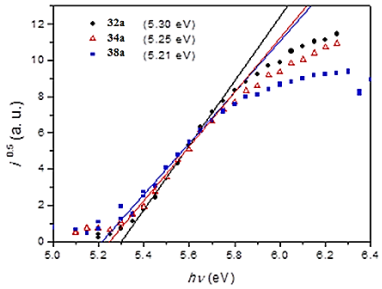

Figure 3.41. Photoemission in air spectra of the investigated HTMs **32a**, **34a** and **38a**. Measurements were made at Vilnius University Department of Solid-state Electronics by dr. V.Gaidelis

To investigate the solar cell performance, the new polymeric HTMs **32a**, **34a**, and **38a** were tested in PSCs without the usual additives or dopants, such as LiTFSI, *t*BP, or tris(2-(1*H*-pyrazol-1-yl)-4-*tert*-butylpyridine)-cobalt(III) tris(bis(trifluoromethylsulfonyl)imide) (CoTFSI). These additives are typically used for increasing hole mobility and conductivity, but may have an adverse effect on the stability of the devices. A device stack of fluorine-doped tin oxide (FTO)/compact TiO_2/mesoporous TiO_2/triple cation perovskite/HTM/Au was used [170]. Figure 42a presents current density–voltage (*J–V*) curves and corresponding open circuit voltage (V_{OC}), short circuit current density (J_{SC}), fill factor (FF), and PCE under AM

1.5G irradiation at 100 $mWcm^{-2}$. All of the new HTMs show respectable PCEs even without the additives.

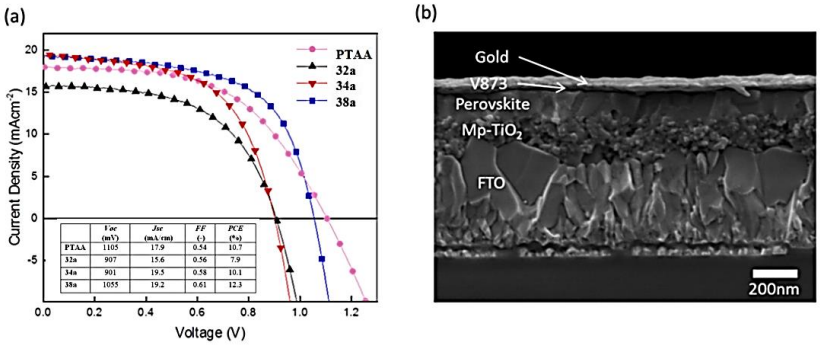

	Voc (mV)	Jsc (mA/cm)	FF (-)	PCE (%)
PTAA	1105	17.9	0.54	10.7
32a	907	15.6	0.56	7.9
34a	901	19.5	0.58	10.1
38a	1055	19.2	0.61	12.3

Figure 3.42. (a) Current density-voltage characteristics for champion devices prepared with PTAA, **32a**, **34a** and **38a** as a HTM. Devices were masked with an aperture of 0.16 cm^2 to define the active area. The curves are recorded with a scan rate of 10 mV s^{-1} from forward bias to short circuit condition. (b) Cross sectional scanning electron microscopy (SEM) image of the device with **38a** (measurement code *V873*). Device was made and measured in EPFL by dr. M.Saliba

In particular, the device based on additive-free **38a** achieved a PCE of 12.3% with a V_{OC} of 1055 mV, a J_{SC} of 19.2 $mAcm^{-2}$, and a *FF* of 0.61, which was better than the device with additive-free PTAA (the most used polymeric HTM in the field). It is noticible, that the additive-free PTAA reaches PCEs of 10.7%, which is one of the highest reported values for this architecture. The optimized concentration of **38a** and PTAA solution is 5 and 10 $mgmL^{-1}$, respectively. Figure 43b shows the cross sectional SEM image of the device with **38a**. The thickness of optimized **38a** is less than 20 nm. The study noticed that **38a** in toluene solution has better wettability on the perovskite film compared with PTAA in toluene solution. Reasearchers speculate that the **38a**/perovskite interface is more beneficial owing to the presence of double bonds that interact with the perovskite absorber, resulting in improved device operation compared with the PTAA/perovskite interface. The study note that LiTFSI and *t*BP, which are often used for chemical oxidation of many other HTMs, do not work for **38a** in the same way. The lower ionization potential of **38a** (-5.21 eV), compared with PTAA (-5.16 eV), could be the reason why **38a** is not oxidized as readily. The device stability under thermal stress was investigated for the created champion additive-free HTM, **38a**. The long-term stability was studied by placing the devices on a hotplate at 85°C in a nitrogen-filled glove box. Figure 43a shows the PCE of the representative devices with **38a** measured at different times; the heating procedure was briefly interrupted for performing a *J*–*V* scan at room temperature.

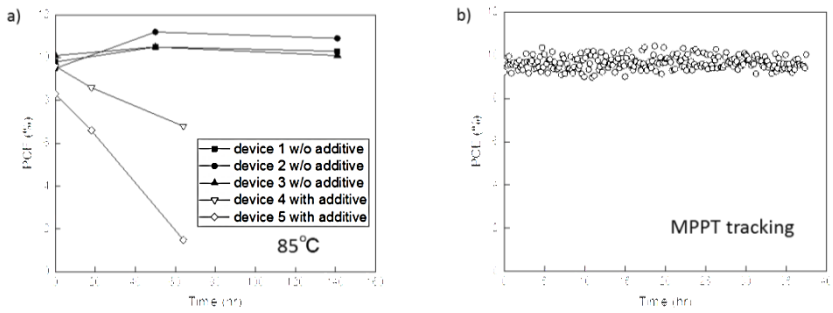

Figure 3.43. a) Thermal stability of 3 independent devices with additive free **38a** and 2 independent devices with additive doped **38**. b) Maximum power point tracking (MPPT) of the device with additive free **38a** under 1 sun illumination. Device was made and measured in EPFL by M.Saliba.

The data reveals that the device with additive-free **38a** is remarkably stable at 85 °C for more than 140 h, with almost no change in the PCE. On the other hand, to investigate the effect of additives for stability, the study conducted the same stability test at 85 °C with **38a** containing LiTFSI and tBP. The concentration of additives is in a similar range to that of PTAA as previously reported [195, 196]. The data reveals that the devices with additive-doped **38a** show a significant degradation at 85 °C, which is strong evidence for the negative effect of additives. In addition, the devices were placed in a nitrogen atmosphere held at room temperature under constant illumination MPPT. The device with additive-free **38a** shows no signs of degradation under 1sun illumination at working conditions for around 40 h. These results indicate that the long-term thermal stability of the devices is highly dependent on the HTM used, shedding light on the importance of interface engineering with additive free HTMs. Researchers note that heat testing is not yet very yet for PSCs and that the study result is one of the few [197-199], indicating the important role of additive-free HTMs towards achieving heat stable perovskite.

Perovskite based solar cells created with polymers bearing 2-phenyl propenyl (**32a**, **38a**) or 2,2-diphenylethenyl groups (**34a**) demonstrated good efficiency and excellent stability. This could be explained by the polymeric HTM coverage on the perovskite surface. The SEM photos of polymer drops on the perovskite surface in Figure 44 demonstrate that the massive substituents possessing double bond influence better compatibility than in the PTAA case, and protect the hybrid organic-inorganic perovskite. In the case of polymer **38a** this angle reaches 4.6°, and in PTAA this angle is higher by 2.7° and reaches 7.3°.

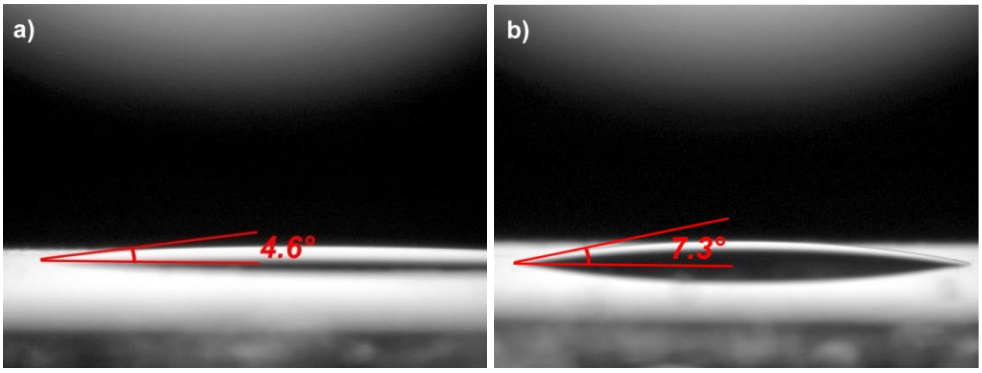

Figure 3.44. SEM photos of contact angle on perovskite surface measurements: a) **38a**, b) **PTAA**

In conclusion, three new polymeric triarylamine derivatives with methyl phenylethenyl and diphenylethenyl functional groups were synthesized and tested as HTMs for the PSC construction. These materials work without any additives, which research shows to be particularly detrimental for PSC stability. Polymer **38a**, bearing poly[bis(4-phenyl)-(3,5-dimethylphenyl)amine] main chain with methyl phenylethenyl fragments attached to it, demonstrates PCE of 12.3% without any additives, which is better than the usually used PTAA. Furthermore, PSCs with **38a** is stable under full sun illumination at MPPT for around 40 h, and under elevated temperature (85 °C) in the dark for more than 140 h. These results indicate that **38a** is a very attractive HTM for highly stable PSCs. More generally, this finding is very promising towards the prospect of commercializing PSCs, because with the astonishing rise in efficiency, the next big step is to demonstrate stability of the PSCs under industrially compatible stress tests.

4. EXPERIMENTAL PART

4.1. Instrumentation

The ^{1}H and ^{13}C NMR spectra were taken from the Varian Unity Inova (300 MHz) and Brucker Avance III (400 MHz) spectrometer at room temperature. The chemical shifts are given in ppm, downfield from tetramethylsilane (TMS, 0 ppm), used as internal standard. Used deuterated solvents are indicated for each compound.

The course of reactions products was monitored by TLC on ALUGRAM SIL, G/UV254 plates and developed with UV light. Silica gel (grade 9385, 230-400 mesh, 60 Ā, Aldrich) was used for column chromatography.

Elemental analysis (C, H and N) was performed with an Exeter Analytical CE-440 elemental analyser.

The UV/Vis spectra were recorded on a Spectronic Genesys 8 or Perkin Elmer Lamba 35 UV/Vis spectrometer in 10^{-4} M solutions of the investigated TM in THF; microcell with an internal width of 1 mm was used.

Infrared (IR) spectra were measured on the Perkin Elmer Spectrum GX FT-IR system spectrometer using KBr pellets. Fluorescence (FL) spectra were recorded with a Hitachi MPF-4 spectrophotometer.

Electrothermal MEL-TEMP capillary melting point apparatus was used for the determination of melting points.

Mass spectra were recorded on a Waters Micromass ZQ 2000 instrument or on an Agilent 1100 series mass spectrometer using direct inlet system.

Cyclic voltammetry (CV) measurements were carried out by a three-electrode assembly cell from Bio-Logic SAS and micro-AUTOLAB Type III potentiostat-galvanostat. The measurements were carried out with glassy carbon electrode in DCM solutions containing 0.1 M tetrabuthylammonium hexafluorophosphate as electrolyte, $Ag/AgNO_3$ as the reference electrode and a Pt wire counter electrode.

Thermal properties were examinated by using a Netzsch STA 409 PC Luxx apparatus under inert atmosphere. The samples were prepared by placing 5 mg of compound into an aluminium sample pan and crimping the upper lid to produce a hermetically sealed sample for DSC testing. During the first heating, the melting points were measured. After melting, the samples were cooled with the same rate. The resulting glasses were heated again under the same conditions to measure the glass transition temperatures. A scan rate for all DSC cycles was 10°C/min.

Thermogravimetric analysis (TGA) data were collected using TGA 4000 from PerkinElmer. Degradation temperatures investigated from 5% weight loss at 10°C/min, N_2 atmosphere.

The charge carrier mobility was measured by the xerographic time of flight method at the Department of Solid State Electronics, Vilnius University. Samples were prepared by casting the solutions of the investigated compounds or mixtures of the investigated compounds with binder material PC-Z (Iupilon Z-200 from Mitsubishi Gas Chemical Co.) at a mass proportion 1:1 in THF. The substrate was polyester film with an Al layer. After coating, the samples were heated at 80°C for 1 h. The hole drift mobility was measured by XTOF technique. Positive corona generated at the layer surface by illumination with pulses of nitrogen laser (pulse

duration was 2 ns, wavelength 337 nm). The layer surface potential decrease as a result of pulse illumination was up to 1-5% of initial potential before illumination. The capacitance probe that was connected to the wide frequency band electrometer measured the speed of the surface potential decrease dU/dt. The transit time t_t was determinated by the kink on the curve of the dU/dt transient in linear or double logarithmic scale. The drift mobility was calculated by the formula $\mu = d^2/U_0 t_t$, where d is the layer thickness, U_0 – the surface potential at the moment of illumination.

The ionization potential (*Ip*) was measured by the electron photoemission in air method and the electron photoemission in air (PESA) method at the Department of Solid State Electronics, Vilnius University. Samples were prepared by dissolving TM in THF or $CHCl_3$ and coating on Al plates precoated with 0.5 μm thick methylmethacrylate and methacrylic acid copolymer sublayer. The thickness of the TM layer was 0.5-1 μm. Usually, ionization potential measurements are carried out in high vacuum, this is one of the main requirements of these measurements. If the vacuum is not high enough, sample surface oxidation and gas adsorbtion are possible and influence the results. In this case, however, the organic materials are stable enough in oxygen and the measurements may be carried out in the air.

Photovoltaic devices with **18** and **22** were made by the following procedure: Conductive FTO glass (NSG10) was sequentially cleaned by sonication in a 2 % Helmanex solution and isopropanol for 15 min each, followed by a 10 min UV-ozone treatment. A 30 nm titania blocking layer was applied on the substrates by spraying a solution of titanium diisopropoxide bis(acetylacetonate) in ethanol at 450 degrees. For the 150 nm mesoporous TiO2 layer, 30 NR-D titania paste from Dyesol diluted in ethanol (150mg/ml) was applied by spin-coating at 4000 rpm for 10s followed by a sintering step at 450 degrees for 30 min. The perovskite layers were fabricated by a single step spin-coating procedure reported by Soek et al. [201] For the perovskite precursor solution, 507 mg of PbI_2 (1.1 mmol) and 159 mg 1 mmol) of CH_3NH_3I were dissolved in 800 μl DMSO. The perovskite solution was spun at 4000 rpm for 30s using a ramp of $2000 rpms^{-1}$. 10 s prior to the end of the spincoating sequence 100 μl chlorobenzene were poured onto the spinning substrate. Afterwards the substrates were transferred onto a heating plate and annealed at 100°C for 1h. The hole-transporting materials were applied from 60 mM and 20 mM solutions in chlorobenzene for spiro and **22** and from a 10 mM solution in a 1 to 1 mixture of chlorobenzene/tetrachloroethane for **18**, respectively. Tert-butylpyridine (Tbp), Tris(2-(1H-pyrazol-1-yl)-4-tert-butylpyridine)cobalt(III) (FK209) and Tris(bis(trifluoromethylsulfonyl) imide) (Li-TFSI) were added as additives. Equimolar amounts of additives were added for all hole-transporters: 330 mol% Tbp, 50 mol% Li-TFSI from a 1.8 M stock solution in acetonitrile and 3 mol% FK209 from a 0.25M stock solution in acetonitrile. The 4 final HTM solutions were spin-coated onto the perovskite layers at 4000 rpm for 20 s. The gold electrodes were fabricated by thermal evaporation of 100 nm gold in high vacuum conditions.

The solar cells were measured using a 450 W xenon light source (Oriel). The spectral mismatch between AM1.5G and the simulated illumination was reduced by the use of a Schott K113 Tempax filter (Präzisions Glas & Optik GmbH). The light intensity was calibrated with a Si photodiode equipped with an IR-cutoff filter

(KG3, Schott), and was recorded during each measurement. Current-voltage characteristics of the cells were obtained by applying an external voltage bias while measuring the current response with a digital source meter (Keithley 2400). The voltage scan rate was 10 mV s^{-1} and no device preconditioning, such as light soaking or forward voltage bias applied for long time, was applied before starting the measurement. The starting voltage was determined as the potential at which the cells furnish 1 mA in forward bias, no equilibration time was used. The cells were masked with a black metal mask (0.16 cm^2) to fix the active area and reduce the influence of the scattered light.

Aging under maximum power point tracking was carried out on masked devices, which were mounted on a temperature controlled plate. The aging was performed under nitrogen atmosphere and 1-sun equivalent illumination provided by an array of white LEDs. The devices were aged by means of keeping them under maximum load under illumination. The maximum power point was updated every 500 s by measuring the current response to a small perturbation in potential. Additionally, a full JV scan was taken every 15 min (at a scan rate of 100 mV s -1 starting from forward bias) which was used to extract the displayed parameters for the aging data.

4.2. Materials

All chemicals were purchased from Aldrich Chemical Co and TCI Europe and used as received without further purification. All solvents were purified using standard procedures as described in [200].

General procedure A

Appropriate carbazole or triphenylamine derivative was dissolved in toluene, phenylacetaldehyde, bis(4-methoxyphenyl)acetaldehyde, bis(4-methylphenyl)acetaldehyde, or 2-phenylpropionaldehyde (1.5 equiv per reactive functional group) and (±)-camphor-10-sulfonic acid (1.0 equiv) were added, and the mixture was refluxed for the indicated time using a Dean-Stark trap. After termination of the reaction (TLC control), the mixture was extracted with toluene. The organic layer was dried over anhydrous $MgSO_4$, filtered, the solvent was removed, and the residue was purified by column chromatography.

General procedure B

3,6-disubsituted carbazole containing benzyl group in the 9^{th} position, was dissolved in DMSO at room temperature, and KO*t*Bu solution (1M in THF, *molar proportion with carbazole 1:10)* was added dropwise. An uncovered flask was stirred for 2 h and water (10 to 1 proportion to organic phase) was added and the suspension was mixed overnight. After this time, the mixture was filtered and precipitate was purified by column chromatography.

General procedure C

Dibromoalkane (1mmol) and 9*H*-3,6-substituted carbazole (2.2 mmol) were dissolved in toluene, an equal volume 40% KOH in water and TBABr was added

and the mixture was stirred in 80°C temperature until termination (TLC control). Organic phase was separated, washed with water and brine, dried on Na_2SO_4, filtered, and solvent was removed. The crude product was purified *via* column chromatography.

3,6-Bis(2,2-diphenylethenyl)-9-ethylcarbazole (1a)

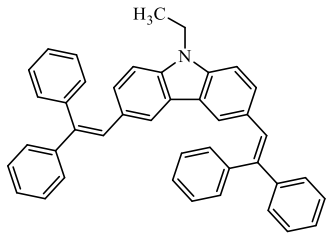

Following general procedure A, a mixture of 9-ethylcarbazole (0.5 g, 2.56 mmol), (+/-)-camphor-10-sulfonic acid (0.59 g, 2.56 mmol), diphenylacetaldehyde (1.51 g, 7.68 mmol) and toluene (15 ml) was refluxed for 3 hours. The product was purified by column chromatography using acetone/*n*-hexane (1/49, *v*/*v*) as an eluent to give **1a** (1.01 g, 72 %) as a bright yellow powder. MS ($APCI^+$, 20 V, m/z): 552 $[M+H]^+$. ^1H NMR (300 MHz, $CDCl_3$, 25°C, TMS): δ= 7.3 (s, 2H, 4,5-H carb.); 7.39-7.21 (m, 20H, 1,2,7,8-H carb. and 2,3,4,5,6-H Ph); 7.13 (s, 2H, =CH-); 7.1-7.05 (m, 4H, 4-H Ph); 4.20-4.13 (m, 2H, $-CH_2-$); 1.34-1.29 (t, 3H, $-CH_3$). ^{13}C NMR (75 MHz, $CDCl_3$, 25°C, TMS): δ= 144.12, 141.23, 140.32, 139.44, 130.86, 129.31, 129.07, 128.84, 128.49, 127.87, 127.73, 127.52, 127.40, 123.02, 121.96, 108.19, 37.87, 14.15. Elemental analysis calcd (%) for $C_{42}H_{33}N$: C 91.43, H 6.03, N 2.54; found: C 91.55, H 6.09, N 2.36.

***3,6-bis[2,2-bis(4-methoxyphenyl)ethenyl]-9-ethylcarbazole (1b*)**

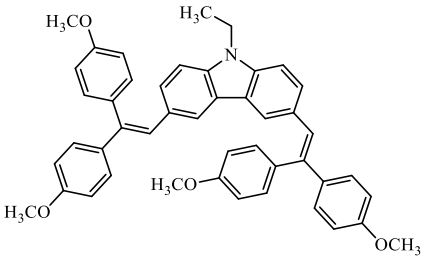

Following general procedure A, a mixture of 9-ethylcarbazole (0.5 g, 2.56 mmol), (+/-)-camphor-10-sulfonic acid (0.59 g, 2.56 mmol), bis(4-methoxyphenyl)acetaldehyde (1.97 g, 7.68 mmol) and toluene (15 ml) was refluxed for 6.5 hours. The product was purified by column chromatography using THF/*n*-hexane (2/23, *v*/*v*) as an eluent to give **1b** (1.08 g, 62 %) as a pale yellow powder. MS ($APCI^+$, 20 V, m/z): 672 $[M+H]^+$. ^1H NMR (300 MHz, $CDCl_3$, 25°C, TMS): δ= 8.02-7.66 (s, 2H, 4,5-H carb.), 7.51-7.42 (m, 2H, 1,8-H carb.), 7.35-6.78 (m, 16H, 2,3,5,6-H 4-CH_3O-Ph); 6.73-6.69 (m, 2H, 2,7-H carb.), 6.65-6.46 (m, 2H, =CH-); 4.46-4.24 (m, 2H, $-CH_2-$); 3.92-3.75 (m, 12H, $-OCH_3$); 1.35-1.27 (m, 3H, CH_3). ^{13}C NMR (75 MHz, $CDCl_3$, 25°C, TMS): δ= 159.06, 158.08, 140.89, 139.85, 139.38, 137.30, 136.92, 135.59, 133.45, 131.90, 130.75, 130.43, 129.16, 128.92, 128.80, 128.74, 128.35, 127.25, 127.12, 126.18, 125.77, 125.42, 114.23, 114.14, 113.65, 113.50, 108.04, 55.43, 55.22, 37.83, 14.09. Elemental analysis calcd (%) for $C_{46}H_{41}NO_4$: C 82.24, H 6.15, N 2.08; found: C 82.42, H 5.97, N 2.15.

3,6-Bis(2,2-diphenylethenyl)-9-isopentyl-9H-carbazole (2a)

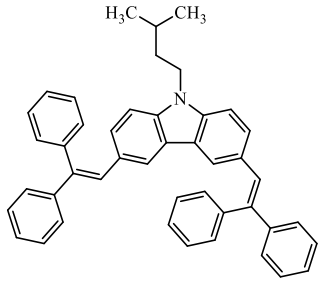

Following general procedure A, a mixture of 9-isopentylcarbazole (0.5 g, 2.1 mmol), (+/-)-camphor-10-sulfonic acid (0.48 g, 2.1 mmol), diphenylacetaldehyde (1.237 g, 6.3 mmol) and toluene (15 ml) was refluxed for 7 hours. The product was purified by column chromatography using dichloromethane/*n*-hexane (1/24, *v*/*v*) as an eluent to give **2a** (0.79 g, 63 %) as a yellow powder. MS (APCI$^+$, 20 V, m/z): 594 $[M+H]^+$. ^{1}H NMR (300 MHz, $CDCl_3$, 25°C, TMS): δ= 7.69-7.63 (m, 2H, 4,5-H carb); 7.52-7.35 (m, 26H, 2,3,4,5,6-Ph, 1,2,7,8-H carb); 7.25 (s, 2H, =CH-); 4.24-4.15 (m, 2H, -N-CH_2-); 1.81-1.62 (m, 3H, -CH-, - CH_2-); 1.10-1.01 (d, 6H, -CH_3). ^{13}C NMR (75 MHz, $CDCl_3$, 25°C, TMS): δ= 144.18, 141.30, 140.34, 139.85, 130.91, 129.36, 129.12, 128.86, 128.53, 127.83, 127.50, 123.03, 121.99, 108.34, 41.74, 37.79, 26.44, 22.89. Elemental analysis calcd (%) for $C_{45}H_{39}N$: C 91.02, H 6.62, N 2.36; found: C 91.00, H 6.69, N 2.31.

3,6-Bis(2,2-bis(4-metoxyphenyl)ethenyl)-9-isopentyl-9H-carbazole (2b)

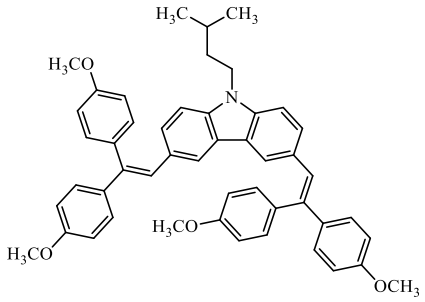

Following general procedure A, a mixture of 9-isopentylcarbazole (0.5 g, 2.1 mmol), (+/-)-camphor-10-sulfonic acid (0.50 g, 2.1 mmol), bis(4-methoxyphenyl)acetaldehyde (1.616 g, 6.3 mmol) and toluene (20 ml) was refluxed for 11 hours. The product was purified by column chromatography using acetone/*n*-hexane (1/9, *v*/*v*) as an eluent to give **2b** (0.67 g, 45 %) as a yellow powder. MS (APCI$^+$, 20 V, m/z): 714 $[M+H]^+$. ^{1}H NMR (400 MHz, $CDCl_3$, 25°C, TMS): δ= 8.11-7.66 (m, 2H, 4,5-H carb.), 7.54-7.53 (m, 2H, 1,8-H carb.), 7.53-6.60 (m, 20H, 2,3,5,6-H 4-CH_3O-Ph, 2,7-H carb, =CH-); 4.43-4.15 (m, 2H, -N-CH_2-), 3.95-3.74 (m, 12H, –OCH_3), 1.93-1.67 (m, 3H, -CH-, -CH_2), 1.15-1.01 (d, 6H, -CH_3). ^{13}C NMR (100 MHz, $CDCl_3$, 25°C, TMS): δ= 158.81, 158.06, 139.31, 137.31, 135.52, 131.80, 130.80, 128.74, 127.16, 126.04, 125.61, 114.23, 113.51, 108.09, 55.44, 55.23, 37.47, 26.32, 22.48. Elemental analysis calcd (%) for $C_{49}H_{47}NO_4$: C 82.44, H 6.64, N 1.96; found: C 82.50, H 6.55, N 1.98.

3,6-Bis(2,2-diphenylethenyl)-9-(2-ethylhexyl)-9H-carbazole (3a)

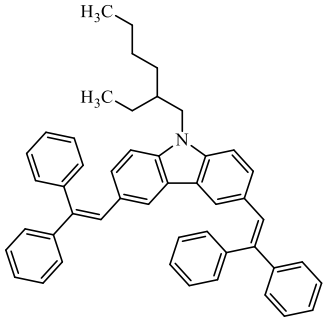

Following general procedure A, a mixture of 9-(2-ethylhexyl)-carbazole (0.5 g, 1.79 mmol), (+/-)-camphor-10-sulfonic acid (0.42 g, 1.79 mmol), diphenylacetaldehyde (1.09 g, 5.37 mmol) and toluene (20 ml) was refluxed for 7 hours. The product was purified by column

chromatography using acetone/*n*-hexane (1/24, *v*/*v*) as an eluent to give **3a** (0.66 g, 62 %) as a yellow powder. MS (APCI$^+$, 20 V, m/z): 636 [M+H]$^+$. ^{1}H NMR (300 MHz, $CDCl_3$, 25°C, TMS): δ= 7.62-7.52 (m, 2H, 4,5-H carb.); 7.48-7.30 (m, 20H, 1,2,7,8-H carb.; 2,3,4,5,6-H Ph); 7.21 (s, 2H, =CH-); 7.17-7.10 (m, 4H, 4-H Ph); 4.20-4.13 (d, J=7,30 Hz, 2H, -N-CH_2); 2.03-1.99 (m, 1H, -CH-); 1.38- 1.29 (m, 8H,-CH_2); 0.97-0.88 (m, 6H, -CH_3). ^{13}C NMR (75 MHz, $CDCl_3$, 25°C, TMS): δ= 140.30, 140.47, 141.25, 130.29, 130.87, 129.52, 127.11, 122.92, 121.83, 108.73, 47.74, 39.61, 31.16, 28.94, 24.56, 23.33, 14.33, 11.15. Elemental analysis calcd (%) for $C_{49}H_{47}N$: C 90.55, H 7.29, N 2.16; found: C 90.36, H 7.45, N 2.19.

3,6-Bis(2,2-bis(4-metoxyphenyl)ethenyl)-9-(2-ethylhexyl)-9H-carbazole (3b)

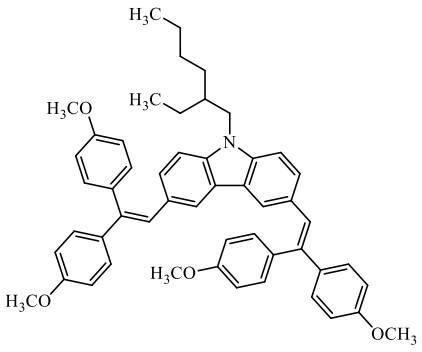

Following general procedure A, a mixture of 9-(2-ethylhexyl)-carbazole (0.5 g, 1.79 mmol), (+/-)-camphor-10-sulfonic acid (0.42 g, 1.79 mmol), bis(4-methoxyphenyl)acetaldehyde (1.38 g, 5.37 mmol) and toluene (20 ml) was refluxed for 8 hours. The product was purified by column chromatography using acetone/*n*-hexane (2/23, *v*/*v*) as an eluent to give **3b** (0.38 g, 28 %) as a yellow powder. MS (APCI$^+$, 20 V, m/z): 756 [M+H]$^+$. ^{1}H NMR (300 MHz, $CDCl_3$, 25°C, TMS): δ= 8.15-7.61 (m, 2H, 4,5-H carb), 7.55-6.57 (m, 22H, 1,8-H carb., 2,3,5,6-H 4-CH_3O-Ph, 2,7-H carb, =CH-), 4.29-4.02 (m, 2H, -N-CH_2), 3.96-3.73 (m, 12H, -OCH_3), 2.19-1.97 (m, 1H, -CH-); 1.53-1.22 (m, 6H, -CH_2), 1.06-0.86 (m, 6H, -CH_3).^{13}C NMR (75 MHz, $CDCl_3$, 25°C, TMS): δ= 158.96, 158.69, 158.50, 157.96, 147.10, 140.80, 139.24, 133.38, 131.97, 131.81, 131.55, 130.68, 130.64, 130.55, 128.95, 128.73, 128.61, 127.17, 125.76, 124.12, 123.21, 114.13, 114.06, 113.84, 113.81, 113.56, 113.53, 113.43, 113.36, 108. 46, 55.34, 55.29, 55.19, 55.13, 47.44, 39.48, 30.96, 28.80, 28.76, 23.10, 14.10, 11.00. Elemental analysis calcd (%) for $C_{52}H_{53}NO_4$: C 82.62, H 7.07, N 1.85; found: C 82.60, H 7.06, N 1.94.

3,6-Bis(2,2-diphenylethenyl)-9-nonyl-9H-carbazole (4a)

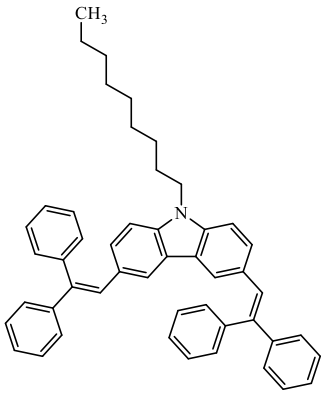

Following general procedure A, a mixture of 9-nonylcarbazole (1.29 g, 4.40 mmol), (+/-)-camphor-10-sulfonic acid (1.02 g, 4.40 mmol), diphenylacetaldehyde (2.59 g, 13.19 mmol) and toluene (15 ml) was refluxed for 1.5 hours. The product was purified by column chromatography using acetone/*n*-hexane (0.2/24.8, *v*/*v*) as an eluent to give **4a** (1.86 g, 65 %) as a pale yellow powder. MS (APCI$^+$, 20 V, m/z): 650 [M+H]$^+$. ^{1}H NMR (400 MHz, $CDCl_3$, 25°C, TMS): δ= 7.53 (s, 2H, 4,5-carb), 7.39–7.23 (m, 20H, Ph, carb), 7.13 (s, 2H, =CH-), 7.09–7.03 (m, 4H, Ph), 4.11 (t, 2H, -N-CH_2-), 1.75

(m, 2H, -CH_2-), 1.35–1.16 (m, 12H, -CH_2-), 0.86 (t, 3H, -CH_3). ^{13}C NMR (100 MHz, $CDCl_3$, 25°C, TMS): δ= 143.87, 140.97, 140.02, 139.68, 130.58, 129.03, 128.77, 128.52, 128.19, 127.09, 122.65, 121.60, 108.12, 43.17, 31.80, 29.44, 29.34, 29.20, 28.96, 27.25, 22.63, 14.09. Elemental analysis calcd (%) for $C_{49}H_{47}N$: C 90.55, H 7.29, N 2.16; found: C 90.51, H 7.38, N 2.11.

9-(tridecan-7-yl)carbazole (5)

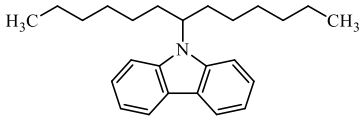

To a solution of carbazole (2 g, 11.96 mmol) and 7-bromotridecane (9.45 g, 35.88 mmol) in DMF (8 ml), anhydrous Na_2SO_4 (1.27 g, 8.97 mmol) and KOH (2.37 g, 35.88 mmol) were added by 3 equal portions. The reaction mixture was stirred at 70°C for 1 hour. After termination of the reaction (TLC control), the mixture was extracted with ethyl acetate. The organic layer was dried over anhydrous Na_2SO_4, filtered, the solvent removed, and the residue was purified by column chromatography using *n*-hexane as an eluent. The yield was 2.82 g (90 %) of white solid **5**. MS (ESI$^+$, m/z): 351 [M+H]$^+$. ^{1}H NMR (400 MHz, $CDCl_3$, 25°C, TMS): δ= 8.15-8.05 (m, 2H, carb), 7.62-7.33 (m, 4H, carb), 7.25-7.12 (m, 2H), 4.65-4.50 (m, 1H, -N-CH-), 2.37-2.17 (m, 2H, -CH_2-), 1.99-1.84 (m, 2H, -CH_2-), 1.33-0.93 (m, 16H, -CH_2-), 0.77 (t, 6H, -CH_3). ^{13}C NMR (100 MHz, $CDCl_3$, 25°C, TMS): δ= 139.01, 125.96, 125.52, 120.81, 120.50, 118.86, 112.01, 109.22, 56.80, 34.19, 32.01, 29.53, 27.24, 22.97, 14.43. Elemental analysis calcd (%) for $C_{25}H_{35}N$: C 85.90, H 10.09, N 4.01; found: C 86.16, H 10.39, N 3.45.

3,6-Bis(2,2-diphenylethenyl)-9-(tridecan-7-yl)-9H-carbazole (5a)

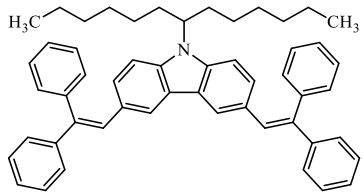

Following general procedure A, a mixture of 9-(tridecan-7-yl)carbazole (1.50 g, 4.29 mmol), (+/-)-camphor-10-sulfonic acid (1.5 g, 6.30 mmol), diphenylacetaldehyde (2.53 g, 12.87 mmol) and toluene (15 ml) was refluxed for 4 hours. The product was purified by column chromatography using acetone/*n*-hexane (0.2/24.8, *v/v*) as an eluent to give **5a** (1.82 g, 60 %) as a yellow powder. MS (ESI$^+$, m/z): 706 [M+H]$^+$. ^{1}H NMR (400 MHz, $CDCl_3$, 25°C, TMS): δ= 7.56 (s, 2H, 4,5-carb), 7.41–7.21 (m, 20H, Ph, carb), 7.12 (s, 2H, =CH-), 7.08–6.97 (m, 4H, Ph, carb), 4.38–4.32 (m, 1H, -N-CH-), 2.22–2.08 (m, 2H, -CH_2-), 1.86–1.77 (m, 8H, -CH_2-), 1.30–1.00 (m, 16H, -CH_2-), 0.85–0.74 (m, 6H, -CH_3). ^{13}C NMR (100 MHz, $CDCl_3$, 25°C, TMS): δ= 143.68, 140.77, 130.54, 129.57, 129.44, 128.80, 128.18, 127.86, 127.74, 127.41, 127.20, 127.05, 108.24, 56.39, 33.62, 31.52, 28.97, 26.68, 22.51, 13.91. Elemental analysis calcd (%) for $C_{53}H_{55}N$: C 90.16, H 7.85, N 1.99; found: C 90.19, H 7.76, N 2.05.

3,6-Bis(2,2-diphenylethenyl)-9-phenyl-9H-carbazole (6a)

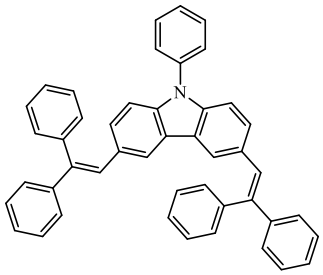

Following general procedure A, a mixture of 9-phenylcarbazole (0.5 g, 2.00 mmol), (+/-)-camphor-10-sulfonic acid (0.48 g, 2.00 mmol), diphenylacetaldehyde (1.178 g, 6.00 mmol) and toluene (20 ml) was refluxed for 10 hours. The product was purified by column chromatography using acetone/*n*-hexane (0.1/24.9, *v*/*v*) as an eluent to give **6a** (0.45 g, 37 %) as pale a yellow powder. MS (APCI$^+$, 20 V, m/z): 600[M+H]$^+$. ^{1}H NMR (300 MHz, $CDCl_3$, 25°C, TMS): δ= 7.52-7.15 (m, 31H, Ph, carb), 7.07 (s, 2H, =CH-),7.03-6.94 (m, 4H, Ph, carb). ^{13}C NMR (75 MHz, $CDCl_3$, 25°C, TMS): δ= 159.12, 158.45, 157.03, 142.86, 141.25, 140.11, 136.93, 136.44, 130.72, 130.11, 129.90, 126.54, 121.95, 120.69, 120.20, 120.05, 117.30, 116.73. Elemental analysis calcd (%) for $C_{46}H_{33}N$: C 92.12, H 5.55, N 2.43; found: C 92.01, H 5.93, 1.06.

9-(p-Metoxyphenyl)carbazole (7)

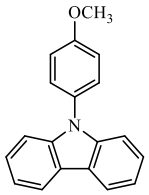

The mixture of carbazole (6.0 g, 35.9 mmol), 4-methoxyiodobenzene (10.51 g 44.9 mmol), copper (2.85 g, 44.9 mmol), 18-crown-6 (1.186 g, 4.49 mmol) and K_2CO_3 (7.44 g, 53.8 mmol) in *o*-dichlorobenzene (40 ml) was purged with argon for 20 min. The reaction mixture was then refluxed for 17 hours, and afterwards filtered to separate the residues of copper and basis. The product has crystallized in the filtrate and was filtered, washed with hexane and recrystallized from 2-propanol to yield 8.93 g (78%) of white crystals. MS (APCI$^+$, 20 V, m/z): 274 [M+H]$^+$. ^{1}H NMR (300 MHz, $CDCl_3$, 25°C, TMS): δ=8.45-8.38 (m, 2H, carb); 8.16-8.04 (m, 2H, carb), 7.39-7.28 (m, 4H, Ar), 7.14-7.02 (m, 4H, Ar), 3.82 (s, 3H, -OCH_3). Elemental analysis calcd (%) for $C_{19}H_{15}NO$: C 83.49, H 5.53, N 5.12; found: C 83.96, H 5.47, N 5.07.

3,6-Bis(2,2-bis(4-metoxyphenyl)ethenyl)-9-(4-metoxyphenyl)-9H-carbazole (7b)

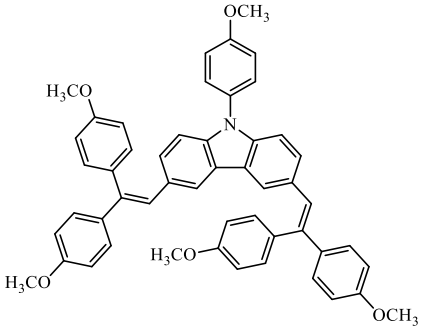

Following general procedure A, a mixture of 9-(*p*-methoxyphenyl)carbazole (0.5 g, 1.83 mmol), (+/-)-camphor-10-sulfonic acid (0.43 g, 1.83 mmol), bis(4-methoxyphenyl)acetaldehyde (1.41 g, 5.49 mmol) and toluene (20 ml) was refluxed for 17 hours. The product was purified by column chromatography using acetone/*n*-hexane (2/23, *v*/*v*) as an eluent to give **7b** (0.34 g, 25 %) as a bright yellow powder. MS (APCI$^+$, 20 V, m/z): 750 [M+H]$^+$. ^{1}H NMR (300 MHz, $CDCl_3$, 25°C, TMS): δ= 8.00-6.58 (m, 26H, Ar, =CH-); 4.13-3.35 (m, 15H, -OCH_3). ^{13}C NMR (75 MHz, $CDCl_3$, 25°C, TMS): δ= 159.02, 158.12, 156.98, 142.60, 141.57, 140.16, 136.78, 136.43, 130.92, 130.13, 129.13, 126.82,

121.95, 120.99, 120.77, 120.35, 117.42, 116.37, 56.28, 55.96, 55.45, 55.18. Elemental analysis calcd (%) for $C_{51}H_{43}NO_5$: 81.68, H 5.78, N 1.87; found: C 81.50, H 5.78, N 1.95.

9-benzyl-9H-carbazole (Bn-Cbz)

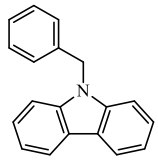

5 g of *N*-carbazole (29.9 mmol) was dissolved in 35 ml toluene, 40 ml 12M NaOH solution in water, 1.2 g tetrabutylamonnium bromide (3.7 mmol) and 4.25 ml benzyl bromide (35.8 mmol) were added and the mixture was stirred for 2h at room temperature. The reaction mixture was extracted with ethyl acetate, dried on $NaSO_4$. After evaporation, the resin was crystalized using acetone/*n*-hexane (1:1) as solvent. 7.0 g white crystals were obtained (91%). ^{1}H NMR (400 MHz, $CDCl_3$, 25°C, TMS): δ= 8.10 (d, J = 7.8 Hz, 2H, 4,5H-carb.), 7.42 – 7.35 (m, 2H, Ph), 7.31 (d, J = 8.2 Hz, 2H, Ph), 7.26 – 7.16 (m, 5H, Ph), 7.12 – 7.06 (m, 2H, Ph), 5.43 (s, 2H, -CH_2-). ^{13}C NMR (101 MHz, $CDCl_3$, 25°C, TMS): δ= 140.76, 137.28, 128.85, 127.53, 126.50, 125.95, 123.13, 120.49, 119.31, 109.00, 46.60.

9-benzyl-3,6-bis(2,2-diphenylvinyl)-9H-carbazole (8a)

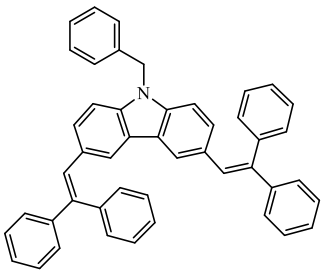

Following general procedure A, 3g Bn-Cbz (11.65 mmol) was dissolved in 15ml toluene, 2.71 g CSA (11.65 mmol) and 6.86 g diphenylacetaldehyde (34.9 mmol) were added and refluxed for 3 h. The product was purified by column chromatography with acetone: *n*-hexane (1:4, *v:v*) and recrystalized from ethyl ether yielded 5.51 g (77%). ^{1}H NMR (400 MHz, DMSO, 25°C, TMS): δ= 7.48 – 7.39 (m, 10H, Ph, carb.), 7.39 – 7.28 (m, 12H, Ph, carb.), 7.23 – 7.16 (m, 8H, Ph), 7.14 – 7.10 (m, 2H, Ph), 7.07 (s, 2H, =CH-), 5.51 (s, 2H, -CH_2-).^{13}C NMR (101 MHz, DMSO), δ, ppm: 143.32, 140.88, 139.90, 137.98, 130.32, 129.52, 128.86, 128.11, 127.74, 127.28, 122.41, 121.33, 109.67, 46.07.

9-benzyl-3,6-bis(2,2-bis(4-methoxyphenyl)vinyl)-9H-carbazole (8b)

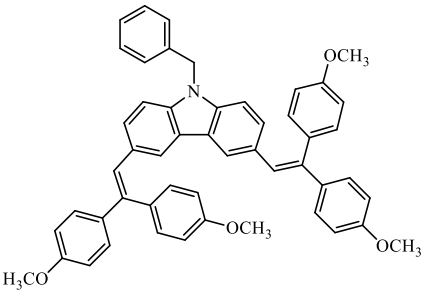

Following general procedure A, mixture of 1 g Bn-Cbz **(**3.886 mmol), 0.9 g CSA (3.886 mmol), 2.99 g bis(4-methoxyphenyl)acetaldehyde (1.166 mmol) in 15ml toluene, was stirred for 5 h in reflux (TCL control). Solvent was evaporated and compound was purified using chromatographic column. ^{1}H NMR (400 MHz, $CDCl_3$): δ= 7.72 (s, 2H, 4,5H-carb), 7.24 (m, 4H, Ph), 7.23 – 7.20 (m, 3H, Ph), 7.18 – 7.14 (m, 12H, Ar), 7.11 – 7.00 (m, 6H, Ar), 6.97 (s, 1H, =CH-), 6.95 (s, 1H, =CH-), 5.31 (s, 2H, -CH_2-), 3.84 (s, 6H, -OCH_3), 3.82 (s, 6H, -OCH_3). ^{13}C NMR (101 MHz,

$CDCl_3$): δ= 142.20, 141.04, 140.73, 139.12, 138.30 – 137.62, 131.45, 129.67, 128.02, 127.91, 127.62 – 127.51, 126.40, 122.35, 121.47, 107.11, 55.15, 55.30, 45.15.

9-benzyl-3,6-bis(2,2-di-p-tolylvinyl)-9H-carbazole (8c)

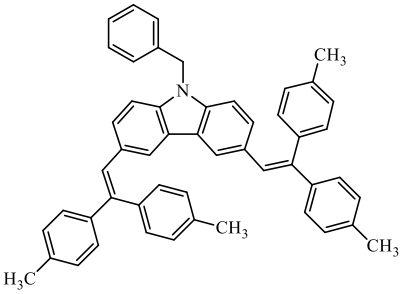

Following general procedure A, mixture of 2 g (7.77 mmol), Bn-Cbz 1.8 g (7.77 mmol) CSA, 5.23 g (23.31 mmol) bis(4-methylphenyl)acetaldedhyde in 15 ml toluene was stirred for 3 h. After termination (TLC control), the mixture was diluted with ethyl acetate and washed with water and brine. The organic part was dried on Na_2SO_4 and filtered. Solvent was evaporated and compound was purified using chromatographic column (acetone: *n*-hexane, 1:9, *v:v*). ^{1}H NMR (400 MHz, $CDCl_3$): δ= 7.57 (s, 2H, 4,5H-carb), 7.24 (t, *J* = 7.5 Hz, 4H, Ph), 7.22 – 7.17 (m, 3H, Ar), 7.16 – 7.09 (m, 12H, Ar), 7.08 – 7.01 (m, 6H, Ar), 6.99 (s, 1H, =CH-), 6.97 (s, 1H, =CH-), 5.29 (s, 2H, -CH_2-), 2.37 (s, 6H, -CH_3), 2.35 (s, 6H, -CH_3). ^{13}C NMR (101 MHz, $CDCl_3$), δ, ppm: 141.30, 140.14, 139.81, 138.04, 137.10 – 136.72, 130.42, 129.43, 128.86, 127.89, 127.75 – 127.31, 126.40, 122.96, 121.70, 108.41, 46.60, 21.42, 21.20.

3,6-bis(2,2-diphenylvinyl)-9H-carbazole (9a)

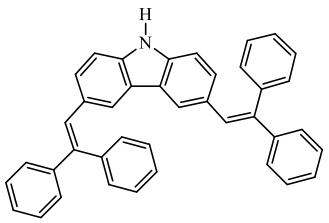

Following general procedure B, 0.5 g (0.81 mmol) **8a** was dissolved in 20 ml dry DMSO, 10 ml 1M *t*-BuOK in THF were added and the reaction was stirred for 2 h in RT in an open flask. 100 ml of H_2O was added and the mixture was stirred overnight. Yellow precipitate were filtrated and purified *via* column chromatography with THF: *n*-hexane (1:4, *v:v*). 0.4 g light yellow crystals were obtained (94%). ^{1}H NMR (400 MHz, Acetone): δ= 10.31 (s, 1H, NH), 7.56 (s, 2H, 4,5H-carb.), 7.46 – 7.33 (m, 22H, Ar), 7.10 (s, 2H, -CH=). ^{13}C NMR (101 MHz, Acetone): δ=143.73, 141.09, 139.93, 139.43, 139.35, 130.34, 128.91, 128.64, 128.21, 127.76, 127.17, 122.90, 121.17, 110.32.

3,6-bis(2,2-bis(4-methoxyphenyl)vinyl)-9H-carbazole (9b)

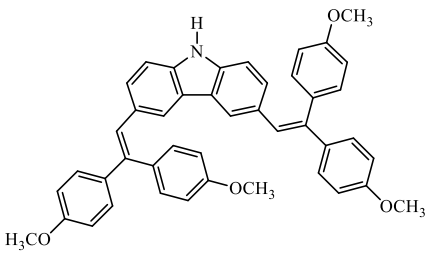

Following general procedure B, 1g **8b** (1.36 mmol) dissolved in 20ml DMSO, reacted with 14 ml 1M *t*-BuOK in THF. After addition of water and overnight stirring, the mixture was filtrated and precipitate was purified by column chromatography (acetone: *n*-hexane, 1:4, *v:v*). 0.85g (93% yield) of

yellow material was obtained. ^{1}H NMR (400 MHz, Acetone): δ= 11.35 (s, 1H, NH), 7.59 (s, 2H, 4,5H-carb.), 7.52 – 7.27 (m, 20H, Ar), 7.02 (s, 2H, =CH-), 3.57 (s, 6H, -OCH_3), 3.37 (s, 6H, -OCH_3). ^{13}C NMR (101 MHz, DMSO): δ= 131.59, 130.80, 129.44, 128.60, 127.32, 114.86, 114.65, 114.01, 113.18, 67.49, 66.82, 55.52.

3,6-bis(2,2-di-p-tolylvinyl)-9H-carbazole (9c)

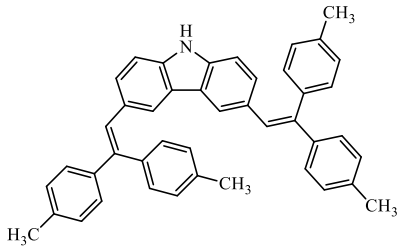

Following general procedure B, 1g **8c** (1.49 mmol) was dissolved in 20ml DMSO, reacted with 15 ml 1M KO*t*Bu in THF. After the addition of water and overnight stirring, the mixture was filtrated and precipitate was purified by column chromatography (acetone: *n*-hexane, 1:4, *v:v*). 0.79g (92% yield) of yellow material **9c** was obtained. ^{1}H NMR (400 MHz, $CDCl_3$): δ= 7.83 (s, 1H, -NH), 7.54 (s, 2H, 4,5H-carb), 7.29 –7.05 (m, 20H, Ar), 6.97 (s, 2H, =CH-), 1.44 (s, 3H, -CH_3), 1.27 (s, 3H, -CH_3). ^{13}C NMR (101 MHz, $CDCl_3$): δ= 141.25, 140.27, 138.52, 137.95, 136.85, 130.44, 129.47, 128.90, 127.92, 127.52, 123.24, 121.54, 109.94, 21.37, 21.16.

3,6,9-tris(2,2-diphenylvinyl)-9H-carbazole (10a)

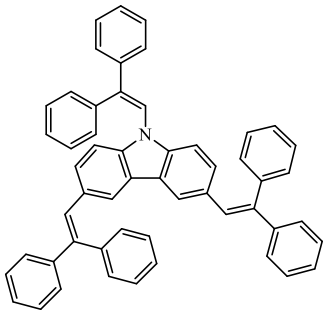

Following general procedure A, 0.4 g (0.7638 mmol) 3,6-bis(2,2-diphenylvinyl)-9*H*-carbazole **9a** reacted with 0.2245g (1.1457 mmol) diphenylacetaldehyde in the presence of 0.1772g (0.7638 mmol) (+/-) camphor-sulphonic acid. After 15min reaction the mixture was extracted with ethyl acetate, evaporated and the resin was purified by column chromatography. ^{1}H NMR (400 MHz, $CDCl_3$), δ, ppm: 7.44 (s, 2H, 4,5-carb), 7.38 – 7.26 (m, 22H, Ar), 7.21 (dt, J = 6.0, 3.2 Hz, 4H, Ar), 7.10 – 7.01 (m, 6H, Ar), 7.01 – 6.95 (m, 2H, Ar), 6.87 (s, 3H, -CH=). ^{13}C NMR (101 MHz, $CDCl_3$), δ, ppm: 143.76, 140.67, 138.66, 130.52, 129.84, 129.43, 128.77, 128.27, 127.77, 127.49, 127.22, 123.48, 121.04, 120.29, 110.04.

3,6,9-tris(2,2-bis(4-methoxyphenyl)vinyl)-9H-carbazole (10b)

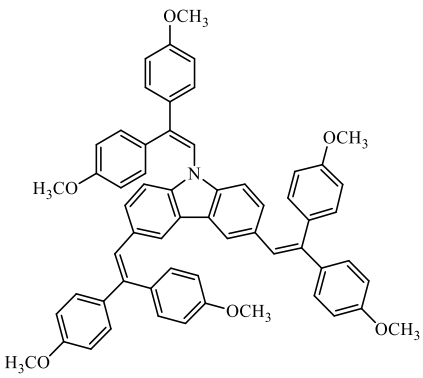

Following general procedure A, 0.1 g (0.1479mmol) 3,6-bis(2,2-bis(4-methoxyphenyl)vinyl)-9*H*-carbazole (**9b**) reacted with 0.056 g (0.2218 mmol) bis(4-methoxyphenyl)acetaldehyde in the presence of 0.1479 mmol (+/-) camphor-sulphonic acid. After 3 min reaction the

mixture was extracted with ethyl acetate, evaporated and the resin was purified by column chromatography. ^{1}H NMR (400 MHz, $CDCl_3$): δ= 7.46 (s, 2H, 4,5H-carb.), 7.30 – 7.20 (m, 6H, Ar), 7.19 – 7.05 (m, 12H, Ar), 7.04 – 6.94 (m, 6H, Ar), 6.93 – 6.80 (m, 7H, Ar, -CH=), 2.38 (s, 9H, -OCH_3), 2.36 (s, 9H, -OCH_3). ^{13}C NMR (101 MHz, DMSO): δ= 159.01, 131.54, 131.03, 130.30, 130.11, 128.53, 114.82, 114.31, 114.24, 113.54, 55.81, 55.17.

3,6,9-tris(2,2-di-p-tolylvinyl)-9H-carbazole (10c)

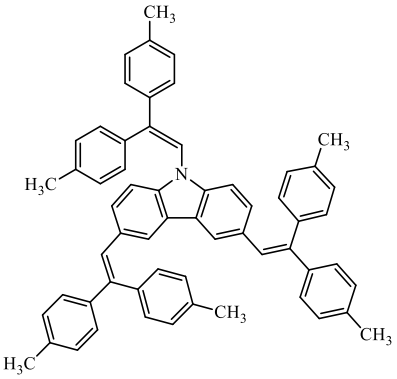

Following general procedure A, 0.2 g (0.3449mmol) 3,6-bis(2,2-bis(4-methylphenyl)vinyl)-9*H*-carbazole (**9c**) reacted with 0.116 g (0.5173 mmol) bis(4-methoxyphenyl)acetaldehyde in the presence of 0.080 g (0.3449 mmol) (+/-) camphor-sulphonic acid. After 10 min reaction the mixture was extracted with ethyl acetate, evaporated and the resin was purified by column chromatography. ^{1}H NMR (400 MHz, $CDCl_3$): δ= 7.46 (s, 2H, 4,5-carb), 7.30 – 7.20 (m, 6H, Ar), 7.19 – 7.05 (m, 12H, Ar), 7.04 – 6.94 (m, 6H, Ar), 6.93 – 6.80 (m, 7H, Ar, -C<u>H</u>=), 2.38 (s, 9H, -CH_3), 2.36 (s, 9H, -CH_3). ^{13}C NMR (101 MHz, $CDCl_3$): δ= 141.25, 140.32, 139.87, 138.75, 137.97, 137.41, 136.84, 135.32, 130.39, 129.94, 129.36, 128.99, 128.78, 127.83, 127.46, 123.47, 121.09, 119.34, 110.04, 21.27.

1,3-di(9H-carbazol-9-yl)propane (11)

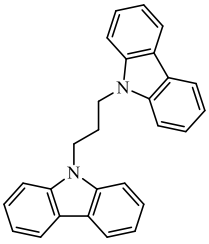

Following general procedure C, 10g (59.80mmol) 9*H*-carbazole and 5.75g (28.48 mmol) 1,3-dibromopropane was dissolved in 25 ml toluene/ 50ml 40% KOH in a water mixture, 0.01g TBABr was added and this mixture was stirred at 80 °C for 48h. After extraction with toluene, the crude product was purified *via* crystallization from THF: EtOH, 1:1, v:v. 9.8g (92.1%) of white crystals was obtained. ^{1}H NMR (400 MHz, DMSO): δ= 8.14 (d, J = 7.7 Hz, 4H carb.), 7.38 (dd, J = 11.3, 4.1 Hz, 4H, carb.), 7.63 – 6.91 (m, 4H, carb), 7.18 (t, J = 7.4 Hz, 4H, carb.), 4.48 (t, J = 7.4 Hz, 4H, -N-CH_2-), 3.41 (s, 2H, -CH_2-). ^{13}C NMR (101 MHz, DMSO): δ= 140.28, 126.19, 122.62, 120.84, 119.31, 109.44, 28.11.

1,6-di(9H-carbazol-9-yl)hexane (12)

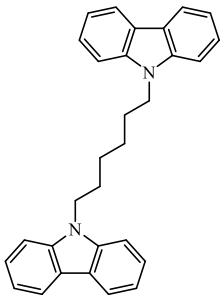

Following general procedure C, 2g (11.96 mmol) 9*H*-carbazole and 1.326 g (5.436 mmol) 1,6-dibromohexane was dissolved in 10.4 ml toluene/20 ml 40% KOH in a water mixture, 0.01 g TBABr was added and this mixture was stirred at 80 °C for 12h. After extraction with toluene, the crude product was purified *via* column chromatography

(THF: *n*-hexane, 1:4, *v:v*). 1.9 g (84%) of white crystals was obtained. ^{1}H NMR (400 MHz, $CDCl_3$): δ= 8.05 (d, *J* = 7.8 Hz, 4H, carb.), 7.43 – 7.35 (m, 4H, carb.), 7.25 (d, *J* = 8.2 Hz, 4H, carb.), 7.18 (t, *J* = 7.4 Hz, 4H, carb.), 4.12 (t, *J* = 7.1 Hz, 4H, N-CH_2-), 1.88 – 1.58 (m, 4H, -CH_2-), 1.33 – 1.20 (m, 4H, -CH_2-). ^{13}C NMR (101 MHz, $CDCl_3$): δ= 140.44, 125.70, 122.90, 120.45, 118.86, 108.69, 42.82, 28.85, 27.09.

1,9-di(9H-carbazol-9-yl)nonane (13)

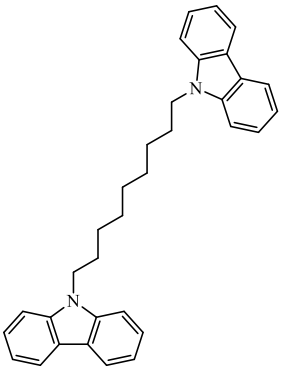

Following general procedure C, 10g (59.80 mmol) 9*H*-carbazole and 8.97 g (29.90 mmol) 1,9-dibromononane was dissolved in 25 ml toluene/ 50 ml 40% KOH in a water mixture, 0.01 g TBABr was added and this mixture was stirred at 80 °C for 24h. After extraction with toluene, the crude product was recrystallized from THF: *n*-hexane, 1:1, *v:v*). 13.1g of pure product was obtained (91%). ^{1}H NMR (400 MHz, $CDCl_3$): δ= 8.08 (d, *J* = 7.8 Hz, 4H, carb.), 7.46 – 7.39 (m, 4H, carb.), 7.35 (d, *J* = 8.2 Hz, 4H, carb.), 7.24 – 7.14 (m, 4H, carb.), 4.22 (t, *J* = 7.2 Hz, 4H, -N-CH_2-), 1.93 – 1.73 (m, 4H, -CH_2-), 1.50 – 0.98 (m, 10H, -CH_2-). ^{13}C NMR (101 MHz, $CDCl_3$): δ= 140.48, 125.62, 122.86, 120.40, 118.76, 108.71, 43.06, 29.34, 28.97, 27.27.

1,3-bis(3,6-bis(2,2-diphenylvinyl)-9H-carbazol-9-yl)propane (14a)

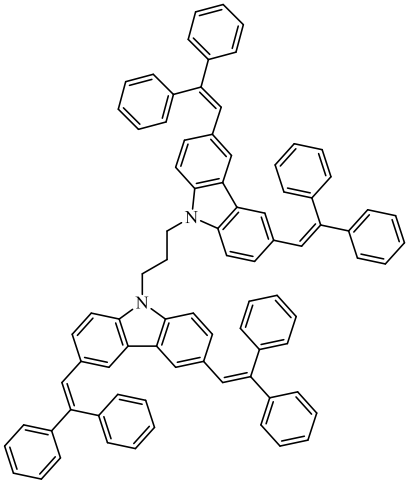

Following general procedure C, 3,6-bis(2,2-diphenylvinyl)-9*H*-carbazole (**9a**) and 1,3-dibromopropane was dissolved in toluene/40% KOH in a water mixture, TBABr was added and this mixture was stirred at 80 °C for 12h. After extraction with toluene, the crude product was purified *via* column chromatography (THF:hexane, 1:25, *v:v*). ^{1}H NMR (400 MHz, $CDCl_3$): δ= 7.50 (s, 4H, 4,5-carb), 7.40 – 7.21 (m, 40H, Ar), 7.11 (s, 4H, -CH=), 7.00 (dd, *J* = 8.6, 1.0 Hz, 4H), 6.82 (d, *J* = 8.6 Hz, 4H), 4.09 (t, 4H, -N-CH_2-), 2.29 – 2.21 (m, 2H, -CH_2-). ^{13}C NMR (101 MHz, $CDCl_3$): δ= 143.78, 140.85, 140.42, 139.30, 130.57, 128.91, 128.25, 127.77, 127.34, 122.85, 121.69, 107.86, 40.62, 27.91.

1,3-bis(3,6-bis(2,2-bis(4-methoxyphenyl)vinyl)-9H-carbazol-9-yl)propane (14b)

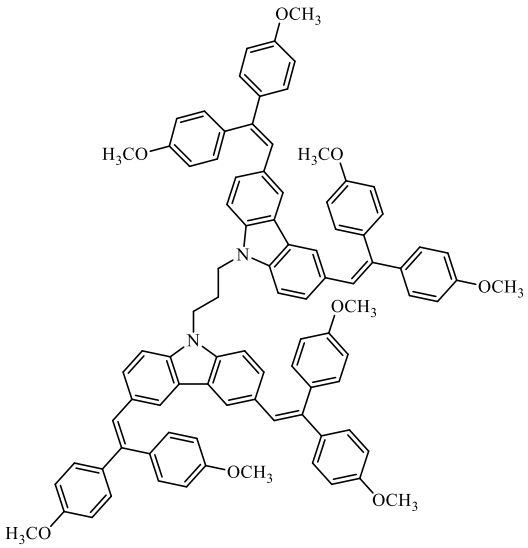

Following general procedure C, 3,6-bis-(2,2-bis(4-methoxyphenyl)vinyl)-9*H*-carbazole (**9b**) and 1,3-dibromopropane was dissolved in toluene/40% KOH in a water mixture, TBABr was added and this mixture was stirred at 80 °C for 12h. After extraction with toluene, the crude product was purified *via* column chromatography (THF:hexane, 1:25, *v:v*). ^{1}H NMR (400 MHz, $CDCl_3$): δ= 7.34 (s, 4H, 4,5-carb), 7.20-7.04 (m, 40H, Ar), 6.90 (s, 4H, -CH=C-), 4.03 (t, 4H, -N-CH_2-), 3.88- 3.67 (m, 24H, -OCH_3), 2.28 – 2.22 (m, 2H, -CH_2-). ^{13}C NMR (101 MHz, $CDCl_3$): δ= 157.99, 131.72, 130.62, 128.64, 114.14, 113.47, 55.22.

1,6-bis(3,6-bis(2,2-diphenylvinyl)-9H-carbazol-9-yl)hexane (15a)

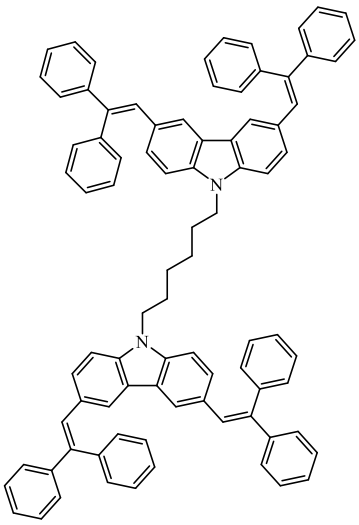

Following general procedure C, 3,6-bis(2,2-diphenylvinyl)-9*H*-carbazole (**9a**) and 1,6-dibromohexane was dissolved in toluene/40% KOH in a water mixture, TBABr was added and this mixture was stirred at 80 °C for 12h. After extraction with toluene, the crude product was purified *via* column chromatography (THF:hexane, 1:25, *v:v*). ^{1}H NMR (400 MHz, $CDCl_3$): δ= 7.50 (s, 4H, 4,5-carb), 7.39 – 7.21 (m, 40H, Ar), 7.11 (s, 4H, =CH-), 7.04 (dd, J = 8.6, 1.4 Hz, 4H), 6.96 (d, J = 8.6 Hz, 4H), 4.03 (t, J = 6.9 Hz, 4H), 1.67 (s, 4H), 1.24 (d, J = 9.8 Hz, 4H). ^{13}C NMR (101 MHz, $CDCl_3$): δ= 143.83, 140.95, 140.13, 139.59, 130.58, 128.79, 128.22, 127.54, 127.19, 122.66, 121.60, 108.06, 42.86, 28.79, 26.95.

1,6-bis(3,6-bis(2,2-bis(4-methoxyphenyl)vinyl)-9H-carbazol-9-yl)hexane (15b)

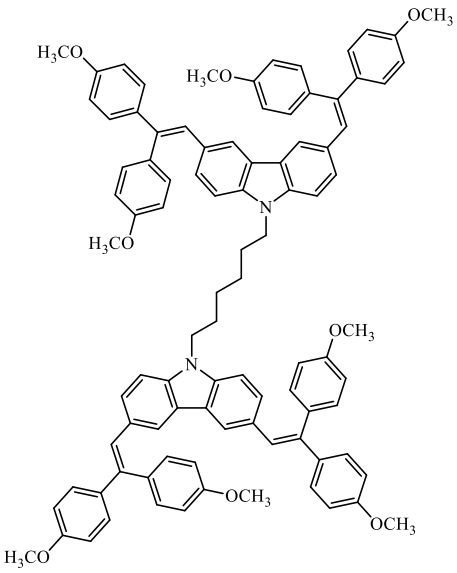

Following general procedure C, 3,6-bis(2,2-bis(4-methoxyphenyl)vinyl)-9*H*-carbazole (**9b**) and 1,6-dibromohexane was dissolved in toluene/40% KOH in a water mixture, TBABr was added and this mixture was stirred at 80 °C for 12h. After extraction with toluene, the crude product was purified *via* column chromatography (THF:hexane, 1:25, *v:v*). ^{1}H NMR (400 MHz, $CDCl_3$): δ= 7.50 (s, 4H, 4,5-carb), 7.05 – 6.78 (m, 44H, Ph, -CH=C-), 4.43 – 4.05 (m, 4H, -N-CH_2-), 3.82 (s, 12H, -OCH_3), 3.73 (s, 12H, -OCH_3), 1.83-1.79 (m, 4H, -CH_2-), 1.69 – 1.49 (m, 4H, -CH_2-). ^{13}C NMR (101 MHz, $CDCl_3$); δ= 158.80, 157.96, 131.75, 130.62, 128.69, 114.12, 113.45, 55.48, 54.97, 43.03, 27.69, 27.02.

1,9-bis(3,6-bis(2,2-diphenylvinyl)-9H-carbazol-9-yl)nonane (16a)

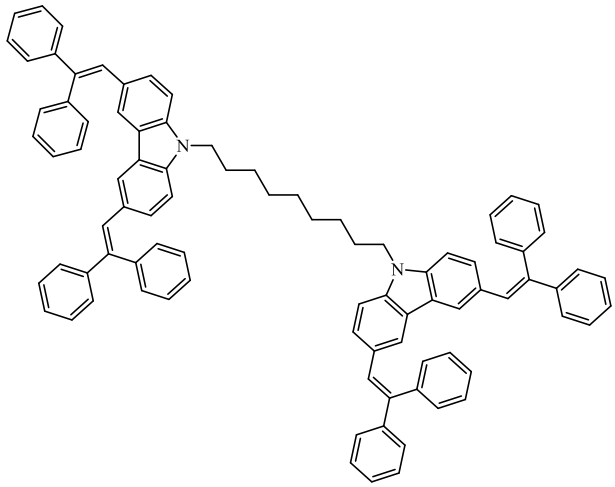

Following general procedure C, 3,6-bis(2,2-diphenylvinyl)-9*H*-carbazole (**9a**) 0.5 g (0.954 mmol) reacted with 0.124 g (0.433mmol) 1,9-dibromononane in 5 ml toluene in the presence of 5ml 40% aqueous KOH for 48 h. After workup procedure, 0.42 g (82%) of yellow powder was obtained. ^{1}H NMR (400 MHz, $CDCl_3$): δ= 7.52 (s, 4H, 4,5H-carb), 7.34 (tt, *J* = 9.5, 4.7 Hz, 28H, Ar), 7.29 – 7.22 (m, 14H, Ar), 7.11 (s, 4H, =CH-), 7.08 – 7.01 (m, 8H, Ar), 4.07 (t, *J* = 7.1 Hz, 4H, N-C$\underline{H_2}$-), 1.77 – 1.67 (m, 4H, -CH_2-), 1.21 (m, 10H, -CH_2-). ^{13}C NMR (101 MHz, $CDCl_3$): δ= 143.86, 140.98, 140.06, 139.67, 130.59, 129.01, 128.79, 128.56, 128.22, 127.51, 127.18, 122.67, 121.64, 108.12, 43.11, 29.23, 28.93, 27.15.

1,9-bis(3,6-bis(2,2-bis(4-methoxyphenyl)vinyl)-9H-carbazol-9-yl)nonane (16b)

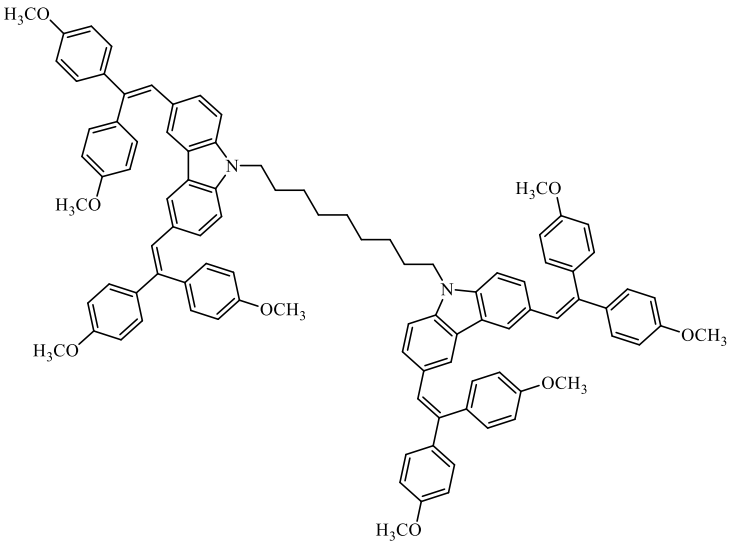

Following general procedure C, 3,6-bis(2,2-bis(4-methoxyphenyl)vinyl)-9*H*-carbazole (**9b**) and 1,3-dibromopropane was dissolved in toluene/40% KOH in a water mixture, TBABr was added and this mixture was stirred at 80 °C for 12h. After extraction with toluene, the crude product was purified *via* column chromatography (THF:hexane, 1:25, *v:v*). ^{1}H NMR (400 MHz, $CDCl_3$): δ= 7.43 (s, 4H, 4,5-carb), 7.20 – 6.88 (m, 44H, Ph, -CH=C-), 4.43 – 4.05 (m, 4H, -N-CH_2-), 3.81 (s, 12H, -OCH_3), 3.72 (s, 12H, -OCH_3), 1.76 – 1.65 (m, 4H, -CH_2-), 1.22-1.16 (m, 10H, -CH_2-).^{13}C NMR (101 MHz, $CDCl_3$): δ= 158.80, 157.96, 131.75, 130.62, 128.69, 114.12, 113.45, 55.48, 54.97, 43.07, 29.21, 28.92, 27.13, 21.36, 21.13.

1,9-bis(3,6-bis(2,2-bis(4-methylphenyl)vinyl)-9H-carbazol-9-yl)nonane (16c)

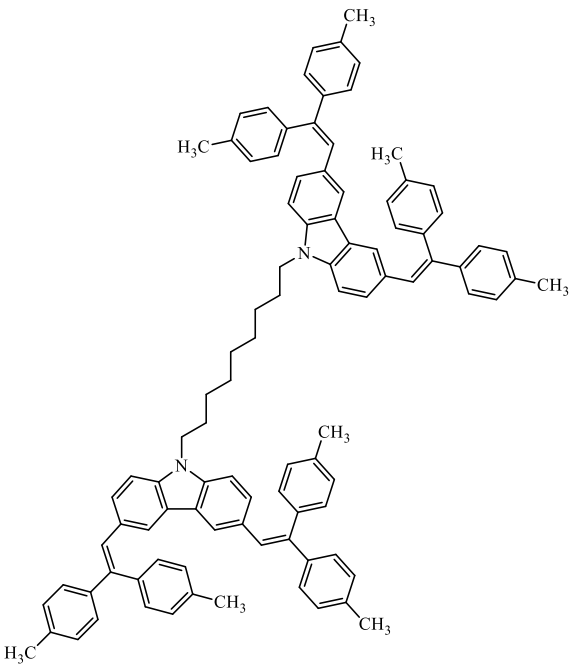

Following general procedure C, 3,6-bis(2,2-bis(4-methylphenyl)vinyl)-9*H*-carbazole (**9c**) and 1,9-dibromononane was dissolved in toluene/40% KOH in a water mixture, TBABr was added and this mixture was stirred at 80 °C for 12h. After extraction with toluene, the crude product was purified via column chromatography (THF:hexane, 1:25, *v:v*). ^{13}C NMR (101 MHz, $CDCl_3$): δ= 141.27, 139.86, 139.51, 138.03, 136.74, 130.39, 129.42, 128.82, 127.93, 127.31, 122.65, 121.62, 108.04, 43.07, 29.21, 28.92, 27.13, 21.36, 21.13.

5,11-dihydroindolo[3,2-b]carbazole (17)

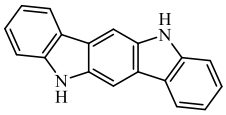

3.7 g (0.02 mol) 3,3′-bisindolylmethane and 2.46 ml triethoxymethane were mixed in 70 ml MeOH at RT. Then the mixture was heated for 15 min at 130°C. After cooling down, the light yellow crystals were filtrated and washed with MeOH. Yield 2.3g (60%). ESI-QTOF-MS: [M] 256.1001, [M+H] 257.1079, [M+2] 258.1115. ^{1}H NMR (400 MHz, DMSO): δ= 11.03 (s, 2H, NH), 8.21- 8.19 (d, 2H, Ph), 8.12 (s, 2H, 6^{th},12^{th}H), 7.47-7.45 (d, 2H, Ph), 7.40- 7.36 (t, 2H, Ph), 7.15 - 7.11 (t, 2H, Ph).

5,11-diethyl-5,11-dihydroindolo[3,2-b]carbazole (18)

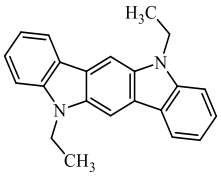

N,N- ICZ derivative **17** (1.5 g, 5.85 mmol) was disolved in 15 mL of dry DMSO at 60 °C. Afterwards, NaH (0.41 g, 17.10 mmol) was added to the obtained a solution and the mixture was stirred for 1 h at the same temperature. Then iodoethane (2.67 g, 17.10 mmol) was added and the reaction temperature was raised to 120 °C. After 2 h the reaction mixture was poured in to water. The formed precipitate was filtered off and flushed with a huge quantity of water. The crude product was purified by column chromatography using 7:18 *v/v* DCM/*n*-hexane as an eluent to collect the product **18** (1.6 g, 88%). ^{1}H NMR (400 MHz, DMSO-d_6): δ= 8.35 (s, 2H, 6^{th},12^{th}H), 8.29 (d, J = 7.7 Hz, 2H, Ph), 7.59 (d, J = 8.2 Hz, 2H, Ph), 7.49-7.45 (m, 2H, Ph), 7.21-7.18 (m, 2H, Ph), 4.56-4.54 (m, 4H, -N-CH_2-), 1.39 (t, J = 7.0 Hz. 6H, -CH_3). ^{13}C NMR (176 MHz, $CDCl_3$): δ= 140.80, 138.63, 129.72, 123.55, 122.85, 121.48, 119.81, 110.32, 103.25, 41.71, 15.48. Anal. Calcd. for $C_{22}H_{20}N_2$: C, 84.58; H, 6.45; N, 8.87; found: C, 84.37; H, 6.39; N, 8.60.

2,8-bis-[2,2-bis(4-methoxyphenyl)ethenyl]-5,11-diethyl-5,11-dihidroindolo[3,2-b]carbazole (19)

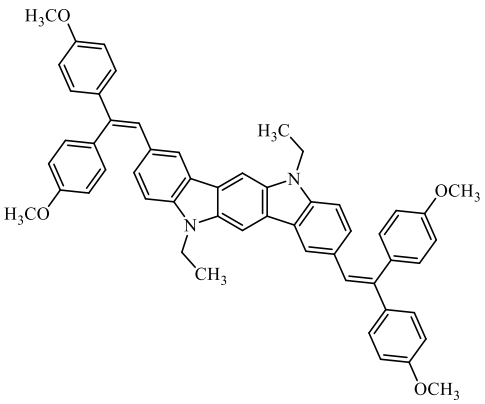

Alkylated ICZ derivative **18** (0.7 g, 2.24 mmol) was dissolved in toluene (20 mL+volume of the Dean– Stark trap), CSA (0.52 g, 2.24 mmol) was added, and the obtained mixture was heated at reflux for 20 min. Afterwards, the 2,2-bis(4-methoxyphenyl)acetaldehyde (1.45 g, 5.4 mmol) was added, and heating at reflux was continued in an apparatus fitted with a Dean–Stark trap. After termination of the reaction (3 h), the mixture was extracted with DCM. The organic layer was dried over anhydrous $MgSO_4$, filtered, the solvent was removed, and the obtained residue was purified by column chromatography using THF/*n*-hexane (1:5, v/v) as an eluent to collect the product. After precipitation from THF to MeOH, **19** was obtained as a pure yellow

powder (0.7 g, 40%). ^{1}H NMR (400 MHz, DMSO-d_6): δ = 7.85 (s, 2H, Ar), 7.75 (s, 2H, Ar), 7.37 (d, J = 8.6 Hz, 4H, Ar), 7.27 (d, J = 8.6 Hz, 4H, Ar), 7.22-7.08 (m, 6H, Ar, -CH=C-), 6.95 (d, J = 8.6 Hz, 4H, Ar), 6.90 (d, J = 8.6 Hz, 4H, Ar), 4.50-4.27 (m, 4H, -N-CH_2-), 3.88, 3.87 (two s, 12H, -OCH_3), 1.47 (t, J = 7.2 Hz, 6H, -CH_3). ^{13}C NMR (101 MHz, THF-d_8): δ = 160.3, 160.2, 141.1, 139.9, 137.8, 137.0, 134.7, 132.7, 129.3, 128.4, 128.0, 124.1, 124.0, 122.4, 115.1, 114.4, 108.4, 99.5, 55.6, 38.4, 14.0. ESI-QTOF-MS: [M+] 788.3622 [M+H] 789.3671, [M+Na] 811.3517. Anal. Calcd. for $C_{54}H_{48}N_2O_4$: C, 82.21; H, 6.13; N, 3.55; found: C, 81.97; H, 5.99; N, 3.21.

10,15-dihydro-5H-diindolo[3,2-a:3',2'-c]carbazole (20)

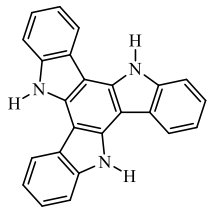

10 g (0,03901 mol) 2-oxindole was disolved in 50 ml $POCl_3$ in a nitrogen atmosphere and heated for 8h at 100 °C. After this time, the mixture was added to an ice bath and saturated aqueous solution of KOH was added until pH=7. After filtration, precipitate were purified by flash column with DCM. The product was crystalized from acetone. 4.3 g (95%) of light yellow crystals were obatained.

^{1}H NMR (400 MHz, DMSO-d_6) δ 11.90 (s, 3H, NH), 8.71-8.69 (d, 3H, Ar), 7.76-7.74 (d, 3H, Ar) 7.43- 7.33 m, 6H, Ar).

5,10,15-triethyl-10,15-dihydro-5H-indolo-[3,2-a:3`,2`-c]carbazole (21)

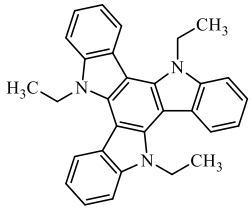

To a solution of triazatruxene **20** (1.6 g, 4.63 mmol) in dry DMSO (15 ml), NaH (0.4 g, 18.52 mmol) was added at 60°C and stirred for 1 h at the same temperature. Then iodoethane (2.89 g, 18.52 mmol) was added and the temperature was raised to 120 °C. After 2h the reaction mixture was cooled and poured in to water. The formed precipitate was filtered off and flushed with a huge quantity of water. The crude product was purified by column chromatography using 7:18 *v/v* DCM/*n*-hexane as an eluent to collect the product 4 (1.8 g, 90%). ^{1}H NMR (400 MHz, DMSO-d_6): δ= 8.32(d, J = 8.0 Hz, 3H, Ar) 7.82 (d, J = 8.0 Hz, 3H, Ar), 7.48-7.35 (m, 6H, Ar), 5.00 (q, J = 7.0 Hz, 6H, -N-CH_2-), 1.44 (t, J = 7.0 Hz, 9H, -CH_3). ^{13}C NMR (101 MHz, $CDCI_3$): δ = 140.80, 138.63, 123.55 122.85, 121.48, 119.81, 110.32, 103.25, 41.71, 29.70. Anal. Calcd. for $C_{30}H_{27}N_3$: C, 83.88; H, 6.34; N, 9.78; found: C, 83.39; H, 6.29; N, 9.30.

3,8,13–tris[2,2-bis(4-methoxyphenyl)ethenyl]-5,10,15-triethyl-10,15-dihydro-5H-indolo-[3,2-a:3`,2`-c]carbazole (22)

Alkylated triazatruxene **21** (0.5 g, 1.16 mmol) was dissolved in toluene (20 mL+volume of the Dean– Stark trap), CSA (0.27 g, 1.16 mmol) was added, and the obtained mixture was heated at reflux for 20 min. Afterwards, 2,2-bis(4-methoxyphenyl)acetaldehyde (1.20 g, 4.64 mmol) was added, and heating at reflux was continued in an apparatus fitted with a Dean–Stark trap. After termination of the reaction (5 h, TLC control), the mixture was extracted with DCM. The organic layer was dried over anhydrous $MgSO_4$, filtered, the solvent was removed, and the

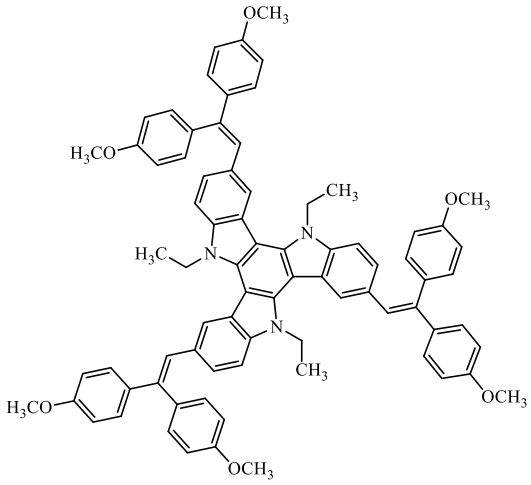

obtained residue was purified by column chromatography using THF/*n*-hexane (1:5, *v/v*) as an eluent. After precipitation from THF to MeOH **22** was obtained as a pure light yellow powder (0.45 g, 35%). ^{1}H NMR (700 MHz, DMSO-d_6): δ= 8.22-8.00 (m, 3H, Ar), 7.76-6.51 (m, 33H, Ar), 4.58-4.27 (m, 6H, -CH_2-), 3.88- 3.67 (m, 18H, -OCH_3), 1.35-1.03 (m, 9H, -CH_3). ^{13}C NMR (101 MHz, THF-d_8): δ = 160.6, 160.0, 142.9, 142.7, 140.8, 138.4, 138.2, 133.2, 131.6, 120.1, 115.2, 114.4, 110.7, 104.4, 55.7, 42.5, 15.9. ESI-QTOF-MS: [M+] 1143.5170, [M+H] 1144.5231, [M+2] 1145.5273 [M+Na] 1166.5076. Anal. Calcd. for $C_{78}H_{69}N_3O_6$: C, 81.86; H, 6.08; N, 3.67; found: C, 81.53; H, 5.89; N, 3.39.

1-ethylindolin-2-one (23)

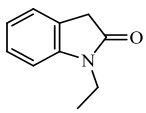

25 g isatin (0.1699 mol) was dissolved in 125 ml of dry DMF, cooled to 0°C in an argon atmosphere. 4.9g (0.20388 mol) NaH was added in three parts while cooling. After 15 min, 26.5 g (0.20388 mol) iodoethane was added dropwise and the mixture was left over night. The mixture was extracted with ethyl ether, the organic layer was washed with brine and dried on Na_2SO_4. The residue was dissolved in 50 ml hydrazine hydrate and heated at 130 °C for 3h. After extraction with EtOAc, the organic layer was washed with saturated $NaHCO_3$, brine and dried on Na_2SO_4. Concentrate was purified by column chromatography (*n*-hexane:ethyl acetate, 5:3, *v:v*). ^{1}H NMR (400 MHz, $CDCl_3$): δ= 7.30 – 7.19 (m, 2H, Ar), 7.01 (t, *J* = 7.5 Hz, 1H, Ar), 6.83 (d, *J* = 7.8 Hz, 1H, Ar), 3.75 (q, *J* = 7.2 Hz, 2H, -N-CH_2-), 3.48 (s, 2H, 3th –CH_2-), 1.26 (t, *J* = 7.2 Hz, 3H, -CH_3). ^{13}C NMR (101 MHz, $CDCl_3$): δ= 174.62, 144.29, 127.79, 124.61, 122.08, 108.17, 35.81, 34.60, 12.67.

5-bromo-1-ethylindolin-2-one (24)

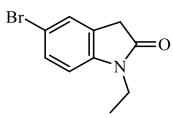

11g (68.23 mmol) of 1-ethylindolin-2-one was dissolved in 200ml acetonitrile at -5˚C with 12.5g (70.02 mmol) NBS added in three equal portions at the same temperature. After 1h, the temperature reached RT and the reaction was kept for 2h. Reaction mixture was extracted with CH_3Cl and the crude product was crystalized from THF:EtOH (1:1, *v:v*). ^{1}H NMR (400 MHz, $CDCl_3$): δ= 7.31 (ddd, *J* = 11.9, 8.0, 2.8 Hz, 2H, 6th,7thH), 6.64 (dd, *J* = 8.2, 3.1 Hz, 1H, 4thH), 3.67 (qd, *J* = 7.2, 3.5 Hz, 2H, -N-CH_2-), 3.43 (d, *J* = 3.7 Hz, 2H, -CH_2-), 1.17 (td, *J* = 7.2, 3.2 Hz, 3H, -CH_3). ^{13}C NMR (101 MHz, $CDCl_3$): δ= 173.96, 143.37, 130.67, 127.71, 126.76, 114.71, 109.50, 35.64, 34.77, 12.57.

3,8,13-tribromo-5,10,15-triethyl-10,15-dihydro-5H-diindolo[3,2-a:3',2'-c]carbazole (25)

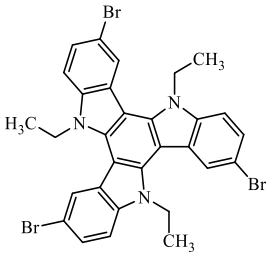

2 g (8.32 mmol) 5-bromo-1-ethylindolin-2-one (**24**) was disolved in 50 ml $POCl_3$ in a nitrogen atmosphere and heated for 8h at 100 °C. Atfer this time, the mixture was added to an ice bath and saturated aqueous solution of KOH was added until pH=7. After filtration, the precipitate were purified by flash column with DCM. The product was crystalized from acetone. 0.643 g (35%) of light yellow crystals were obtained. ^{1}H NMR (400 MHz, $CDCl_3$): δ= 8.24 (d, J = 1.4 Hz, 3H, Ar), 7.51 (dd, J = 8.6, 1.5 Hz, 3H, Ar), 7.42 (d, J = 8.6 Hz, 3H, Ar), 4.69 (q, J = 7.1 Hz, 6H, -CH_2-), 1.50 (t, J = 7.1 Hz, 9H, -CH_3). ^{13}C NMR (101 MHz, $CDCl_3$): δ= 139.13, 138.80, 125.67, 124.67, 123.94, 113.10, 111.58, 102.20, 67.97, 41.66, 15.37.

2-(2,2-bis(4-methoxyphenyl)vinyl)-4,4,5,5-tetramethyl-1,3,2-dioxaborolane (26)

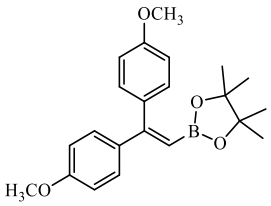

In an argon atmosphere, 5g (26.73mmol) of bromoanisole was dissolved in 25 ml of dry toluene, 1.87g (12.15mmol) vinylboronate pinacol ester, 4.91 g (48.56 mmol) iPr$_2$NH and 0.31 g (0.6 mmol) Pd[P(t-Bu)$_3$]$_2$ were added and the mixture was heated at 80°C for 24h. After extraction, the crude product was purified *via* column chromatography. ^{1}H NMR (400 MHz, $CDCl_3$): δ= 7.27 – 7.20 (m, 4H, Ph), 7.16 – 7.06 (m, 4H, Ph), 6.04 (s, 1H, -CH=C-), 3.82 (s, 3H, -CH_3), 3.80 ((s, 3H, -CH_3), 1.30 (s, 12H, -CH_3).

N,N-Bis(4-methylphenyl)-4-[2,2-bis(4-methoxyphenyl)etenyl]aniline (27b)

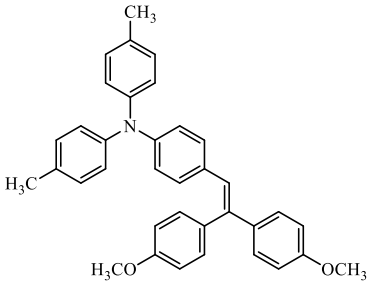

Following general procedure A, 4,4′-dimethyltriphenylamine (0.5 g, 1.83 mmol), (+/-)-camphor-10-sulfonic acid (0.42 g, 1.83 mmol), and bis(4-methoxyphenyl)acetaldehyde (0.56 g, 2.2 mmol) were mixed (reaction time 6 hours). After extraction (toluene), the crude product was purified by column chromatography (acetone/*n*-hexane 3/22, *v*/*v*) to give **27b** (0.7 g, 75%) as a bright yellow powder. m.p. 167–169 °C.^{1}H NMR (300 MHz, $CDCl_3$): δ= 7.34-7.21 (m, 8H, 2,3,5,6-H 4-OCH_3-Ph); 7.16-7.04 (m, 8H, 2,3,4,5,6-H 4-CH_3-Ph); 6.93 (s, 1H, =CH-); 6.99-6.94 (m, 4H, 2,3,5,6-H 1,4-subst. Ph), 3.91-3.88 (2s, 6H, –OCH_3); 2.38 (s, 6H, -CH_3). ^{13}C NMR (75 MHz, $CDCl_3$, 25°C, TMS): δ= 159.1, 159.0, 146.7, 145.2, 139.7, 136.8, 133.3, 132.8, 131.6, 131.0, 130.2, 130.0, 128.7, 126.1, 125.0, 121.5, 114.3, 113.7, 55.4, 21.0; elemental analysis calcd (%) for $C_{36}H_{33}NO_2$: C 84.51, H 6.50, N 2.74; found: C 84.34, H 6.63, N 2.89.

N,N-Bis(4-methylphenyl)-4-[2,2-bis(4-methylphenyl)etenyl]aniline (27c)

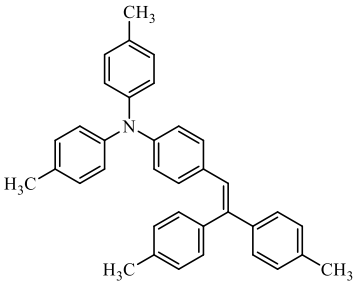

Following general procedure A, 4,4′-dimethyltriphenylamine (0.5 g, 1.83 mmol), (+/-)-camphor-10-sulfonic acid (0.42 g, 1.83 mmol), and bis(4-methylphenyl)acetaldehyde (0.49 g, 2.2 mmol) were mixed (reaction time 5 hours). After extraction (toluene), the crude product was purified by column chromatography (acetone/*n*-hexane 3/22, *v*/*v*) to give **27c** (0.7 g, 75%) as a bright yellow powder. ^{1}H NMR (300 MHz, $CDCl_3$, 25°C, TMS): δ= 7.20-7.18 (m, 2H, Ph), 7.14-7.07 (m, 6H, Ph), 7.03-7.01 (m, 4H, Ph), 6.95-6.94 (m, 4H, Ph), 6.85-6.82 (m, 3H, Ph, -CH=C-), 6.75-6.73 (m, 2H, Ph), 2.36 (s, 3H, $-CH_3$), 2.33 (s, 3H, $-CH_3$), 2.28 (s, 6H, $-CH_3$). ^{13}C NMR (101 MHz, $CDCl_3$): δ= 146.69, 145.07, 141.11, 140.15, 137.89, 136.86, 136.85, 132.64, 130.69, 130.16, 130.11, 129.85, 129.48, 128.87, 127.24, 126.72, 124.87, 121.35, 21.36, 21.13, 20.83.

4-(2-Methyl-2-phenylethenyl)-N,N-bis[(4-methyl)phenyl]aniline (27d)

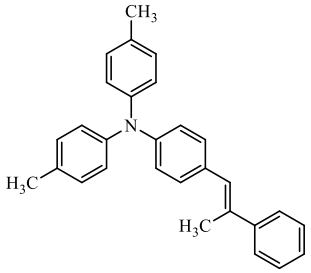

Following general procedure A, 4,4′-dimethyltriphenylamine (0.5 g, 1.83 mmol), (+/-)-camphor-10-sulfonic acid (0.42 g, 1.83 mmol), and 2-phenylpropionaldehyde (0.29 g, 2.2 mmol) were mixed (reaction time 3 hours). After extraction (toluene), the crude product was purified by column chromatography (acetone/*n*-hexane 1/249, *v*/*v*) to give **27d** (0.52 g, 73%) as a yellow oil. ^{1}H NMR (300 MHz, $CDCl_3$, 25°C, TMS): δ= 7.53–7.46 (m, 2H, Ph), 7.35 (t, *J*= 7.4 Hz, 2H, Ph), 7.29–7.18 (m, 3H, Ph), 7.09–6.98 (m, 8H, Ph), 6.90 (s, 1H, -CH=C-), 6.76–6.71 (m, 2H, Ph), 2.33–2.14 (m, 9H, $-CH_3$); ^{13}C NMR (75 MHz, $CDCl_3$, 25°C, TMS): δ= 146.8, 145.4, 144.6, 136.1, 132.7, 131.8, 130.1, 130.0, 128.5, 127.7, 127.1, 126.1, 124.9, 122.3, 21.0, 17.9; elemental analysis calcd (%) for $C_{29}H_{27}N$: C 89.42, H 6.99, N 3.60; found: C 89.50, H 7.10, N 3.40.

4-Metyl-N,N-bis{4-[2,2-bis(4-methoxyphenyl)ethenyl]phenyl}aniline (28b)

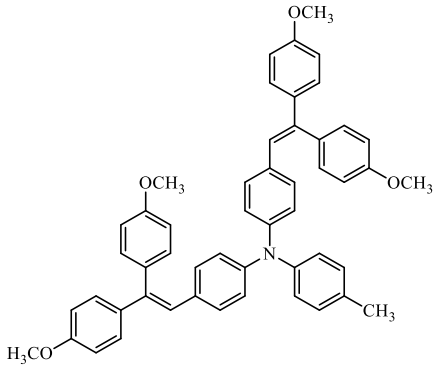

Following general procedure A, 4-methyltriphenylamine (0.5 g, 1.93 mmol), (+/-)-camphor-10-sulfonic acid (0.45 g, 1.93 mmol), and bis(4-methoxyphenyl)acetaldehyde (1.19 g, 4.63 mmol) were mixed (reaction time 6 hours). After extraction (toluene), the crude product was purified by column chromatography (acetone/*n*-hexane 3/22, *v*/*v*) to give **28b** (0.99 g, 70 %) as a bright yellow powder. ^{1}H NMR (300 MHz, $CDCl_3$, 25°C, TMS): δ= 7.29–6.94 (m, 16H, 2,3,5,6-H 4-OCH_3-Ph), 6.92–6.84 (m, 4H, 2,3,4,5,6-H 4-CH_3-Ph), 6.82 (s, 2H, =CH-);), 6.80–6.74 (m, 8H, 2,3,5,6-H 1,4-subst. Ph), 3.81-3.72 (m, 12H, –OCH_3), 2.31–2.27 (m, 3H, -CH_3); ^{13}C NMR (75 MHz, $CDCl_3$, 25°C, TMS): δ= 159.2, 158.3, 146.1, 144.8, 140.1, 137.9, 136.8, 133.2, 131.6, 130.8, 130.2, 128.7, 128.2, 125.9, 125.6, 123.2, 122.7, 114.3, 113.8, 113.6, 55.4, 21.1; elemental analysis calcd (%) for $C_{51}H_{45}NO_4$: C 83.24, H 6.16, N 1.90; found: C 83.39, H 6.07, N 1.72.

4-Metyl-N,N-bis{4-[2,2-bis(4-methylphenyl)ethenyl]phenyl}aniline (28c)

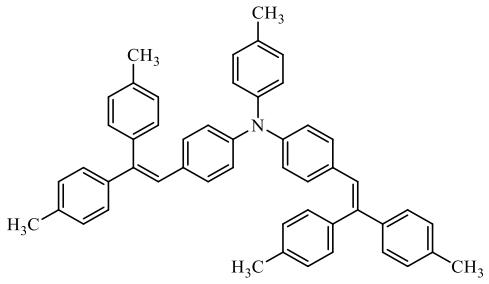

Following general procedure A, 4-methyltriphenylamine (0.5 g, 1.93 mmol), (+/-)-camphor-10-sulfonic acid (0.45 g, 1.93 mmol), and bis(4-methylphenyl)acetaldehyde (1.04 g, 4.63 mmol) were mixed (reaction time 5 hours). After extraction (toluene), the crude product was purified by column chromatography (acetone/*n*-hexane 3/22, *v*/*v*) to give **28c** (0.95 g, 63 %) as a bright yellow powder. ^{1}H NMR (400 MHz, $CDCl_3$): δ= 7.18 (t, *J* = 8.7 Hz, 4H, Ph), 7.15 – 7.05 (m, 8H, Ph), 7.02 (d, *J* = 8.1 Hz, 6H, Ph), 6.98 – 6.92 (m, 6H, Ph), 6.84 (dd, *J* = 9.2, 1.7 Hz, 4H, Ph), 6.78 (s, 2H, -CH=C-), 2.36 (s, 3H, -CH_3), 2.33 (s, 6H, -CH_3), 2.28 (s, 6H, -CH_3). ^{13}C NMR (101 MHz, $CDCl_3$): δ= 146.69, 145.07, 141.11, 140.15, 137.89, 136.86, 132.64, 130.69, 130.13, 129.85, 129.48, 128.87, 127.24, 126.72, 124.87, 121.35, 25.65, 21.36, 21.13, 20.83.

N, N-Bis[4-(2-methyl-2-phenylethenyl)phenyl]-4-methylaniline (28d)

Following general procedure A, 4-methyltriphenylamine (0.5 g, 1.93 mmol), (+/-)-camphor-10-sulfonic acid (0.45 g, 1.93 mmol), and 2-phenylpropionaldehyde (0.62 g, 4.63 mmol) were mixed (reaction duration 5 hours). After extraction (toluene), the crude product was purified by column chromatography (acetone/*n*-hexane 1/249, *v*/*v*) to give **28d** (0.54 g, 57 %) as a yellow oil. ^{1}H NMR (300 MHz, $CDCl_3$, 25°C, TMS): δ= 7.55–7.45 (m, 3H, Ph), 7.35 (t, *J*= 7.4 Hz, 3H, Ph), 7.30–

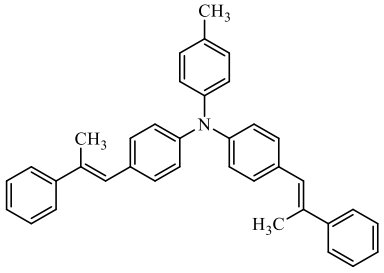

7.16 (m, 8H, Ph), 7.14–6.94 (m, 8H, Ph), 6.82 (s, 2H, -CH=C-), 2.38–2.12 (m, 9H, -CH_3); ^{13}C NMR (75 MHz, $CDCl_3$, 25°C, TMS): δ= 146.4, 145.1, 144.5, 136.4, 133.4, 132.5, 130.2, 130.1, 129.8, 128.8, 128.5, 128.3, 127.6, 127.2, 126.2, 125.5, 123.2, 122.8, 21.1, 17.9; elemental analysis calcd (%) for $C_{37}H_{33}N$: C 90.39, H 6.77, N 2.85; found: C 90.53, H 6.49, N 2.98.

Tris{4-[2,2-bis(4-methoxyphenyl)ethenyl]phenyl}amine (29b)

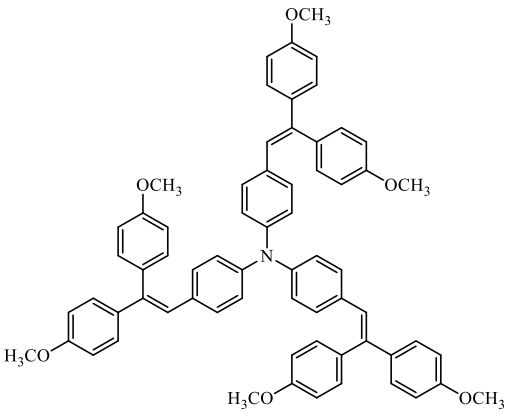

Following general procedure A, triphenylamine (0.5 g, 2.04 mmol), (+/-)-camphor-10-sulfonic acid (0.47 g, 2.04 mmol), and bis(4-methoxyphenyl)acetaldehyde (1.88 g, 7.34 mmol) were mixed (reaction duration 10 hours). After extraction (toluene), the crude product was purified by column chromatography (acetone/*n*-hexane 2/23, *v*/*v*) to give **29b** (1.5 g, 77 %) as a bright yellow powder. ^{1}H NMR (300 MHz, $CDCl_3$, 25°C, TMS): δ= 7,30-6,93 (m, 24H, 2,3,5,6-H 4-OCH_3-Ph); 6,86 (s, 3H, =CH-); 6,81-6,73 (m, 12H, 2,3,5,6-H 1,4-subst. Ph); 3,84-3,70 (m, 18H, –OCH_3). ^{13}C NMR (75 MHz, $CDCl_3$, 25°C, TMS): δ= 145.7, 140.4, 136.7, 133.2, 132.5, 131.8, 131.6, 130.9, 130.4, 128.8, 128.3, 126.4, 125.9, 124.5, 124.0, 123.6, 114.3, 113.7, 113.6, 55.4; elemental analysis calcd (%) for $C_{66}H_{57}NO_6$: C 82.56, H 5.98, N 1.46; found: C 82.43, H 5.85, N 1.59.

Tris{4-[2,2-bis(4-methylphenyl)ethenyl]phenyl}amine (29c)

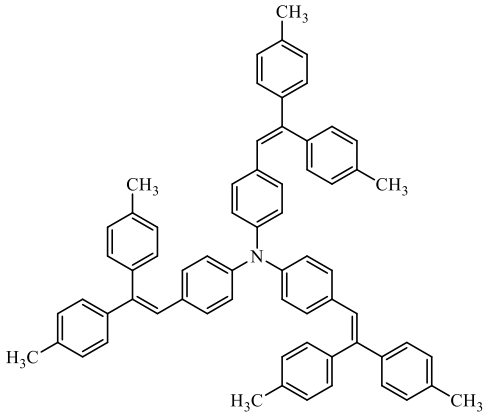

Following general procedure A, triphenylamine (0.5 g, 2.04 mmol), (+/-)-camphor-10-sulfonic acid (0.47 g, 2.04 mmol), and bis(4-methylphenyl)acetaldehyde (1.65 g, 7.34 mmol) were mixed (reaction duration 8 hours). After extraction (toluene), the crude product was purified by column chromatography (acetone/*n*-hexane 1/24, *v*/*v*) to give **29c** (1.4 g, 79 %) as a bright yellow powder. ^{1}H NMR (400 MHz, $CDCl_3$): δ= 7.69-7.61 (m, 8H, Ph), 7.48 – 6.97 (m, 31H, Ph, -CH=C-), 2.47 (s,

9H, -CH_3), 2.43(s, 9H, -CH_3). ^{13}C NMR (101 MHz, $CDCl_3$) δ: 142.98, 137.29, 136.65, 135.29, 133.54, 128.40, 128.35, 127.31, 126.53, 25.67, 21.68, 21.15.

Tris[4-(2-methyl-2-phenylethenyl)phenyl]amine (29d)

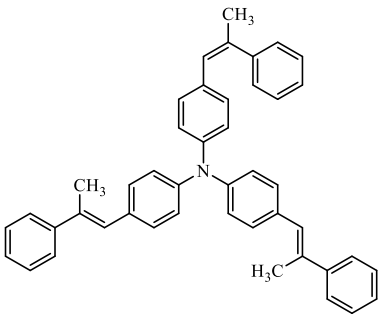

Following general procedure A, triphenylamine (0.5 g, 2.04 mmol), (+/-)-camphor-10-sulfonic acid (0.47 g, 2.04 mmol), and 2-phenylpropionaldehyde (0.98 g, 7.34 mmol) were mixed (reaction duration 5 hours). After extraction (toluene), the crude product was purified by column chromatography (THF/*n*-hexane 1/49, *v*/*v*) to give **29d** (0.86 g, 71 %) as a yellow powder. ^{1}H NMR (300 MHz, $CDCl_3$, 25°C, TMS): δ= 7.59–7.43 (m, 5H, Ph), 7.41–7.19 (m, 15H, Ph), 7.16 (d, *J*= 8.6 Hz, 3H, Ph), 7.06 (d, *J*= 8.5 Hz, 2H, Ph), 6.91–6.69 (m, 5H, Ph, -CH=C-), 2.38–2.13 (m, 9H, -CH_3); ^{13}C NMR (75 MHz, $CDCl_3$, 25°C, TMS): δ= 146.0, 144.5, 137.9, 136.7, 133.1, 130.3, 129.9, 128.8, 128.5, 127.5, 126.2, 123.9, 123.6, 17.9; elemental analysis calcd (%) for $C_{45}H_{39}N$: C 91.02, H 6.62, N 2.36; found: C 91.27, H 6.51, N 2.22.

4-bromo-N-(4-bromophenyl)-N-phenylaniline (30)

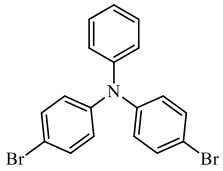

15g (61.14 mmol) triphenylamine was dissolved in 50ml DCM, cooled down to -5˚C and 22.85 g (128.3 mmol) *N*-bromosuccinimide was added in the dark by three portions at the same temperature and then the reaction mixture was left in RT for 12h. After extraction, the crude product was purified by column chromatography (*n*-hexane). 23 g (93.3%) of pure compound was obtained.

4-bromo-N-(4-bromophenyl)-N-[4-(2-phenylprop-1-en-1-yl)phenyl]aniline (31)

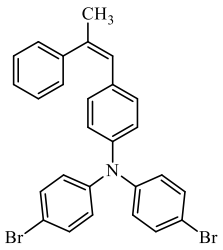

4,4′-dibromotriphenylamine (4.00 g, 9.92 mmol), (+/-)-camphor-10-sulfonic acid (2.30 g, 9.92 mmol), and 2-phenylpropionaldehyde (2.00 g, 14.88 mmol) were dissolved in toluene (20 ml) and the mixture was heated at reflux for 8 h using a Dean-Stark trap. After termination of the reaction (TLC: *n*-hexane), the solution was extracted with toluene. The organic layer was dried over anhydrous $MgSO_4$, filtered, the solvent was removed and the residue purified by column chromatography (*n*-hexane) to give **31** (3.19 g, 62 %) as a light yellow powder. ^{1}H NMR (400 MHz, $CDCl_3$): δ= 7.51 (d, J = 7.2 Hz, 2H, Ph), 7.42 – 7.32 (m, 6H, Ph), 7.32 – 7.22 (m, 3H, 3,4,5H- nonsubstituted-Ph), 7.05 (d, J = 8.6 Hz, 2H, Ph), 6.97 (d, J = 8.8 Hz, 4H, Ph), 6.76 (s, 1H, =CH-), 2.31 (d, J = 1.2 Hz, 3H, -CH_3). ^{13}C NMR (101 MHz, $CDCl_3$): δ= 146.49, 145.25, 144.20, 137.08, 133.80, 132.51, 130.44, 128.47, 127.28, 127.11, 126.09, 125.67, 124.02, 115.72, 17.84. Elemental analysis calcd (%) for $C_{27}H_{21}Br_2N$: C 62.45, H 4.08, N 2.70; found: C 62.43, H 4.24, N 2.86.

Poly[N,N-diphenyl-4-(2-phenylprop-1-en-1-yl)aniline-4′,4′′-diyl] (32)

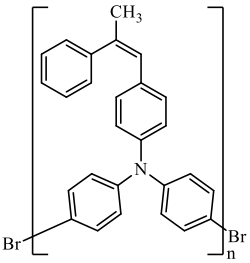

$NiCl_2$ (0.056 g, 0.43 mmol), zinc powder (1.221 g, 18.67 mmol), 2,2′-bipyridine (0.109 g, 0.70 mmol) and triphenylphosphine (1.141 g, 4.35 mmol) were dispersed in dry and degassed N,N-dimethylacetamide (7 ml) under an argon atmosphere. The mixture was stirred for 1 h, during this time the color changed from grey to brown. Monomer **31** (1.59 g, 3.06 mmol), was added and the mixture was heated at 80 °C for 6 h. Afterwards, chlorobenzene (1 ml) was added and the stirring was continued for another 2 h. After termination of the reaction, the solution was filtered through celite, extracted using a mixture of dichloromethane/THF (3:1). The organic layer was dried over anhydrous $MgSO_4$, filtered, the solvent was removed and the residue was filtered through a short (5 cm) silica gel column. Impurities and low molecular weight products were eluted with acetone and THF was then used to isolate the main product. The polymer was precipitated from THF to 10-fold excess of methanol 3 times to give **32** (0.63 g, 57 %) as a bright yellow powder. ^{1}H NMR (700 MHz, $CDCl_3$): δ= 7.59 – 6.99 (m, 17H, Ph), 6.78 (s, 1H, -CH=C-), 2.32 (s, 3H, -CH_3). ^{13}C NMR (176 MHz, $CDCl_3$): δ= 146.44, 145.84, 144.24, 136.44, 134.99, 130.15, 130.09, 129.30, 128.31, 127.40, 127.28, 127.01, 125.95, 124.51, 124.43, 124.25, 123.68, 123.51, 17.72.

4-bromo-N-(4-bromophenyl)-N-[4-(2,2-diphenylethenyl)phenyl]aniline (33)

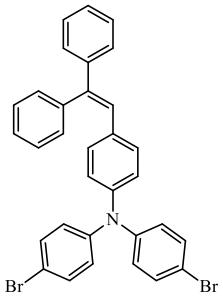

4,4′-dibromotriphenylamine (5.00 g, 12.40 mmol), (+/-)-camphor-10-sulfonic acid (2.88 g, 12.40 mmol), and diphenylacetaldehyde (3.65 g, 18.60 mmol) were dissolved in toluene (20 ml) and the mixture was heated at reflux for 9 h using a Dean-Stark trap. After termination of the reaction (TLC: *n*-hexane), the solution was extracted with ethyl acetate. The organic layer was dried over anhydrous $MgSO_4$, filtered, the solvent was removed and the residue purified by column chromatography (*n*-hexane) to give **33** (4.76 g, 66 %) as a light yellow powder. ^{1}H NMR (400 MHz, $CDCl_3$): δ= 7.42 – 7.18 (m, 14H, Ph), 6.95 – 6.84 (m, 7H, Ph, -CH=), 6.78 (d, J = 8.7 Hz, 2H, Ph). ^{13}C NMR (101 MHz, $CDCl_3$): δ= 146.28, 145.49, 143.44, 141.62, 140.61, 132.55, 132.48, 130.71, 130.30, 128.94, 128.35, 127.61, 127.51, 127.49, 127.35, 125.89, 123.22, 115.88. Elemental analysis calcd (%) for $C_{32}H_{23}Br_2N$: C 66.11, H 3.99, N 2.41; found: C 65.94, H 4.20, N 2.46.

Poly[4-(2,2-diphenylethenyl)-N,N-diphenylaniline-4′,4′′-diyl] (34)

$NiCl_2$ (0.027 g, 0.21 mmol), zinc powder (0.590 g, 9.02 mmol), 2,2′-bipyridine (0.054 g, 0.35 mmol) and triphenylphosphine (0.552 g, 2.10 mmol) were dispersed in dry and degassed N,N-dimethylacetamide (7 ml) under an argon atmosphere. The mixture was stirred for 1 h, during this time the color changed from grey to brown. Monomer **33** (1.78 g, 3.06 mmol), was added and the mixture was heated at 80 °C for 6 h. Afterwards, chlorobenzene (1 ml) was added and the stirring was continued

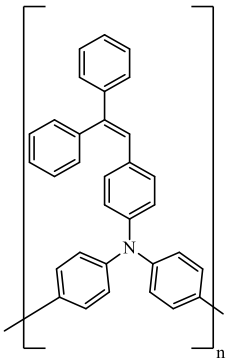

for another 2 h. After termination of the reaction, the solution was filtered through celite, extracted using a mixture of dichloromethane/THF (3:1). The organic layer was dried over anhydrous $MgSO_4$, filtered, the solvent was removed and the residue was filtered through a short (5 cm) silica gel column. Impurities and low molecular weight products were eluted with acetone and THF was then used to isolate the main product. The polymer was precipitated from THF to 10-fold excess of methanol 3 times to give **34** (0.90 g, 70 %) as a bright yellow powder. ^{1}H NMR (700 MHz, THF-d_8): δ= 7.61 – 6.46 (m, 23H, Ar). ^{13}C NMR (176 MHz, THF-d_8): δ= 148.05, 145.27, 142.71, 137.05, 133.55, 132.25, 131.92, 130.54, 129.78, 129.09, 128.94, 128.80, 126.40, 124.42.

Bis(4-bromophenyl)amine (35)

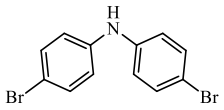

4.52g (26.75 mmol) of diphenylamine was dissolved in 30 ml DCM, cooled down to -5˚C and 10 g (56.18 mmol) *N*-bromosuccinimide was added in the dark by three portions at the same temperature and then the reaction mixture was left in RT for 24h. After extraction, the crude product was purified by column chromatography (*n*-hexane). 8.2 g (93.3%) of pure compound was obtained.

N,N-bis(4-bromophenyl)-3,5-dimethylaniline (36)

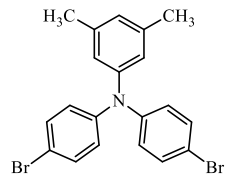

4,4′-dibromodiphenylamine (5.00 g, 15.29 mmol), 3,5-dimethyliodobenzene (3.90 g, 16.82 mmol), copper(I) iodide (0.23 g, 1.22 mmol), 1,10-phenanthroline (0.22 g, 1.22 mmol) and crushed potassium hydroxide pellets (8.07 g, 122.32 mmol) were added to the degassed toluene (40 ml) under an argon atmosphere and the mixture was heated at reflux for 6 h using a Dean-Stark trap. After termination of the reaction (TLC: *n*-hexane) the solution was filtered through celite and extracted with toluene. The organic layer was dried over anhydrous $MgSO_4$, filtered, the solvent was removed and the residue purified by column chromatography (*n*-hexane) to give **36** (4.27 g, 65 %) as a yellow powder. ^{1}H NMR (400 MHz, $CDCl_3$): δ= 7.32 (d, J = 8.9 Hz, 4H, Ph), 6.91 (d, J = 8.8 Hz, 4H, Ph), 6.72 (s, 1H, 4-H trisubst. Ph), 6.67 (s, 2H, 1,5-H trisubst. Ph), 2.22 (s, 6H, -CH_3). ^{13}C NMR (101 MHz, $CDCl_3$): δ= 146.89, 146.82, 139.39, 132.34, 125.92, 125.37, 122.83, 115.17, 21.42. Elemental analysis calcd (%) for $C_{20}H_{17}Br_2N$: C 55.71, H 3.97, N 3.25; found: C 55.92, H 3.89, N 3.20.

N,N-bis(4-bromophenyl)-3,5-dimethyl-4-(2-phenylprop-1-en-1-yl)aniline (37)

Triphenylamine derivative **36** (2.00 g, 4.64 mmol), (+/-)-camphor-10-sulfonic acid (1.08 g, 4.64 mmol), and 2-phenylpropionaldehyde (0.93 g, 6.96 mmol) were dissolved in toluene (15 ml) and the mixture was heated at reflux for 18 h using a Dean-Stark trap. After termination of the reaction (TLC: acetone/*n*-hexane 1/24, *v*/*v*) the solution was extracted with ethyl acetate. The organic layer was dried over

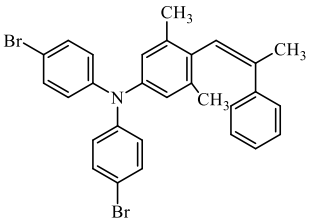

anhydrous $MgSO_4$, filtered, the solvent was removed and the residue purified by column chromatography (*n*-hexane) to give 37 (1.88 g, 74 %) as a light yellow powder. ^{1}H NMR (400 MHz, $CDCl_3$): δ= 7.57 (d, J = 7.2 Hz, 2H, Ph), 7.39 (t, J = 7.5 Hz, 2H, Ph), 7.34 (d, J = 8.9 Hz, 4H, Ph), 7.31 – 7.27 (m, 1H, 4H-nonsubst. Ph), 6.95 (d, J = 8.9 Hz, 4H, Ph), 6.77 (s, 2H, 1,5-H tetrasubst. Ph), 6.68 (s, 1H, =CH-), 2.14 (s, 6H, -CH_3), 1.90 (d, J = 1.1 Hz, 3H, -CH_3). ^{13}C NMR (101 MHz, $CDCl_3$): δ= 146.79, 145.17, 142.72, 138.17, 138.01, 133.57, 132.36, 128.50, 127.42, 125.89, 125.61, 125.36, 123.63, 115.14, 20.55, 17.06. Elemental analysis calcd (%) for $C_{29}H_{25}Br_2N$: C 63.64, H 4.60, N 2.56; found: C 63.46, H 4.52, N 2.77.

Poly[3,5-dimethyl-N,N-diphenyl-4-(2-phenylprop-1-en-1-yl)aniline-4',4''-diyl] (38)

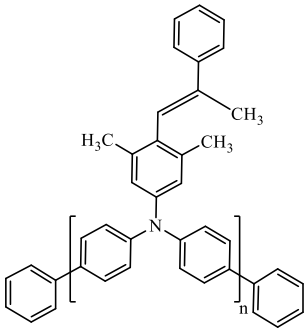

$NiCl_2$ (0.027 g, 0.21 mmol), zinc powder (0.590 g, 9.02 mmol), 2,2′-bipyridine (0.054 g, 0.35 mmol) and triphenylphosphine (0.552 g, 2.10 mmol) were dispersed in dry and degassed *N*,*N*-dimethylacetamide (6 ml) under an argon atmosphere. The mixture was stirred for 1 h, during this time the color changed from grey to brown. Monomer **37** (0.81 g, 1.48 mmol), was added and the mixture was heated at 80 °C for 6 h. Afterwards, chlorobenzene (1 ml) was added and the stirring was continued for another 2 h. After termination of the reaction, the solution was filtered through celite and extracted using a mixture of dichloromethane/THF (3:1). The organic layer was dried over anhydrous $MgSO_4$, filtered, the solvent was removed and the residue was filtered through a short (5 cm) silica gel column. Impurities and low molecular weight products were eluted with acetone and then THF was used to isolate the main product. The polymer was precipitated from THF to 10-fold excess of methanol 3 times to give 38 (0.36 g, 64 %) as a bright yellow powder. ^{1}H NMR (700 MHz, $CDCl_3$): δ= 7.57 (d, J = 7.3 Hz, 2H, Ph), 7.55 – 7.41 (m, 5H, Ph), 7.38 (t, J = 7.2 Hz, 2H, Ph), 7.33 – 7.24 (m, 1H, 4H-nonsubst. Ph), 7.19 (d, J = 7.2 Hz, 3H, Ph), 6.89 (s, 2H, 1,5-H trisubst. Ph), 6.72 (s, 1H, =CH-), 2.16 (s, 6H, -CH_3), 1.93 (s, 3H, -CH_3). ^{13}C NMR (176 MHz, $CDCl_3$): δ= 146.71, 145.76, 142.76, 137.86, 137.54, 134.54, 132.66, 129.16, 128.34, 127.23, 125.83, 125.76, 124.11, 123.33, 20.43, 16.93.

CONCLUSIONS

1. Interaction of 9*H*-carbazole and its 9-substituted derivatives with acetaldehydes in the presence of (±)-camphorsulfonic acid as a catalyst was studied. It has been found that:

1.1. The corresponding 3,6,9-tri or 3,6-diaryletenyl substituted derivatives of 9*H*-carbazole are formed during this reaction.

1.2. This simple one-step synthesis method has been demonstrated to be suitable for the synthesis of carbazole-based charge transporting materials with the extended π-conjugated system in the case of one carbazole chromophore. In addition, electrophilic substitution takes place at the 3rd and 6th positions.

1.3. The investigation of the synthetic routes for the preparation of carbazole-based charge transporting materials with the extended π-conjugated system has revealed the necessity of protection-deprotection methodology at the *N*(9)-position in carbazole in the case of several carbazole chromophores participating in the reaction and electrophilic substitution taking place at the 3rd, 6th, and 9th positions.

1.4. The novel organic solution-processable, film-forming carbazole-based derivatives possessing diarylethenyl fragments are attractive for optoelectronic applications, owing to their high hole drift mobility exceeding 10^{-3} cm^2 /V·s at 3.6×10^5 V/cm electric field under ambient conditions.

2. Investigation of the interaction of 9-substituted derivatives of 5,11-dihydroindolo[3,2-*b*]- and 10,15-dihydro-5*H*-indolo-[3,2-*a*:3`,2`-*c*]carbazoles with acetaldehydes in the presence of (±)-camphorsulfonic acid as a catalyst has revealed that the corresponding 2,8-bis- and 3,8,13–tris[2,2-bis(4-methoxyphenyl)ethenyl] derivatives form during this reaction.

3. The synthesized indolecarbazole-based derivatives with 2,2-bis(4-methoxyphenyl)ethenyl substituents at the 2,8- or 3,8,13-positions are attractive for optoelectronic applications. Hole drift mobilities of their solid solutions in bisphenol Z polycarbonate reach 10^{-3} cm^2 /V·s at 3.6×105 V/cm electric field under ambient conditions. The ionization potentials of the hole transporting materials are 5.28 eV and 5.34 eV, respectively, and thus make them suitable for application in perovskite solar cells.

4. Remarkable power conversion efficiency of 15.24% was achieved using the indolocarbazole-based derivative, containing triazatruxene as a central linking fragment and three equivalent 2,2-bis(4-methoxyphenyl)ethenyl side arms, as hole transporting material and composite perovskite as absorber, which is on a par with that of spiro-OMeTAD (17.03%).

5. Interaction of triphenylamine with arylacetaldehydes in the presence of (±)-camphorsulfonic acid as a catalyst was studied. It has been found that:

5.1. Facile one-step electrophilic substitution reaction takes place between arylacetaldehyde and any of the triphenylamine rings with the subsequent loss of water molecules.

5.2. This simple method enables synthesis of star-shaped charge transporting materials whose optical, physicochemical and electrical properties depend on the number of arylethenyl substituents and their nature.
5.3. The highest hole mobility, reaching up to 0.017 cm^2 V^{-1} s^{-1} at strong electric fields, was observed for the derivative of triphenylamine, possessing the diphenylethenyl substituent at all para-positions.
5.4. The newly synthesized star-shaped charge transporting materials are applicable as semiconducting materials in electrophotographic photoreceptors (Al/titanyl phthalocyanine/star-shaped triphenylamine-based charge transporting material). The organic photoreceptor devices were constructed using these materials. Their test results have demonstrated that novel materials outperform the well-known hole transporting material TPD.
6. Dibrominated triphenylamines with phenylethenyl side groups can be used successfully in the reductive Yamamoto homopolymerization. It has been found that:
6.1. The corresponding solution-processable polymers with weight and number-average molecular mass reaching 14400 and 7500, respectively, are formed during this reaction.
6.2. The molecular structure of the synthesized polymers allows them to exist in a stable amorphous state with high thermal stability (decomposition starts at temperatures above 400 °C), which is desired to form uniform HTM films in optoelectronic devices.
6.3. HOMO energy levels of the synthesized polymers are in the range of (-5.3 eV)-(-5.21eV) and are favourable for the hole transport.
6.4. The highest power conversion efficiency (12.3%) of perovskite solar cells (FTO)/compact TiO_2/mesoporous TiO_2/triple cation perovskite/HTM/Au) without any additives has been observed for the polymer containing poly[bis(4-phenyl)-(3,5-dimethylphenyl)amine] main chain with methyl phenylethenyl fragments attached to it. This result is better than the one for the well investigated and usually used poly[bis(4-phenyl)(2,4,6-trimethylphenyl)amine] (10.7%).
6.5. Introduction of phenylethenyl fragments into the structure of polymers has been shown to determine better compatibility with the perovskite surface and protect hybrid organic-inorganic perovskite to give highly stable PSCs.

REFERENCES

1. STROHRIEGL, P., GRAZULEVICIUS, J.V., Charge-Transporting Molecular Glasses. *Adv. Mater*, 2002, 14, 1439–1452. https://doi.org/10.1002/1521-4095(20021016)14:20<1439::AID-ADMA1439>3.0.CO;2-H.
2. LYGAITIS, R., GETAUTIS, V., GRAZULEVICIUS, J. V., Hole-Transporting Hydrazones. *Chem. Soc. Rev*., 2008, 37, 770–788. doi:10.1039/B702406C.
3. WEISS, D. S., ABKOWITZ, M., Advances in Organic Photoconductor Technology. *Chem. Rev*., 2010, 110, 479. DOI: 10.1021/cr900173r.
4. SHIROTA, Y. Organic Materials for Electronic and Optoelectronic Devices. *J. Mater. Chem*., 2000, 10, . 1–25. 10.1039/A908130E.
5. MARTINS, J. S., et al, New Class of Organic Hole-Transporting Materials Based on Xanthene Derivatives for Organic Electronic Applications, *J. Phys. Chem. C*, 2017, 121, 24, p. 12999–13007, 10.1021/acs.jpcc.7b02034.
6. SHIROTA, Y., KAGEYAMA, H. Charge Carrier Transporting Molecular Materials and Their Applications in Devices. *Chem. Rev.*, 2007, 107, 4, 953–1010, DOI: 10.1021/cr050143+.
7. BORSENBERGER, P. M., et al. Hole transport in 1,1-bis(di-4-tolylaminophenyl)cyclohexane. *J. Chem. Phys*., 1991, 94, p. 8276, https://doi.org/10.1063/1.460112.
8. PLATER, J. M., JACKSON, T., Polyaromatic amines. Part 4: Synthesis of poly(ethynyl) linked aromatic amines. *Tetrahedron*, 2003, 59, p. 4673, https://doi.org/10.1016/S0040-4020(03)00521-0.
9. NANDAKUMAR, M. V., VERKADE, G., One-Pot Sequential *N* and *C* Arylations: An Efficient Methodology for the Synthesis of trans 4-N,N-Diaryl Aminostilbenes. *Angew. Chem.*, 2005, 117, 3175, DOI: 10.1002/anie.200462938.
10. ALLARD, S., et al. Organic Semiconductors for Solution-Processable Field-Effect Transistors (OFETs). *Angew.Chem. Int. Ed*., 2008, 47,4070; https://doi.org/10.1002/anie.200701920.
11. FACCHETTI, A., π-Conjugated Polymers for Organic Electronics and Photovoltaic Cell Applications. *Chem.Mater*., 2011, 23, 733; DOI: 10.1021/cm102419z.
12. WANG, H., et al. Semiconducting π-Conjugated Systems in Field-Effect Transistors: A Material Odyssey of Organic Electronics. *Chem. Rev*., 2012, 112, 2208, DOI: 10.1021/cr100380z.
13. DRIVER, M.S.; HARTWIG, J.F., A Rare, Low-Valent Alkylamido Complex, a Diphenylamido Complex, and Their Reductive Elimination of Amines by Three-Coordinate Intermediates. *J. Am. Chem. Soc*., 1995, 117, 16, p. 4708–4709, DOI: 10.1021/ja00121a030.
14. GURAM, A.S., et al. A Simple Catalytic Method for the Conversion of Aryl Bromides to Arylamines. *Angewandte Chemie International Edition*, 34 (12): 1348–1350, 1995 https://doi.org/10.1002/anie.199513481.

15. ULLMANN, F., BIELECKI, J., , Ueber Synthesen in der Biphenylreihe. *Chemische Berichte*. 34 (2): 2174–2185, 1901, https://doi.org/10.1002/cber.190103402141.
16. MIYAURA, N., et al. "A new stereospecific cross-coupling by the palladium-catalyzed reaction of 1-alkenylboranes with 1-alkenyl or 1-alkynyl halides. *Tetrahedron Letters*, 20 (36): 3437–3440, 1979, https://doi.org/10.1016/S0040-4039(01)95429-2
17. MIYAURA, N., SUZUKI, A., , Stereoselective synthesis of arylated (*E*)-alkenes by the reaction of alk-1-enylboranes with aryl halides in the presence of palladium catalyst. *Chem. Comm.*, (19): 866–867, 1979 DOI:10.1039/C39790000866
18. COREY, E.; ENDERS, D., Applications of *N,N*-dimethylhydrazones to synthesis. Use in efficient, positionally and stereochemically selective C_C bond formation; oxidative hydrolysis to carbonyl compounds. *Tetrahedron Letters*, 17 (1): 3–3, 1976, DOI: 10.1016/S0040-4039(00)71307-4
19. VOGEL, A. Anthraquinone:, in Ullmann Qs Encyclopedia of Industrial Chemistry, Wiley-VCH, Weinheim, 2000.
20. COLLIN, G. Anthracene: in Ullmann Qs Encyclopedia of Industrial Chemistry,Wiley-VCH, Weinheim, 2006;
21. DONALD, S.D., et al. Synthesis of Heterocycles from Hydrogen Cyanide Derivatives. *Advances in Heterocyclic Chemistry*, Volume 41, 1987, Pages 1-40;
22. MARTIN, E.L., A Modification of the Clemmensen Method of Reduction. *J. Am. Chem. Soc*, 1936, 58,1438, DOI: 10.1021/ja01299a038.
23. WEISSERMEL, K., ARPE, H.J., Aromatics-Production and Conversion. in *Industrial Organic Chemistry*, Fourth Edition,Wiley-VCH, Weinheim, 2003, pp.328–331, DOI: 10.1021/ja033656b.
24. ROY, J., et al., Recent trends in the synthesis of carbazoles: an update. *Tetrahedron*, 2012, 68,6099, https://doi.org/10.1016/j.tet.2012.05.007.
25. NAGAO, I. et al., 9-Stannafluorenes: 1,4-Dimetal Equivalents for Aromatic Annulation by Double Cross-Coupling. *Angew.Chem. Int. Ed*., 2009, 48, 7573, https://doi.org/10.1002/anie.200903779.
26. TOGUEM, S.-M. T et al., Synthesis of Dibenzothiophenes and Carbazoles by Sequential 'Tetra-Fold Heck/6 π-Electrocyclization/Dehydrogenation' Reactions of Tetrabromothiophene and Tetrabromo-N-methylpyrrole. *Adv.Synth. Catal*., 2012, 354,1819, https://doi.org/10.1002/adsc.201200057;
27. JIA, X., et al. Catalytic Radical Cation Salt Induced Csp3–H Functionalization of Glycine Derivatives: Synthesis of Substituted Quinolines. *Org.Lett*., 2012, 14, 78, DOI: 10.1021/ol301909g.
28. NI, Y. et al.,*Org. Lett*. 2009, 11,3702.
29. HUANG, W. et al., Pd-Catalyzed Reactions of o-Diiodoarenes with Alkynes for Aromatic Ring Extension. *Org.Lett*., 2004, 6,2429, DOI: 10.1021/ol049176m.
30. TAKAHASHI, T. et al., Copper-Mediated Coupling of Zirconacyclopentadienes with Dihalo Aromatic Compounds. Formation of Fused Aromatic Rings. *J. Am. Chem. Soc*. 1996, 118,5154, DOI: 10.1021/ja960407x.

31. SCOTT, L. T., et al., Geodesic polyarenes with exposed concave surfaces. *Pure Appl. Chem*., 1999, 71,2 09,http://dx.doi.org/10.1351/pac199971020209.
32. WATSON, M. D., et al., Big Is Beautiful−"Aromaticity" Revisited from the Viewpoint of Macromolecular and Supramolecular Benzene Chemistry. *Chem.Rev.*,2001, 101,1267, DOI: 10.1021/cr990322p.
33. TSEFRIKAS, V.M., SCOTT, L.T., Geodesic Polyarenes by Flash Vacuum Pyrolysis. *Chem. Rev*., 2006, 106, 4868, DOI: 10.1021/cr050553y.
34. WU, J., et al., Graphenes as Potential Material for Electronics, *Chem. Rev*. 2007, 107, 718, DOI: 10.1021/cr068010r.
35. FENG, X., et al., Large polycyclic aromatic hydrocarbons: Synthesis and discotic organization. *Pure Appl. Chem*., 2009, 81, 2203, http://dx.doi.org/10.1351/PAC-CON-09-07-07
36. SCHAMALTZ, B., et al., Polyphenylene-Based Materials: Control of the Electronic Function by Molecular and Supramolecular Complexity. *Adv.Mater*., 2009, 21, 1067, https://doi.org/10.1002/adma.200802016.
37. RIEGER, R., MGLLEN, J., Forever young: polycyclic aromatic hydrocarbons as model cases for structural and optical studies. *J. Phys.Org.Chem.*, 2010, 23,315, https://doi.org/10.1002/poc.1644.
38. SYGULA, A., Chemistry on a Half-Shell: Synthesis and Derivatization of Buckybowls. *Eur.J.O rg.Chem*., 2011, 1611, https://doi.org/10.1002/ejoc.201001585.
39. CHEN, L., et al., From nanographene and graphene nanoribbons to graphene sheets: chemical synthesis. *Angew.Chem.Int.Ed*., 2012, 51, 7640, doi: 10.1002/anie.201201084.
40. ITAMI, K., Toward controlled synthesis of carbon nanotubes and graphenes. *Pure Appl. Chem.*, 2012, 84, 907, http://dx.doi.org/10.1351/PAC-CON-11-11-15.
41. SUN, Z., et al., Low band gap polycyclic hydrocarbons: from closed-shell near infrared dyes and semiconductors to open-shell radicals. *Chem. Soc. Rev*., 2012, 41,7857, DOI:10.1039/C2CS35211G.
42. MOLLER, M., et al, *Advances in Polymer Science*, 2013, 262, 61.
43. WU, D., et al., Arynes in the synthesis of polycyclic aromatic hydrocarbons, *RSC Adv.*, 2013, 3,22727, DOI:10.1039/C3RA43804J.
44. MULLEN, K., Evolution of Graphene Molecules: Structural and Functional Complexity as Driving Forces behind Nanoscience. *ACS Nano*, 2014, 8, 6531, DOI: 10.1021/nn503283d.
45. SUN, Z., et al., Zethrenes, Extended p-Quinodimethanes, and Periacenes with a Singlet Biradical Ground State. *Acc.Chem. Res.*, 2014, 47, 2582, DOI: 10.1021/ar5001692.
46. BALL, M., et al., Contorted Polycyclic Aromatics. *Acc.Chem. Res*., 2015, 48, 267, DOI: 10.1021/ar500355d.
47. NARITA, A., et al., Bottom-up synthesis of chemically precise graphene nanoribbons. *Chem. Rec.*, 2015, 15, 295, DOI: 10.1002/tcr.201402082.
48. NARITA, A., et al., New advances in nanographene chemistry. *Chem. Soc.Rev.*, 2015, 44, 6616, DOI:10.1039/C5CS00183H.

49. SEGAWA, Y., et al., Synthesis of Extended π-Systems through C–H Activation. *Angew.Chem. Int. Ed.*, 2015, 54,66, https://doi.org/10.1002/anie.201403729.
50. SEGAWA, Y., et al., Structurally uniform and atomically precise carbon nanostructures. *Nat. Rev.Mater.*, 2016, 1, 15002, https://doi.org/10.1038/natrevmats.2015.2.
51. OZAKI, K., et al., One-shot K-region-selective annulative π-extension for nanographene synthesis and functionalization. *Nat. Commun*., 2015, 6, 6251, https://doi.org/10.1038/ncomms7251.
52. ITO, H., et al. Annulative π-Extension (APEX): Rapid Access to Fused Arenes, Heteroarenes, and Nanographenes. *Angew.Chem. Int. Ed*., 2017, 56,11144–11164, https://doi.org/10.1002/anie.201701058.
53. ZHU, X.-H., et al., Solution-processable single-material molecular emitters for organic light-emitting devices. *Chem. Soc.Rev*. 2011, 40, 3509, DOI:10.1039/C1CS15016B.
54. MISHRA, A., et al., Functional Oligothiophenes: Molecular Design for Multidimensional Nanoarchitectures and Their Applications, *Chem. Rev.*, 2009, 109,1141, DOI: 10.1021/cr8004229.
55. MURPHY, A.R., et al., Organic Semiconducting Oligomers for Use in Thin Film Transistors. *Chem. Rev.*, 2007, 107,1066, DOI: 10.1021/cr0501386.
56. SEED, A., Synthesis of self-organizing mesogenic materials containing a sulfur-based five-membered heterocyclic core. *Chem. Soc.Rev,*. 2007, 36, 2046, DOI: 10.1039/b612666a.
57. YAMAGUCHI, J., et al., C-H bond functionalization: emerging synthetic tools for natural products and pharmaceuticals. *Angew.Chem.Int.Ed*., 2012, 51, 8960, DOI: 10.1002/anie.201201666.
58. MAGANO, J., et al., Large-Scale Applications of Transition Metal-Catalyzed Couplings for the Synthesis of Pharmaceuticals. *Chem. Rev.*, 2011, 111, 2177, DOI: 10.1021/cr100346g.
59. SCHIMDT, A.W., et al., Occurrence, biogenesis, and synthesis of biologically active carbazole alkaloids. *Chem. Rev.,* 2012, 112, 3193, DOI: 10.1021/cr200447s.
60. MANEERAT, W., et al., Bioactive Carbazole Alkaloids from Clausena wallichii Roots. *J. Nat. Prod.*, 2012, 75, 741, DOI: 10.1021/np3000365.
61. DELANDES, S., et al., *Mar.Drugs*, 2009, 7,754. doi:10.3390/md7040754.
62. YAMASHITA, M., et al., Fused Ring Construction around Pyrrole, Indole, and Related Compounds via Palladium-Catalyzed Oxidative Coupling with Alkynes. *J. Org.Chem.*, 2009, 74,7481, DOI: 10.1021/jo9016698.
63. JAZZAR, R., et al., Functionalization of Organic Molecules by Transition-Metal-Catalyzed C(sp^3)-H Activation. *Chem. Eur.J*., 2010, 16, 2654, https://doi.org/10.1002/chem.200902374.
64. SONG, G., et al., Synthesis of Quinolines via Rh(III)-Catalyzed Oxidative Annulation of Pyridines. *J. Org. Chem.*, 2011, 76, 7583, DOI: 10.1021/jo201266u.

65. QIAN, Z.-C., et al., Efficient Synthesis of Isoquinolines via Rh(III)-Catalyzed Oxidative Annu-lation of Picolinamides with Alkynes. *Synlett*, 2014, 25,103, DOI: 10.1055/s-0033-1340870.
66. MATSUDA, Y., et al., Formal [4+2] Reaction between 1,3-Diynes and Pyrroles: Gold(I)-Catalyzed Indole Synthesis by Double Hydroarylation. *Chem. Eur.J*., 2015, 21,1463, https://doi.org/10.1002/chem.201405903.
67. OZAKI, K., et al., One-shot indole-to-carbazole π-extension by a Pd–Cu–Ag trimetallic system. *Chem. Sci.*, 2013, 4, 3416, DOI:10.1039/C3SC51447A.
68. GUO, T., et al., Copper(I)-catalyzed enantioselective hydroboration of cyclopropenes: facile synthesis of optically active cyclopropylboronates. *Org.Chem. Front.*, 2014, 1707, DOI:10.1039/C4QO00157E.
69. VERMA, A.K., et al., Palladium-Catalyzed Triple Successive C–H Functionalization: Direct Synthesis of Functionalized Carbazoles from Indoles. *Org. Lett.*, 2015, 17,3658, DOI: 10.1021/acs.orglett.5b01476.
70. LAHA, J., et al., A Tandem Approach to Functionalized Carbazoles from Indoles via Two Successive Regioselective Oxidative Heck Reactions Followed by Thermal Electrocyclization. *Org.Lett.*, 2015, 17, 4742, DOI: 10.1021/acs.orglett.5b02265.
71. THIES, N., et al., Synthesis of 2- and 2,7-Functionalized Pyrene Derivatives: An Application of Selective C-H Borylation. *Chem. Eur.J*. 2012, 18,6302, https://doi.org/10.1002/chem.201103774.
72. DAWANDE, S. G., et al., Rhodium Enalcarbenoids: Direct Synthesis of Indoles by Rhodium(II)-Catalyzed [4+2] Benzannulation of Pyrroles, *Angew.Chem. Int. Ed.* 2014, 53,4076, https://doi.org/10.1002/anie.201400161
73. WU, J.-Q., et al., From Indoles to Carbazoles: Tandem Cp*Rh(III)-Catalyzed C–H Activation/Brønsted Acid-Catalyzed Cyclization Reactions. *ACS Catal.*, 2015, 5,6453, DOI: 10.1021/acscatal.5b01801.
74. PARIA, S., REISER, O., Visible Light-Mediated Coupling of α-Bromochalcones with Alkenes. *Adv.Synth. Catal.*, 2014, 356, 557, https://doi.org/10.1002/adsc.201400638.
75. WU, Y., et al., Palladium catalyzed dual C–H functionalization of indoles with cyclic diaryliodoniums, an approach to ring fused carbazole derivatives. *Org.Biomol.Chem.*, 2014, 12,9777, DOI:10.1039/C4OB02170C.
76. OZAKI, K., et al., Annulative π-Extension (APEX) of Heteroarenes with Dibenzosiloles and Dibenzogermoles by Palladium/o-Chloranil Catalysis. *Org.Lett*., 2017, 19, 1930, DOI: 10.1021/acs.orglett.7b00684.
77. YANO, Y., et al., Helically Twisted Tetracene: Synthesis, Crystal Structure, and Photophysical Properties of Hexabenzo[a,c,fg,j,l,op]tetracene. *Synlett,* 2016, 27, 2081, DOI: 10.1055/s-0035-1561455.
78. DANN, O., et al., *Chem.Ber.*,1954, 87,140.
79. FLETCHER, H., 1,3,4,7-Substituted isoindoles and isoindolenines. *Tetrahedron*, 1966, 22, 2481, https://doi.org/10.1016/S0040-4020(01)99037-4.
80. CRANWELL, P. A., et al., A synthesis of ellipticine. *J. Chem.Soc.*,1962, 3482, DOI:10.1039/JR9620003482.

81. ABID, M., et al., Solvent-Free Solid Acid-Catalyzed Electrophilic Annelations: A New Green Approach for the Synthesis of Substituted Five-Membered *N*-Heterocycles. *Adv.Synth. Catal.*, 2006, 348, 2191, https://doi.org/10.1002/adsc.200606200.
82. KULKARNI, A., et al Microwave-Assisted Solid-Acid-Catalyzed Friedel-Crafts Alkylation and Electrophilic Annulation of Indoles Using Alcohols as Alkylating Agents. *Synthesis*, 2009, 4010, DOI: 10.1055/s-0029-1217052.
83. ZHENG, X., et al., Benzannulation of Indoles to Carbazoles and Its Applications for Syntheses of Carbazole Alkaloids. *Org.Lett.*, 2014, 16,5156, DOI: 10.1021/ol5025053.
84. MAFTOUH, M., et al., Synthesis and cytotoxic activity of hydroxylated derivatives of olivacine in relation with their biotransformation. *J. Med. Chem.*, 1985, 28, 708, DOI: 10.1021/jm00383a004.
85. SUAREZ, A., et al., Brønsted Acid-Catalyzed Straightforward Synthesis of Benzo[b]carbazoles from 2,3-Unsubstituted Indoles. *Adv.Synth. Catal*., 2014, 356, 374, https://doi.org/10.1002/adsc.201300868.
86. THOLANDER, J., BERGMAN, J., Synthesis of 6,12-disubstituted 5,11-dihydroindolo[3,2-b]carbazoles, including 5,11-dihydroindolo[3,2-b]carbazole-6,12-dicarbaldehyde, an extremely efficient ligand for the TCDD (Ah) receptor. *Tetrahedron*, 1999, 55, 12577, https://doi.org/10.1016/S0040-4020(99)00733-4.
87. ZHAO, H.-P., et al., *Chem. Phys.Lett.*, 2007, 439, 132.
88. DEB, M. L., et al., A Facile Synthesis of 6,12-Disubstituted 5,7-Dihydroindolo[2,3-b]carbazoles from the Reaction of 1H-Indole and Aldehydes Catalyzed by Molecular Iodine. *Synthesis*, 2008,286, DOI: 10.1055/s-2008-1000849.
89. DUPEYRE, G. et al., A one-pot synthesis of 7-phenylindolo[3,2-a]carbazoles from indoles and β-nitrostyrenes, via an unprecedented reaction sequence. *Org. Biomol. Chem.*, 2011, 9, 7780, DOI:10.1039/C1OB06108A.
90. SURESHABABU, R., et al., Lewis Acid Mediated One-Pot Synthesis of Aryl/Heteroaryl-Fused Carbazoles Involving a Cascade Friedel–Crafts Alkylation/Electrocyclization/Aromatization Reaction Sequence. *Eur.J.Org. Chem*., 2011, 922, https://doi.org/10.1002/ejoc.201001309.
91. DHAYALAN, J. A., et al., A Versatile Synthesis of Annulated Carbazole Analogs Involving a Domino Reaction of Bromomethylindoles with Arenes/Heteroarenes. *Eur.J.Org. Chem.*, 2009, 531, https://doi.org/10.1002/ejoc.200801018.
92. CLEMENT, J. A., et al., Lewis-Acid-Mediated Domino Reactions of Bis(diacetoxymethyl)-Substituted Arenes and Heteroarenes. *Eur.J.Org.Chem.*, 2011,569, https://doi.org/10.1002/ejoc.201001174.
93. RAFIQ, S. M., Lewis Acid/Brønsted Acid Mediated Benz-Annulation of Thiophenes and Electron-Rich Arenes. *Org. Lett.*, 2014, 16, 2720, DOI: 10.1021/ol501006t.
94. GIOMI, D., CECCHI, M., Study on direct benzoannelations of pyrrole and indole systems by domino reactions with 4,5-dicyanopyridazine. *Tetrahedron*, 2002, 58, 8067, https://doi.org/10.1016/S0040-4020(02)00958-4.

95. NAPOLITANO, A., A reinvestigation of the reactions between 5,6-dihydroxyindoles and quinones. *Tetrahedron*, 1987, 43, 2749, https://doi.org/10.1016/S0040-4020(01)86880-0.
96. LLPE-ALVARADO, P., et al., One-pot assembly of large heterocyclic quinones through three-component reactions. *TetrahedronLett.*, 2001,42,7971, https://doi.org/10.1016/S0040-4039(01)01725-7.
97. ALONSO, M., et al., Regioselective Diels–Alder reactions of 3-indolylquinones. *Tetrahedron*, 2003, 59, 2821, https://doi.org/10.1016/S0040-4020(03)00340-5.
98. PRAKASH, K. S., et al., A General Method for the Synthesis of 5H-Benzo[b]-, Carbazolo[2,3-b]- and Indolo[2,3-b]carbazole Derivatives via Copper(II) Triflate-Catalyzed Heteroannulation. *Adv.Synth. Catal.*, 2012, 354,1566, https://doi.org/10.1002/adsc.201100887.
99. SHIROTA, Y., KAGEYAMA, H., Charge Carrier Transporting Molecular Materials and Their Applications in Devices. *Chem. Rev.*, 2007;107:953–1010, DOI: 10.1021/cr050143+.
100. SATHIYAN, G., et al. Review of carbazole based conjugated molecules for highly efficient organic solar cell application. *Tetrahedron Letters*, 2016; 57, 243–52, https://doi.org/10.1016/j.tetlet.2015.12.057.
101. WANG, H., et al. Facile Synthesis and High Performance of a New Carbazole-Based Hole-Transporting Material for Hybrid Perovskite Solar Cells. *ACS Photonics*, 2015; 2, 849–55, DOI: 10.1021/acsphotonics.5b00283.
102. GRATIA, P., et al. A Methoxydiphenylamine-Substituted Carbazole Twin Derivative: An Efficient Hole-Transporting Material for Perovskite Solar Cells. *Angew. Chem. Int. Ed.*, 2015;11409–13, https://doi.org/10.1002/anie.201504666.
103. WANG, J., et al. A new carbazole-based hole-transporting material with low dopant content for perovskite solar cells. *Electrochimica Acta*, 2016;210:673–80, https://doi.org/10.1016/j.electacta.2016.05.203.
104. NAJARI, A., et al. High Open-Circuit Voltage Solar Cells Based on New Thieno[3,4-c]pyrrole-4,6-dione and 2,7-Carbazole Copolymers. *Macromolecules*, 2012; 45:1833–38, DOI: 10.1021/ma202540j.
105. DUAN, L., et al. Strategies to Design Bipolar Small Molecules for OLEDs: Donor-Acceptor Structure and Non-Donor-Acceptor Structure. *Adv. Mater.*, 2011; 23,1137–44, https://doi.org/10.1002/adma.201003816.
106. MATULAITIS, T., et al., Synthesis and properties of bipolar derivatives of 1,3,5-triazine and carbazole. *Dyes Pigments*, 2016;127:45–58, https://doi.org/10.1016/j.dyepig.2015.11.001.
107. ZHU, W., et al. A novel family of twisted molecular luminescent materials containing carbazole unit for single-layer organic electroluminescent devices. *J. Photochem. Photobiol. A Chem.*, 2003; 154, 169–177, https://doi.org/10.1016/S1010-6030(02)00325-8.
108. CHERPAK, V.V., et al., 3,6-Di(9-carbazolyl)-9-(2-ethylhexyl)carbazole based single-layer blue organic light emitting diodes. *Syn Metals*, 2011, 161, 1343–1346, https://doi.org/10.1016/j.synthmet.2011.04.035.

109. YANG, T., et al. Three carbazole-based host materials: facile synthesis, photophysical properties and performances in PhOLED. *Tetrahedron*, 2016; 72, 8066–72, https://doi.org/10.1016/j.tet.2016.10.044
110. AMEEN, SH., et al,. Diphenylaminocarbazoles by 1,8-functionalization of carbazole: Materials and application to phosphorescent organic light-emitting diodes. *Dyes and Pigments*, 2016, https://doi.org/10.1016/j.dyepig.2015.08.027.
111. BUCINSKAS, A., et al. *N*-Annelated perylenes as effective green emitters for OLEDs. *RSC Adv.* 2015;5:78150–9, DOI:10.1039/C5RA15075B.
112. REIG, M., et al. Easy accessible blue luminescent carbazole-based materials for organic light-emitting diodes. *Dyes and Pigments*, 2017, 137, 24–35, DOI:10.1039/C5RA21959K.
113. REIG M., et al. New solution-processable carbazole derivatives as deep blue emitters for organic light-emitting diodes. *RSC. Adv.*, 2016,6, 9247–53, DOI:10.1039/C5RA21959K.
114. SHEN, J.Y., et al., Ambipolar conductive 2,7-carbazole derivatives for electroluminescent devices. *Adv. Funct. Mater*., 2007, 17, 983–95, https://doi.org/10.1002/adfm.200600921.
115. ADHIKARI, R.M., et al., Synthesis and photophysical properties of carbazole-based blue light-emitting dendrimers. *J. Org. Chem.*, 2007; 72, 4727–32.
116. SONNTAG, M., STROHRIEGL, P., Novel 2,7-Linked Carbazole Trimers as Model Compounds for Conjugated Carbazole Polymers. *Chem. Mater.*, 2004; 16, 4736–42, DOI: 10.1021/cm040142i.
117. MORIN, J.F, et al., Siove A. Polycarbazoles: 25 years of progress. *Macromol. Rapid Commun.*, 2005, 26, 761–78, https://doi.org/10.1002/marc.200500096.
118. SUNG, S.D et al. 14.8% Perovskite Solar Cells Employing Carbazole Derivatives as Hole Transporting Materials. *Chem. Commun.*, 2014, 14161–3, DOI:10.1039/C4CC06716A.
119. KANG, M.S., et al. Novel Carbazole-Based Hole-Transporting Materials with Star-Shaped Chemical Structures for Perovskite-Sensitized Solar Cells. *ACS Appl. Mater. Interfaces*, 2015, 7, 22213–7, DOI: 10.1021/acsami.5b04662.
120. LYGAITIS, R., et al. Hole-transporting hydrazones. *Chem. Soc. Rev.*, 2008, 37, 770–88, doi: 10.1039/b702406c.
121. BUBNIENE, G., et al. Synthesis of new hole-transporting molecular glasses with pendant carbazolyl-based hydrazone moieties. *Synth. Met.*, 2009, 159, 1695–700, https://doi.org/10.1016/j.synthmet.2009.05.008.
122. GETAUTIS, V., et al. An Efficient Scalable Synthesis of 2,3-Epoxypropyl Phenylhydrazones. *Molecules*, 2006, 11, 64–71, https://doi.org/10.3390/11010064.
123. BUBNIENE, G., et al., Easily functionalizable carbazole based building blocks with extended conjugated systems for optoelectronic applications. *Tetrahedron*, 2010; 66, 3199–206, https://doi.org/10.1016/j.tet.2010.02.086.
124. DASKEVICIENE, M., et al. 1,3-Diphenylethenylcarbazolyl-Based Monomer for Cross-Linked Hole Transporting Layers. *Molecules*, 2015;20:9124−9138, DOI: 10.3390/molecules20059124.

125. BUCINSKAS, A., et al. Structure-property relationship of isomeric diphenylethenyl-disubstituted dimethoxycarbazoles. *RSC Adv.*, 2015, 5, 49577−89, DOI:10.1039/C5RA09161F.
126. BUBNIENE, G. et al., Easily functionalizable carbazole based building blocks with extended conjugated systems for optoelectronic applications. *Tetrahedron*, 2010, 66, 3199–206, https://doi.org/10.1016/j.tet.2010.02.086.
127. CEKAVICIUTE, M., et al., Structure-properties relationship of phenylethenyl-substituted triphenylamine, *J Phys Chem C*, 2013, 117, 7973−80, DOI: 10.1021/jp3099297.
128. MATOLIUSKYTE, A., et al. Carbazole-containing enamines as charge transport materials for electrophotography. *Synthetic Metals*, 158, 2008, 462–467, https://doi.org/10.1016/j.synthmet.2008.03.020.
129. MALINAUSKAS, T., Krūvininkus transportuojančių ir šviesą išspinduliuojančių medžiagų sintezė iš hidrazonų, karbazolo ir 1,4,5,8-naftalentetrakarbksiimido 2,3 –epoksipropilinių darinių, Kaunas, Technologija, 2007.
130. HU, X., et al., 5,11-Dihydro-5,11-di-1-naphthylindolo[3,2-b]carbazole: Atropisomerism in a Novel Hole-Transport Molecule for Organic Light-Emitting Diodes. *J. Am. Chem. Soc*., 1999, 121, 5097, DOI: 10.1021/ja9906554.
131. WAKIM, S., et al., Organic Microelectronics: Design, Synthesis, and Characterization of 6,12-Dimethylindolo[3,2-b]Carbazoles. *Chem. Mater.*, 2004, 16, 4386, DOI: 10.1021/cm049786g.
132. LI, Y., et al., Polyindolo[3,2-b]carbazoles: A New Class of p-Channel Semiconductor Polymers for Organic Thin-Film Transistors. *Macromolecules*, 2006, 39, 6521, DOI: 10.1021/ma0612069.
133. LI, Y., et al., Novel Peripherally Substituted Indolo[3,2-b]carbazoles for High-Mobility Organic Thin-Film Transistors. *Adv. Mater*., 2005, 17, 849, https://doi.org/10.1002/adma.200401290.
134. BLOUIN, N., et al., Optical, Electrochemical, Magnetic, and Conductive Properties of New Polyindolocarbazoles and Polydiindolocarbazoles. *Macromol. Chem. Phys*., 2006, 207, 166, https://doi.org/10.1002/macp.200500423.
135. WU, Y., et al., Indolo[3,2-b]carbazole-Based Thin-Film Transistors with High Mobility and Stability. *J. Am. Chem. Soc*., 2005, 127, 614, DOI: 10.1021/ja0456149.
136. VELASCO, D., et al., Indolo[3,2-b]carbazole derivatives as hole transporting materials for electrophotography. *Synt. Met*., 2009, 159, 654, https://doi.org/10.1016/j.synthmet.2008.12.011.
137. KULSHRESHTHA, G., C. et al., New interfacial materials for rapid hole-extraction in organic photovoltaic cells. *J. Mater. Chem. A*, 2013, 1, 4077, DOI:10.1039/C3TA00808H.
138. SHELTON, S. W., et al., Solution-Processable Triindoles as Hole Selective Materials in Organic Solar Cells. *ACS Appl. Mater. Interfaces*, 2012, 4, 2534, https://pubs.acs.org/doi/abs/10.1021/am300228w.

139. RAMOS, F. J., et al., Rational design of triazatruxene-based hole conductors for perovskite solar cells. *RSC Adv.*, 2015, 5, 53426, DOI:10.1039/C5RA06876B.
140. RAKSTYS, K. et al., Triazatruxene-Based Hole Transporting Materials for Highly Efficient Perovskite Solar Cells. *J. Am. Chem. Soc.*, 2015, 137, 16172, DOI: 10.1021/jacs.5b11076.
141. PINDUR, U., et al., Indolo[3,2-b]carbazol: Reaktionsprodukt der Umsetzung von 3,3′-Bisindolylmethan mit Orthoameisensäuretriethylester. *Arch. Pharm.* (Weinheim), 1987, 320, 280, https://doi.org/10.1002/ardp.19873200317.
142. TORRES, A., REGO, L.G., Surface Effects and Adsorption of Methoxy Anchors on Hybrid Lead Iodide Perovskites: Insights for Spiro-MeOTAD Attachment. *J. Phys. Chem. C*, 2014, 118, 26947, DOI: 10.1021/jp510595s.
143. GINNARI-SATRIANI, L et al., A hydrophilic three side-chained triazatruxene as a new strong and selective G-quadruplex ligand. *Org. Biomol. Chem*., 2009, 7, 2513, DOI:10.1039/B904723A.
144. HUANG, C.-H., et al., Enhanced Photovoltaic Response in Hydrogen-Bonded All-Organic Devices. *Org. Lett*., 2005, 7, 3409, DOI: 10.1021/ol050966l.
145. HOFFMANN, K.J., et al., *Synth. Met.*, 2000, 113, 3944.
146. MALINAUSKAS, T., et al., Enhancing Thermal Stability and Lifetime of Solid-State Dye-Sensitized Solar Cells via Molecular Engineering of the Hole-Transporting Material Spiro-OMeTAD. *ACS Appl. Mater. Interfaces*, 2015, 7, 11107, DOI: 10.1021/am5090385.
147. BELLETETE, M., et al., Optical and Photophysical Properties of Indolocarbazole Derivatives. *J. Phys. Chem. A*, 2006, 110, 13696, DOI: 10.1021/jp066143a.
148. KIM, H., et al., Planar heterojunction organometal halide perovskite solar cells: roles of interfacial layers. *Energy Environ. Sci.*, 2016, 9, 12, DOI:10.1039/C5EE02194D.
149. SNAITH, H. J., et al., *J. Phys. Chem. Lett*., 2014, 5, 1511.
150. UNGER, E. L., et al., Hysteresis and transient behavior in current–voltage measurements of hybrid-perovskite absorber solar cells. *Energy Environ. Sci.*, 2014, 7, 3690, DOI:10.1039/C4EE02465F.
151. CHRISTIANS, J. A., et al., Best Practices in Perovskite Solar Cell Efficiency Measurements. Avoiding the Error of Making Bad Cells Look Good. *J. Phys. Chem. Lett.*, 2015, 6, 852, DOI: 10.1021/acs.jpclett.5b00289.
152. BORSENBERGER, P. M., WEISS, D.S., Organic Photoreceptors for Imaging Systems, Marcel Dekker Inc, New York, 1993.
153. BORSENBERGER, P. M., et al., Charge transport in disordered molecular solids. *J. Chem. Phys*., 1991, 94, 5447, https://doi.org/10.1063/1.460506.
154. ALLARD, S., et al., Organic semiconductors for solution-processable field-effect transistors (OFETs), *Angew. Chem. Int. Ed*., 2008, 47, 4070, DOI: 10.1002/anie.200701920.
155. SHIROTA, Y., KAGEYAMA, H., Charge Carrier Transporting Molecular Materials and Their Applications in Devices. *Chem. Rev.*, 2007, 107, 953, DOI: 10.1021/cr050143+.

156. STROHRIEGL, P., GRAZULEVICIUS, J.V., Charge-Transporting Molecular Glasse. *Adv. Mater*., 2002, 14, 1439, https://doi.org/10.1002/1521-4095(20021016)14:20<1439::AID-ADMA1439>3.0.CO;2-H.
157. BORSENBERGER, P. M., et al., Hole transport in 1,1-bis(di-4-tolylaminophenyl)cyclohexane. *J. Chem. Phys.*, 1991,94, 8276, https://doi.org/10.1063/1.460112.
158. VERES, J., et al., Low-k Insulators as the Choice of Dielectrics in Organic Field-Effect Transistors. *Adv. Funct. Mater*., 2003, 13, 199, https://doi.org/10.1002/adfm.200390030.
159. SONNTAG, M., et al., Novel Star-Shaped Triphenylamine-Based Molecular Glasses and Their Use in OFETs. *Chem. Mater*., 2005, 17, 3031, DOI: 10.1021/cm047750i.
160. SASAKI, M. (Ricoh Company Ltd.), US Patent US 4859556, 1989.
161. NAGAI, K., et al. (Ricoh Company Ltd., Hodogaya Chemical Co., Ltd.), Jpn. Kokai Tokkyo Koho JP 09278723, 1997.
162. SASAKI, M., (Ricoh Company Ltd.), Ger. Offen. DE 3414141, 1984.
163. MONTRIMAS, E., et al., *Lith. J. Phys.*, 1966, 6, 569.
164. VAEZI-NEJAD, S. M., Xerographic time of flight experiment for the determination of drift mobility in high resistivity semiconductors. *Int. J. Electron.*, 1987, 62, 361; https://doi.org/10.1080/00207218708920988.
165. ARCHIE, Y., et al., *Int. J. Electron.*, 1987, 62, 625.
166. KIRKUS, M., et al., New indole–carbazole hybrids as glass-forming high-triplet-energy materials. *Synth. Met.* 2009, 159, 729, https://doi.org/10.1016/j.synthmet.2008.12.027.
167. MIYAMOTO, E., et al., *Electrophotography*, 1989, 28, 364.
168. CORDONA, M., et al., Two-layer organic photovoltaic cell. *Top. Appl. Phys.*, 1978, 26, 1, https://doi.org/10.1063/1.96937.
169. KOJIMA, A., et al., Organometal Halide Perovskites as Visible-Light Sensitizers for Photovoltaic Cells. *J Am Chem Soc*., 2009, 131, 6050-6051, DOI: 10.1021/ja809598r.
170. SALIBA, M., et al., Cesium-containing triple cation perovskite solar cells: improved stability, reproducibility and high efficiency. *Energ Environ Sci*., 2016, DOI: 10.1039/C5EE03874J.
171. MASUKO, K., et al., Achievement of More Than 25% Conversion Efficiency With Crystalline Silicon Heterojunction Solar Cell. *Ieee J Photovolt.*, 2014, 4, 1433-1435, DOI: 10.1109/JPHOTOV.2014.2352151.
172. SALIBA, M., et al., A molecularly engineered hole-transporting material for efficient perovskite solar cells. *Nature Energy*, 2016, 1, 15017, https://doi.org/10.1038/nenergy.2015.17.
173. MALINAUSKAS, T., et al., Branched methoxydiphenylamine-substituted fluorene derivatives as hole transporting materials for high-performance perovskite solar cells. *Energ Environ Sci*., 2016, 9, 1681-1686, DOI:10.1039/C5EE03911H.

174. HAWASH, Z., et al., Air-Exposure Induced Dopant Redistribution and Energy Level Shifts in Spin-Coated Spiro-MeOTAD Films. *Chem. Mater.*, 2015, 27, 562-569, DOI: 10.1021/cm504022q.
175. DOMANSKI, K., et al., Not All That Glitters Is Gold: Metal-Migration-Induced Degradation in Perovskite Solar Cells. *ACS Nano*., 2016,10, 6, 6306-14, DOI: 10.1021/acsnano.6b02613.
176. ABATE, A., et al., Lithium salts as "redox active" p-type dopants for organic semiconductors and their impact in solid-state dye-sensitized solar cells. *Phys. Chem. Chem. Phys.*, 2013, 15, 2572-2579, DOI:10.1039/C2CP44397J.
177. NOH, J. H., et al. Nanostructured TiO2/CH3NH3PbI3 heterojunction solar cells employing spiro-OMeTAD/Co-complex as hole-transporting material. *J Mater Chem A* 2013, 1, 11842-11847, DOI:10.1039/C3TA12681A.
178. HEO, J. H., et al., Efficient inorganic–organic hybrid heterojunction solar cells containing perovskite compound and polymeric hole conductors. *Nat. Photonics*, 2013, 7, 486 – 491, https://doi.org/10.1038/nphoton.2013.80.
179. YANG, W. S., et al., High-performance photovoltaic perovskite layers fabricated through intramolecular exchange. *Science*, 2015, 348, 1234 – 1237, DOI: 10.1126/science.aaa9272.
180. BAILIE, C. D et al., Melt-infiltration of spiro-OMeTAD and thermal instability of solid-state dye-sensitized solar cells. *Phys Chem Chem Phys*, 2014, 16, 4864-4870, DOI:10.1039/C4CP00116H.
181. NIU, G. D et al., Review of recent progress in chemical stability of perovskite solar cells. *J. Mater. Chem. A*, 2015, 3, 8970-8980, DOI:10.1039/C4TA04994B.
182. QIN, P., et al., Perovskite Solar Cells with 12.8% Efficiency by Using Conjugated Quinolizino Acridine Based Hole Transporting Material. *J. Am. Chem. Soc.*, 2014, 136, 8516-8519, DOI: 10.1021/ja503272q.
183. FRANCKEVICIUS, M, et al., A dopant-free spirobi[cyclopenta[2,1-b:3,4-b′]dithiophene] based hole-transport material for efficient perovskite solar cells. *Mater. Horiz.*, 2015, 2, 613-618, DOI:10.1039/C5MH00154D.
184. KAZIM, S., et al., A dopant free linear acene derivative as a hole transport material for perovskite pigmented solar cells. *Energ. Environ. Sci.*, 2015, 8, 1816-1823, DOI:10.1039/C5EE00599J.
185. LIU, J., et al., A dopant-free hole-transporting material for efficient and stable perovskite solar cells. *Energ. Environ. Sci*., 2014, 7, 2963-2967, DOI:10.1039/C4EE01589D.
186. ZHANG, F., et al., A Novel Aluminum–Graphite Dual-Ion Battery. *Adv. Energy Mater.*, 2016, https://doi.org/10.1002/aenm.201502588.
187. LIU, Y. S., et al. Perovskite Solar Cells Employing Dopant-Free Organic Hole Transport Materials with Tunable Energy Levels. *Adv. Mater.*, 2016, 28, 440, https://doi.org/10.1002/adma.201504293.
188. HUANG, C. Y et al., Dopant-Free Hole-Transporting Material with a C3h Symmetrical Truxene Core for Highly Efficient Perovskite Solar Cells. *J. Am. Chem. Soc.*, 2016, 138, 2528-2531, DOI: 10.1021/jacs.6b00039.

189. CHEN, W. Y., et al., Simple planar perovskite solar cells with a dopant-free benzodithiophene conjugated polymer as hole transporting material. *J. Mater. Chem. C* 2015, 3, 10070-10073, DOI:10.1039/C5TC01856K.
190. KIM, G.-W., et al., Dopant-free polymeric hole transport materials for highly efficient and stable perovskite solar cells. *Energ. Environ. Sci.*, 2016, 9, 2326-2333, DOI:10.1039/C6EE00709K.
191. Japanese Industrial Standard 8938.
192. SONG, Y. K., et al., Energy level tuning of TPB-based hole-transporting materials for highly efficient perovskite solar cells. *Chem. Commun.*, 2014, 50, 15239-15242, DOI:10.1039/C4CC06493C.
193. RYU, S., et al., Voltage output of efficient perovskite solar cells with high open-circuit voltage and fill factor. *Energ. Environ. Sci.*, 2014, 7, 2614-2618, DOI:10.1039/C4EE00762J.
194. KIM, H., et al., Planar heterojunction organometal halide perovskite solar cells: roles of interfacial layers. *Energ. Environ. Sci.*, 2016, 9, 12-30, DOI:10.1039/C5EE02194D.
195. YANG, W. S., et al., High-performance photovoltaic perovskite layers fabricated through intramolecular exchange. *Science*, 2015, 348, 1234-1237, DOI: 10.1126/science.aaa9272.
196. YANG, W., et al., Poly(carboxybetaine) nanomaterials enable long circulation and prevent polymer-specific antibody production. *Nano*, 2014, 9, 10. https://doi.org/10.1016/j.nantod.2014.02.004.
197. MEI, A., et al., A hole-conductor-free, fully printable mesoscopic perovskite solar cell with high stability. *Science*, 2014, 345, 295-298, DOI: 10.1126/science.1254763.
198. LI, X., et al., Outdoor Performance and Stability under Elevated Temperatures and Long-Term Light Soaking of Triple-Layer Mesoporous Perovskite Photovoltaics. *Energy Technology*, 2015, 3, 551-555, https://doi.org/10.1002/ente.201500045.
199. BUSH, K. A., et al. Thermal and Environmental Stability of Semi-Transparent Perovskite Solar Cells for Tandems Enabled by a Solution-Processed Nanoparticle Buffer Layer and Sputtered ITO Electrode. *Adv. Mater*., 2016, 28, 3937-3943, https://doi.org/10.1002/adma.201505279.
200. HARDWOOD, L.M., et al, Organic chemistry. Principles and practice. O. Mead et al. Eds., *Blackwell Science*, 1989.
201. JEON, N.J., et al. Solvent engineering for high-performance inorganic-organic hybrid perovskite solar cells. *Nat. Mater.*, 13, 1–7 (2014), DOI: 10.1038/nmat4014.

LIST OF PUBLICATION

1. Malinauskas, T., Daskeviciene, M., Bubniene, G., Petrikyte, I., Raisys, S., Kazlauskas, K., Gaidelis, V., Jankauskas, V., Maldzius, R., Jursenas, S., Getautis, V. Phenylethenyl-Substituted Triphenylamines: Efficient, Easily Obtainable, and Inexpensive Hole-Transporting Materials. Chemistry - A European Journal, Weinheim: Wiley-VCH. 2013, vol. 19, p. 15044 –15056;
2. Matsui, T., Petrikyte, I., Malinauskas, T., Domanski, K., Daskeviciene, M., Steponaitis, M., Gratia, P., Tress, W., Correa-Baena, JP., Abate, A., Hagfeldt, A., Grätzel, M., Nazeeruddin, MK., Getautis, V., Saliba, M. Additive-free transparent triarylamine-based polymeric hole-transport materials for stable Perovskite solar cells // ChemSusChem. Weinheim: Wiley-VCH. ISSN: 1864-5631, eISSN: 1864-564X. 2016, vol. 9, iss. 18, p. 2567-2571;
3. Petrikytė, I.; Zimmermann, I., Rakšys, K.; Daškevičienė, M.; Malinauskas, T.; Jankauskas, V.; Getautis, V.; Nazeeruddin, MK. Efficiency enhancement of perovskite solar cells via incorporation of phenylethenyl side arms into indolocarbazole-based hole transporting materials // Nanoscale. Cambridge: Royal Society of Chemistry. ISSN: 2040-3364, eISSN: 2040-3372. 2016, vol. 8, iss. 16, p. 8530-8535.

PUBLICATIONS IN INTERNATIONAL AND LITHUANIAN CONFERENCE PROCEEDINGS

1. Petrikytė, I.; Tomkutė-Lukšienė, D.; Bubnienė, G.; Daškevičienė, M.; Malinauskas, T.; Jankauskas, V.; Raišys, S.; Kazlauskas, K.; Juršėnas, S.A.; Barvainienė, B.; Getautis, V. Effective carbazole-based hole transporting materials with extended conjugation. In: Chemistry and chemical technology 2017: proceedings of the international conference, April 28th, 2017, Kaunas. Kaunas: Kauno technologijos universitetas, 2017, pp. 40-40. ISSN 2538-7359.
2. Matsui, T.; Petrikytė, I.; Malinauskas, T.; Domanski, K.; Daškevičienė, M.; Steponaitis, M.; Gratia, P.; Tress, W.; Correa-Baena, J.-P.; Abate, A.; Hagfeldt, A.; Graetzel, M.; Nazeeruddin, M.K.; Getautis, V. Saliba, M. Additive-free polymeric triarylamine derivatives as hole transporting materials for stable perovskite solar cells. In: Open readings 2017: 60 scientific conference for students of physics and natural sciences, March 14-17, 2017 Vilnius, Lithuania: programme and abstracts. Vilnius: Vilnius University, 2017, pp. 235-235. ISSN 2029-4425.
3. Matsui, T.; Petrikytė, I.; Malinauskas, T.; Domanski, K.; Daškevičienė, M.; Steponaitis, M.; Gratia, P.; Tress, W.; Correa-Baena, J.-P.; Abate, A.;

Hagfeldt, A.; Graetzel, M.; Nazeeruddin, M.K.; Getautis, V.; Saliba, M. Additive-free triarylamine derivative polymeric hole transport materials for stable perovskite solar cells. In: Baltic polymer symposium 2016: Klaipeda, September 21-24, 2016: programme and abstracts. Kaunas University of Technology, Vilnius University, Klaipeda University. Kaunas: Kaunas University of Technology, 2016, pp. 110110. ISBN 9786090212356.

4. Petrikytė, I.; Zimmermann, I.; Rakštys, K.; Daškevičienė, M.; Malinauskas, T.; Jankauskas, V.; Magomedov, A.; Getautis.; V. Efficiency enhancement of perovskite solar cells via incorporation of phenylethenyl side arms into indolocarbazole-based hole transporting materials. In: Chemistry and chemical technology: international conference of Lithuanian Society of Chemistry: Lithuanian Academy of Science, Vilnius, Lithuania, April 28-29, 2016: book of abstracts. Fizinių ir technologijos mokslų centras, Vilniaus universitetas, Lietuvos mokslų akademija, Kauno technologijos universitetas. [S.l.]: [s.n.], 2016, pp. 236-236. ISBN 9786099551135.
5. Bikbajevas, V.; Medeišienė, G.; Kazlauskienė, V.; Miškinis, J.; Tamošiūnas, R.; Urnikaitė, S.; Petrikytė, I.; Getautis, V.; Sahraoui, B. Chemical functionalization of GaN surface by self assemble monolayer of azophenylcarbazoles. In: 40-oji Lietuvos nacionalinė fizikos konferencija: programa ir pranešimų tezės, Vilnius, 2013 m. birželio 10-12 d. Vilnius: Vilniaus universiteto leidykla, 2013, pp. 97-97. ISBN 9786094592102.
6. Urnikaitė, S.; Petrikytė, I.; Daškevičienė, M.; Malinauskas, T.; Gaidelis, V.; Maldzius, R.; Jankauskas, V.; Getautis, V. . Solution processable C60 fullerene-hydrazone dyads for optoelectronics. In: ICHMS'2009: Hydrogen Materials Science and Chemistry Carbon Nanomaterials: XI International Conference, 25-31 August,Yalta, Ukraine. Kiev: AHEU, 2009, pp. 710-711.

SL344. 2018-10-26, 17,25 leidyb. apsk. l. Tiražas 15 egz. Užsakymas 295.
Išleido Kauno technologijos universitetas, K. Donelaičio g. 73, 44249 Kaunas
Spausdino leidyklos „Technologija“ spaustuvė, Studentų g. 54, 51424 Kaunas